Hydrological Drought Atlas for the State of Texas

Texas Water Resources Institute TR-474
February 2013

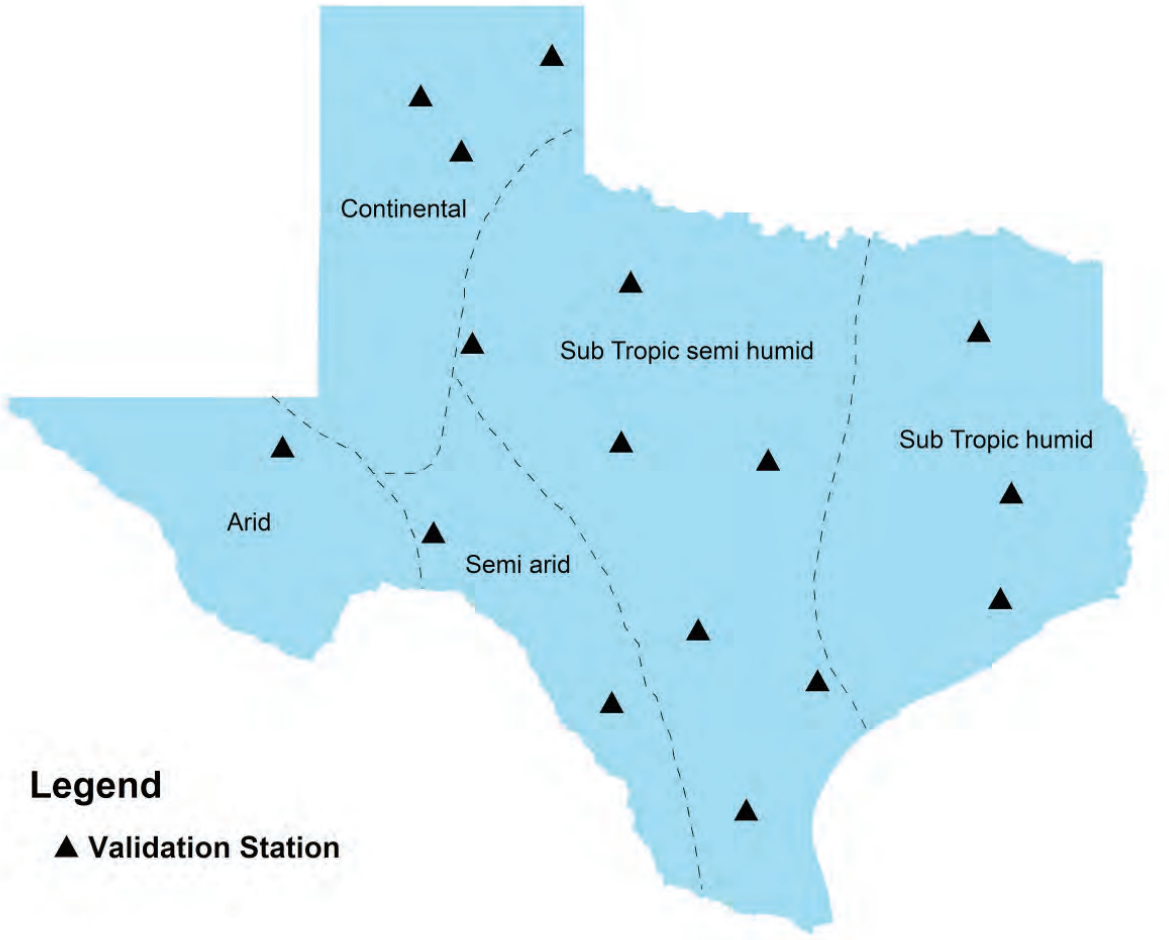

Texas Water Resources Institute
make every drop count

Deepthi Rajsekhar, Vijay P. Singh,
Department of Biological and Agricultural Engineering,
Texas A&M University
Ashok Mishra, Glenn Department of Civil Engineering,
Clemson University

Hydrological Drought Atlas for the State of Texas

For Durations from 3 Months to 36 Months and

Return Periods from 5 Years to 100 Years

Prepared by

Deepthi Rajsekhar

Graduate student, BAEN department, Texas A&M University

Dr. Vijay P. Singh

Professor, BAEN department, Texas A&M University

Dr. Ashok Mishra

Assistant Professor, Glenn Department of Civil Engineering, Clemson University

for

United States Geological Survey (USGS)

Texas Water Resources Institute

Technical Report Number 474

February 2013

College Station, Texas

Preface

This publication serves as a guide for the preparation of hydrological drought frequency maps. The work has been supported by the United States Geological Survey (USGS) grant 2009TX334G to provide the required material to aid drought planning and management.

The report is divided into four parts. The first part describes the methodology employed for developing drought severity-duration-frequency (S-D-F) relationships for uniform grids over Texas, and presents results and discusses them. The second part includes drought iso-severity maps generated for drought durations ranging from 3 to 36 months and return periods from 5 years to 100 years. Third and fourth parts include the maps derived using the same methodology, drought durations and return periods, but the data used for deriving the drought properties are precipitation and naturalized stream flow, respectively. Parts 3 and 4, hence, serve as a validation for the drought maps constructed. An illustrative example with sample calculations for each step is also included in the report.

Contents

Abstract

Maps depicting the spatial variation of hydrological drought severity for Texas are presented in this report. The return periods chosen are 5, 10, 25, 50 and 100 years for drought durations of 3, 6, 9, 12, 18, 24 and 36 months, respectively. The maps were constructed using the drought severity-duration-frequency (S-D-F) relationship derived using a copula-based multivariate probabilistic approach. For purposes of deriving drought properties, monthly stream flow simulations from a large scale land surface model, known as variable infiltration Capacity (VIC) model, were utilized. The stream flow time series obtained was gridded at $1/8^{th}$ degree resolution over Texas. The marginal distribution most suitable for fitting each of the drought variables was determined after testing commonly used distributions, such as exponential, gamma, log-normal, and Weibull. The marginal distributions of drought severity and duration with the smallest root mean square error (RMSE) value between observed and theoretical probabilities were selected. For modeling the joint distribution of drought characteristics, the following classes of bivariate copulas were considered: Archimedean, extreme value, Plackett and elliptical families. The best performing copula, determined using the RMSE and the Akaike information criterion (AIC), were used to determine the conditional and joint return periods and hence derive the drought S-D-F curves. The information obtained from the S-D-F curves was used for the preparation of drought atlas, which depicts the spatial variation of drought severity for specific drought durations and return periods in Texas.

Keywords: Drought atlas, copula, hydrological drought, S-D-F curves

Introduction

A drought can generally be defined as a temporary meteorological event that starts with shortage of precipitation, and may affect streamflow, soil moisture, and ground water. This is considered as a recurring normal event that occurs in all climate regions. Since it is a creeping phenomenon, it is often difficult to detect its beginning, thus making it a complex natural phenomenon which is difficult to quantify and manage (Wilhite and Glantz, 1985).

Droughts are dynamic and are characterized by multiple attributes, like severity, duration and magnitude (Mishra and Singh, 2010). For any drought event, the cumulative deficit of the variable of interest during the drought event is defined as drought severity. Drought duration is the time between the onset and the end of a drought event. Drought magnitude is the average deficit per unit duration. A significant problem associated with drought analysis is the assessment of the rarity of events, such as long or severe droughts. This is of particular interest from a design point of view. Just like intensity-duration-frequency curves have been used for a long time to synthesize a “design storm”, a similar approach can also be taken in the case of droughts.

The purpose of this study is to develop a relationship between drought parameters, severity, duration and frequency, and then utilize it for plotting drought iso-severity curves, thus improving the hydroclimatic design for the state of Texas.

Historical Review

Previous works, cited in the literature, which focused on the construction of drought maps, are briefly reviewed. Dalezios et al. (2000) developed S-D-F relationships for wet periods and drought events for Greece using an extreme value distribution and prepared iso-severity maps of various return periods and durations over the region. The drought events in this study were characterized using the Palmer drought severity index (PDSI). Saghafian et al. (2003) analyzed meteorological droughts in Iran using the run theory and then derived the S-D-F curves and iso-severity maps for the region. In these studies, analysis of extreme events was performed using an empirical relationship based on a plotting position formula. Yoo et al. (2008) applied a rectangular Pulse Poisson Process Model (RPPM) for quantification and analysis of droughts in Korea. The occurrence of drought was assumed as a Poisson process, and the overlap probability between consecutive rectangular pulses was estimated. Based on model structure of RPPM, they presented a theoretical methodology for drought S-D-F analysis. Santos et al. (2012) investigated regional frequency analysis of droughts in Portugal using monthly precipitation data from 144 rain gauge stations. In their study, drought was modeled using the Standardized Precipitation Index (SPI) at multiple time scales (1, 3, 6 and 12 consecutive months) and three spatially defined regions were identified using L-moments analysis. Then, drought magnitude maps of the region were developed using the kriging technique for various return periods. In this study, rather than going for the empirical approaches previously used for deriving drought maps, an analytical approach derived by Shiau et al. (2006) was applied, since it accounts for the multi-attribute nature of droughts in a simple manner.

Part 1. Analysis

Data

Since fine scale observed data is essential to account for spatial heterogeneity of droughts, it might not be wise to use stream gauge data because stream gauges integrate over large spatial areas and thus do not account for the spatial variability of droughts (Andreadis et al., 2005). Besides, in Texas, the distribution of gauging stations is not uniform, since most of the stations are concentrated in the eastern part and relatively few stations are located in the western part of the state. To avoid this problem and to overcome the lack of long-term continuous stream flow data from all over Texas, a land surface model, called Variable Infiltration Capacity (VIC) model, was used to simulate stream flow for a period of 1950-2000, and results were validated against observed values from several USGS stream gauges. This particular model was chosen, since it focuses on simulating hydrological processes relevant to the water and energy balance

over the land surface for studying the effect of climate change on stream flow generation. Distinguishing characteristics of the model include sub-grid variability in land surface vegetation classes, sub-grid variability in the soil moisture storage capacity, and drainage from the lower soil moisture zone (base flow) as a nonlinear recession.

The data used in the study can be divided into three categories: (1) Stream flow simulation obtained from the hydrological model; (2) meteorological forcing, soil and vegetation data used for driving the hydrological model; and (3) naturalized stream flow data from hydro-climatic data network (HCDN) stream gauges.

(1) ***Stream flow simulation using Variable infiltration capacity (VIC) model***

The VIC-3L is a large scale land surface model and is used for simulating land-atmosphere fluxes by solving water and energy balance at a daily or sub-daily temporal scale (Liang et al., 1994). The land surface is essentially divided into grids of specified resolution. Each of these cells is simulated independent of each other. Land surface is divided into different vegetation covers in such a way that multiple vegetation classes can exist within a cell. The soil moisture distribution, infiltration, drainage between soil layers, surface runoff, and subsurface runoff are all calculated for each land cover tile at each time step. Then, for each grid cell, the total heat fluxes (latent heat, sensible heat, and ground heat), effective surface temperature, and the total surface and subsurface runoff are obtained by summing over all the land cover tiles weighted by the fractional coverage. It should thus be noted that the VIC model does not account for the interflow between grids. Because of the absence of observed data for evaporation, soil moisture and runoff for each grid, to evaluate the model simulation results a routing model should be used as a post processing tool to produce stream flow at the points of interest.

In the VIC-3L model, soil is typically partitioned into three layers vertically, with variable soil depths and the main soil parameters include hydraulic conductivity, thickness of each soil layer, soil moisture diffusion parameters, initial soil moisture, bulk density and particle density. The VIC model has been widely used, particularly for stream flow and soil moisture simulations. Abdulla et al. (1996), Nijssen et al. (1997), Lohmann et al. (1998), and Nijssen et al. (2001) used VIC primarily for stream flow simulation. Sheffield et al. (2004), Andreadis and Lettenmaeir (2006), Sheffield and Wood (2008), and Shukla and Wood (2008) demonstrated the use of VIC simulated soil moisture and runoff in the context of droughts. Since the grid-based VIC model simulates the time series of runoff only for each grid cell, which is non-uniformly distributed within the cell, a stand-alone routing model (Lohmann et al., 1996, 1998a) is employed to transport grid cell surface runoff and base flow to the outlet of that grid cell and then into the river system. In this routing scheme, the surface runoff simulated by VIC in each grid cell is transported to the outlet of the grid cell using a unit hydrograph approach. Then, runoff from each grid cell is routed through the channel using a linearized Saint-Venant equation.

In this study, the model was run separately for each of the twenty three river basins in Texas and once stream flow simulations within each grid cell were obtained, the routing model was employed to transport grid cell surface runoff and base flow to the outlet of that grid cell and then into the river system.

(2) *Data requirements for the model*

For this study, the VIC model for stream flow simulation was run at 1/8th degree resolution and hence all input files, including forcing files, soil and vegetation parameters had this resolution. This is the default resolution at which the VIC model runs (Salathe, 2003). This resolution was chosen by taking into consideration the availability of gridded daily forcing data of precipitation (mm), maximum and minimum temperature (^{o}C) and wind speed (m/s) which are needed to drive the model at the 1/8th resolution from Maurer et al. (2002) who have provided a data base for 15 delineated basins in the United States, Canada and Mexico. The time period of data used was for the latter half of the 20th century: 1949-2000. The year 1949-1950 was considered as the spin up year for the model. Apart from the forcing data, soil and land cover data is also required by the VIC model. The soil characteristics which were not considered for calibration were taken from gridded 1/8 degree datasets developed as part of the Land Data Assimilation System (LDAS) project (Mitchell et al., 1999). Within the conterminous United States, these datasets are based on the 1-km-resolution dataset produced by the Pennsylvania State University (Miller and White, 1998). Soil texture in the LDAS dataset is divided into 16 classes for each of 11 layers, inferring specific soil characteristics (e.g., field capacity, wilting point, saturated hydraulic conductivity) based on the work of Cosby et al. (1984) and Rawls et al. (1993), and Reynolds et al. (2000). These LDAS datasets were used to specify the relevant soil parameters required by the VIC model directly. For the remaining soil characteristics (e.g., soil quartz content), values were specified using the soil texture from the 1-km database, which were then indexed to published parameter values [the primary source was Rawls et al. (1993)], and aggregated to the 1/8th degree model resolution. Vegetation parameters needed were also obtained from LDAS. The land cover characterization was based on the University of Maryland global vegetation classification described by Hansen et al. (2000), which has a spatial resolution of 1 km, and a total of 14 different land cover classes. From these global data we identified the land cover types present in each 1/8 grid cell in the model domain and the proportion of the grid cell occupied by each, as described by Maurer et al. (2001). The leaf area index (LAI) needed was derived from the gridded (1/4 degree) monthly global LAI database of Myneni et al. (1997), which is inverted using the Hansen et al. (2000) land cover classification to derive monthly mean LAIs for each vegetation class for each grid cell.

The data needed for the routing scheme includes a fraction file, flow direction file, Xmask file, flow velocity and diffusion files, and unit hydrograph file. ArcMap was used for the preparation of files, and the DEM files needed for creating the required files were obtained from the USGS hydro 1k datasets.

(3) ***Station data used for model validation***

Since the model simulated stream flow was used for analysis in this study, validation of the results was carried out with respect to the actual flow values. The stream flow obtained after calibrating the model parameters was validated using the USGS hydro climatic data network (HCDN) stream flow data. The HCDN stream flow data provides the naturalized stream flow data which can be used for analyzing the hydrologic response to climate change. Since VIC model simulates naturalized stream flow, it makes sense to validate it using HCDN data rather than the data from the original USGS gauge network.

Figure 1 shows five major climate zones within Texas, namely arid, semi-arid, subtropical semi humid, subtropical humid and continental steppe, and locations of stream gauge stations used for validating the stream flow obtained from the VIC model. Table 1 gives details of the validation stations.

Table 1. Information on validation stations within Texas

Station Name	Station ID	Latitude	Longitude	Validation Period	Climate Zone
Frio River Near Derby	8205500	31.436	-103.467	1951-1952	Arid
Spring Creek Near Spring	8068520	35.471	-101.880	1981-1982	Continental
Village Creek Near Kountze	8041500	34.837	-101.414	1968-1969	Continental
Neches River Near Neches	8032000	35.935	-100.371	1965-1966	Continental
Nueces River Near Three rivers	8210000	30.452	-101.733	1975-1976	Semiarid
Nueces River Below Uvalde	8192000	28.5	-99.682	1959-1960	Semiarid
Mill Creek Near Bellville	8111700	32.628	-101.285	1989-1990	Subtropical
North Concho River Near Carlsbad	8134000	31.494	-99.574	1969-1970	Subtropical
Millers Creek Near Munday	8082700	33.329	-99.465	1972-1973	Subtropical
Ecleto Creek Near Runge	8186500	29.335	-98.689	1982-1983	Subtropical
Cowhouse Creek at Pidcoke	8101000	31.285	-97.885	1955-1956	Subtropical
Coleto Creek Near Victoria	8177300	28.752	-97.317	1979-1980	Subtropical
Los Olmos Creek Near Falfurrias	8212400	27.2645	-98.136	1967-1968	Subtropical

Big cow Creek Near Newton	8029500	32.763	-95.463	1982-1983	Subtropical
Long king Creek Near Livingston	8066200	30.907	-95.088	1991-1992	Subtropical
Bayou Toro Near Toro	8025500	29.6947	-95.216	1973-1974	Subtropical

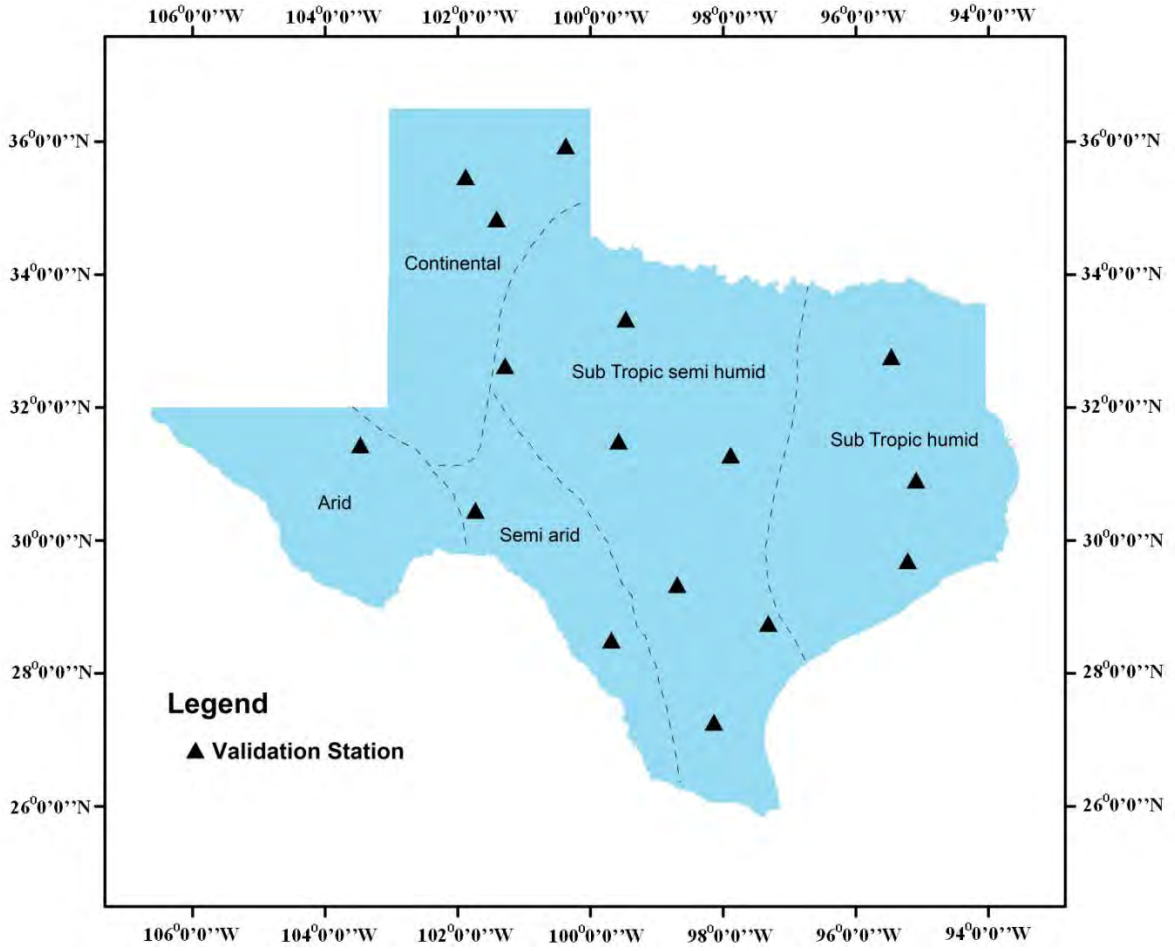

Figure 1. Location of validation stations within different climate zones in Texas

Data Processing

(1) *Gridding of Meteorological Forcing data*

The default resolution of the VIC model is 1/8th degree. Hence, all the forcing parameters required to run the model should be in gridded data format with the same resolution. Maurer et al. (2002) explains how the gridding of forcing data can be done to match the model resolution. The VIC model was designed to use daily precipitation, maximum and minimum temperature and daily averaged wind speed. Out of these, the daily 10-m wind fields were obtained from the

NCEP–NCAR reanalysis and regridded from the T62 Gaussian grid, which is 1.9° grid, to the 1/8° grid using linear interpolation. Daily precipitation data was obtained from National Oceanic and Atmospheric Administration (NOAA) Cooperative Observer (Co-op) stations. The precipitation gauge data were gridded to the $1/8^0$ resolution using the synergraphic mapping system (SYMAP) algorithm of Shepard (1984). The gridded daily precipitation data were then scaled to match the long-term average of the parameter-elevation regressions on independent slopes model (PRISM) precipitation climatology, which is a comprehensive dataset of 12 monthly means for 1961–90 that is statistically adjusted to capture local variations due to complex terrain. The scale factor would be the ratio of mean monthly PRISM precipitation for the period 1961-1990 to the unscaled mean monthly observed precipitation for the grid during 1961-1990. For each grid, there would be a different scaling factor for each month. For the minimum and maximum temperatures the same procedure for precipitation was followed for gridding.

(2) ***Stationarity checking for stream flow data***

Before using stream flow data for drought classification and further analysis, the time series was checked for stationarity. The assumption of stationarity might no longer be valid for time series of hydrological variables due to substantial climate change brought about by human intervention (Milly et al., 2008). If the time series was found to be non-stationary, it was rendered stationary by means of a transformation, like data differencing or detrending, which is given as:

$$X_i^* = X_{i+1} - X_i, i = 1, 2...N-1 \quad (1)$$

where X_i , i=1, 2,…, N, is the monthly time series under consideration. To test for stationarity, two tests were used. The augmented Dickey Fuller test (ADF), proposed by Dickey and Fuller (1979), which tests the difference stationarity, and KPSS test, proposed by Kwiatkowski et al. (1992), which tests trend stationarity, were used. The ADF tests were conducted through ordinary least squares (OLS) estimation of regression models with either an intercept or a linear trend. The KPSS test complements the Dickey-Fuller unit root test. In this test, the series is decomposed into the sum of a deterministic trend, a random walk, and a stationary error. The null hypothesis for the test is that the intercept is a fixed element. Both tests were carried out at the 5% significance level. If the time series fails to pass the KPSS test, detrending is carried out to remove the trend component from the series. If it fails the ADF test, data differencing is carried out to achieve stationarity.

From this step onwards, a small example subset will be used to illustrate the calculations involved in each step. The observed stream flow data from the USGS station: Brazos River near upper bend has been utilized for this purpose. The location details of the station are: Latitude is

$33^0$01’ and longitude is $98^0$37’. Figure 2 shows the logarithmized monthly stream flow time series for the time period 1962-2000.

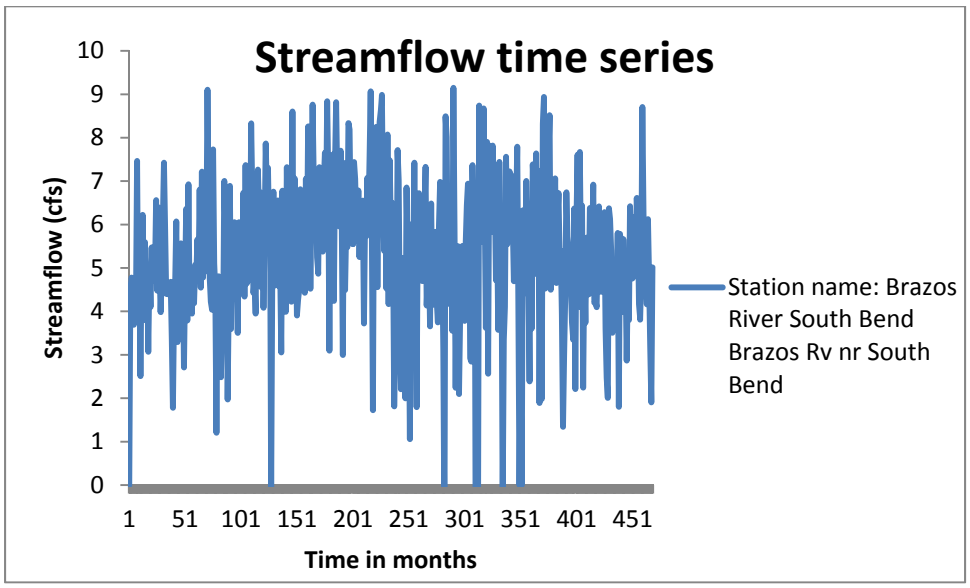

Figure 2. Monthly stream flow time series

Tables 2 and 3 show a sample streamflow data before and after transformation (here logarithm was used for transforming the data). Table 4 shows that the mean and standard deviation of the time series when split into two parts remain almost unchanged after transformation compared to the case before transformation.

Table 2. Sample streamflow data before transformation

91	118.5	100	40.2	53.3	60.4	1743	42.1	223.2	12.3
156.6	502.5	44.7	267.5	99.9	148.6	21.5	133.9	60.5	237.6
110.9	138.4	168.1	706.3	87.9	597.4	177.5	53.6	119.2	414.1
1672	379.5	81.8	82.7	80.8	101.3	107.8	28.7	5.92	58.1
101	433	27	56.9	38.5	261	94.5	182	15	111.1
577.3	44.4	1017	62.7	128.1	51.9	105	66	159.3	119.1
285.1	109.9	900.4	94.2	1359	119.6	274.1	136.7	251.3	8987
705.4	118.9								

Table 3. Sample streamflow values after transformation by taking logarithm

1.96	2.07	2.00	1.60	1.73	1.78	3.24	1.62	2.35	1.09
2.19	2.70	1.65	2.43	2.00	2.17	1.33	2.13	1.78	2.38
2.04	2.14	2.23	2.85	1.94	2.78	2.25	1.73	2.08	2.62
3.22	2.58	1.91	1.92	1.91	2.01	2.03	1.46	0.77	1.76

2.00	2.64	1.43	1.76	1.59	2.42	1.98	2.26	1.18	2.05
2.76	1.65	3.01	1.80	2.11	1.72	2.02	1.82	2.20	2.08
2.45	2.04	2.95	1.97	3.13	2.08	2.44	2.14	2.40	3.95
2.85	2.08								

Table 4. Comparison of mean and standard deviations of time series before and after transformation

Time period	**Before transformation**		**After transformation**	
	Mean	**SD**	**Mean**	**SD**
1951-1954	253.57	392.42	2.122	0.468
1955-1958	477.58	1490.81	2.137	0.593
Error percentages	88.33%	279.9%	0.715%	26.72%

It can be seen from Table 4 that there is considerable improvement in stationarity after transformation. The error percentage, particularly for mean, is quite negligible, when compared over two parts of the time series.

Study area

The area considered for this study is the state of Texas. There are five distinct climate zones in Texas showing the variation from arid to sub-tropic humid zones. The varied physiography in the state of Texas with forests in the east, coastal plains in the south to the elevated plateaus and basins in the north and west, results in a wide variety of weather throughout the year (Benke and Cushing, 2005). The land surface elevation follows a decreasing trend from west to east, with arid climate zone covering higher elevation areas, whereas most of the sub-tropic humid zone and parts of sub-tropic semi-humid zone cover the low lying regions in Texas. There are 13 major river basins in Texas that vary greatly in size, shape and stream patterns. Climate, particularly rainfall and evaporation, strongly controls the flows of rivers and streams in Texas. The region is traversed by a strong decreasing rainfall gradient from east to west and a temperature gradient from north to south that strongly influences vegetation, land use and river flow. In Sabine River basin in east Texas, mean annual rainfall is nearly 60 inches and annual evaporation is less than 70 inches, whereas in Rio Grande basin in west Texas, mean annual rainfall ranges from 8 to 20 inches and annual evaporation is as much as 105 inches. Therefore, east Texas rivers flow year around, whereas most of the west Texas streams flow only part of the year (Bureau of Economic Geology, 1996). Figure 3 shows a river basin map of Texas and the precipitation (annual average in inches) gradient within the state.

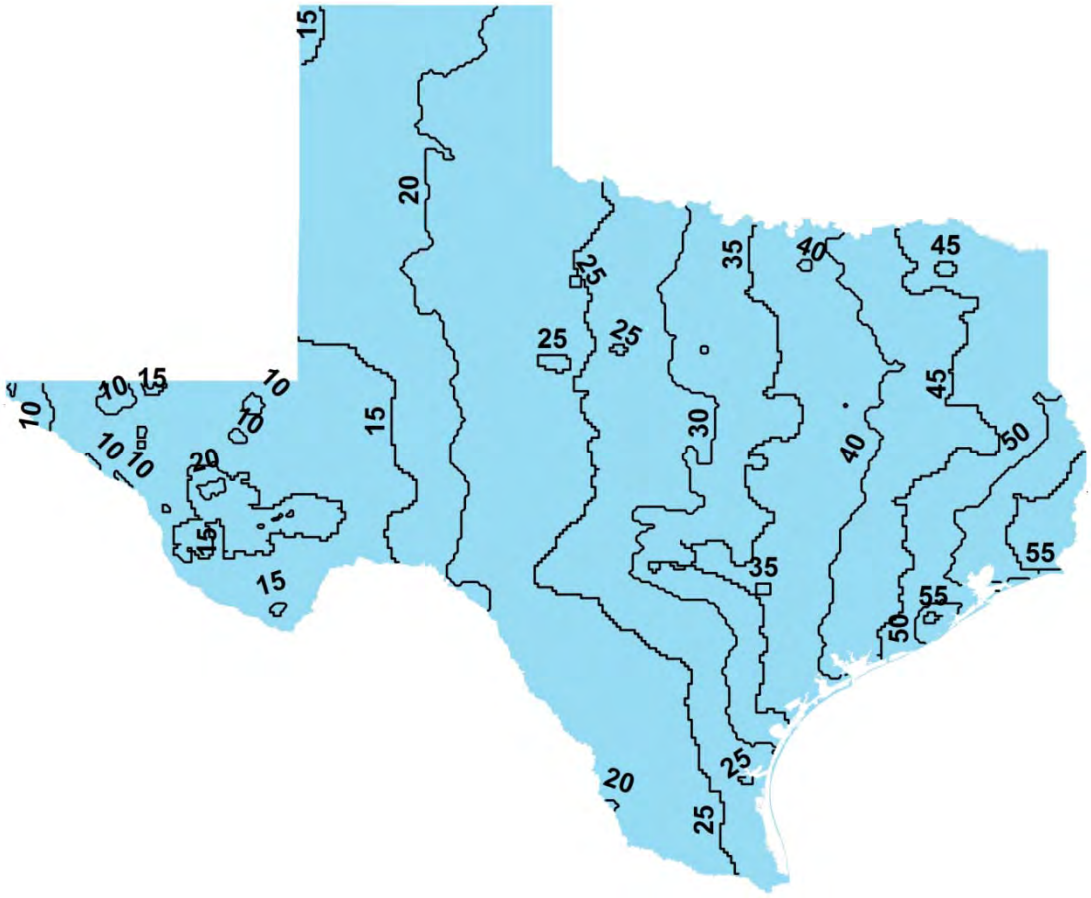

Figure 3. River basin map of Texas with precipitation pattern (annual average Precipitation in inches)

Part 1: Analyses

(1) *Determination of drought severity and duration using theory of runs*

A drought event is characterized by severity, duration and magnitude (Mishra and Singh, 2010). For any drought event, the cumulative deficit of the variable of interest during the drought event is defined as drought severity. Drought duration is the time between the onset and the end of a drought event. Drought magnitude is the average deficit per unit duration. In this study, drought duration and severity were considered. For the monitoring and quantification of drought, a wide range of drought indices are available in the literature (Keyantash and Dracup, 2002). Since this study deals with hydrological droughts, stream flow is the indicator variable of a drought event. Hence, a drought index based on stream flow, namely standardized stream flow index (SSFI), was used in this study to quantify drought properties.

Standardized stream flow index (SSFI)

The concept of SSFI is statistically similar to that of standardised precipitation index (SPI) introduced by McKee (1993) and has been applied by Modarres (2007). Shukla and Wood (2008) used a standardised runoff index (SRI) as a complement to the SPI to assess hydrological aspects of a drought. Table 5 gives the classification of events based on the SSFI values (Modarres, 2007). Following this classification, a threshold value of -0.99 was chosen, since any value below that indicates the onset of a dry event.

Table 5. SSFI Classification

SSFI value	Classification
2.0 or more	Extremely wet
1.5 to 1.99	Very wet
1.0 to 1.49	Moderately wet
-0.99 to 0.99	Near normal
-1.0 to -1.49	Moderately dry
-1.5 to -1.99	Severely dry
-2.0 or less	Extremely dry

The calculation of SSFI involves the following steps: (1) A suitable probability distribution is fitted to the monthly stream flow time series for the time period 1950-2000. (2) From the fitted frequency distribution, the cumulative probability distribution of stream flow is obtained. (3) Cumulative probability is transformed to a standard normal variate of zero mean and unit standard deviation. This is calculated from a numerical approximation to the normal cumulative distribution function (CDF). The approximation given by Abramowitz and Stegun (1964) was used to obtain the standard cumulative normal probability distribution function (CDF). The approximation for $\phi(x)$ for $x>0$ is given as:

$$\phi(x) = 1 - \varphi(x)(b_1 t + b_2 t^2 + b_3 t^3 + b_4 t^4 + b_5 t^5) + \varepsilon(x), \quad t = \frac{1}{1 + b_0 x} \tag{2}$$

where $\varphi(x)$ is the standard normal CDF, b_0=0.2316419, b_1=0.319381530, b_2=-0.356563782, b_3=1.781477937, b_4=-1.821255978, b_5=1.330274429.

Having approximated the normal CDF using eq. (2), the standard normal variate Z can be calculated as:

$$z = t - \frac{c_0 + c_1 t + c_2 t^2}{1 + d_1 t + d_2 t^2 + d_3 t^3} \tag{2a}$$

$$t = \sqrt{-2\ln(\phi(Z))} \; for \; \phi(Z) < 0.5$$

$$t = \sqrt{-2\ln(1 - \phi(Z))} \; for \; 0.5 < \phi(Z) \le 1$$

C_0 = 2.515517, C_1= 0.802853, C_2= 0.010328, d_1= 1.432788, d_2= 0.189269, d_3= 0.001308.

SSFI is essentially the standard Z-variate calculated in the previous step. In other words, *SSFI* for a given series can simply be represented as the standard normal variate with zero mean and unit standard deviation and is given as:

$$SSFI = \frac{F_i - \overline{F}}{\sigma} \qquad (3)$$

where F_i is the flow rate in time interval *i*, $\overline{F}$ is the mean of the series, and σ is the standard deviation of the series. Conceptually it represents the number of standard deviations above or below that an event is from the mean (McKee, 1993).

Considering a number of previous studies, like Zaidman et al. (2001), Kroll and Vogel (2002), McMahon et al. (2007), Shukla and Wood (2008) and Nalbantis and Tsakiris (2009), the log-normal distribution was selected for fitting monthly stream flow data. In a previous study for Texas, the authors identified that log-normal distribution provided a satisfactory fit for stream flow data within various climatic regions in Texas.

The calculations involved in the determination of SSFI are illustrated below:

The first step would be fitting the log-normal distribution to stream flow data. From the log-normal CDF obtained, the calculation of SSFI for one observation is shown below:

x = 6.5, $\phi(x)$ = 0.75, Mean $\overline{F}$ =5.321 and standard deviation σ=1.7478

$$t = \frac{1}{1 + b_0 x} = \frac{1}{1 + 0.2316419 * 6.5} = 0.1249$$

$$\phi(x) = 1 - 0.75(0.319381530 * 0.1249 - 0.356563782 * 0.1249^2 + 1.781477937 * 0.1249^3 - 1.821255978 * 0.1249^4 + 1.330274429 * 0.1249^5) = 0.97195$$

$$t = \sqrt{-2\ln(1 - 0.97195)} = 2.673487$$

$$SSFI = Z = t - \frac{c_0 + c_1 t + c_2 t^2}{1 + d_1 t + d_2 t^2 + d_3 t^3}$$

$$= 2.673487 - \frac{2.515517 + 0.802853 * 2.673487 + 0.010328 * 2.673487}{1 + 1.432788 * 2.673487 + 0.189269 * 2.673487^2 + 0.001308 * 2.673487^3}$$

$$= 1.9181$$

Figure 4 shows the SSFI time series for the data.

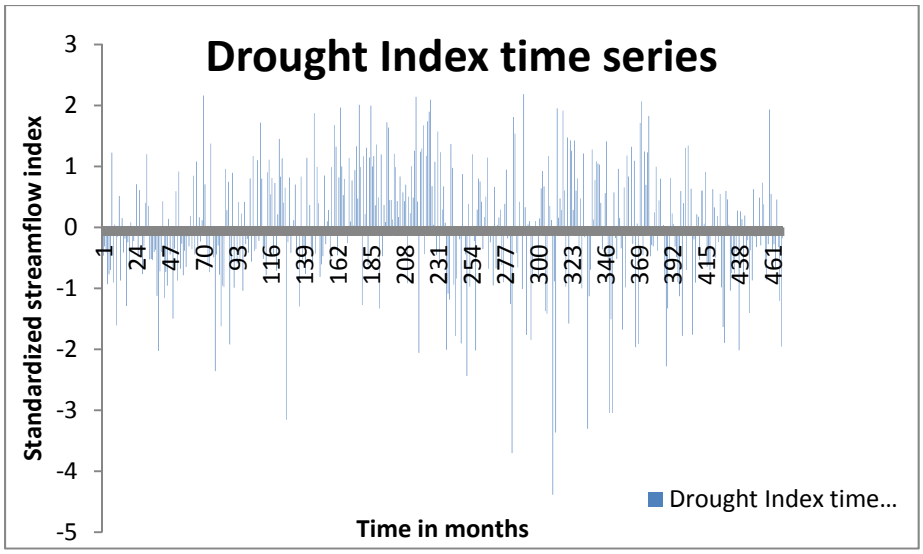

Figure 4. SSFI time series for the station location

The theory of runs was used for deriving drought characteristics from the stream flow time series. This method has been widely used in the field of hydrology. Yevjevich et al. (1967), Rodriguez-Iturbe (1969), Saldarriaga and Yevjevich (1970), Millan and Yevjevich (1971), Guerrero-Salazar and Yevjevich (1975), and Sen (1976,1977) are among the first who applied the run theory in hydrology. A run is defined as a portion of time series of drought variable X_t in which all values are either above or below a threshold level X_0. Accordingly, it can be called a positive or a negative run. The threshold level may be constant or it may vary with time. Thus, the drought characteristics essentially depend upon the threshold chosen (Mishra and Singh, 2010). Figure 5 depicts the drought characteristics derived using SSFI.

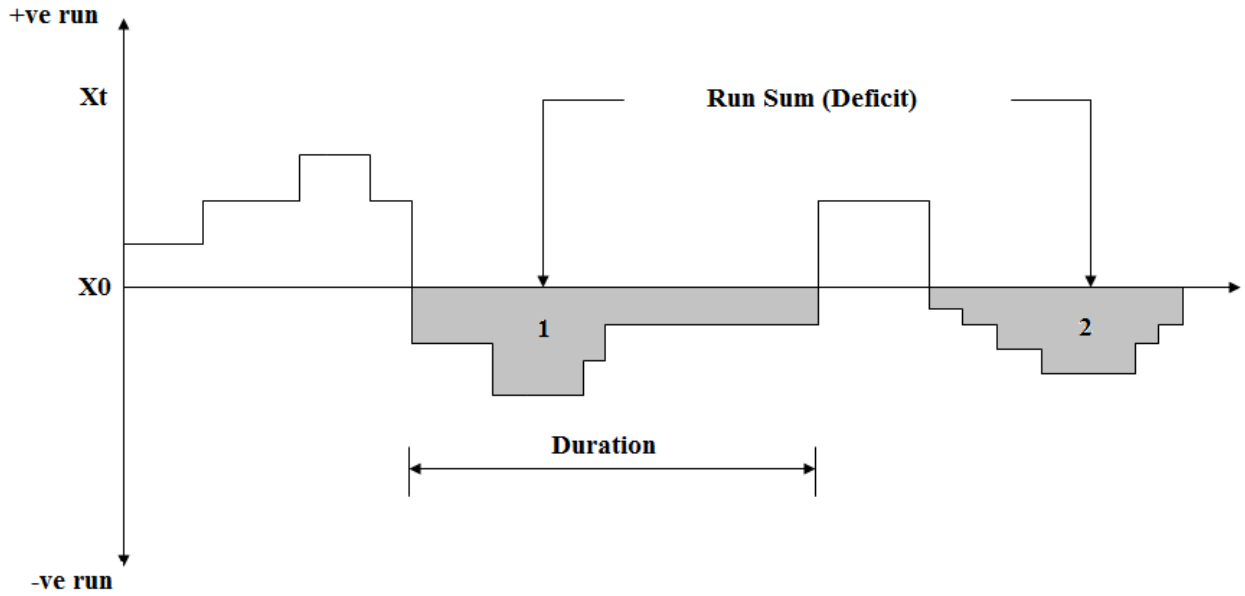

Figure 5. Drought characteristics derived using standardized stream flow index (SSFI)

Having obtained the time series of SSFI from the previous step, the severity and duration values of the drought events can be calculated as follows.

Table 6 shows a portion of the monthly SSFI time series and the calculated severity and duration values.

Table 6. Sample SSFI time series

SSFI	Severity	Duration (months)
-0.464		
-0.312		
-0.409	-1.225	1
-0.931		
-1.225		
-0.905		
-1.609		
-1.124	-4.76	3
-2.027		
-0.720		

From Table 5, it can be seen that any SSFI value falling below -0.99 can be considered as a drought event. From the example subset given in Table 3, the first drought event has a magnitude of -1.225 and lasts for a month. The second drought event has a cumulative magnitude of (-1.609-1.124-2.027) which is -4.76 and lasts over a period of 3 months. Figure 6 shows the scatter plot for the severity-duration values calculated.

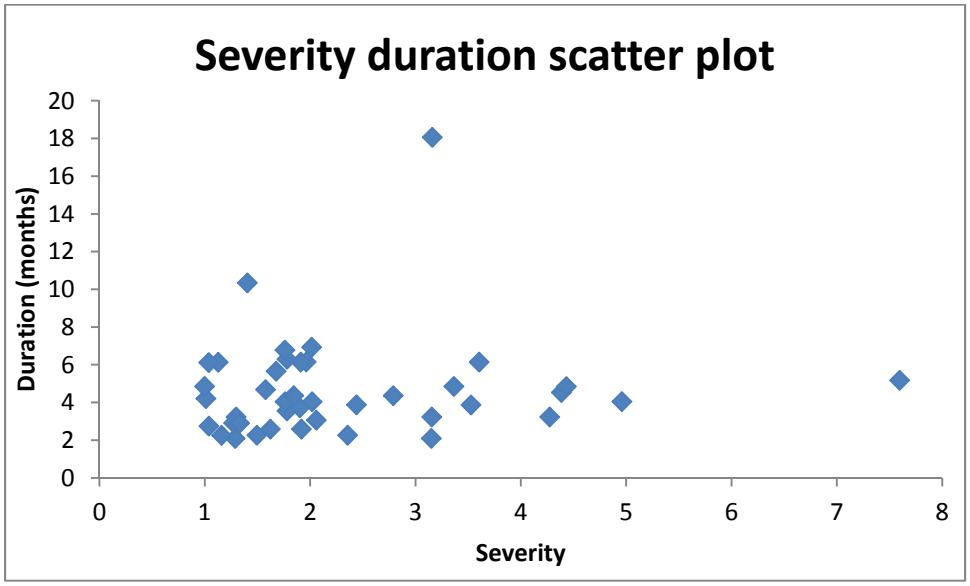

Figure 6. Severity Duration scatter plot

Table 7 gives the summary of the statistics of the drought properties at the station.

A total of 42 drought events were observed.

Table 7. Summary statistics of drought events

Drought property	Severity	Duration (months)
Mean	2.3058825	4.6054762
Standard deviation	1.3375898	2.7289699
Skewness	1.9339718	3.0202531
Minimum	0.9988734	2
Maximum	7.5951209	18

(2) ***Determination of marginal distributions for drought severity and duration***

Distribution Selection

Sklar's theorem requires that the marginal distributions should be continuous. In drought analysis, the two most commonly used continuous distributions are exponential and gamma for fitting the drought duration (Zelenhastic and Salvai, 1987) and drought severity (Shiau, 2006), respectively. However, since there are several grids to be considered, these two distributions might not fit well for all cases. Hence, additional distributions, like Weibull and log normal, which are usually used to describe hydrological variables, were also considered.

Parameter Estimation

Parameters of marginal distributions were estimated using the maximum likelihood estimation method. The procedure of finding the value of one or more parameters for a given statistic makes the known likelihood distribution a maximum. The maximum likelihood estimates are obtained by maximizing the log-likelihood function.

The maximum likelihood method provides one solution to the estimation problem. Let $\{x_i\}$ be a set of observations from a population with probability distribution function:

$$\phi(x; a_1, a_2, \ldots a_n) = \phi(x, \{a\}) \tag{4a}$$

Parameters {a} influence the distribution function, but are generally unknown. The task of estimation is to determine functions of observations {x} to use as estimates of parameters. The probability of obtaining a set of observations {x} from a population with probability distribution function $\phi(x, \{a\})$ is the product of the probabilities of all the observations:

$$L(a) = \prod_i \phi(x_i, \{a\}) \tag{4b}$$

This joint probability function is called the likelihood and depends on parameters $\{a\}$. The value a_k, for which the likelihood reaches its maximum value, is the maximum-likelihood estimate for parameter a. If W= ln(L$\{a\}$), then

$$W = \sum_i \phi(x_i, \{a\}) \tag{4c}$$

The maximum-likelihood estimate of parameters $\{a\}$ satisfies the simultaneous equations:

$$\left.\frac{\partial W}{\partial a_j}\right|_{a_i=a_j} = 0 \tag{4d}$$

Figures 7 and 8 show the histogram of severity and duration data, respectively, and the distribution fits.

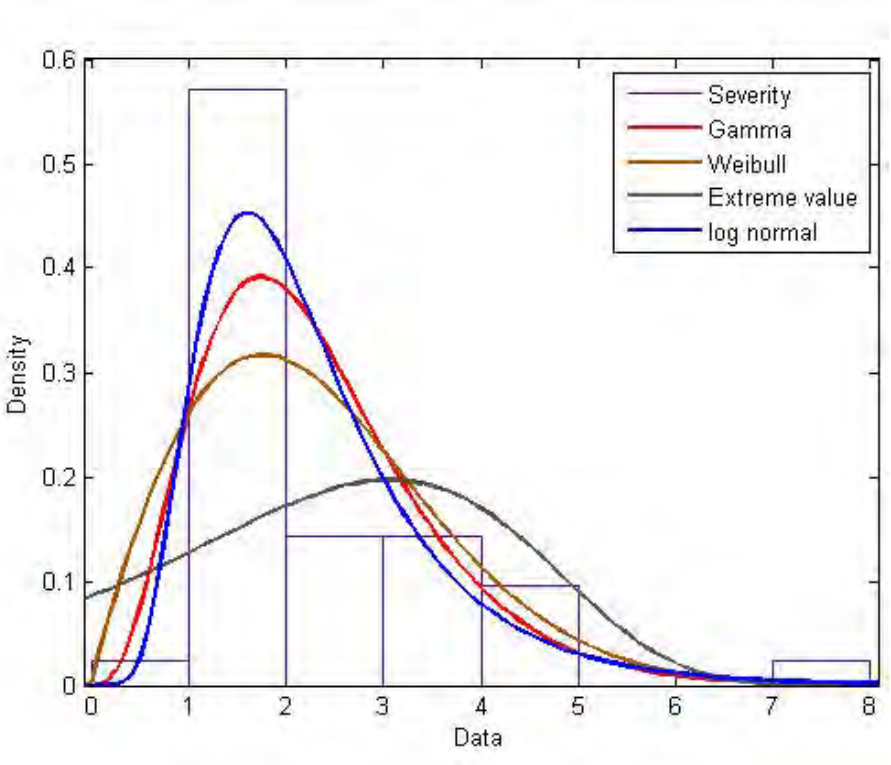

Figure 7. Histogram for severity data and distribution fits

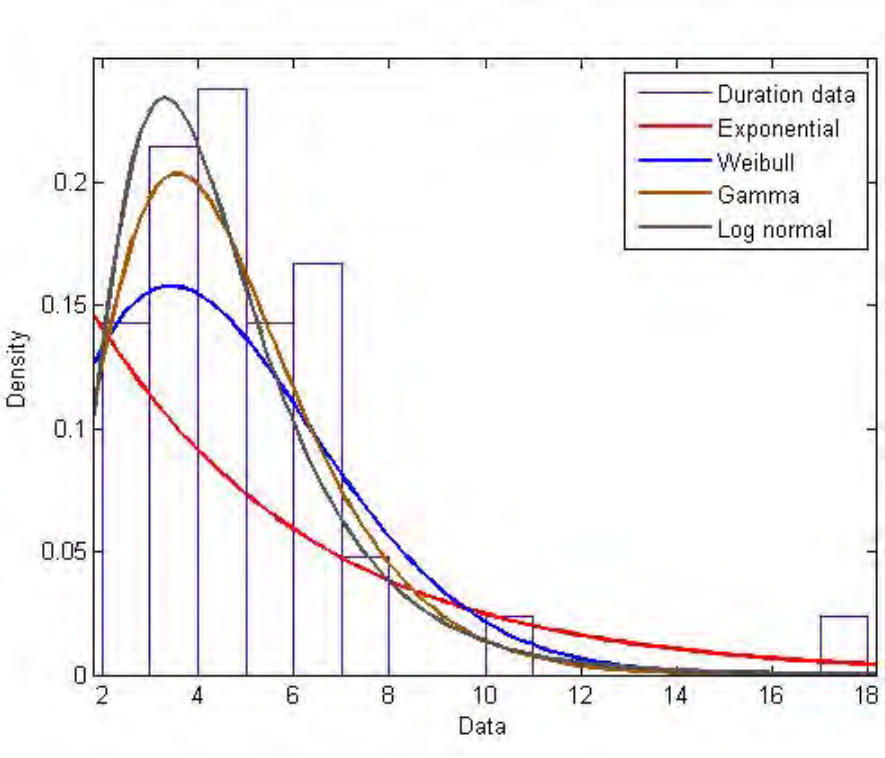

Figure 8. Histogram for duration data and distribution fits

Calculations involved in the parameter estimation for one of the chosen distributions, viz., log normal for severity are shown below:

$$\hat{\mu} = \frac{\sum_k \ln x_k}{n}; \hat{\sigma}^2 = \frac{\sum_k (\ln x_k - \hat{\mu})^2}{n} \quad (4d)$$

where $\hat{\mu}$ is the estimator of mean and $\hat{\sigma}^2$ is the estimator of variance, k is the number of observations, and X_k is the observations. Table 8 gives the values of X_k.

Table 8. Severity values (X_k) used for parameter estimation

1.609	1.289	3.151	1.159	1.495	2.356	1.623	1.917	1.039	3.155
1.297	1.273	1.330	2.058	4.275	1.781	1.902	2.439	2.018	4.959
1.010	1.762	1.844	2.789	4.385	3.365	1.577	0.999	4.432	7.595
1.678	1.963	1.911	3.605	1.128	1.780	1.760	3.528	1.037	2.014
1.404	3.159								

$$\sum_k \ln X_k = 29.728; \hat{\mu} = \frac{29.728}{42} = 0.708$$

$$\sum_k (\ln X_k - \hat{\mu})^2 = 9.811; \hat{\sigma}^2 = \frac{9.811}{42} = 0.234$$

Goodness of fit

For choosing the most suitable marginal distribution from amongst the candidate distributions, goodness of fit statistics, like mean square error (MSE) and Akaike information criterion (AIC), AIC is a goodness of fit statistic which has an information entropy background and represents a relative measure of information lost in the system. The distribution with the lowest AIC was chosen.The AIC is defined as:

$$AIC(m) = n\log(MSE) + 2m \tag{4}$$

where n is the number of observations and m is the number of fitted parameters.

Mean square error denotes the difference between the estimated and true values. The distribution with the smallest MSE values between observed and theoretical probabilities was chosen. *MSE* is the mean square error of the fitted distribution with respect to the empirical distribution and is given as:

$$MSE = \frac{1}{n-m}\sum_{i=1}^{n}(O_i - P_i)^2 \tag{5}$$

where O_i and P_i represent the observed and estimated variables, respectively.

A sample calculation for the estimation of goodness of fit parameters AIC and MSE for log normal distribution fit in the case of severity data is given below. Table 9 shows the observed and estimated severity values.

Table 9. Observed and estimated severity values

Observed severity values (O)	Estimated severity values (P)	$(O-P)^2$
1.6085	1.723473	0.013219
1.288996	1.183367	0.011157
3.150614	3.131783	0.000355
1.158675	0.978645	0.032411
1.494962	1.358948	0.0185
2.356052	2.087721	0.072002
1.622627	1.570525	0.002715
1.917271	1.808434	0.011846
1.038689	1.223807	0.034269
3.155055	3.265075	0.012105
1.297035	1.305006	6.35E-05
1.273248	1.343874	0.004988
1.330372	1.381897	0.002655
2.057645	2.19255	0.018199
4.274602	4.456096	0.03294

1.780895	1.492546	0.083145
1.902308	1.528715	0.139572
2.439114	2.564702	0.015772
2.01824	2.160059	0.020113
4.958802	4.636471	0.103897
1.010203	1.072409	0.00387
1.762338	1.708479	0.002901
1.843975	1.74475	0.009846
2.788553	2.781287	5.28E-05
4.385018	4.818158	0.18761
3.364899	3.855427	0.240618
1.576833	1.893163	0.100065
0.998873	0.931434	0.004548
4.431861	4.970311	0.289928
7.595121	8.009869	0.172016
1.677634	2.050186	0.138796
1.962933	2.091348	0.01649
1.910923	2.133444	0.049515
3.605031	3.765717	0.02582
1.127742	1.220839	0.008667
1.779639	1.663629	0.013458
1.759909	1.613274	0.021502
3.527597	3.361717	0.027516
1.036974	1.141186	0.01086
2.014445	2.463874	0.201986
1.403509	1.517982	0.013104
3.159355	3.695592	0.28755

$\sum (\boldsymbol{O} - \boldsymbol{P})^2 = 2.456$

MSE=2.456/(42-2) = 0.061

AIC(2) = 42*log(0.061) + 2*2 = -46.899

Figure 9 gives the quantile plot with 95% confidence bounds for log-normal distribution which was chosen to fit the severity data.

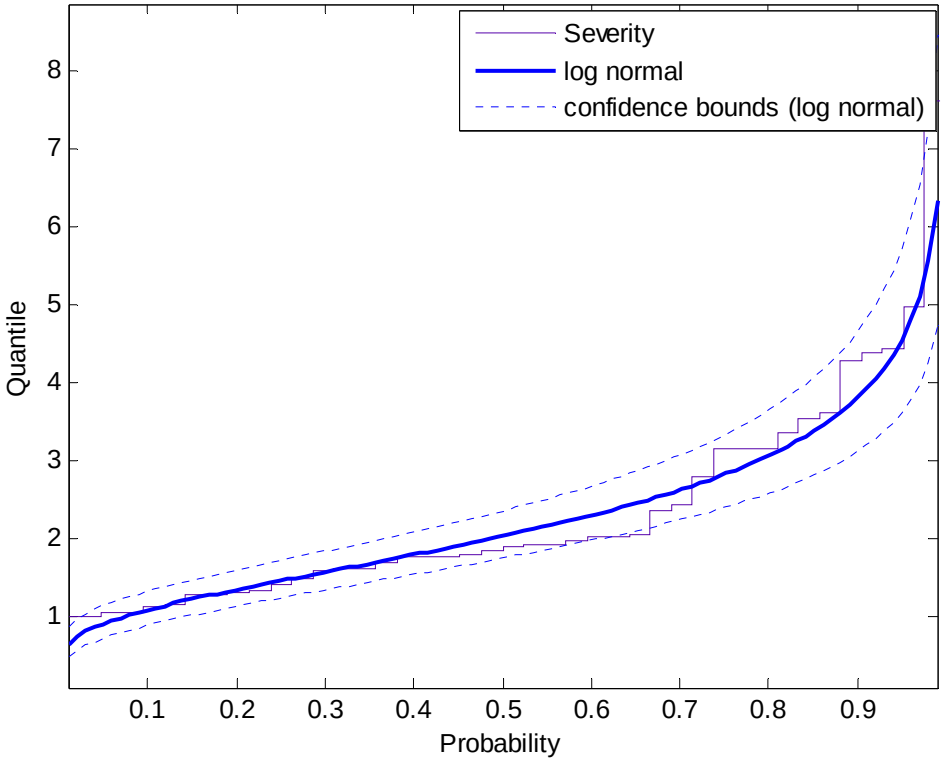

Figure 9. Quantile plot for the log-normal distribution

The chosen log-normal distribution thus has the following parameters: mu (μ) is 0.707 with a standard error of 0.0754 and sigma (σ) is 0.489 with a standard error of 0.054. Figure 10 gives the quantile plot with 95% confidence bounds for the exponential distribution which was chosen to fit the duration data. The chosen exponential distribution has the following parameters: mu is 4.595 with a standard error of 0.0754.

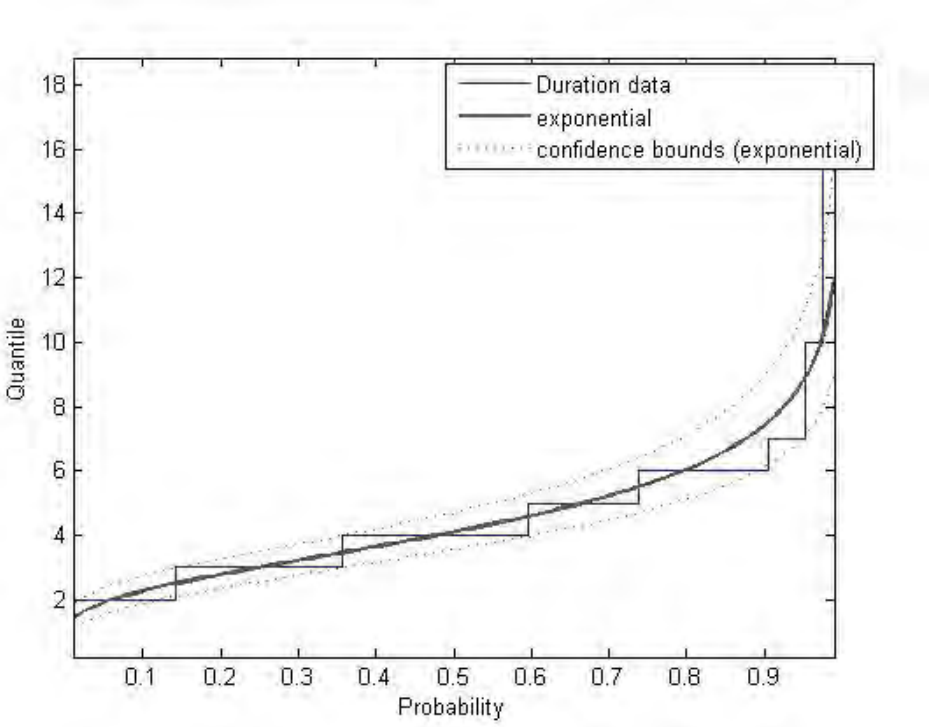

Figure 10. Quantile plot for exponential distribution

(3) ***Construction of joint distribution of drought severity and duration***

Droughts are dynamic and are characterized by multiple attributes, such as severity, duration and magnitude (Mishra and Singh, 2010). Several studies related to drought properties have been conducted in the past. In some of the studies (Tallaksen et al., 1997, Fernández & Salas, 1999; Cancelliere & Salas, 2004) drought properties were investigated separately by unviariate frequency analysis. However, taking into account the fact that droughts are multi-attribute in nature, in several other studies, univariate analysis was extended to bivariate analysis (Shiau and Shen, 2001; Bonaccorso et al., 2003; Kim et al., 2003; González and Valdés, 2003; Salas et al., 2005). However, the derivation of such bivariate distributions poses problems, since the marginal distributions used should belong to the same family, which might not be the case in reality since we use different distribution functions to fit different drought properties. The use of copulas to link marginal distributions to form a joint distribution was found to alleviate such problems and several studies focusing on the use of copulas in the context of drought analysis can be seen in the literature (Shiau, 2006, 2007, 2009; Kao & Govindaraju, 2010; Song & Singh, 2010a,b; Mirakbari et al., 2010).

A bivariate distribution function $F_{X,Y}(x,y)$ of two correlated random variables X and Y with marginal CDFs $F_X(x) = P(X \leq x)$ and $F_Y(y) = P(Y \leq y)$, respectively, can be expressed in terms of copula function C as (Sklar, 1959):

$$F_{X,Y}(x,y) = C[F_X(x)F_Y(y)] = C(u,v) \tag{6}$$

where $F_{X,Y}(x,y)$ is the joint CDF of random variables X and Y.

Copula functions for joint distribution

In this study, four classes of bivariate copulas were considered: Archimedean, extreme value, Plackett and elliptical families.

Archimedean copulas

This family of copulas is related to Laplace transforms of bivariate distribution functions (Joe, 1997). If L denotes the class of Laplace transforms, which consist of strictly decreasing differentiable functions:

$$L = \begin{Bmatrix} \phi : [0,\infty] \to [0,1] \phi^{-1}(0) = 1, \phi^{-1}(\infty) = 0; \\ (-1)^j \phi^{(j)} \geq 0;\ j = 1,...,\infty \end{Bmatrix} \tag{7}$$

then the bivariate copula function $C : [0,1]^2 \to [0,1]$ is defined as (Nelson, 1999):

$$C(u,v) = \phi^{[-1]}[\phi(u) + \phi(v)]\ u,v \in [0,1] \tag{8}$$

where $\phi(.)$ is the copula generator and $\phi^{-1}(.)$ is the pseudo inverse of $\phi(.)$. The Archimedean class of copulas considered in the study include: Clayton and Frank copulas.

Extreme value copulas

A bivariate random variable (X, Y) is said to follow an extreme value distribution with unit exponential margins

$$P(X > x) = e^{-x}, P(Y > y) = e^{-y} (x > 0, y > 0) \text{ for any n} \geq 1 \tag{9}$$
$$F_{X,Y}^n(x,y) = F_{X,Y}(nx,ny)\ \ (x > 0, y > 0)$$

The joint survivor function for any (X, Y) can be expressed as (Tawn, 1988):

$$F_{X,Y}(x,y) = P(Y > y, X > x) = \exp\left[-(x+y)A\left(\frac{y}{x+y} \right) \right] (x > 0, y > 0) \tag{10}$$

where $A(.)$ is the Pickands dependence function. Accordingly, a bivariate extreme value copula can be written in terms of Pickands dependence function as:

$$C(u,v) = P\left[F_X(x) \le u, F_Y(y) \le v\right] = \exp\left[(\log u + \log v)A\left(\frac{\log u}{\log u + \log v}\right)\right] \quad (11)$$

The extreme value copula considered in this study was Gumbel-Hougaard copula.

Elliptical copula

Under this class, Student's *t* copula was considered in the study. This family of copulas does not have closed form expressions.

Plackett copula

The Plackett copula is formed by assuming a constant global cross ratio function. The expressions for the copulas considered in the study and the parameter space are explained in Table 10.

Table 10. Joint cumulative distribution function for various types of copulas used in the study

Names	Equations	Parameters
Clayton	$(u^{-\theta} + v^{-\theta} - 1)^{\frac{-1}{\theta}}$	$0 \in \left[-1, \infty) \setminus \{0\}\right]$
Frank	$\frac{-1}{\theta}\ln(1 + \frac{(e^{-\theta_u} - 1)(e^{-\theta_v} - 1)}{(e^{-\theta} - 1)})$ $\theta \in R$	$\theta \in (-\infty, \infty) \setminus \{0\}$
Gumbel-Hougaard	$\exp\left[-(u^{-\theta} + v^{-\theta})^{1/\theta}\right]$	$\theta \in [1, \infty)$
Student t	$\int_{-\infty}^{t_\nu^{-1}(u)} \int_{-\infty}^{t_\nu^{-1}(v)} \frac{1}{2\Pi\sqrt{(1-r^2)}} \left\{1 + \frac{x^2 - 2rxy + y^2}{\nu(1-r^2)}\right\}^{-(\nu+2)/2} dxdy$ $t_\nu(x) = \int_{-\infty}^{x} \frac{\Gamma[(\nu+1)/2]}{\sqrt{\Pi\nu}\Gamma(\nu/2)} \left(1 + y^2/\nu\right)^{-(\nu+1)/2} dy, \ \nu \neq 0$	$\nu > 2, r \in (0,1]$ r is off-diagonal element of correlation matrix

Plackett	$\frac{1}{2(\theta-1)}(b-c)$ $b=1+(\theta-1)(u+v), c=\sqrt{b^2-4uv\theta(\theta-1)}$	$\theta \in [0,\infty)\setminus\{1\}$

Copula parameter estimation

Copula parameters were estimated following the method proposed by Joe (1997), viz., Inference functions for margins (IFM). This is a two stage approach. In this study, suppose we have a bivariate distribution with *n* observations for each margin, the first step of IFM is to use maximum likelihood estimation (MLE) method to find the vector of marginal parameters β which maximizes the likelihood function:

$$\log L(X_{ij};\beta)=\sum_{i=1}^{n}\sum_{j=1}^{2}\log f_i(X_{ij};\beta_j) \tag{12}$$

where *f*(.) is the marginal pdf. If the likelihood function is simple, we can easily set its partial derivatives equal to zero, or the optimization procedure is usually conducted by iterative methods. Then, the estimated $\widehat{\beta}_{IFM}=(\widehat{\beta}_1^T,\widehat{\beta}_2^T)^T$ from step 1, along with sample data, were used to estimate copula parameters α, which maximize the likelihood function:

$$\log L(X_{ij};\alpha,\beta)=\sum_{i=1}^{n}\log c(F_1(X_{i1};\widehat{\beta}_1),\,F_2(X_{i2};\widehat{\beta}_2)) \tag{13}$$

where *F*(.) is the marginal *CDF*.

Again, iterative methods are applied to optimize the likelihood function to obtain copula parameters $\widehat{\alpha}_{IFM}$.

For the estimation of parameters using the inference function for margins, the original data will be transformed as points represented within a 2-dimensional unit hypercube. This means the data will now be a 42 X 2 matrix with points in the interval [0,1]. Thus, in essence copula is the multivariate distribution on unit hypercube with uniform marginals. Table 11 gives the data in this format.

Table 11. Severity and duration data represented as points within a unit hypercube

Severity (U)	Duration (V)
0.059031	0.078112
0.890036	0.852276
0.330202	0.402932

0.229701	0.112496
0.113949	0.146598
0.310923	0.366604
0.228432	0.248906
0.651997	0.571187
0.06616	0.079638
0.275431	0.795828
0.28182	0.425222
0.880066	0.99172
0.44433	0.42331
0.755914	0.986244
0.603296	0.753069
0.783266	0.710984
0.113931	0.158839
0.978564	0.940248
0.848597	0.89539
0.050647	0.586408
0.466202	0.425831
0.325653	0.363858
0.630205	0.325906
0.230299	0.954493
0.579885	0.60536
0.603156	0.708867
0.599879	0.7625
0.448428	0.439857
0.035424	0.084785
0.513815	0.577633
0.40773	0.490836
0.108046	0.139395
0.459876	0.784427
0.450883	0.314409
0.55114	0.659675
0.805404	0.875285
0.70085	0.78651
0.872236	0.840886
0.052192	0.095428
0.219681	0.108388
0.459642	0.721368
0.958534	0.99183

This data has a linear correlation parameter of 0.805 and hence rho (ρ) = 0.65.

Using this, parameters for various copula families are calculated, as shown in Table 12.

Table 12. Copula parameters estimated for sample example data

Copula family	Parameters
Clayton	Θ = 2.7263
Frank	Θ = 8.7613
Gumbel	Θ = 2.1372
Plackett	Θ = 3.187
Students-t	Θ = 0.8238, r = 2.178

Goodness of fit test

To identify the appropriate copula model among the ones considered, distance based statistics, such as Anderson-Darling (*AD*), integrated Anderson-Darling (*IAD*), and Akaike information criterion (*AIC*) test statistics, were used to evaluate the performance of fitted copula models. The empirical copula can be calculated from the observed data. The empirical forms of *A*D and *IAD* statistics are given as:

$$AD = \max_{1\le i\le n, 1\le j\le n} \frac{\left|\widehat{C}_n(\frac{i}{n},\frac{j}{n}) - C_{p\theta}(\frac{i}{n},\frac{j}{n})\right|}{\sqrt{C_{p\theta}(\frac{i}{n},\frac{j}{n})[1-C_{p\theta}(\frac{i}{n},\frac{j}{n})]}} \tag{14}$$

$$IAD = \sum_{i=1}^{n}\sum_{j=1}^{n} \frac{\left[\widehat{C}_n(\frac{i}{n},\frac{j}{n}) - C_{p\theta}(\frac{i}{n},\frac{j}{n})\right]}{C_{p\theta}(\frac{i}{n},\frac{j}{n})[1-C_{p\theta}(\frac{i}{n},\frac{j}{n})]} \tag{15}$$

where *i* and *j* represent order statistics of random variables *u* and *v*.

The expressions for *AIC* and *MSE* are given by eq. (4) and eq. (5), respectively. The copula family with minimum *AD*, *IAD* and *AIC* statistics were chosen.

Table 13 gives the goodness of fit statistic for each copula family.

Table 13. Goodness of fit statistics for copula families

Copula family	Log-likelihood	AIC
Clayton	**31.786**	**-405.976**
Frank	28.812	-387.518

Gumbel	20.198	-391.276
Plackett	25.729	-377.197
Students-t	18.182	-328.871

(4) ***Conditional distribution for severity based on duration***

Shiau (2006) derived expressions for the distribution of severity conditioned on duration from bivariate copulas for drought variables which can be given as:

$$P(S \le s \mid D \ge d') = \frac{P(S \le s, D \ge d')}{P(D \ge d')} = \frac{F_S(s) - F_{D,S}(d', s)}{1 - F_D(d')} = \frac{F_S(s) - C[F_D(d'), F_S(s)]}{1 - F_D(d')} \quad (16)$$

Similarly, the conditional distribution of duration with respect to severity can be given as:

$$P(D \le d \mid S \ge s') = \frac{P(D \le d, S \ge s')}{P(S \ge s')} = \frac{F_D(d) - F_{D,S}(d, s')}{1 - F_S(s')} = \frac{F_D(d) - C[F_D(d'), F_S(s)]}{1 - F_S(s')} \quad (17)$$

Conditional probability plots are useful in water-supply management systems, where one determines if the drought duration and severity simultaneously exceed certain thresholds, to trigger a drought contingency plan. To evaluate the drought severity distribution given drought duration values exceeding a certain threshold *d*' or to evaluate drought duration distribution given the drought severity exceeding a particular threshold *s*', the conditional probability plots can be used.

Tables 14 and 15 give the conditional probabilities for (a) severities given duration and (b) durations given severity, respectively.

Table 14. Conditional cumulative probability for severity given duration

Severity (S)	**Duration (months) (D)**	**Conditional Cumulative probability $F_{S\|D}$**
1.6085	2	0.5931
1.288996	2	0.6329
3.150614	2	0.558
1.158675	2	0.0585
1.494962	2	0.5743
2.356052	2	0.5275
1.622627	3	0.457
1.917271	3	0.3574
1.038689	3	0.5249
3.155055	3	0.9659
1.297035	3	0.703

1.273248	3	0.9783
1.330372	3	0.3795
2.057645	3	0.976
4.274602	3	0.703
1.780895	4	0.4518
1.902308	4	0.6304
2.439114	4	0.8046
2.01824	4	0.758
4.958802	4	0.9987
1.010203	4	0.3501
1.762338	4	0.4873
1.843975	4	0.0735
2.788553	4	0.9966
4.385018	5	0.499
3.364899	5	0.6364
1.576833	5	0.72
0.998873	5	0.4037
4.431861	5	0.8861
7.595121	5	0.5427
1.677634	6	0.5661
1.962933	6	0.5761
1.910923	6	0.864
3.605031	6	0.1764
1.127742	6	0.6219
1.779639	6	0.743
1.759909	7	0.663
3.527597	4	0.6216
1.036974	6	0.786
2.014445	7	0.0599
1.403509	10	0.8045
3.159355	18	0.9731

Table 15. Conditional cumulative probability for duration given severity

Severity (S)	**Duration (months) (D)**	**Conditional Cumulative probability $F_{D\|S}$**
1.6085	2	0.2089
1.288996	2	0.7438
3.150614	2	0.2658
1.158675	2	0.8358

1.494962	2	0.2246
2.356052	2	0.2855
1.622627	3	0.3319
1.917271	3	0.5852
1.038689	3	0.263
3.155055	3	0.0185
1.297035	3	0.1518
1.273248	3	0.6269
1.330372	3	0.4546
2.057645	3	0.3623
4.274602	3	0.3077
1.780895	4	0.6481
1.902308	4	0.1828
2.439114	4	0.9337
2.01824	4	0.6206
4.958802	4	0.0001
1.010203	4	0.4906
1.762338	4	0.3223
1.843975	4	0.858
2.788553	4	0.005
4.385018	5	0.4251
3.364899	5	0.3486
1.576833	5	0.2945
0.998873	5	0.4338
4.431861	5	0.0343
7.595121	5	0.3508
1.677634	6	0.2836
1.962933	6	0.223
1.910923	6	0.1181
3.605031	6	0.6761
1.127742	6	0.3183
1.779639	6	0.545
1.759909	7	0.4314
3.527597	4	0.7124
1.036974	6	0.083
2.014445	7	0.8326
1.403509	10	0.15
3.159355	18	0.8568

(5) ***Construction of S-D-F curves***

The relationship among drought severity, duration and frequency in terms of recurrence interval for drought events can be represented by the conditional recurrence interval which is given as (Shiau, 2007):

$$T_{S|D}(s \mid d) = \frac{1}{\gamma(1 - F_{S|D}(s \mid d))} \tag{18}$$

where s and d denote the drought severity and duration, respectively; $F_{S|D}(s|d)$ is the conditional CDF of S, given $D=d$; $T_{S|D}(s|d)$ is the conditional recurrence interval of S given $D = d$; and γ is the arrival rate of drought events which need to be fitted to the observed data.

The conditional CDF is given as:

$$F_{S|D}(s \mid d) = \frac{\partial F_{S,D}(s,d)}{\partial F_D(d)} \tag{19}$$

where $F_D(d)$ is the CDF of drought duration, and $F_{S,D}(s,d)$ is the joint CDF of drought severity and duration which will be derived using copulas. The conditional distribution in eq. (19) can be rewritten as:

$$F_{S|D}(s \mid d) = \frac{\partial F_{S,D}(s,d)}{\partial F_D(d)} = \frac{\partial C(F_S(s), F_D(d))}{\partial F_D(d)} = \mathrm{C}_{F_S|F_D}(F_S(s) \mid F_D(d)) \tag{20}$$

where C is the unique copula function that links $F_S(s)$ and $F_D(d)$ to form the joint CDF. Eq. (17) can thus be rewritten as:

$$T_{S|D}(s \mid d) = \frac{1}{\gamma(1 - C_{F_S|F_D}(F_S(s) \mid F_D(d)))} \tag{21}$$

The theoretical drought SDF relationship from eq. (21) can be used to construct the dependence between drought severity, duration and the arrival rate of drought events. This will be a useful tool for water management and project designs, since it helps determine when a certain severe drought of a specific duration may reoccur in the future. From the above equations, solving for $F_S(s)$ and $F_D(d)$ for specific value of $T_{S|D}(s \mid d)$, S-D-F curves for various recurrence intervals were obtained. The drought severity quantiles for specific duration and return period were thus obtained from these curves.

A sample calculation for constructing the S-D-F curve is given below:

For the given data, length of time period considered, N = 51 years
Number of drought events, n = 42
Inter arrival time = n/N = 42/50 = 0.84

Return period, $T_{S|D}(s=1.6 \mid d = 2 \text{ months}) = \frac{1}{0.84*(1-0.2089)} = 1.5$ years

Results

(1) *Model Calibration and validation*

Since the VIC model involves a number of parameters, calibration of the same can become quite tedious. The recommended parameters and the plausible range of values for each of them are given in Table 6. In this study, six soil parameters were considered for calibration purposes. The VIC model calibration was performed using a random auto start simplex method program. The simplex method was applied using random auto start populations of 75-100 parameter sets. The entire cycle was repeated from 5-10 times for each sub-basin. Each auto start yielded different correlation coefficient (R^2) values (usually within +/- 0.1), and different parameter sets. As regards calibration of the routing model, the suggested parameters for adjustment included velocity and diffusivity. The model developers are less specific about the routing model calibration as compared to the VIC model calibration. Application based studies focusing on monthly discharge from large basins have shown that it does not require high accuracy in the routing model parameter. Hence, while parameters like flow direction and contributing fraction can be obtained from the DEM, for other parameters like flow velocity and diffusivity physically reasonable values are chosen without further calibration (www.hydro.washington.edu). If only monthly stream flows are required, diffusivity and velocity values of 800 m^2/s and 1.5 m/s are deemed acceptable. In case daily flows are required, the calibration methodology to be followed for routing parameters is outlined in Lohmann et al. (1996, 1998).

For purposes of comparison, the routing model was used to route the flow to the selected station locations. Results from the routing model were aggregated to a monthly scale (in cfs) and compared with the observed gauge data (in cfs). The three performance criteria selected were correlation coefficient, the Nash-Sutcliffe (N-S) efficiency, and mean flow ratio and these are defined as:

$$\textit{Correlation coefficient, } r = \frac{M\sum_{i=1}^{M} S_i O_i - \sum_{i=1}^{M} S_i \sum_{i=1}^{M} O_i}{\sqrt{M\sum_{i=1}^{M} S_i{}^2 - \left(\sum_{i=1}^{M} S_i\right)^2)(M\sum_{i=1}^{M} O_i{}^2 - \left(\sum_{i=1}^{M} O_i\right)^2}} \quad (22)$$

$$\textit{Nash Sutcliffe efficiency} = 1.0 - \frac{\sum_{i=1}^{M}(O_i - S_i)^2}{\sum_{i=1}^{M}(O_i - \bar{O})^2} \quad (23)$$

$$\textit{Meanflow}(MF)\textit{ ratio} = \frac{\bar{S}}{\bar{O}} \quad (24)$$

where M is the number of months, S_i is the simulated stream flow for the ith month , O_i is the observed stream flow for ith month, and $\overline{S}$ and $\overline{O}$ are the mean monthly simulated and observed stream flows, respectively.

Higher values of correlation coefficient and the Nash-Sutcliffe (N-S) efficiency indicate good performance of the model. The closer the value is to 1, the more accurate the model is. Validation of the results obtained from the calibrated model with respect to the observed stream flow values at the respective gauges are shown in Figure 11. Table 16 gives a summary of performance measures at each of these stations. The validation period was two years. The start and end dates of the validation periods for each station is already given in Table 1. Since the time period considered in the study was lengthy (1950-2000), different validation periods were considered for the stations such that they cover the time period under consideration. The correlation coefficient values for the 16 stations lie within the range 0.65-0.92 which means the model is capable of explaining 42% to 84% of variability in the observed data. The N-S efficiency values range from 0.41-0.78. Since an N-S value of 1 corresponds to a perfect match and 0 corresponds to the situation where simulated values match the mean of observed values, a value of 0.5 may be considered to represent a 'mediocre' model performance. Hence, from the values obtained for the model at all 16 stations, it can be seen that the model performance is satisfactory. The mean flow ratio values for the model ranges from 0.54-1.46. It can also be seen from Table 16 that the mean flow values are lower than 1 at some stations, whereas it is higher than 1 in some others. Thus, the model is not showing any unidirectional bias while simulating stream flow.

Table 16. Goodness of fit test values of model validation at the selected stations

Station Name	Correlation Coefficient	Mean Flow Ratio	Nash Sutcliffe Efficiency
Frio River Near Derby	0.82	0.76	0.79
Spring Creek Near Spring	0.89	0.92	0.69
Village Creek Near Kountze	0.90	0.72	0.74
Neches River Near Neches	0.86	1.04	0.71
Nueces River Near Three rivers	0.69	1.06	0.41
Nueces River Below Uvalde	0.82	0.87	0.57
Mill Creek Near Bellville	0.72	1.12	0.49
North Concho River Near Carlsbad	0.86	1.03	0.75
Millers Creek Near Munday	0.83	1.09	0.74
Ecleto Creek Near Runge	0.69	0.88	0.44
Cowhouse Creek at Pidcoke	0.87	0.54	0.76

Coleto Creek Near Victoria	0.84	1.43	0.73
Los Olmos Creek Near Falfurrias	0.92	1.26	0.78
Big cow Creek Near Newton	0.91	0.82	0.72
Long king Creek Near Livingston	0.85	0.69	0.61
Bayou Toro Near Toro	0.65	1.46	0.63

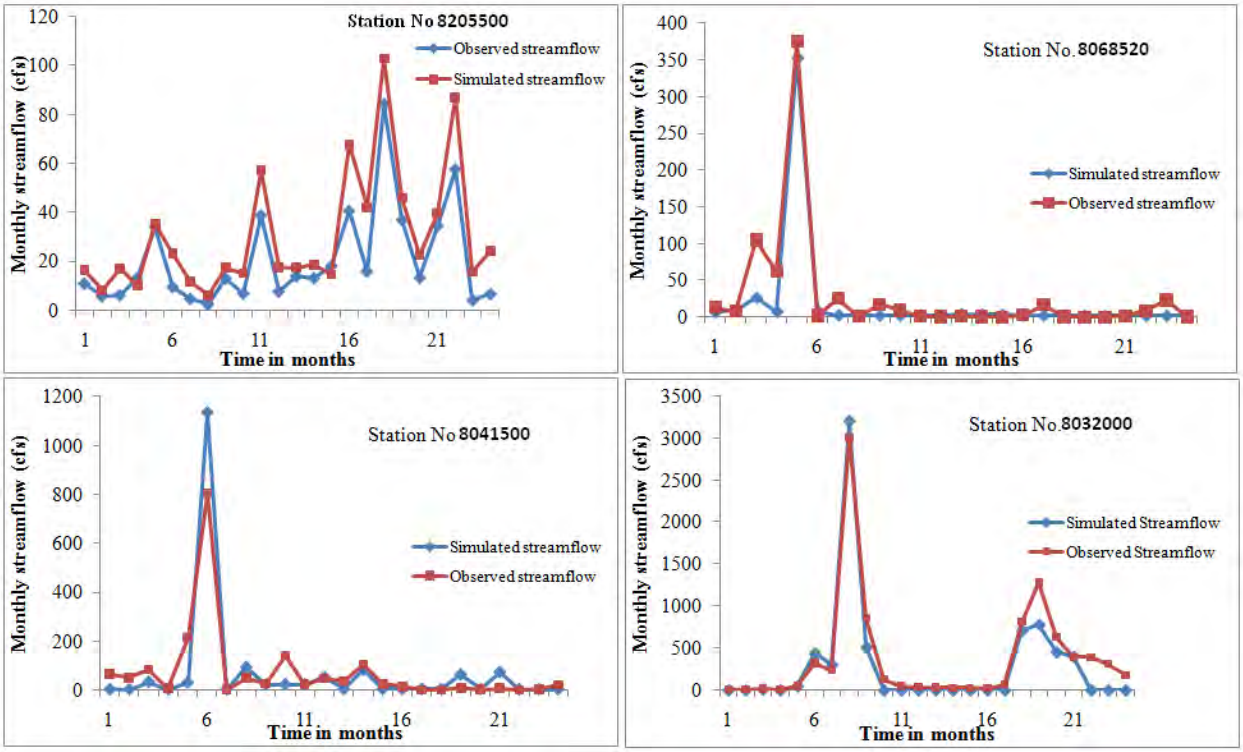

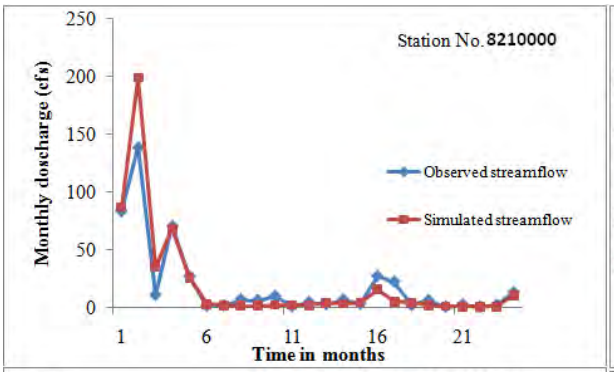
Station No. 8210000
Monthly doscharge (cfs)
Observed streamflow
Simulated streamflow
Time in months

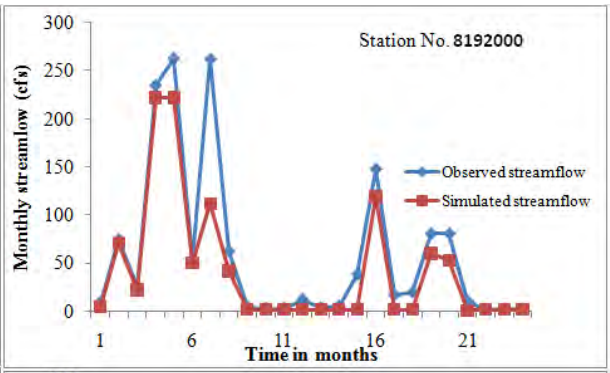
Station No. 8192000
Monthly streamlow (cfs)
Observed streamflow
Simulated streamflow
Time in months

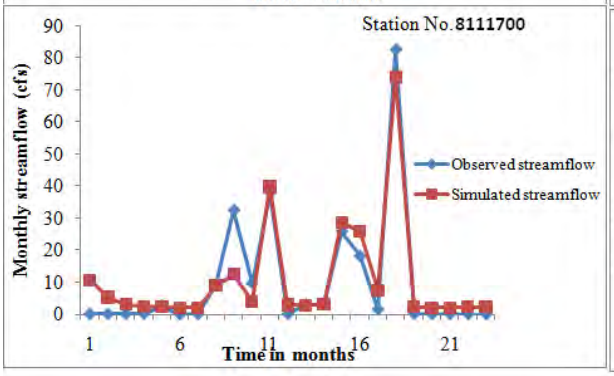
Station No. 8111700
Monthly streamflow (cfs)
Observed streamflow
Simulated streamflow
Time in months

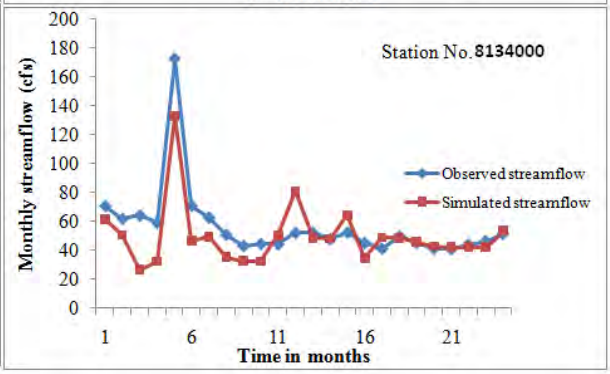
Station No. 8134000
Monthly streamflow (cfs)
Observed streamflow
Simulated streamflow
Time in months

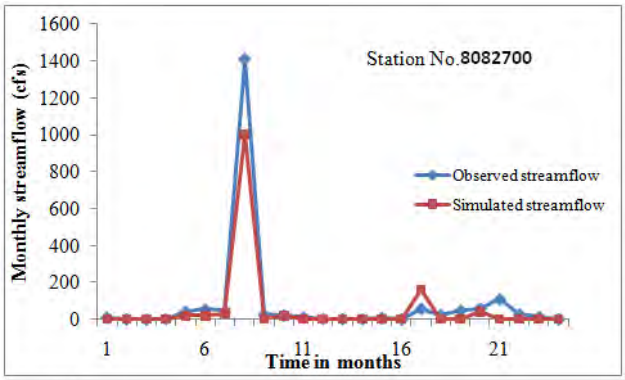
Station No. 8082700
Monthly streamflow (cfs)
Observed streamflow
Simulated streamflow
Time in months

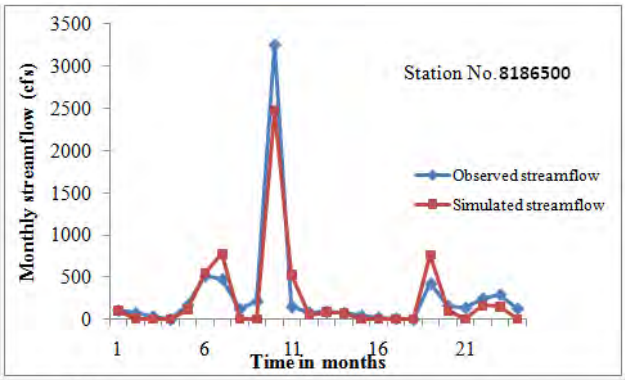
Station No. 8186500
Monthly streamflow (cfs)
Observed streamflow
Simulated streamflow
Time in months

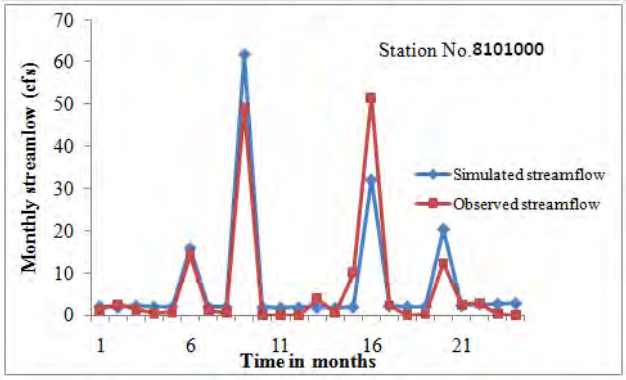
Station No. 8101000
Monthly streamlow (cfs)
Simulated streamflow
Observed streamflow
Time in months

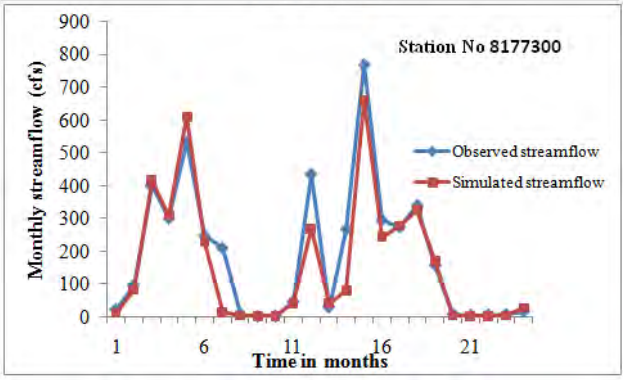
Station No 8177300
Monthly streamflow (cfs)
Observed streamflow
Simulated streamflow
Time in months

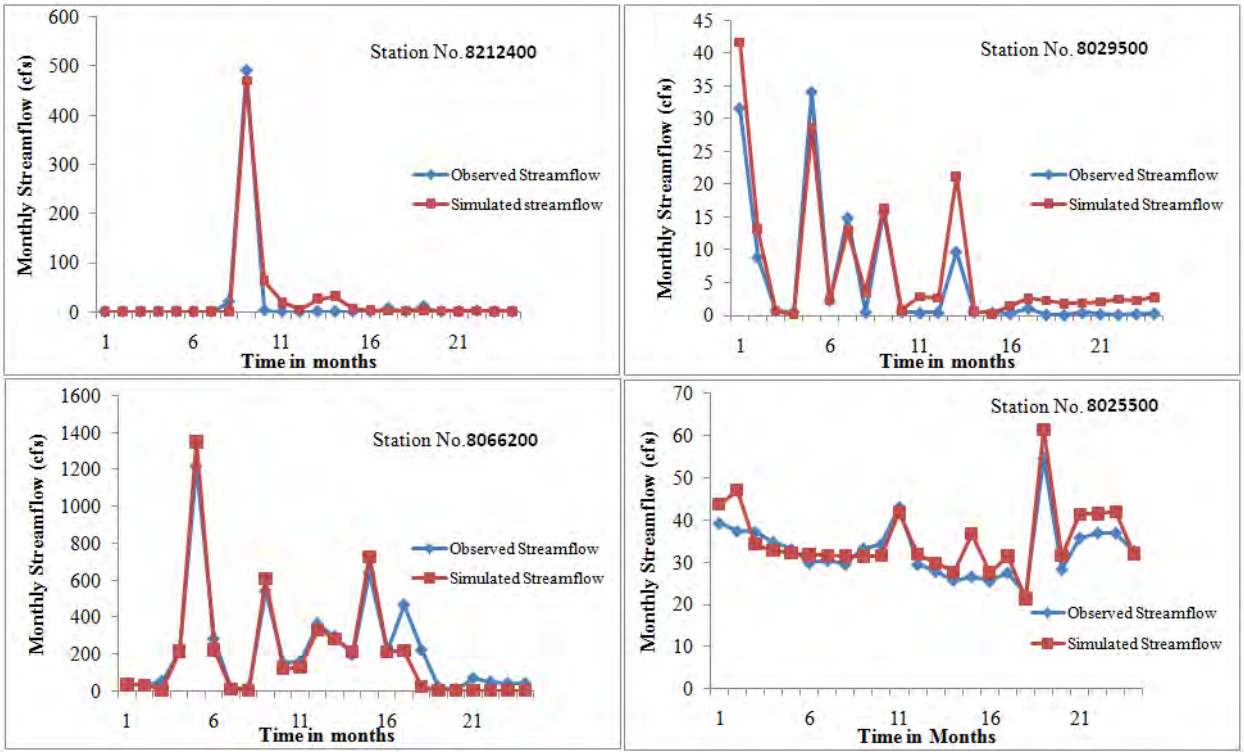

Figure 11. Comparison of simulated and observed stream flows for selected stations

Sample results for one grid are shown for the succeeding steps and the procedure followed is the same for other grids. The location of the grid is given by: latitude 31.3125^0 N and longitude -103.6875^0 E. This grid lies in the arid climatic region of Texas. Drought statistics at the location are summarized in Table 17.

Table 17. Summary of drought statistics for sample grid

Drought variables	Statistics	
Number of droughts		35
Severity	Mean	4.63
	Minimum	1.03
	Maximum	18.52
	Standard deviation	4.14
	Skewness	3.78
Duration	Mean	4.5
	Minimum	1
	Maximum	20
	Standard deviation	3.08
	Skewness	2.91

The S-D-F curves derived for grids belonging to different climate regions are shown in the later section to demonstrate the variations that might accrue due to the change in climate.

(2) ***Marginal distribution of drought variables***

Before using a copula to obtain the bivariate distribution of drought variables, appropriate marginal distributions must be identified for each drought variable. In this study, the best fit among the following distributions, namely gamma, exponential, log normal and Weibull were chosen to fit drought severity and drought duration, respectively. The maximum likelihood method was used for the parameter estimation of these distributions. The best fitted distribution for each drought variable was determined using the mean square error and AIC criteria. Table 18 gives the fitting performance of various distributions. The results can be visually examined by means of PDF, CDF and probability-probability plots. Figure 12 shows the same for drought duration and severity, respectively.

Table 18. Performance of different probability distributions for fitting drought severity and duration

Drought variables	Distributions	MSE	AIC
Severity	Exponential	0.0031	-394.87
	Gamma	0.0016	-422.08
	Weibull	0.0021	-430.23
	Log normal	**0.0014**	**-436.79**
Duration	**Exponential**	**0.0011**	**-389.31**
	Gamma	0.0028	-340.73
	Weibull	0.0019	-332.97
	Log normal	0.0024	-328.56

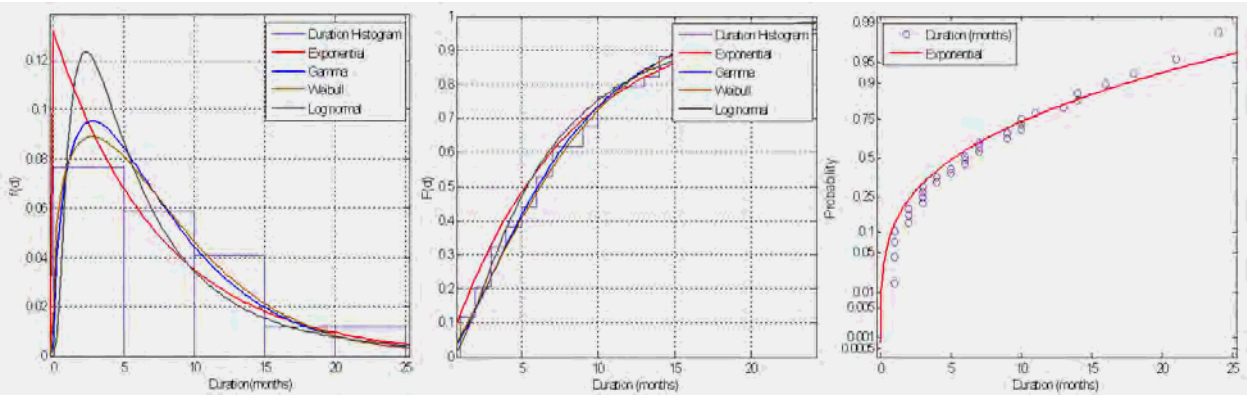

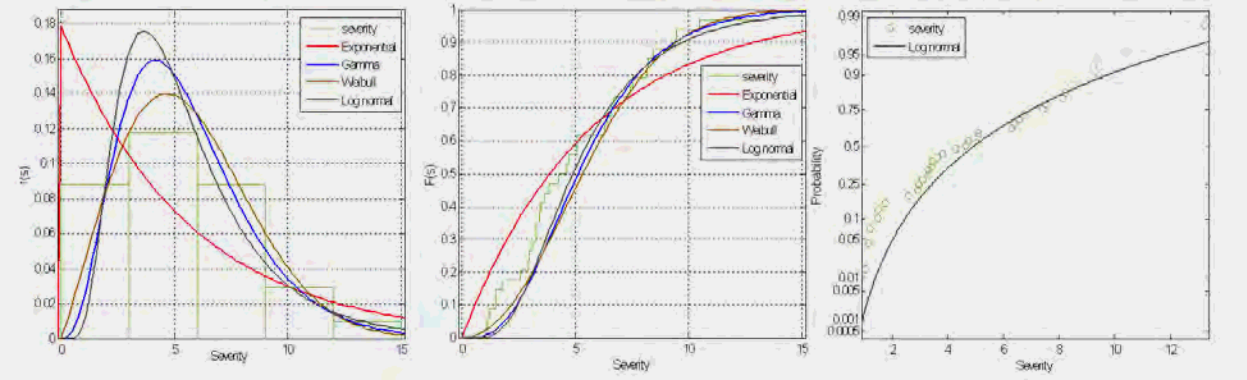

Figure 12. PDF, CDF and probability plot for drought duration (months); PDF, CDF and probability plot for drought severity

In the grid considered, log normal distribution and exponential distribution were found to be satisfactory for fitting drought severity and duration, respectively.

(3) ***Joint probability distribution using copula***

The list of copulas considered in this study and their CDF expressions have already been given in Table 3. The maximum pseudo likelihood method was used for the parameter estimation of copulas. The fitted parameters and the values of AIC criteria, log-likelihood function, and distance statistics, like AD and IAD, are given in Table 19. The log-likelihood function for Gumbel-Hougaard copula which belongs to the extreme value copula class was slightly higher than other classes of copulas. The goodness of fit test was carried out using the distance statistics AD and IAD with respect to the empirical copula. In the case of distance statistics, the Gumbel-Hougaard copula had smaller AD value than the rest of the copulas, whereas the Frank copula showed the least IAD value. Table 20 gives the goodness of fit statistics for all the copula families.

Table 19. Log-likelihood and AIC values for copula functions

Copula families		**Copula parameter**	**Log likelihood**	**AIC**
Archimedean	Clayton	Θ= 1.26	17.29	-389.51
	Frank	Θ=7.52	37.35	-378.09
Extreme value	Gumbel-Hougaard	Θ=4.18	**51.03**	**-412.37**
Elliptical	Student t	γ = 3.25, r= 0.872	28.18	-397.05
Plackett	Plackett	Θ=25.79	41.45	-401.23

Table 20. Goodness of fit results based on distance statistics

Copula families		AD	IAD
Archimedean	Clayton	0.67	1.73
	Frank	0.78	1.39
Extreme value	Gumbel-Hougaard	0.64	1.53
Elliptical	Student t	0.75	1.45
Plackett	Plackett	0.68	1.78

To visualize the results, a scatter plot between the observed severity and duration values and randomly simulated pairs of severity and duration values from each copula class (which would be transformed from the copula scale to original data units) were plotted. Figure 13 shows the scatter plots between observed values and simulated values for all copula classes. The extreme value copula considered in the study, viz., Gumbel-Hougaard copula, adequately modeled the dependence structure between drought variables.

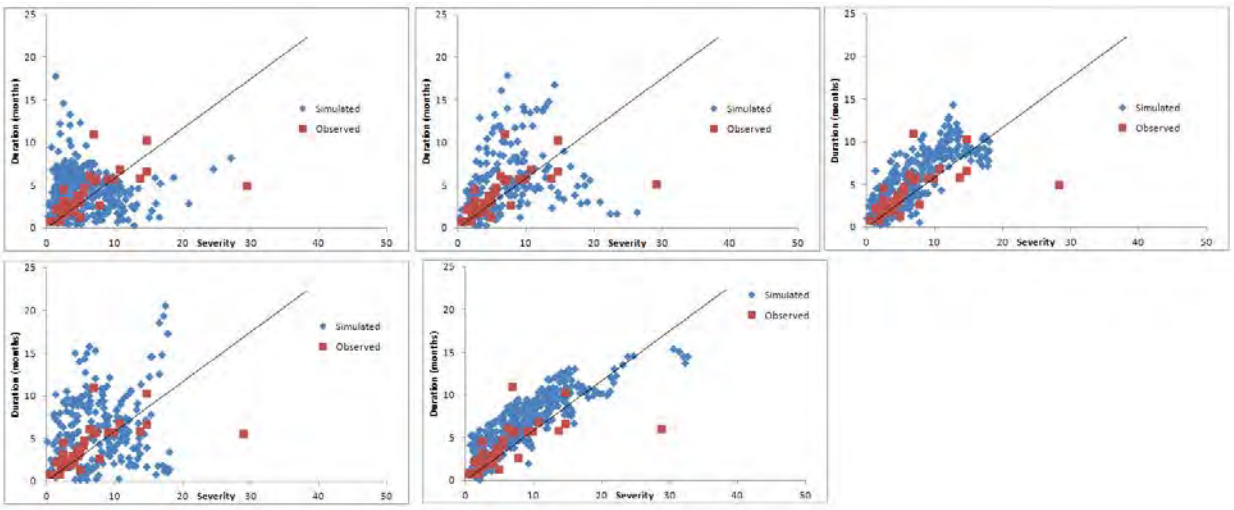

Figure 13. Scatter plot between observed data and simulations from joint distributions belonging to various copula classes: a. Clayton b. Frank c. Gumbel-Hougaard d. Students *t* e. Plackett

(4) ***Conditional distribution***

Shiau (2006) derived an expression for conditional distribution from bivariate copulas for drought variables [Refer to Eqs. (16) and (17)].

Figure 14 shows the conditional probability plots for drought severity and duration, respectively.

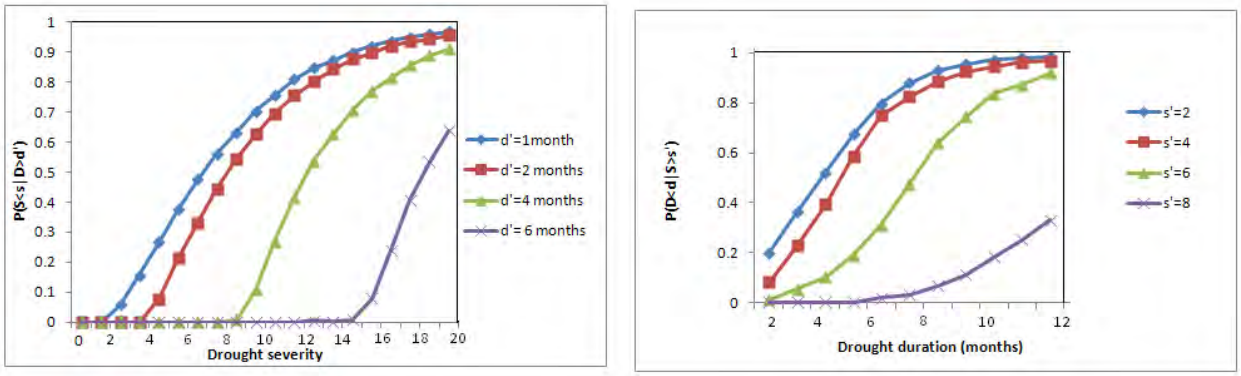

Figure 14. Conditional distribution of a. drought severity and b. drought duration

(5) ***Frequency analysis and derivation of drought S-D-F curves***

Figure 15 shows S-D-F curves for grids belonging to all the five climatic regions in Texas. It can be seen that the grids belonging to arid, semi arid and continental steppe regions showed a convex down pattern for their S-D-F curves. Based on precipitation patterns and visualization of the spatial variation of stream flow droughts over Texas, these regions are found to be more drought prone. Accordingly, from the S-D-F curves, it can be seen that the rate of increase of drought severity is higher for longer durations, whereas it decreases for shorter drought durations. In the case of humid and semi humid regions, the curves show a concave downward pattern. This indicates that the rate at which drought severity increases is more for shorter drought durations, and it reduces with longer durations, ultimately reaching a constant value for very long drought duration. More severe droughts seem to occur in arid, semi-arid and continental steppe regions.

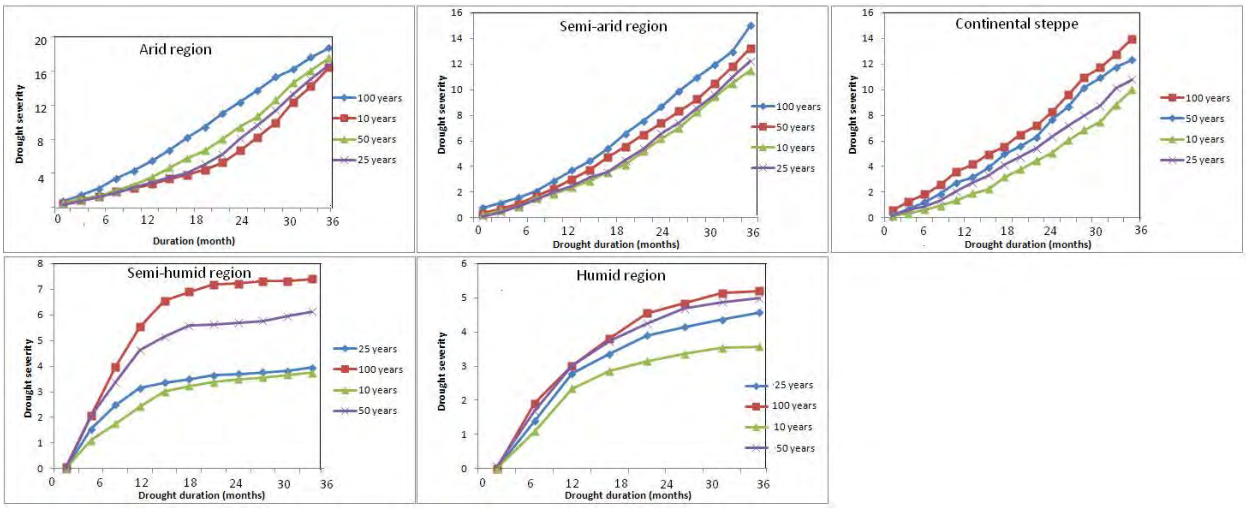

Figure 15. Drought S-D-F curves for grids from: a. Arid, b. Semi-arid, c. Continental, d. Semi humid, and e. humid climatic regions

Drought iso-severity maps for specific durations and return periods

Data used for plotting

For the construction of iso-severity maps, the availability of continuous stream flow data record is an important factor. As previously mentioned, the distribution of the stream flow gauge stations within Texas is not uniform. Likewise, the length of the data recorded need not be continuous or lengthy enough at all the stations. Taking these factors into consideration, simulated stream flow records corresponding to spatially continuous $1/8^{th}$ degree grids within Texas for the time period 1950-2000 was simulated using a hydrologic model: VIC. The results of simulation were then validated at specific stream gauge locations scattered within Texas to ensure that the model results were a good representation of the actual scenario. The drought durations considered for plotting the drought frequency maps were 3, 6, 9, 12, 18, 24 and 36 months, respectively. The return periods considered were 5, 10, 25, 50 and 100 years. The 35 iso-severity maps plotted permits variation of drought severity in two directions – duration and return period. A total of 4197 grids over Texas, each having a size of $1/8^{th}$ degree was considered for plotting these 35 drought frequency maps.

The analyses section explains the methodology followed, for ease of understanding, by taking an example grid whose location is given by: latitude 31.3125^0 N and longitude -103.6875^0 E. Further details of the results are already given under the results section. For convenience, a summary of the various steps to be followed is given below:

1. The simulated stream flow time series corresponding to each grid is converted to standardized stream flow index (SSFI) from which drought severity and duration can be derived using the theory of runs.

2. Suitable marginal distribution from among those listed in Table 6 is fitted to drought severity and duration, respectively. The MSE and AIC criteria are used for judging the best fit candidate distribution.

3. Joint and conditional distributions are obtained from the marginal distributions of severity and duration by choosing a suitable copula. From eqs. (16)-(21) the relationship between drought severity, duration and different return periods are established which can be approximated by SDF curves with severity along the y-axis and duration along x-axis.

4. Thus, by utilizing these curves, for selected recurrence intervals of 5, 10, 25, 50 and 100 years, the drought severity quantile for specific drought durations can be obtained for each of the grids within Texas. This can be an important preliminary data to know while planning for future droughts. For example, for the grid under consideration, if we were to plan for a 3 month duration drought with a 10-year return period, then the drought severity to be considered would be 2.38.

5. The raster data consisting of drought severities for specific durations and return periods are then used for plotting contour maps using arcGIS. Figures 9a to x show the drought severity maps for Texas for different durations and return periods.

Some other points to be noted while plotting the drought frequency maps are listed below:

1. Smoothing of iso-severity lines may be required, since the isolines formed may be irregular while trying to fit all the points on the map. In arcgis, there is a contour smoothening algorithm which follows the Bezier interpolation and fits the Bezier curves between vertices. A Bézier curve is defined by a set of control points P_0 through P_n, where n is called its order (n = 1 for linear, 2 for quadratic, etc.). The first and last control points are the end points of the curve. The intermediate control points do not lie on the curve. The resulting line passes through the vertices of the input line. Bezier curve is generally used in computer graphics and related fields to model smooth curves. This algorithm does not require a tolerance.

2. Results are more reliable, since the spatial sampling error that might arise due to geographical distribution of stations does not arise in this case, as we are using continuously spaced and uniformly sized grids in lieu of stream gauge stations. Hence, it is possible that this has also an advantage of capturing the topographical influence on hydrological droughts

3. The isoline interval ranges from 0.2-1.0, depending on the range of drought severity magnitude. The isolines are plotted at uniform intervals.

4. The drought duration value starts at 3 months, since it can be considered as a sufficiently long enough drought to affect, in particular, the agro-sector. The maximum value of drought duration considered for plotting the maps is 36 months, since droughts longer than this duration might be considered rarer in the study region.

5. Four different return period values, viz., 10, 25, 50 and 100 years, are considered for plotting the maps. One might come across situations, wherein drought severities corresponding to either an intermediate value of drought duration or return period for which no map has been plotted or for return periods greater than 100 years. Construction of additional SDF curves should not be a problem. One may also use an extrapolation technique by plotting the drought severity values for available return periods at the location of interest obtained from all the plotted maps on a probability paper.

Figures 16 a. to ah. show drought severity maps for Texas for different durations and return periods. These maps would be highly useful for knowing the frequency of specific drought events, or for estimating the design severity of a drought event for a given duration and return period. For example, for the grid under consideration, if we were to plan for a 3 month

duration drought with 10 year return period, then the drought severity to be considered would be 2.38. More severe droughts seem to occur in arid, semi-arid and continental steppe regions.

For further comparison and validation purposes respectively, the drought maps have been developed for two more conditions: (a) based on precipitation (b) based on naturalized stream flow from gauges. Figures 10 a. to 10 ah. show the drought severity maps based on precipitation and figures 11 a. to 11 ah. show the maps developed based on the naturalized stream flow values.

Summary and Conclusions

The report presents a hydrological drought atlas for Texas. One major problem that might arise in such a study would be spatial sampling error that might arise due to the geographical distribution of stations. In the case of Texas, stream flow gauges are unevenly distributed with a majority of stations concentrated in east Texas, and very few covering the western part. To counter this problem, we use simulated stream flow over continuously spaced and uniformly sized grids in lieu of stream gauge stations. This can be expected to make the results more reliable. It is possible that this has also an advantage of capturing the topographical influence on hydrological droughts. The results obtained from the study can be summarized as below:

1. The drought severity varies systematically for different durations and return periods, with maximum severity along western and northern Texas and then gradually decreasing towards south western Texas and eastern Texas. This pattern is expected, given that the basic climatic pattern within Texas is fairly simple: annual mean precipitation increases from west to east. Similarly, the prevalence of severe weather, like hurricanes which will contribute to copious amounts of rainfall, increases from west to east.
2. As long as the drought duration increases, the corresponding severity also increases, as expected, although the rate at which it increases seems to depend on the climatic zone.
3. In general, the severity-duration-frequency relationship shows a specific pattern in humid and semi-humid regions, i.e., the drought severity increases rapidly if the drought duration is short. As the drought duration increases, the drought severity also increases but the rate at which the severity increases becomes less for longer drought durations.
4. Arid, semi-arid and continental steppe regions show a pattern for their S-D-F curves wherein it can be seen that the rate of increase of drought severity is higher for longer durations, whereas it decreases for shorter durations.
5. From drought maps, for higher durations the contour lines are closer on the western side, indicating a larger rate of increase in severity along that part. However, in the eastern part, the contour lines are closer for shorter durations, indicating that the rate at which severity increases is higher for small drought durations.

6. Droughts with larger durations appear to have smoother contours than droughts with smaller durations. This might be due to the fact that droughts with durations 12 months and greater seem to be rarer compared to shorter durations like 3-6 months.
7. The maps tally with the water budget climatology of Texas (Norwine et al., 1995). In most of the maps, southern Texas shows higher severities. This tallies with the fact that the deficit component of the water budget (indicating the amount of additional water that plants need, but do not receive) is highest along the southern climate division of Texas due to the combination of high evapotranspiration rates and relatively low precipitation. Understandably, the deficit is on the higher side for western Texas too due to low precipitation.
8. It should be noted that northern Texas too shows relatively higher severities, particularly for longer duration droughts. This tallies with the fact that the surplus component of the water budget, that reflects the water available as runoff, is on the lower side in northern Texas. This might be attributed to the combination of low rainfall and seasonality of the precipitation delivery. A majority of rainfall in this region occurs during summer. The low surplus leading to lower runoff will reflect a more severe hydrological drought event.
9. The drought maps derived based on precipitation and naturalized flows are in fairly good agreement with the maps derived using the simulated flows. On average, there is a better agreement between precipitation and simulated flow results compared to naturalized flow and simulated flow results. The drought properties of severity and duration show error percentiles equal to 42.8 and 52.3%, respectively, between simulated and naturalized flows. But, it lowers down to 12.4 and 32 %, respectively, if precipitation and simulated flow results are compared.

References

Abdulla, F.A., Lettenmaier, D.P., Wood, E.F and Smith, J.A (1996). “Application of a macroscale hydrologic model to estimate the water balance of the Arkansas-Red river basin,” J. Geophys. Res., 101(D3), 7449-7459.

Andreadis, K.. Wood, C.E., Wood, A., Hamlet, A. and Lettenmaier, D. (2005). “Twentieth century drought in conterminous United States,” J. HydroMeteor., 6, 985-1001.

Andreadis, K.M., and Lettenmaier, D.P. (2006). “Trends in 20th century drought over the continental United States,” Geophys. Res. Lett., 33, L10403.

Benke, Arthur C., ed., and Cushing, Colbert E., ed. (2005). “Rivers of North America,” Burlington, Massachusetts: Elsevier Academic Press.

Bonaccorso, B., Cancelliere, A., and Rossi, G. (2003). “An analytical formulation of return period of drought severity,” Stoch. Env. Res. and Risk Assess., 17(3), 157-174.

Bureau of Economic Geology (1996). “River Basin Map of Texas,” University of Texas, Austin

Cancelliere, A. and Salas, J. D. (2004). “Drought length properties for periodic-stochastic hydrological data”, Water Resources Res., 40, W02503 doi:10.1029/2002WR001750.

Cosby, B. J., Hornberger, G. M. Clapp, R. B. and Ginn, T. R. (1984). “A statistical exploration of the relationships of soil moisture characteristics to the physical properties of soils,” Water Resour.Res., 20, 682–690.

Dalezios, N.R. and Tyraskis, P.A. (1999). “Maximum entropy spectra for regional precipitation analysis and forecasting,” J. Hydrol., Vol. 109, pp. 25-42.

Liang, X., Lettenmaier, D.P.,Wood, E.F. and Burges, S.J. (1994). “A Simple hydrologically Based Model of Land Surface Water and Energy Fluxes for GSMs,” J. Geophys. Res., 99(D7), 14415-14428.

Dickey, D.A. and Fuller, W.A. (1979). “Distribution of the estimators for autoregressive time series with a unit root,” J. Am. Stat. Assoc.,74(366),427-431.

Fernández, B. and Salas, J.D. (1999). “Return period and risk of hydrologic events I: mathematical formulation,” J. Hydrol. Eng., 4 (4), 297–307.

González, J. and Valdés, J. B. (2003). “Bivariate drought recurrence analysis using tree ring reconstructions,” J. Hydrol. Eng., 8(5), 247-258.

Guerrero-Salazar, P. and Yevjevich, V. (1975) “Analysis of Drought Characteristics by the Theory of Runs,” Hydrology Paper No. 80, Colorado State University, Fort Collins.

Hansen, M. C., DeFries, R. S. Townshend, J. R. G. and Sohlberg, R. (2000). “Global land cover classification at 1 km spatial resolution using a classification tree approach,” Int. J. Remote Sens., 21, 1331–1364.

Joe, H. (1997). “ Multivariate Models and Dependence Concepts,” Chapman and Hall: New York.

Kao, S. C. and Govindaraju, R. S. (2010). “A copula-based joint deficit index for droughts,” J. Hydrol., 380(1-2), 121-134.

Keyantash, J. and Dracup, J.A. (2002). “The quantification of drought: An evaluation of drought indices,” Bull. Am. Met. Soc., 83, 1167-1180.

Kim, T. W., Valdés, J. B., and Yoo, C. (2003). “Nonparametric approach for estimating return periods of droughts in arid regions,” J. Hydrol. Eng., 8(5), 237-246.

Kroll, C.N. and Vogel, R.M. (2002). “Probability distribution of low streamflow series in the United States,” J. Hydrol., 7, 137-146.

Kwiatkowski, D., Phillips, P.C.B., Schmidt, P. and Shin, Y. (1992). "Testing the null hypothesis of stationarity against the alternative of a unit root: How sure are we that economic time series have a unit root," J. Econometrics, 54,159-178.

Liang, X., Lettenmaier, D.P.,Wood, E.F. and Burges, S.J. (1994). "A Simple hydrologically Based Model of Land Surface Water and Energy Fluxes for GSMs," J. Geophys. Res., 99(D7), 14415-14428.

Lohmann, D., Nolte-Holube, R. and Raschke, E. (1996). "A large-scale horizontal routing model to be coupled to land surface parametrization schemes," Tellus, 48(A), 708-721.

Lohmann, D., Raschke, E., Nijssen, B. and Lettenmaier, D.P. (1998). "Regional scale hydrology: I. Formulation of the VIC-2L model coupled to a routing model," Hydrol. Sci. J., 43(1), 131-141.

Maurer, E. P., B. Nijssen, and D. P. Lettenmaier, (2000). "Use of reanalysis land surface water budget variables in hydrologic studies," GEWEX News, 10 (4), 6–8.

Maurer, E.P., Wood, A.W., Adam, J.C., Lettenmaier, D.P. and Nijssen, B. (2002). " A Long-Term Hydrologically-Based Data Set of Land Surface Fluxes and States for the Conterminous United States," J. Clim., 15(22), 3237-3251.

McKee, T.B., Doesken, N.J., Kleist, J. (1993). "The relationship of drought frequency and duration to time scales," Eight conf. App. Clim., Anaheim, CA.

McMahon, T.A., Pegram, G.G.S., and Vogel, R.M. (2007). "Revisiting reservoir storage yield relationships using a global streamflow database," Advances in Water Resources, 30, 1858-1872.

Millan, J. and Yevjevich, V. (1971). "Probabilities of observed droughts," Hydrology Paper No. 50, Colorado State University, Fort Collins, Colorado.

Miller, D. A., and R. A. White. (1998). "A conterminous United States multilayer soil characteristics dataset for regional climate and hydrology modeling," Earth Interactions, 2.

Mitchell, K., and Coauthors (list them.] (1999). "The GCIP Land Data Assimilation (LDAS) Project—Now underway," GEWEX News, 9 (4), 3–6.

Milly P. C. D., Betancourt J., Falkenmark M., Hirsch R. M., Kundzewicz Z. W., Lettenmaier D. P., and Stouffer, R. J. (2008). "Stationarity is dead: whither water management?," Science, 319, 573-574.

Mirakbari, M., Ganji, A. and Fallah, S.R. (2010). "Regional bivariate frequency analysis of meteorological drought," J. Hydrol., 15(12), 985-1000.

Mishra, A.K. and Singh, V.P. (2010). "A review of drought concepts," J. Hydrol., 391, 202-216.

Modarres, R. (2007). “Streamflow drought time series forecasting,” Stoch. Environ. Res. Risk Assess., 22, 223-233.

Myneni, R. B., Nemani, R. R. and Running, S. W. (1997). “Estimation of global leaf area index and absorbed PAR using radiative transfer models,” IEEE Trans. Geosci. Remote Sens., 35, 1380-1393.

Nalbantis, L. and Tsakiris, G. (2009). “Assessment of hydrologic drought revisited,” Water Res Management, 23, 881-897.

Nelsen, R.B. (1999). “An Introduction to copulas,” Springer: NewYork, NY; 209.

Nijssen, B.N., Lettenmaier, D.P., Liang, X., Wetzel, S.W. and Wood, E.F. (1997). “Streamflow simulation for continental-scale river basins,” Water Resour. Res., 33(4), 711-724.

Nijssen, B.N., O'Donnell, G.M., Lettenmaier, D.P. and Wood, E.F. (2001). “Predicting the discharge of global rivers,” J. Clim., 14, 3307-3323.

Rawls, W. J., Ahuja, L. R. Brakensiek, D. L.and Shirmohammadi, A. (1993). “Infiltration and soil water movement,” Handbook of Hydrology,, D. Maidment, Ed., McGraw-Hill, 5.1–5.51.

Reynolds, C. A., Jackson, T. J. and Rawls, W. J. (2000). “Estimating soil water-holding capacities by linking the Food and Agriculture Organization soil map of the world with global pedon databases and continuous pedotransfer functions,” Water Resourc. Res., 36, 3653–3662.

Rodriquez-Iturbe, I. (1969). “Application of the theory of runs to hydrology,” Water Res. Research, 5(6), 1422-1427.

Saghafian, B., Shokoohi, A. and Raziei, T. (2003). “Drought spatial analysis and development of severity-duration-frequency curves for an arid region,”Proceedings of International Conference on Hydrology of the Mediterranean and Semiarid Regions, Montpellier, 278, 305–311.

Salas, J. D., Fu, C., Cancelliere, A., Dustin, D., Bode, D., Pineda, A., and Vincent, E., (2005) “Characterizing the severity and risk of drought in the Poudre River, Colorado,” J. Water Res. Planning and Mgmt., 131(5), 383-393.

Salathe, E.P. (2003). “Comparison of various precipitation downscaling methods for the simulation of stream flow in a rain shadow river basin,” Int. J. Clim., 23, 887–901.

Saldarriaga, J. and Yevjevich, V. (1970). “Application of run-lengths to hydrologic series,” Hydrology Paper No. 40, Colorado State University, Fort Collins, Colorado.

Santos, J.F., Calvo, I.P. and Portela, M.M. (2012). “Spatial and temporal variability of droughts in Portugal,” Water. Res. Research, 46, 1-13.

Sen, Z. (1976). “Wet and dry periods of annual flow series,” J. Hydraul. Div., American Society of Civil Engineers, Proc. Paper 12457, 102(HY10), 1503-1514.

Sen, Z. (1977). “Run-sums of annual flow series,” J. Hydrol., 35, 311--324.

Sheffield, J., Goteti, G., Wen, F. and Wood, E.F. (2004). “A simulated soil moisture based drought analysis for the United States,” J. Geophys. Res., 109, p. D24108 24110.21029/22004JD005182.

Sheffield, J., and Wood, E.F. (2008). “Global Trends and Variability in Soil Moisture and Drought Characteristics, 1950–2000, from Observation-Driven Simulations of the Terrestrial Hydrologic Cycle,” J. Clim., 21, 432–458.

Shiau, J. T. and Shen, H. W. (2001). “Recurrence analysis of hydrologic droughts of differing severity,” J. Water Res. Planning and Mgmt., 127(1), 30-40.

Shiau, J. (2006). “Fitting Drought Duration and Severity with Two-Dimensional Copulas,” Water Res. Mgmt., 20(5), 795-815.

Shukla, S., and Wood, A.W. (2008). “Use of a standardized runoff index for characterizing hydrologic drought,” Geophys. Res. Letters, 35, L02405.

Shiau, J.-T., Feng, S. and Nadarajah, S. (2007). “Assessment of hydrological droughts for the Yellow River, China, using copulas,” Hydrol. Processes, 21(16), 2157-2163.

Shiau, J.T. and Modarres, R. (2009). “Copula-based drought severity-duration-frequency analysis in Iran,” Met. Applications, 16, 481–489.

Sklar ,A. (1959). “Fonctions de répartition á n dimensions et leurs marges,” Publications de l’Institut de Statistique de l’Université de Paris, 8, 229–231.

Song, S. and Singh, V.P. (2010a). “Meta-elliptical copulas for drought frequency analysis of periodic hydrologic data, Environmental Research and Risk Assessment,” Stoch. Env. Res. and Risk Assess., 24 (3), 425-444.

Song, S. and Singh, V. P. (2010b). “Frequency analysis of droughts using the Plackett copula and parameter estimation by genetic algorithm,” Stoch. Env. Res. and Risk Assess., 24 (5), 783–805.

Tallaksen, L.M., Madsen, H. and Clausen, B. (1997). “On the definition and modeling of stream drought duration and deficit volume,” Hydrol. Sci. J., 42 (1), 15–33.

Tawn, J.A. (1988). “Bivariate extreme value theory: models and estimation,” Biometrika, 75(3), 397–415.

Wilhite, D.A. and Glantz, M.H. (1985). “Understanding the drought phenomenon: the role of definitions,” Water Int., 10, 111-120.

Yevjevich V., Siddiqui, M.M and Downer, R.N. (1967). “Application of Runs to hydrologic droughts,” Proceedings of International Hydrology symposium, Fort Collins, Vol. 1, Paper 63, 496-505.

Yoo, C., Kim, D., Kim, T-W. and Hwang, K-N. (2008). “Quantification of drought using a rectangular pulses Poisson process model,” J. Hydrol., 355: 34–48.

Zaidman, M.D., Ress, H.G. and Young, A.R. (2001). “Spatio-temporal development of streamflow droughts in north-west Europe,” Hydrol. And Earth sys. Sci., 5, 733-751.

Part 2: Iso-severity maps

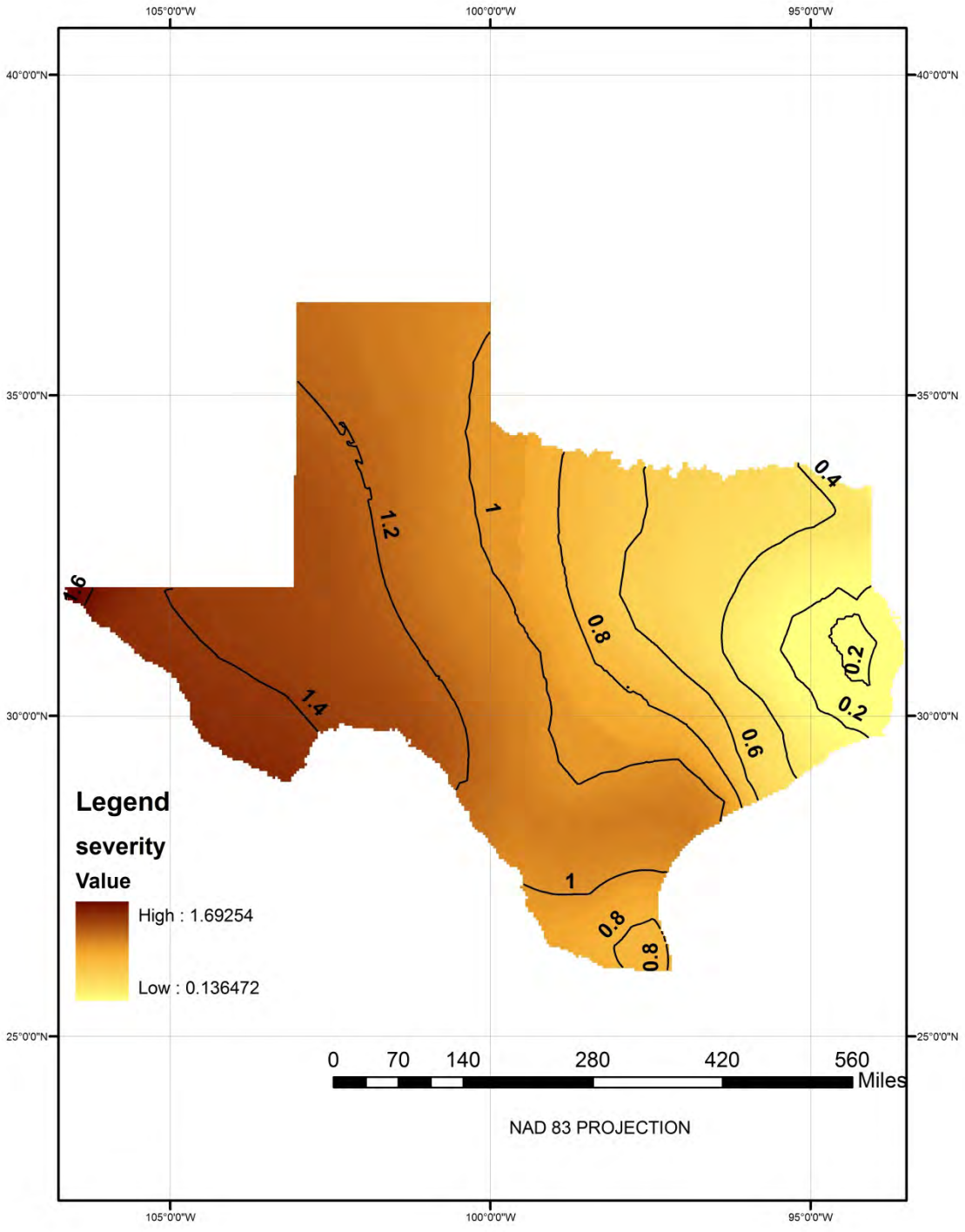

Figure 16a. Iso severity map for 3 months drought duration with a return period of 5

years

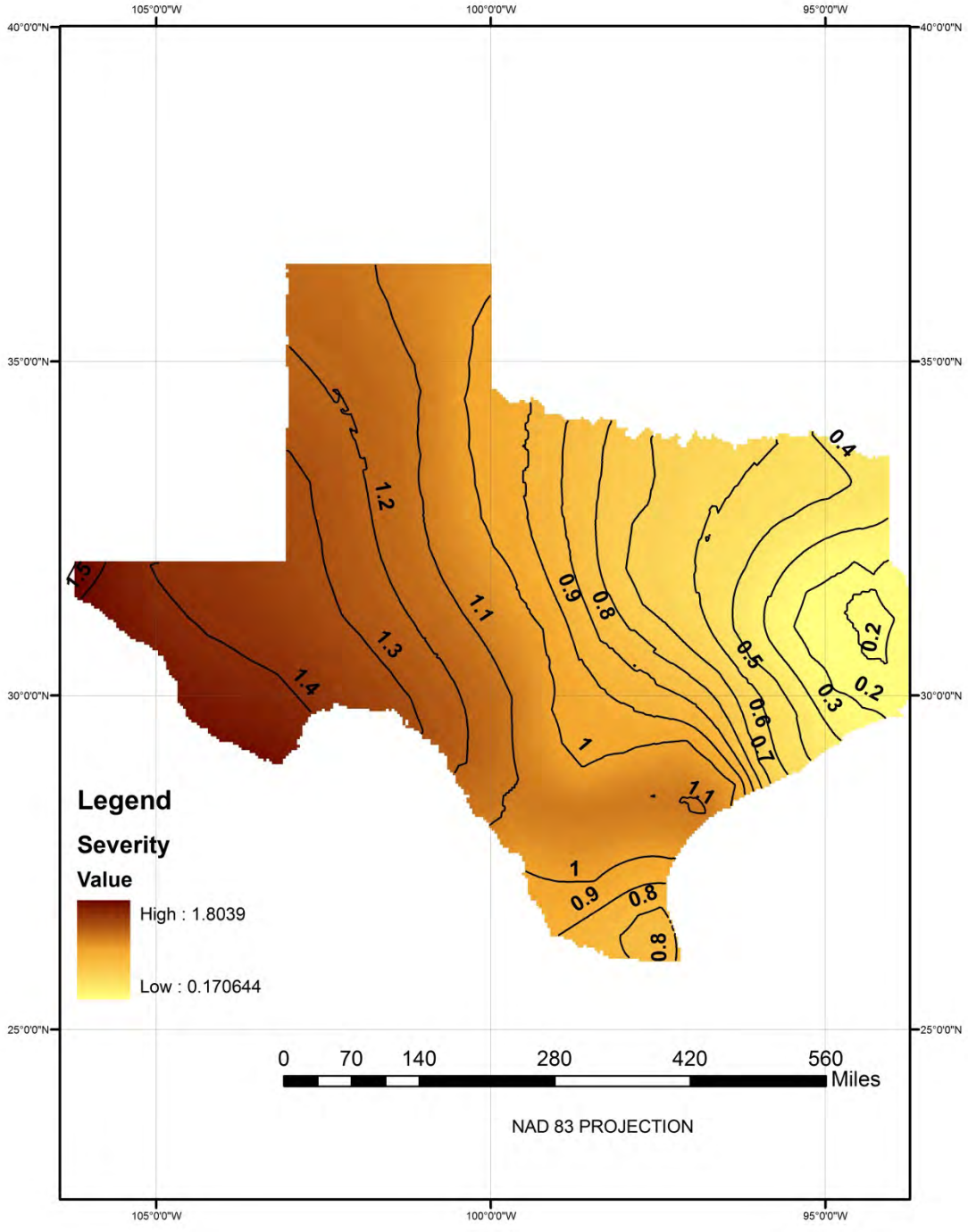

Figure 16b. Iso severity map for 3 months drought duration with a return period of 10 years

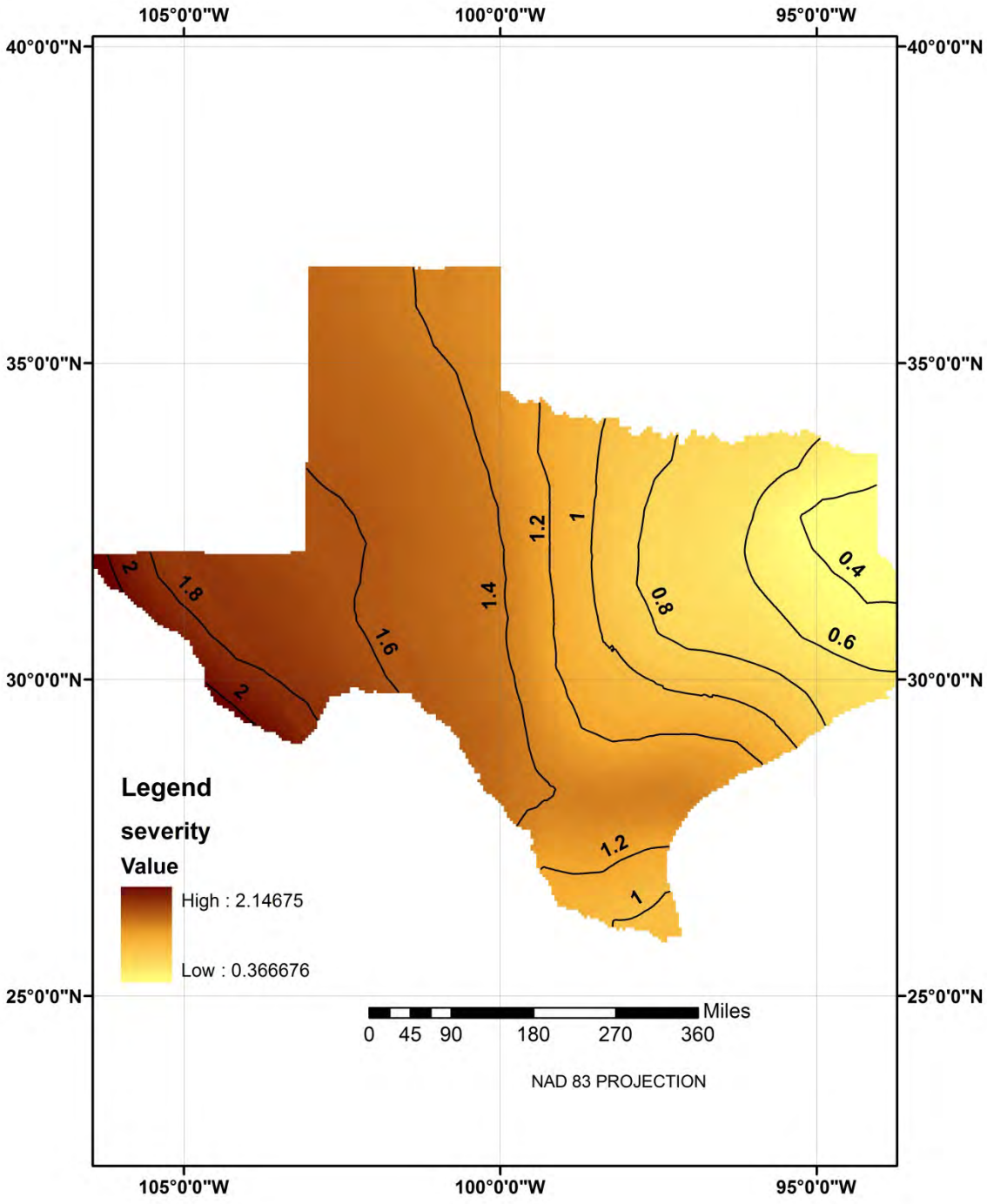

Figure 16c. Iso severity map for 3 months drought duration with a return period of 25 years

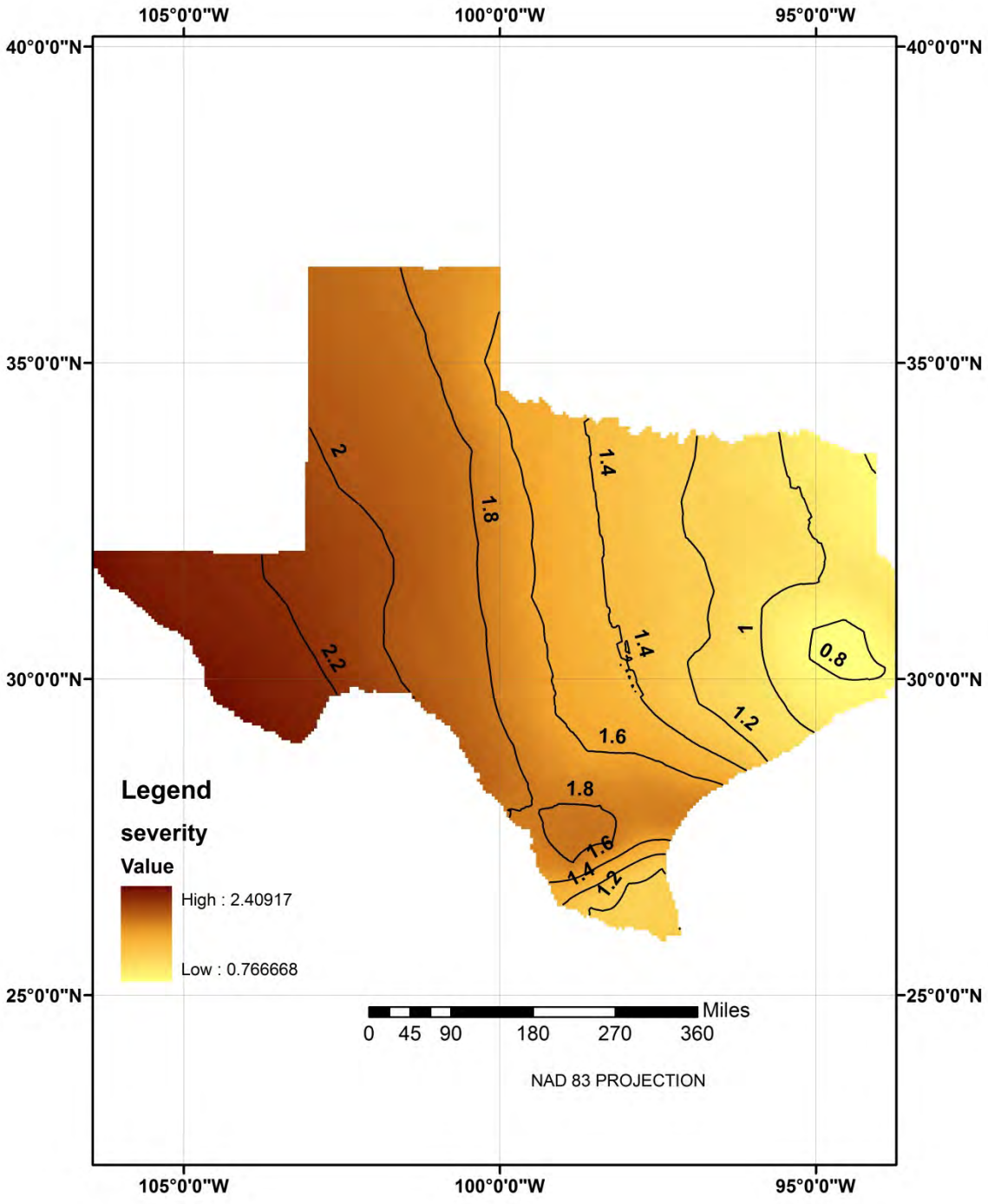

Figure 16d. Iso severity map for 3 months drought duration with a return period of 50 years

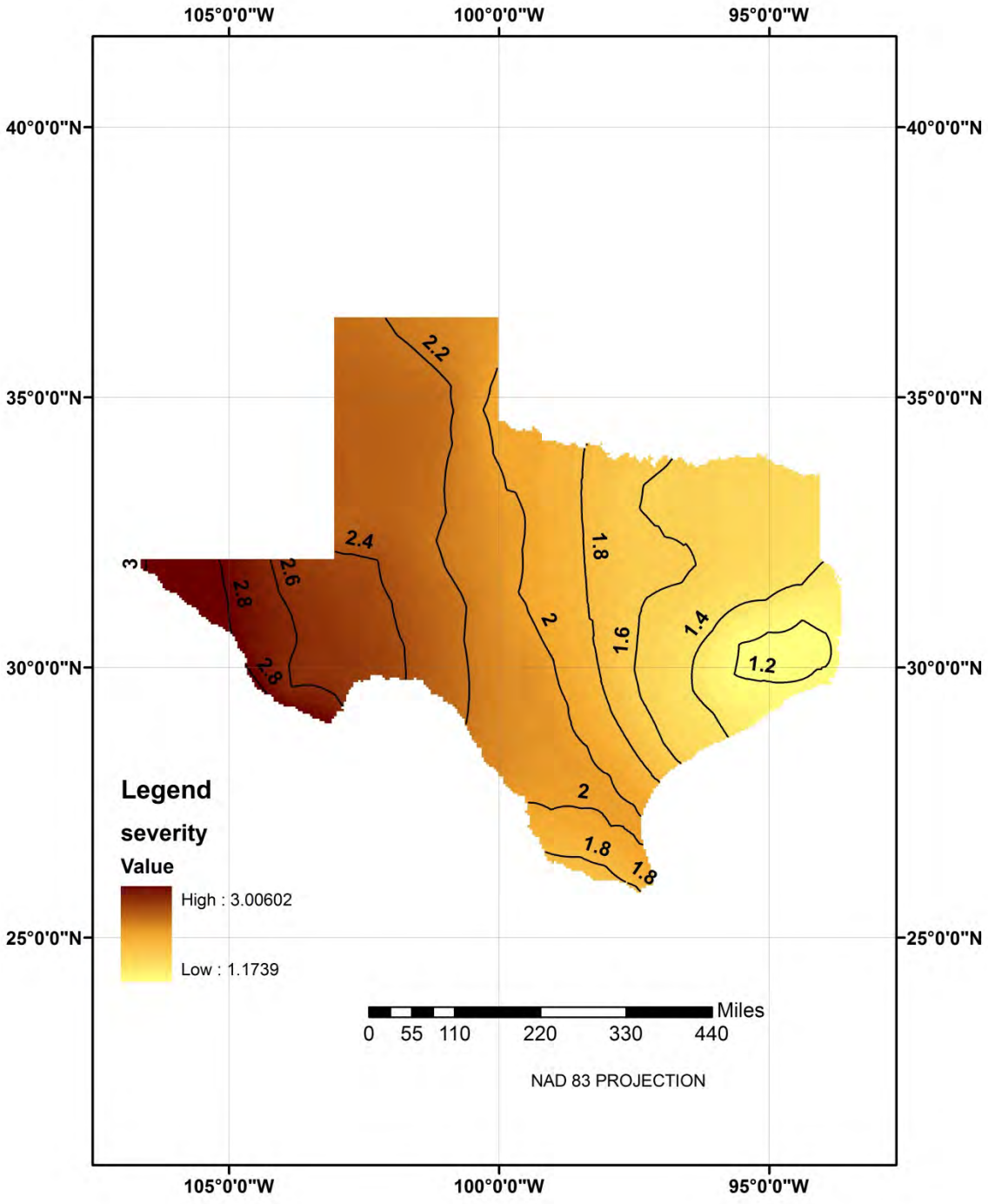

Figure 16e. Iso severity map for 3 months drought duration with a return period of 100 years

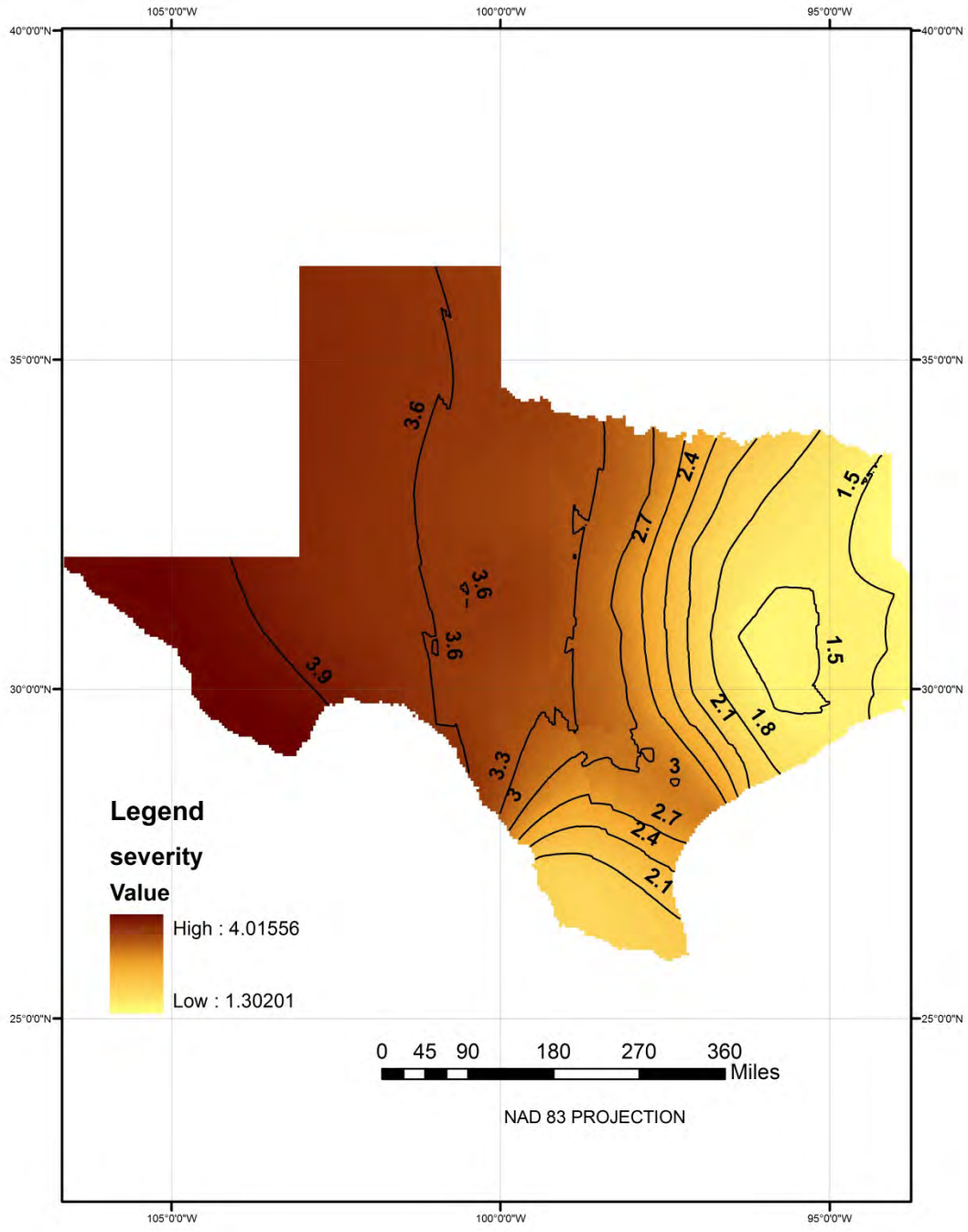

Figure 16f. Iso severity map for 6 months drought duration with a return period of 5 years

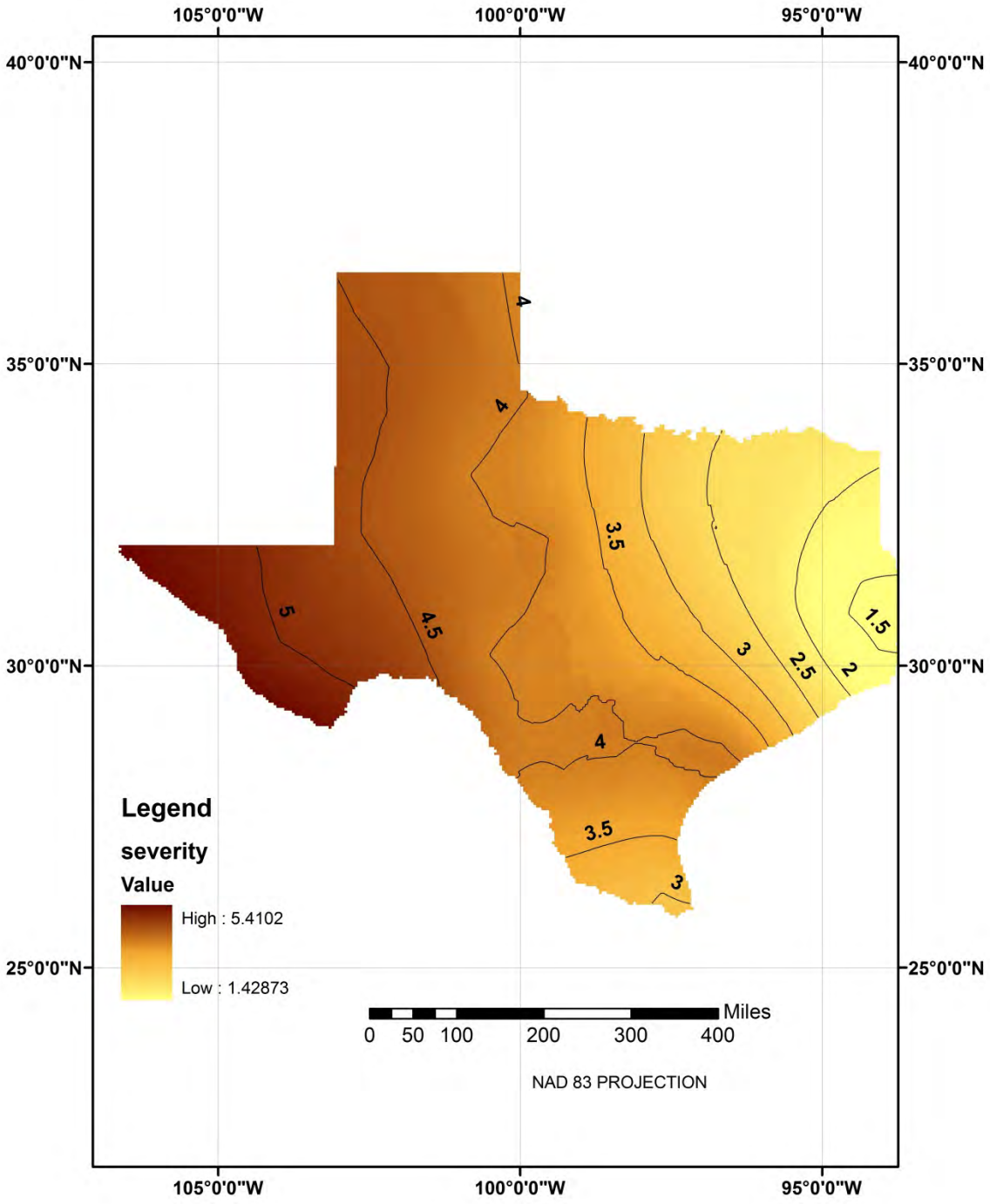

Figure 16g. Iso severity map for 6 months drought duration with a return period of 10 years

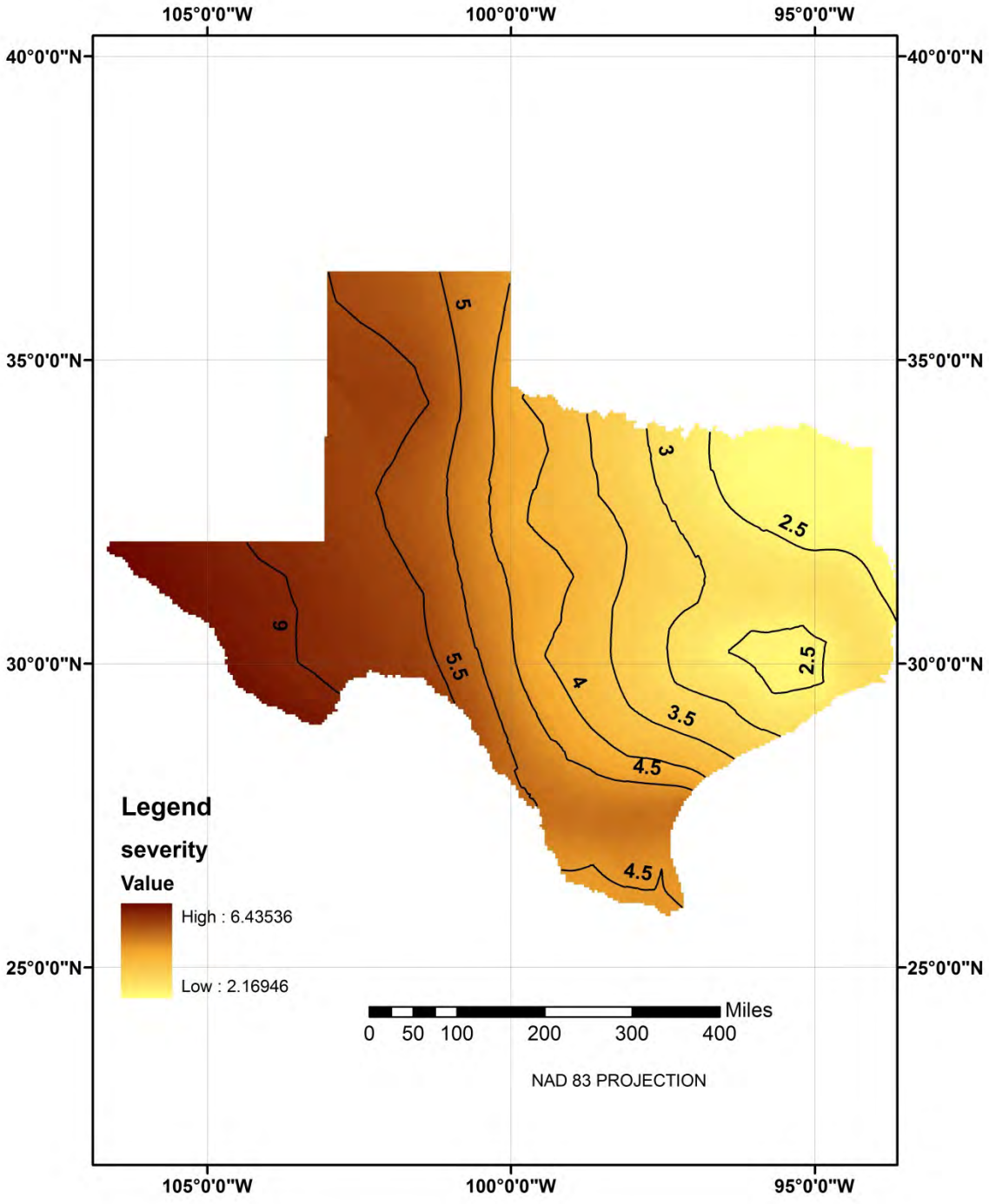

Figure 16h. Iso severity map for 6 months drought duration with a return period of 25 years

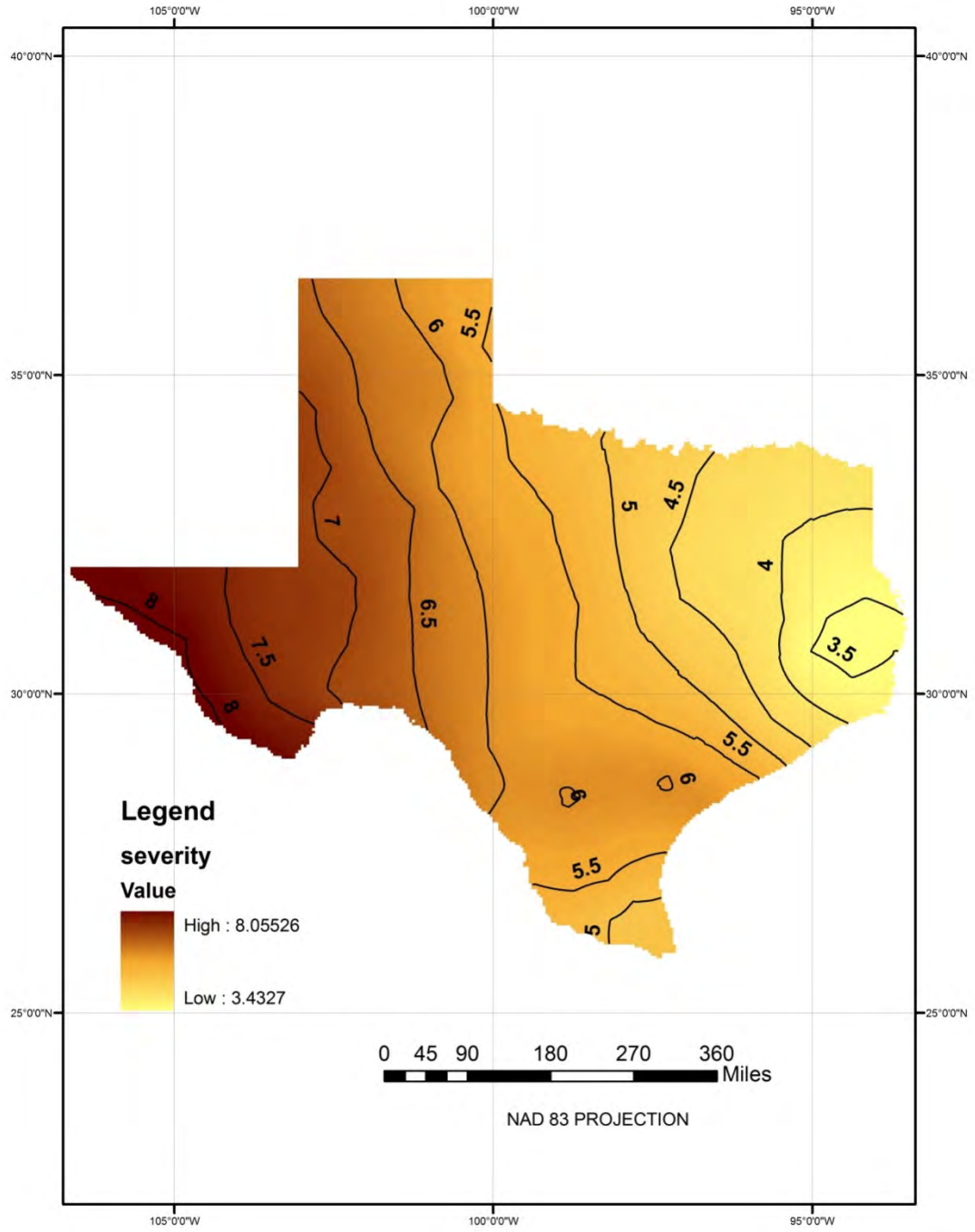

Figure 16i. Iso severity map for 6 months drought duration with a return period of 50 years

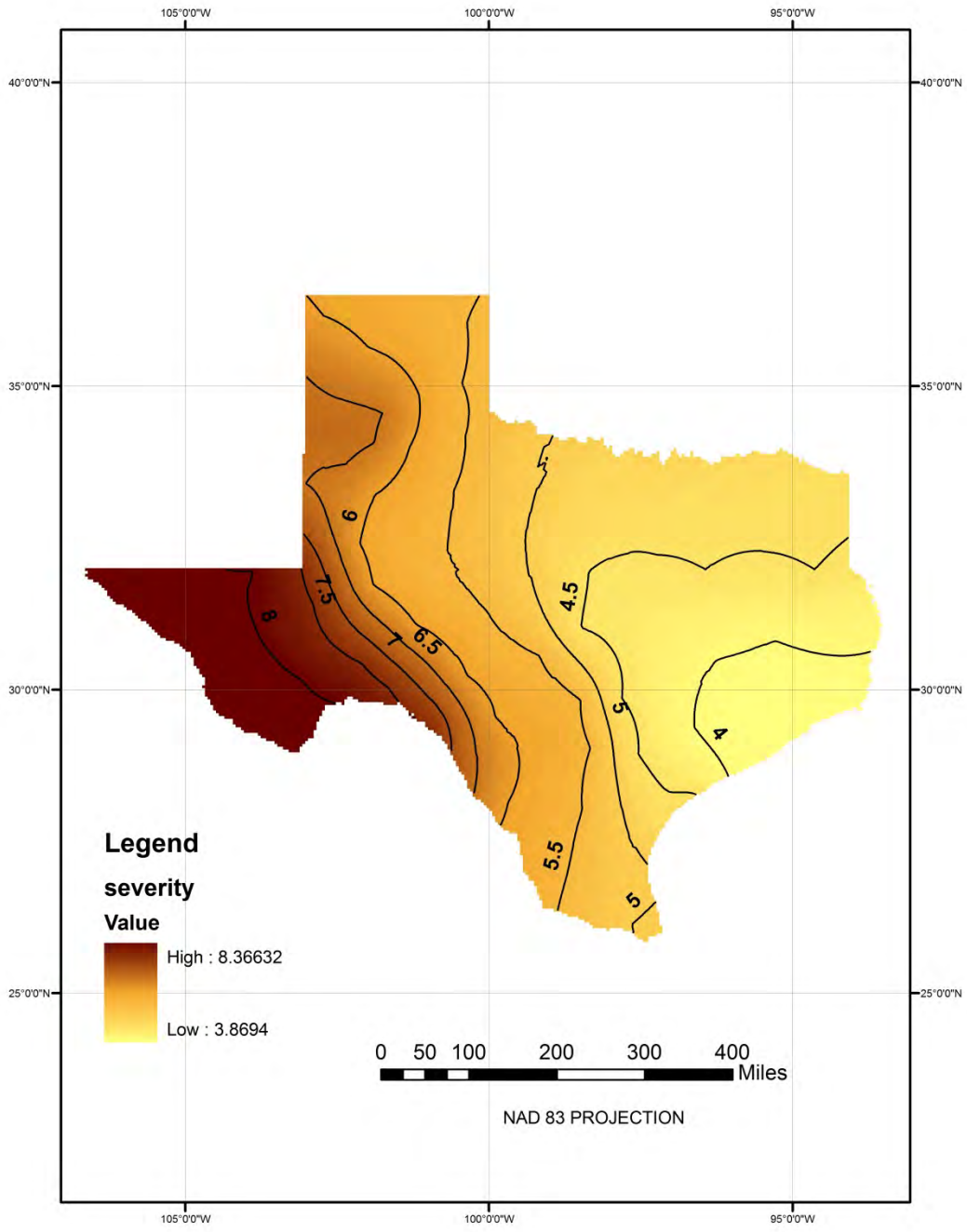

Figure 16j. Iso severity map for 6 months drought duration with a return period of 100 years

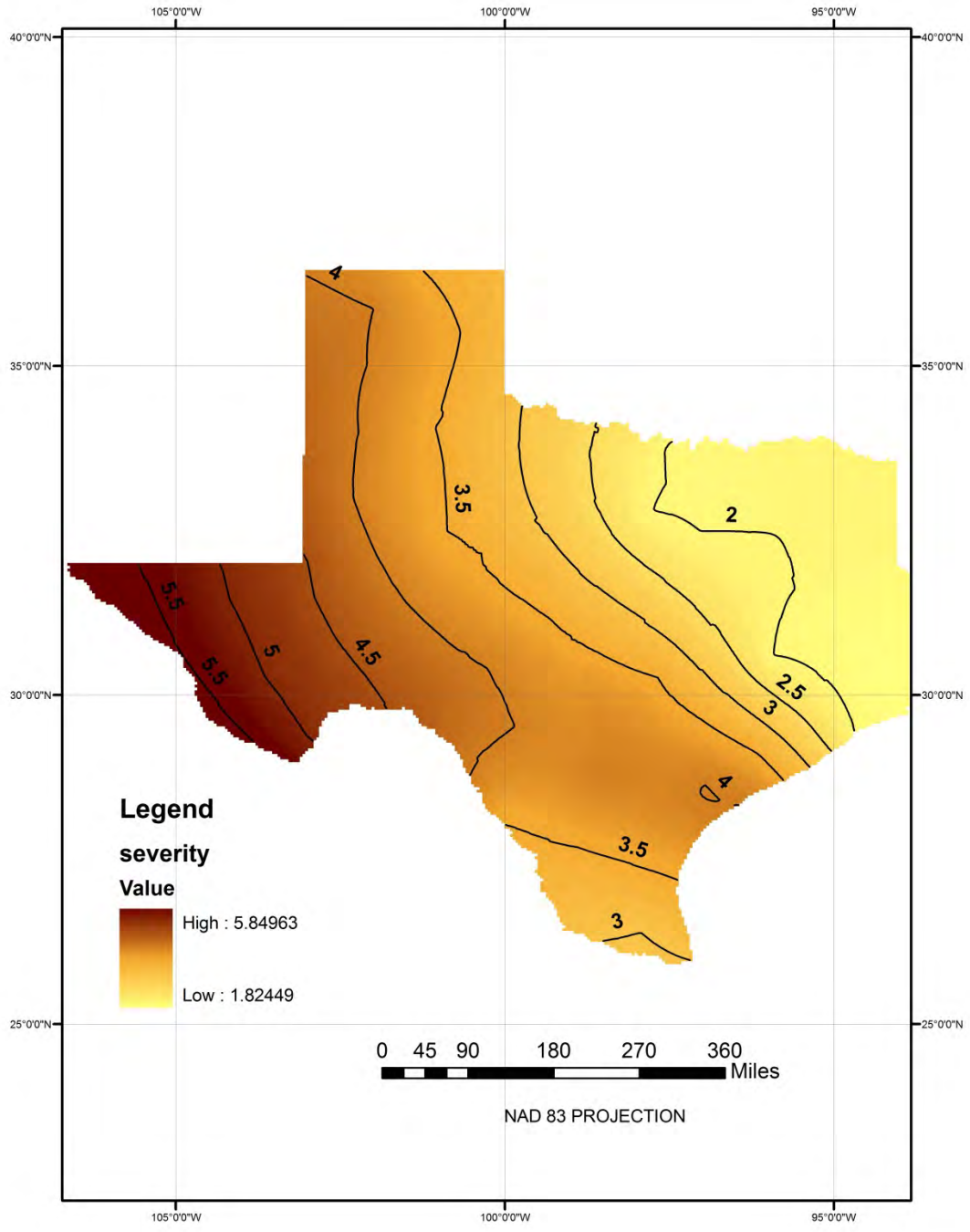

Figure 16k. Iso severity map for 9 months drought duration with a return period of 5 years

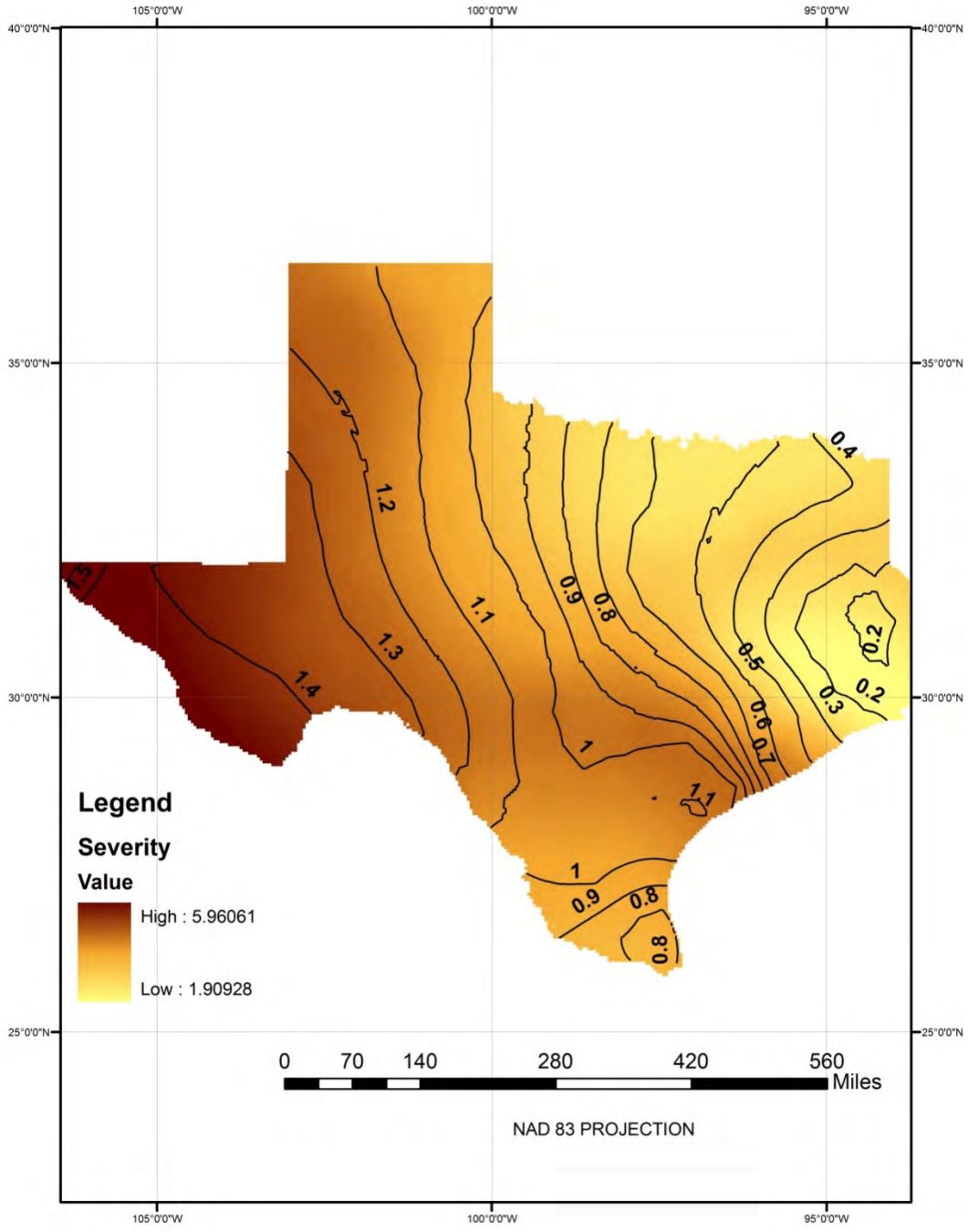

Figure 16l. Iso severity map for 9 months drought duration with a return period of 10 years

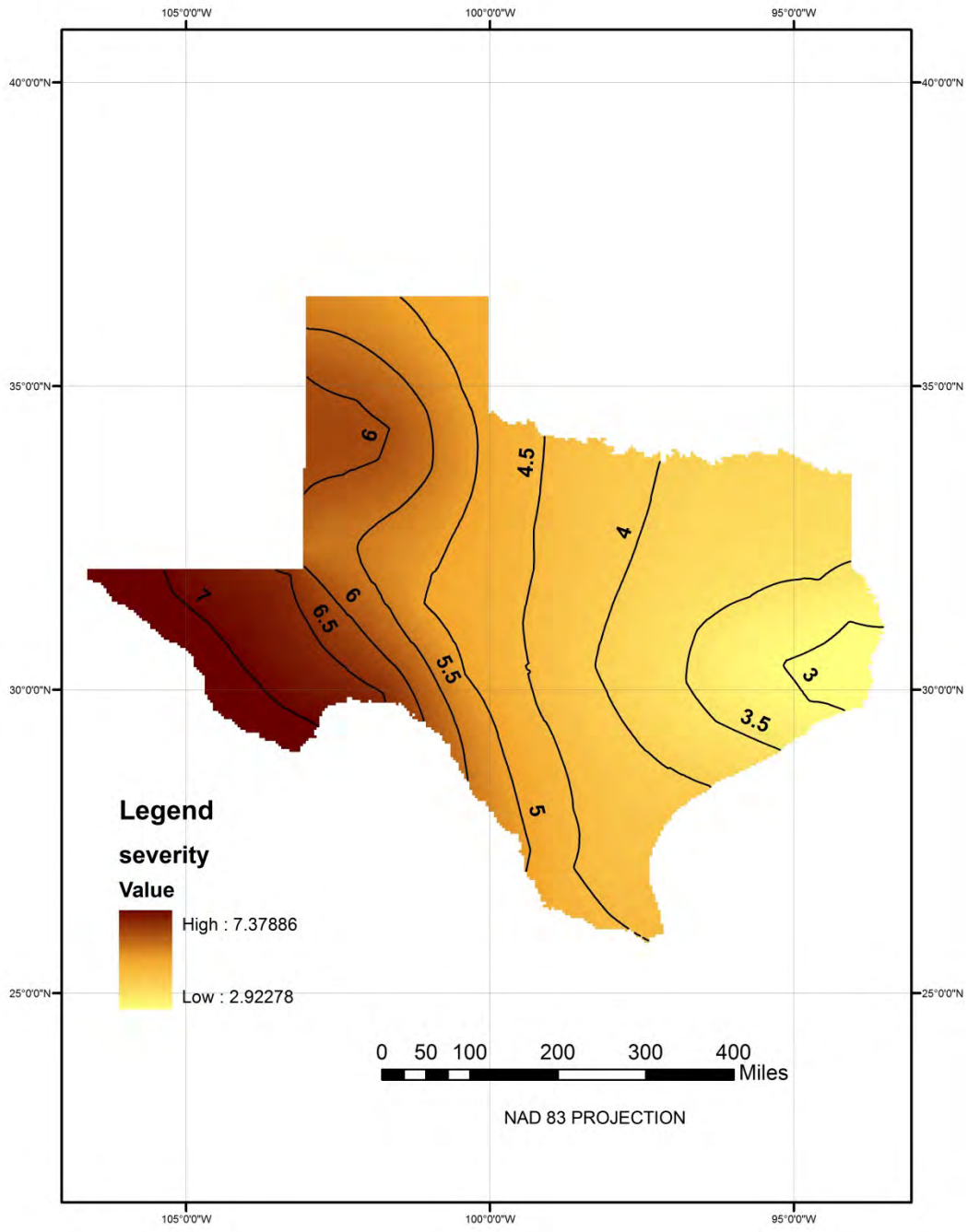

Figure 16m. Iso severity map for 9 months drought duration with a return period of 25 years

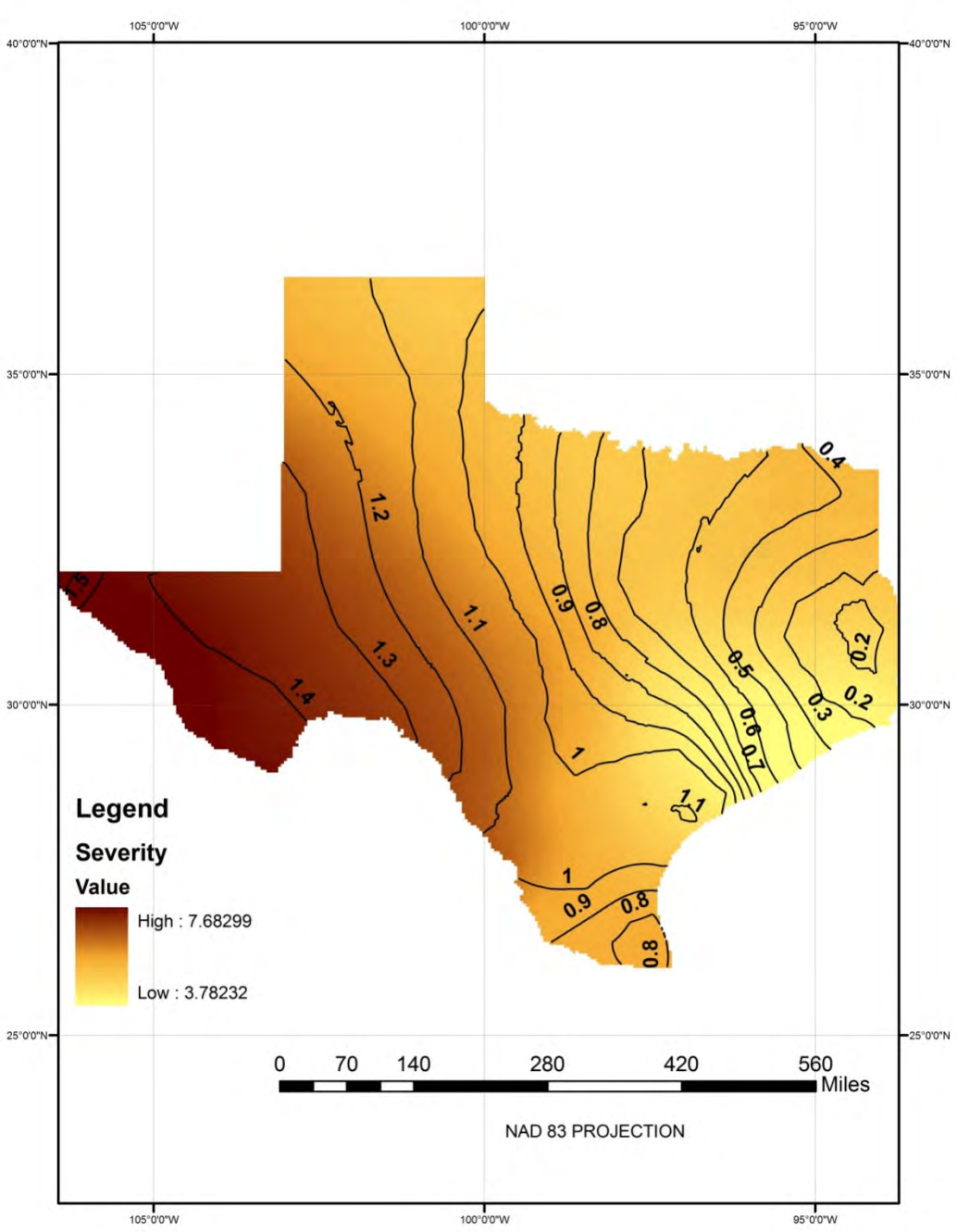

Figure 16n. Iso severity map for 9 months drought duration with a return period of 50 years

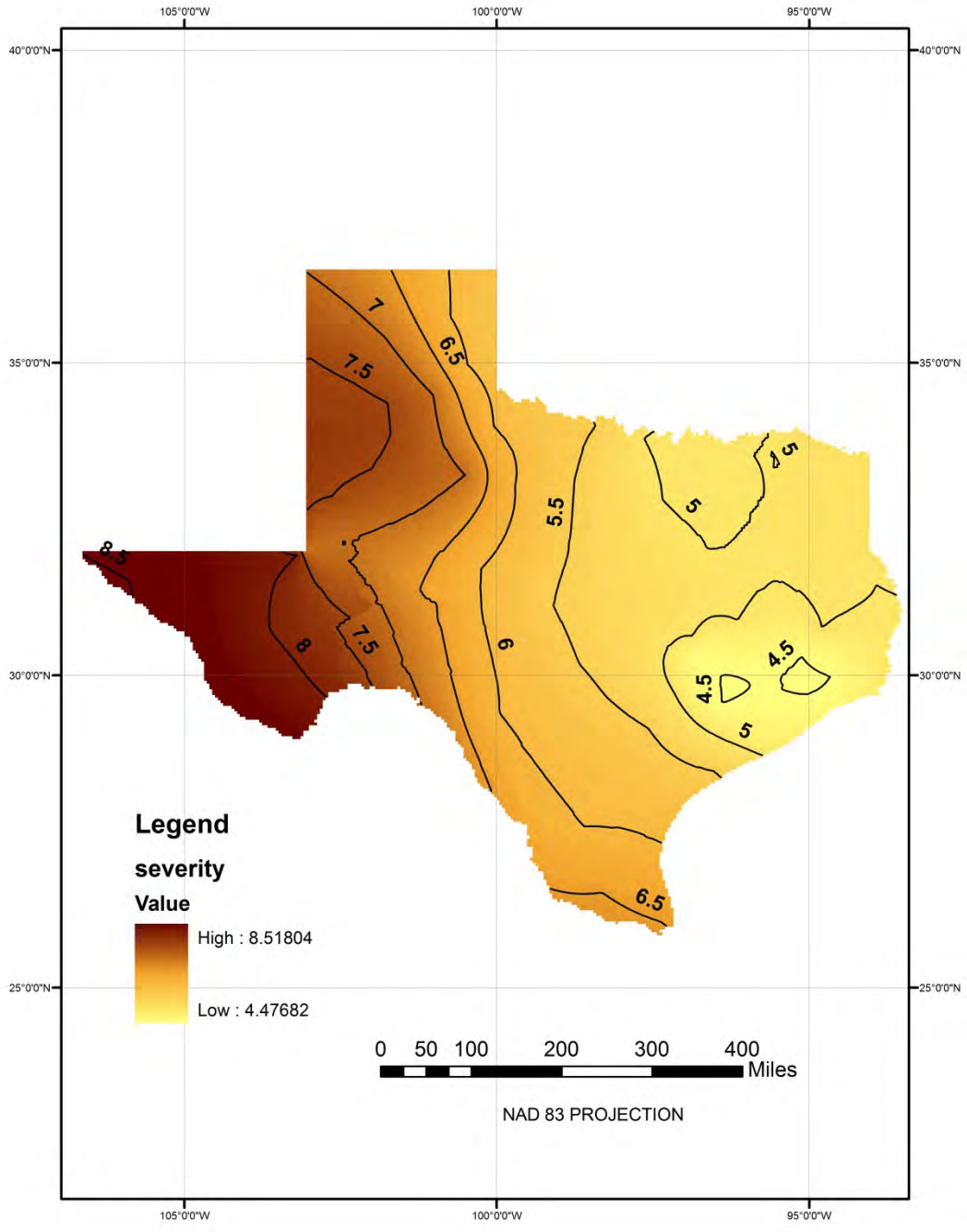

Figure 16o. Iso severity map for 9 months drought duration with a return period of 100 years

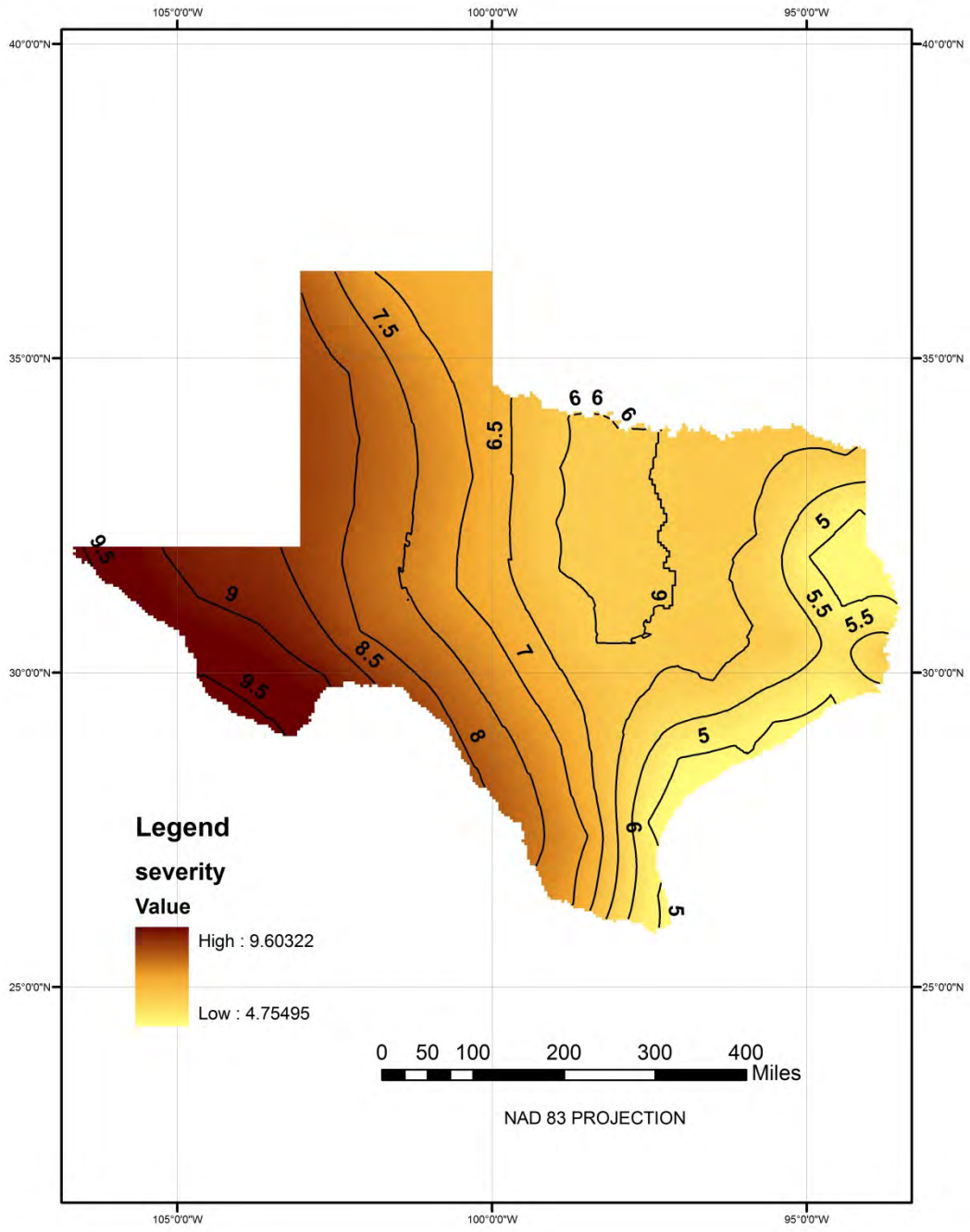

Figure 16p. Iso severity map for 12 months drought duration with a return period of 5 years

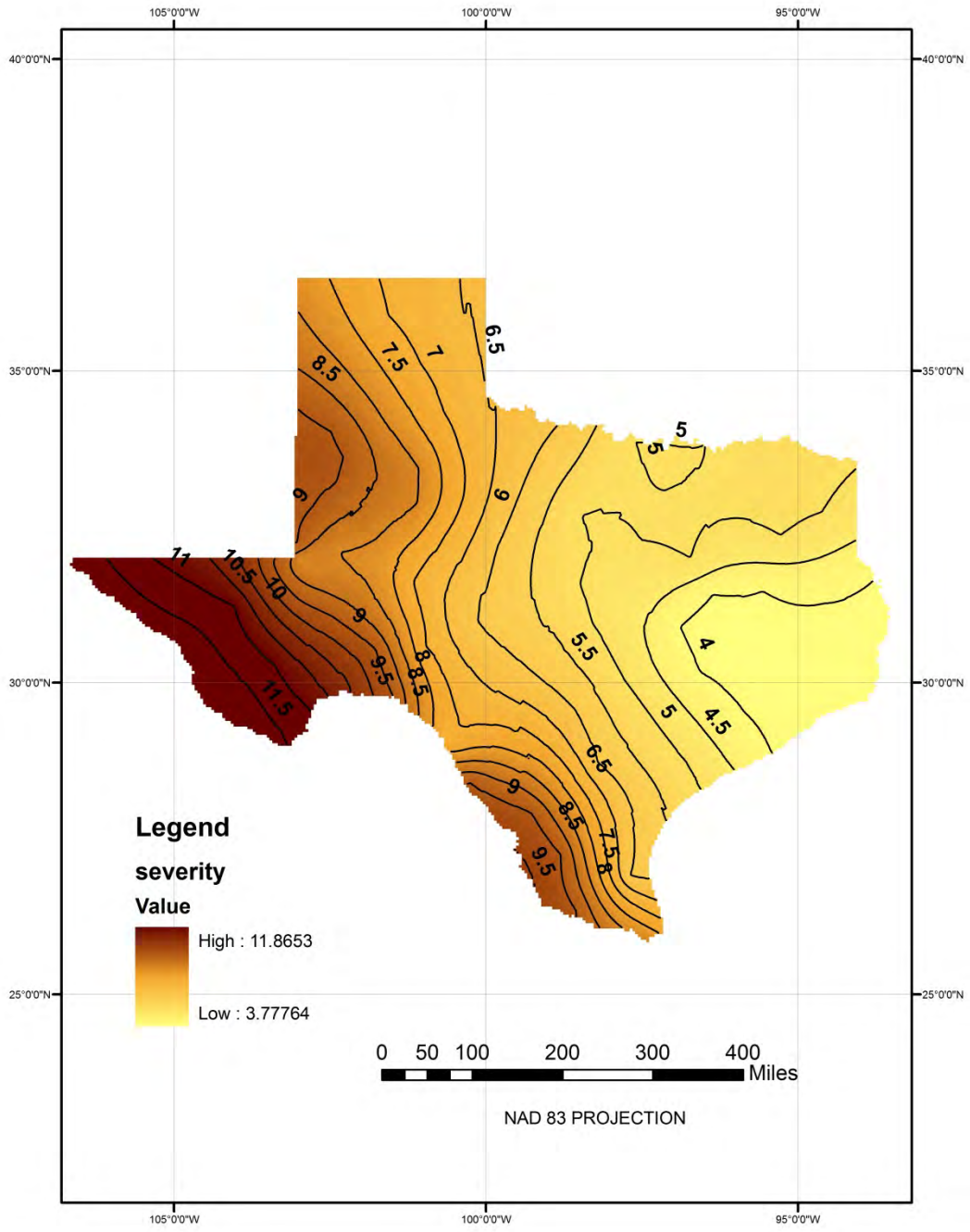

Figure 16q. Iso severity map for 12 months drought duration with a return period of 10 years

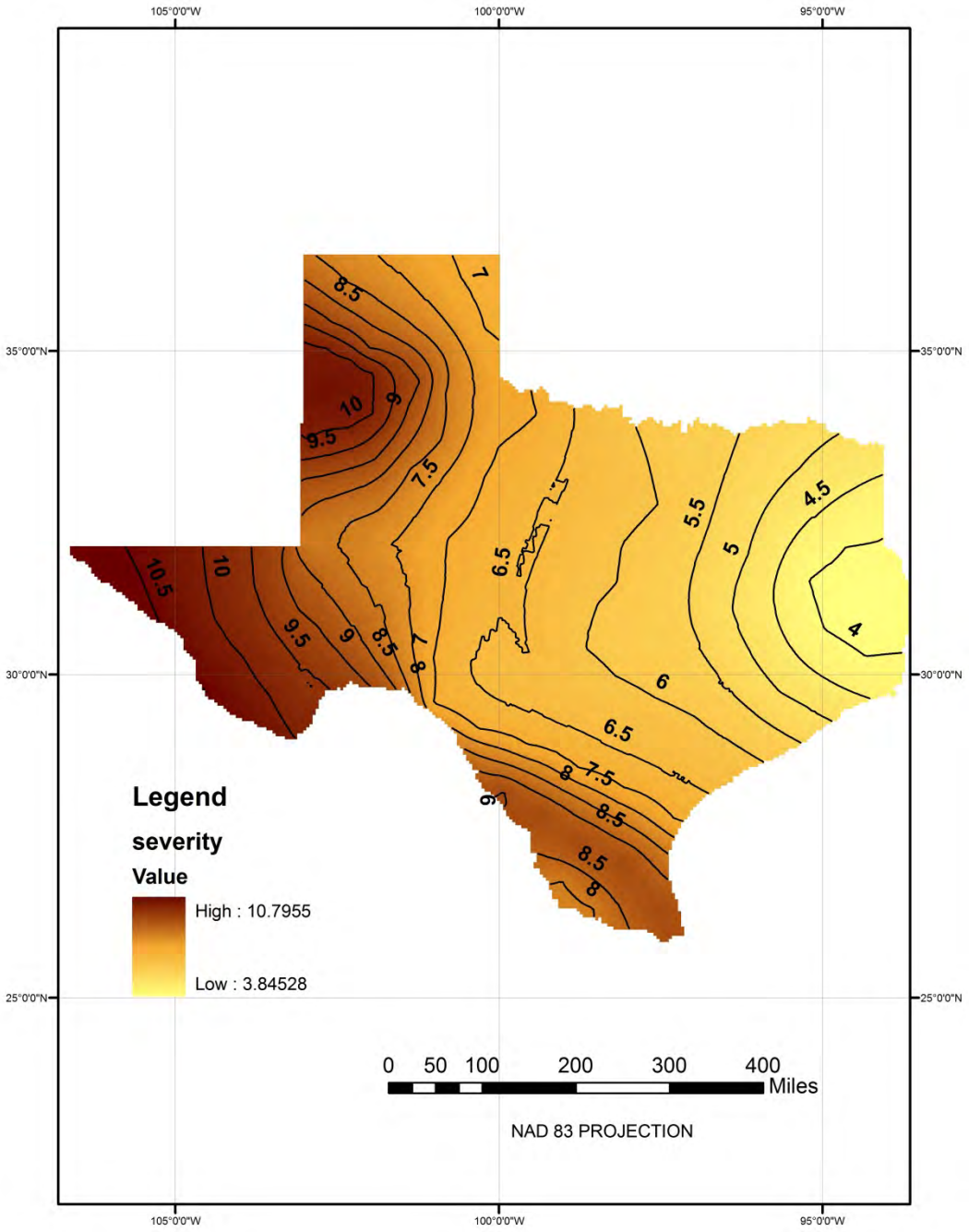

Figure 16r. Iso severity map for 12 months drought duration with a return period of 25 years

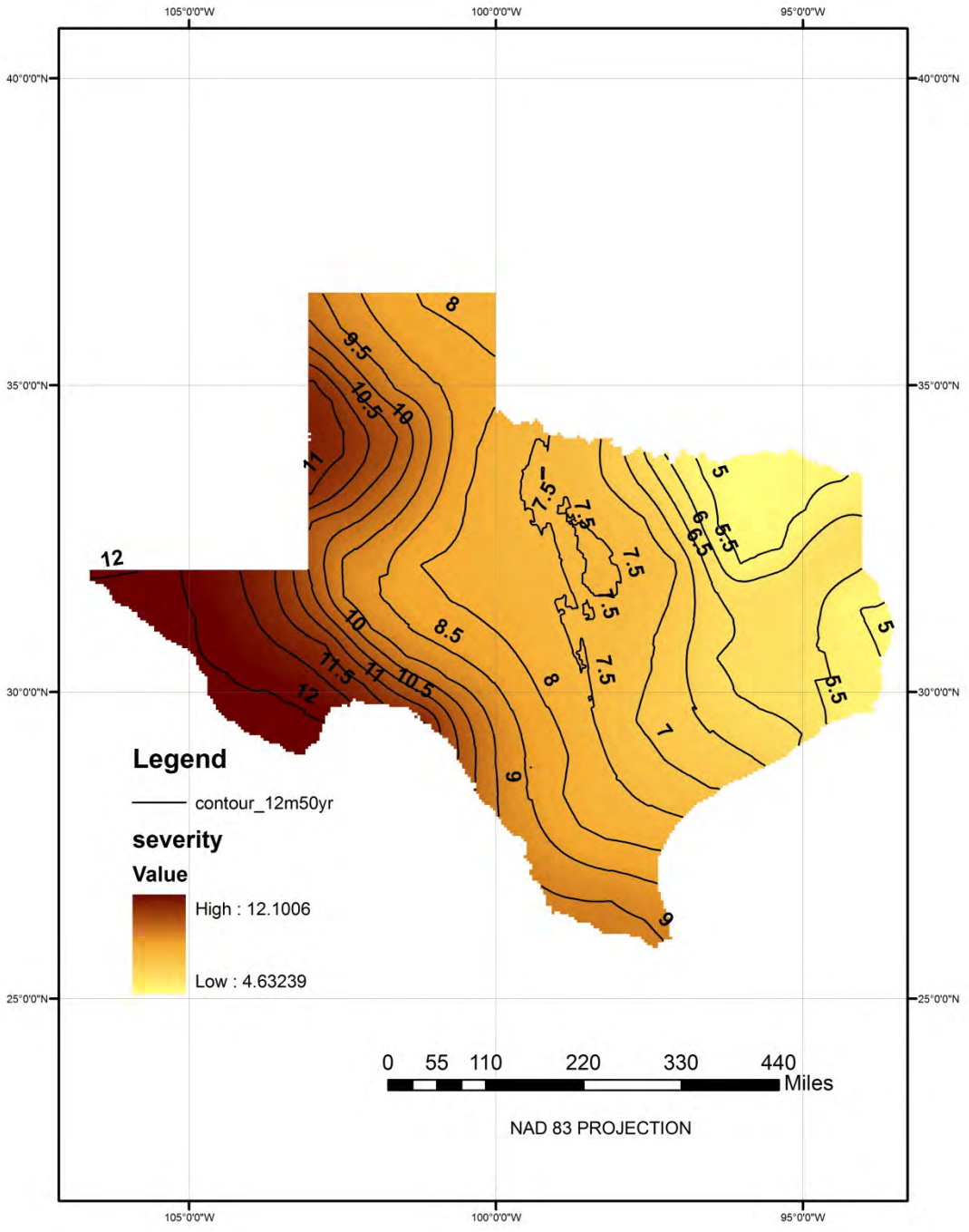

Figure 16s. Iso severity map for 12 months drought duration with a return period of 50 years

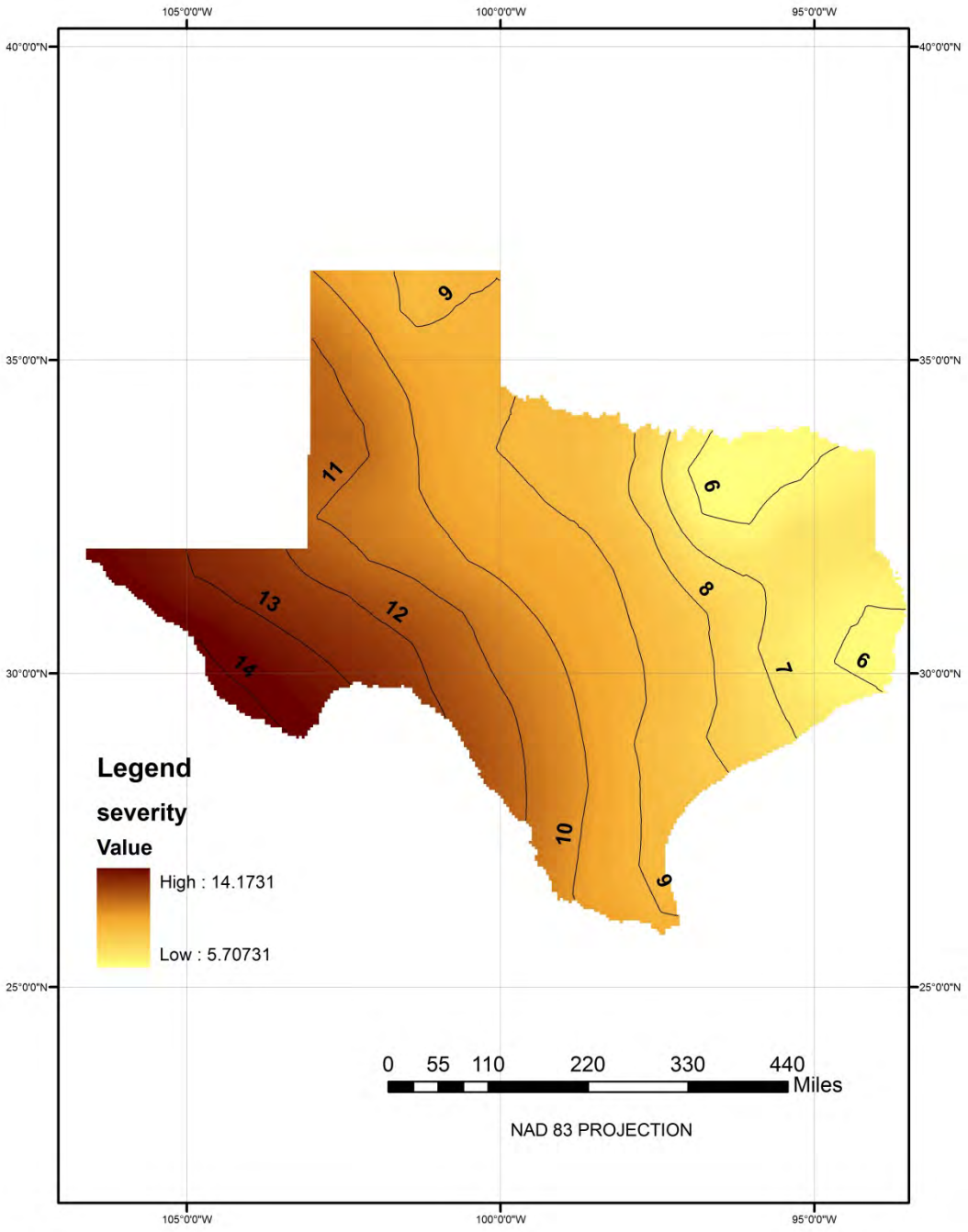

Figure 16t. Iso severity map for 12 months drought duration with a return period of 100 years

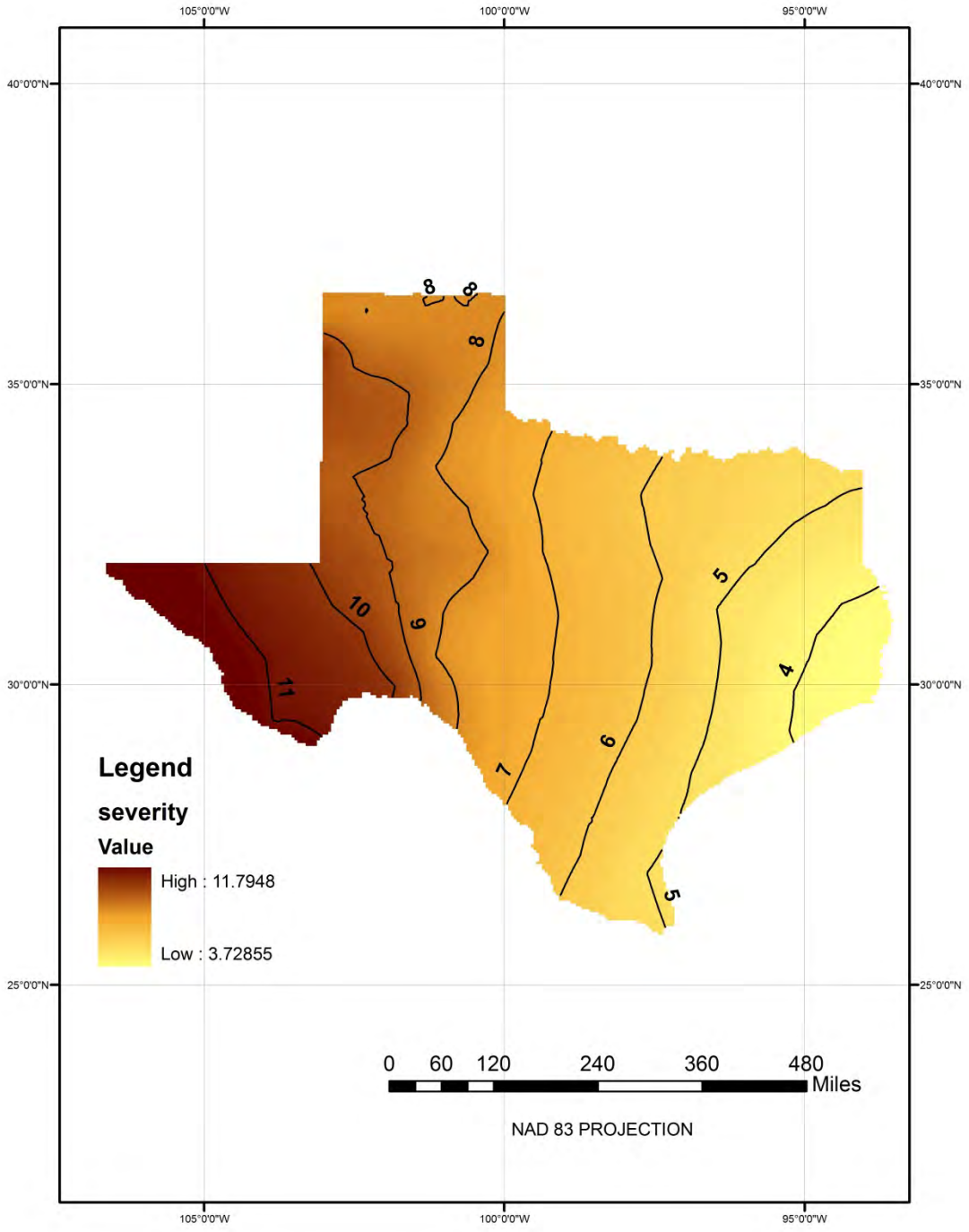

Figure 16u. Iso severity map for 18 months drought duration with a return period of 5 years

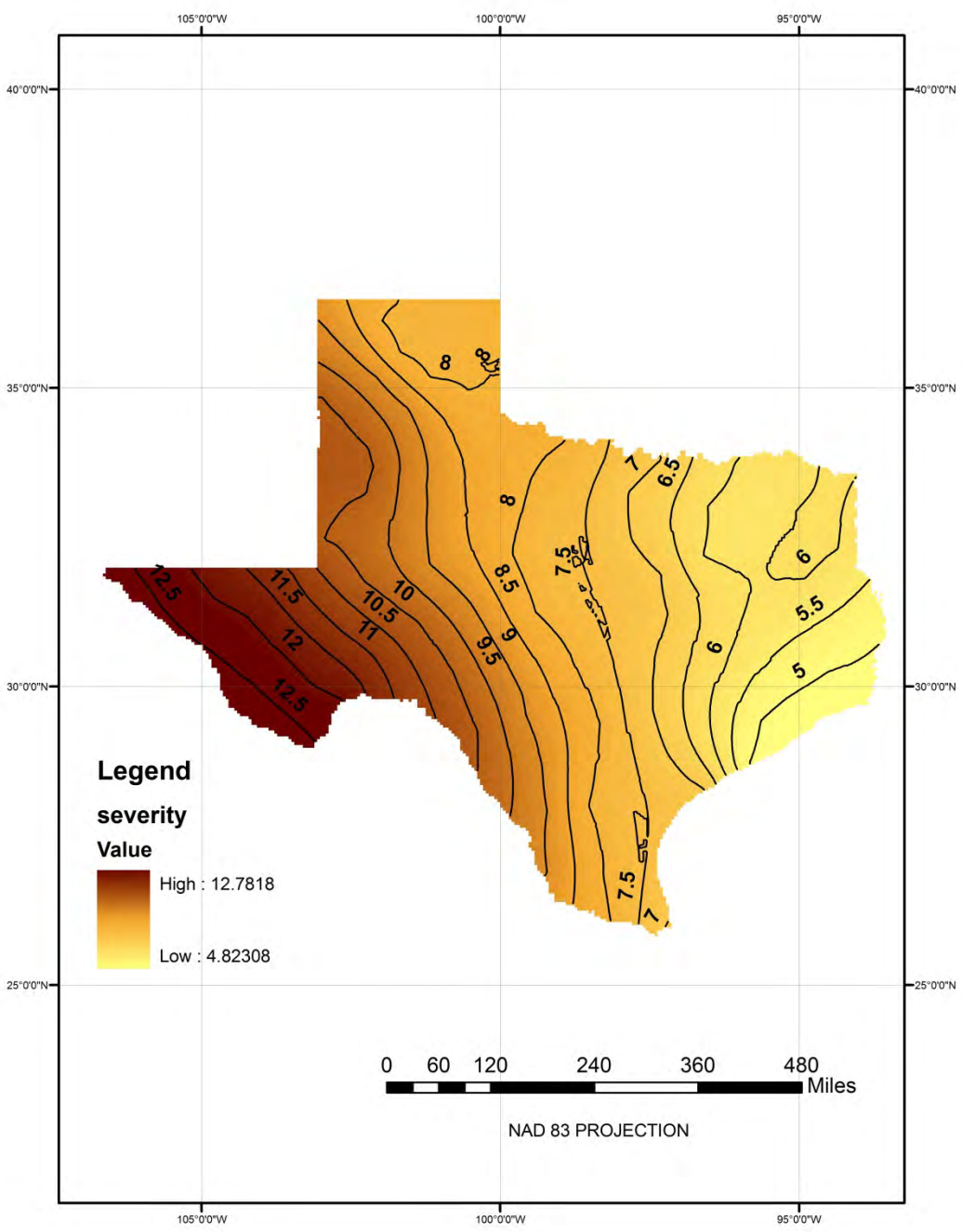

Figure 16v. Iso severity map for 18 months drought duration with a return period of 10 years

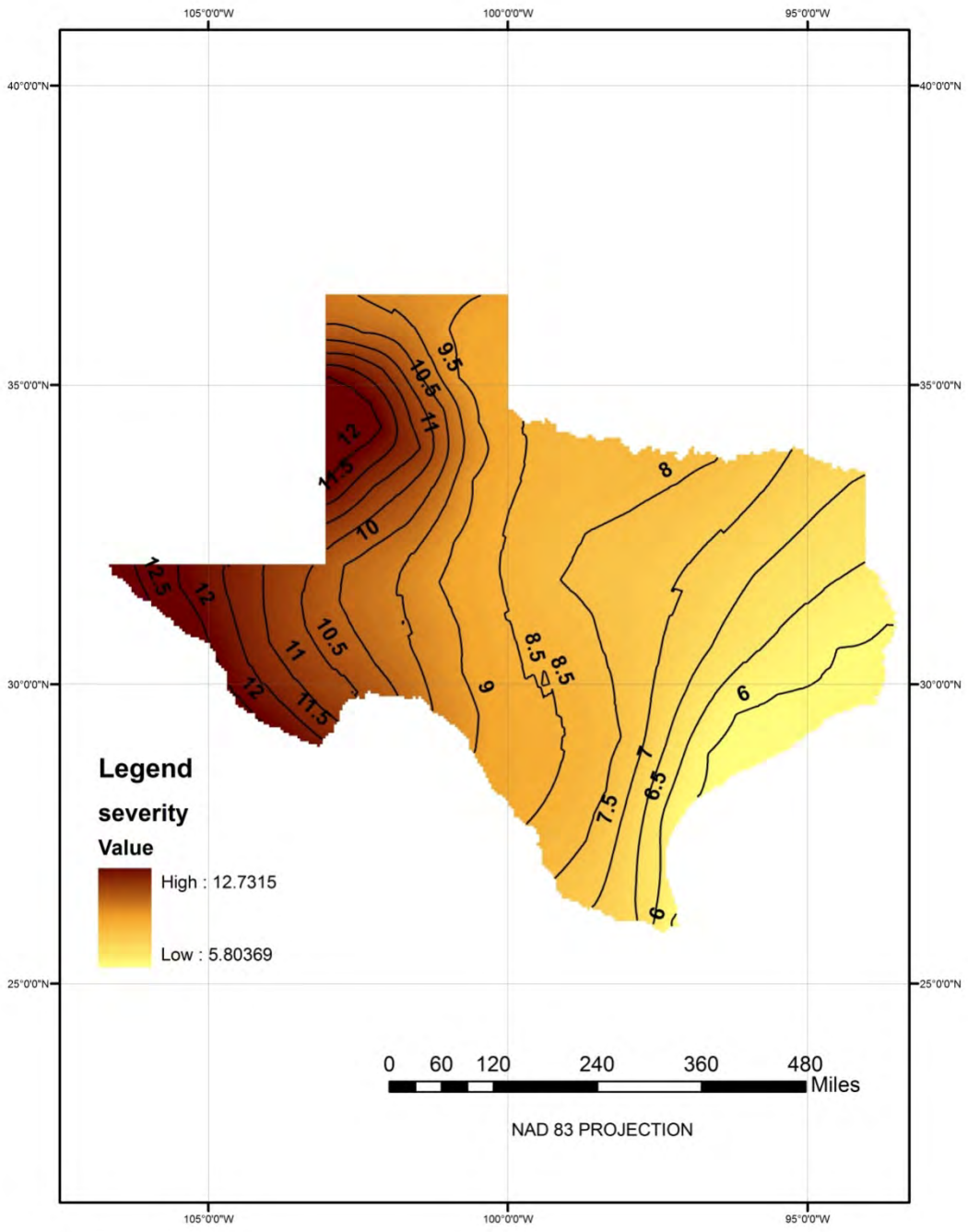

Figure 16w. Iso severity map for 18 months drought duration with a return period of 25 years

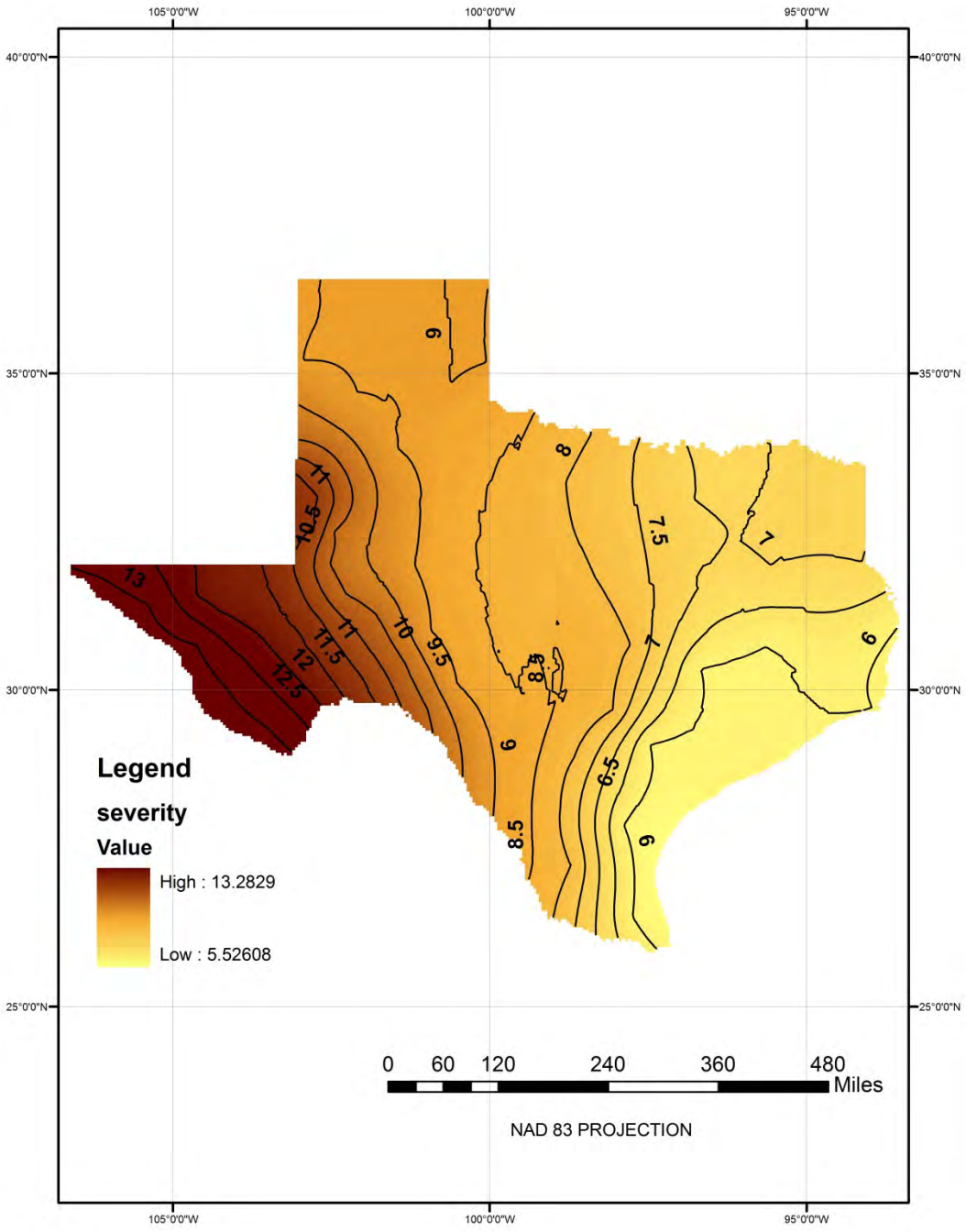

Figure 16x. Iso severity map for 18 months drought duration with a return period of 50 years

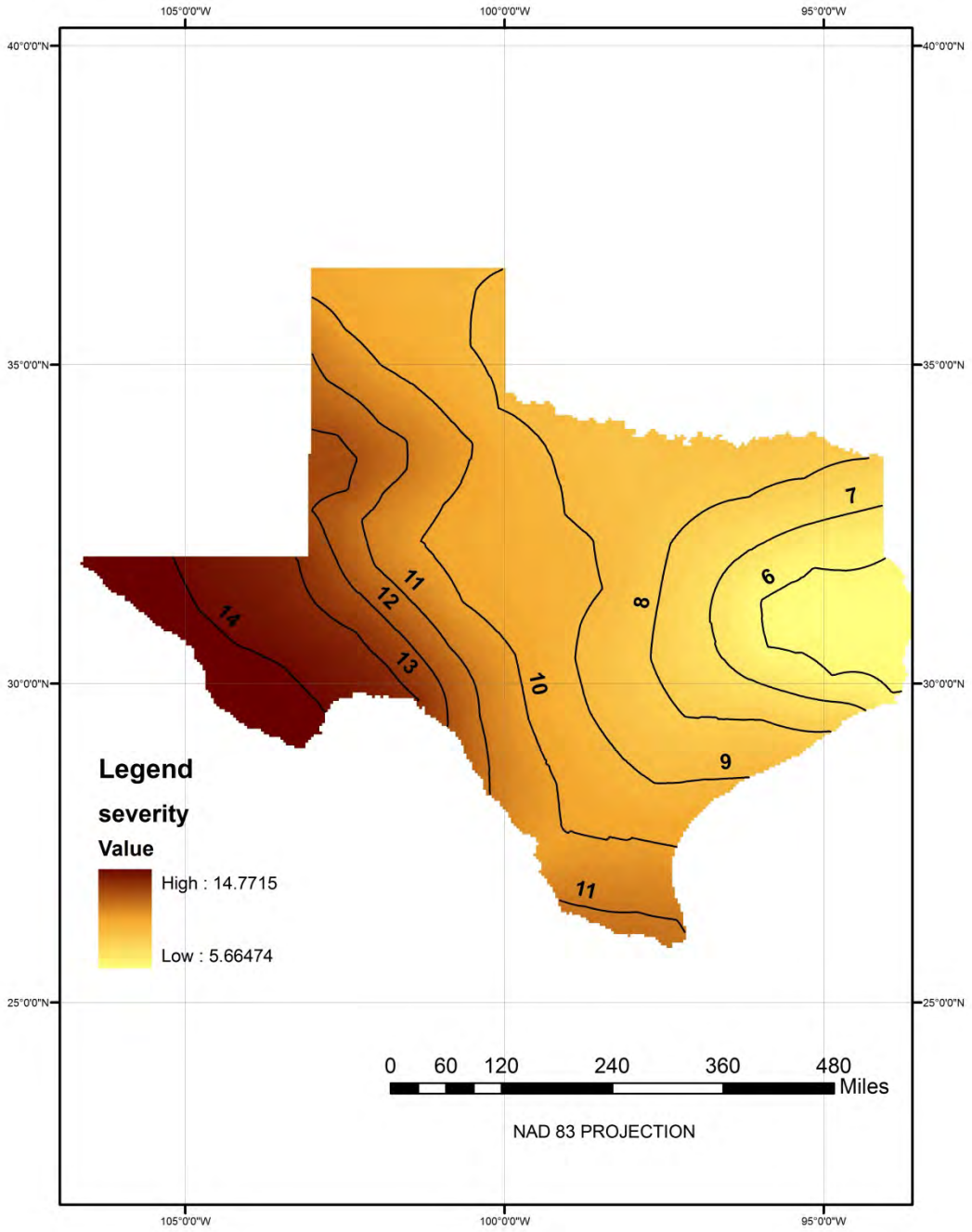

Figure 16y. Iso severity map for 18 months drought duration with a return period of 100 years

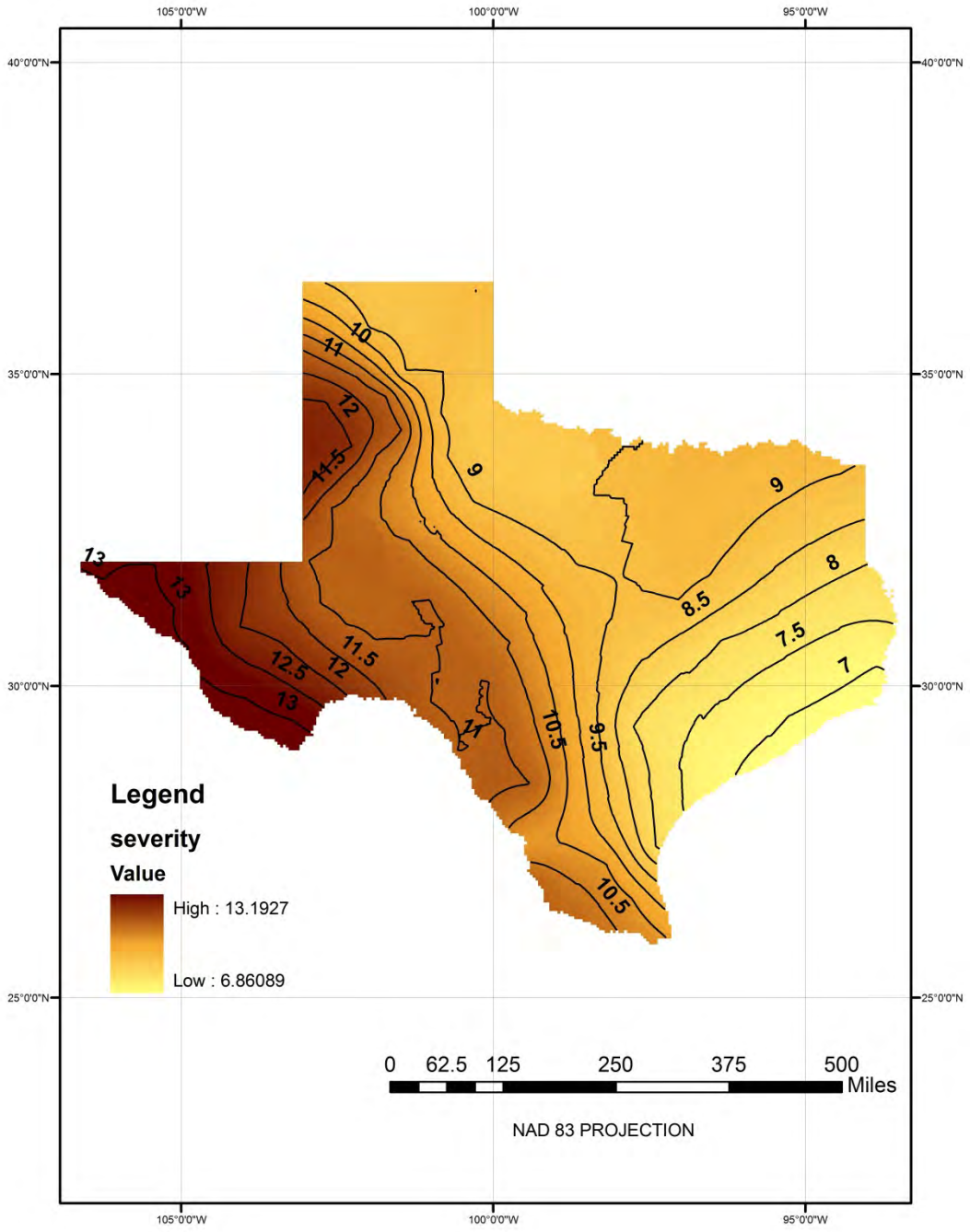

Figure 16z. Iso severity map for 24 months drought duration with a return period of 5 years

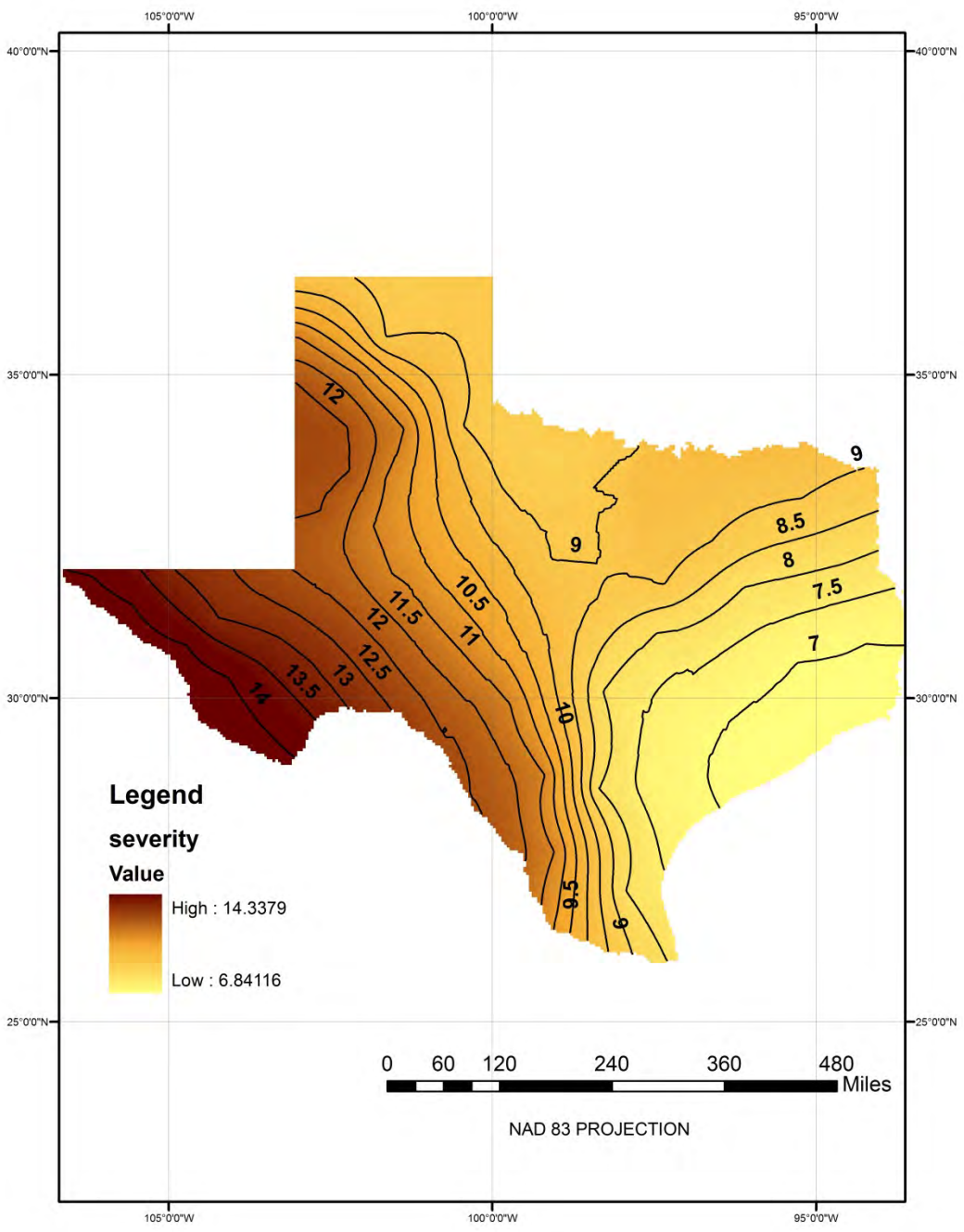

Figure 16aa. Iso severity map for 24 months drought duration with a return period of 10 years

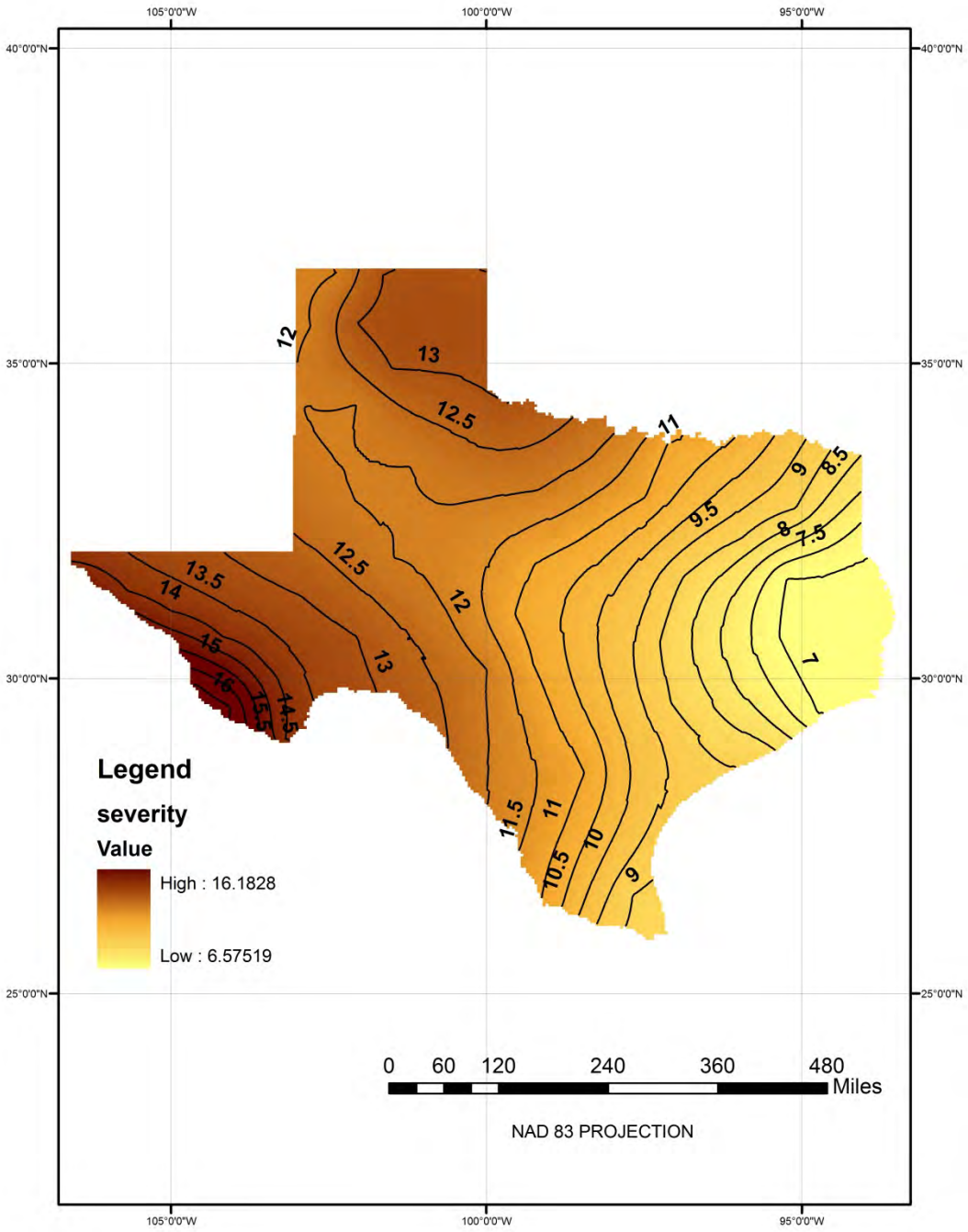

Figure 16ab. Iso severity map for 24 months drought duration with a return period of 25 years

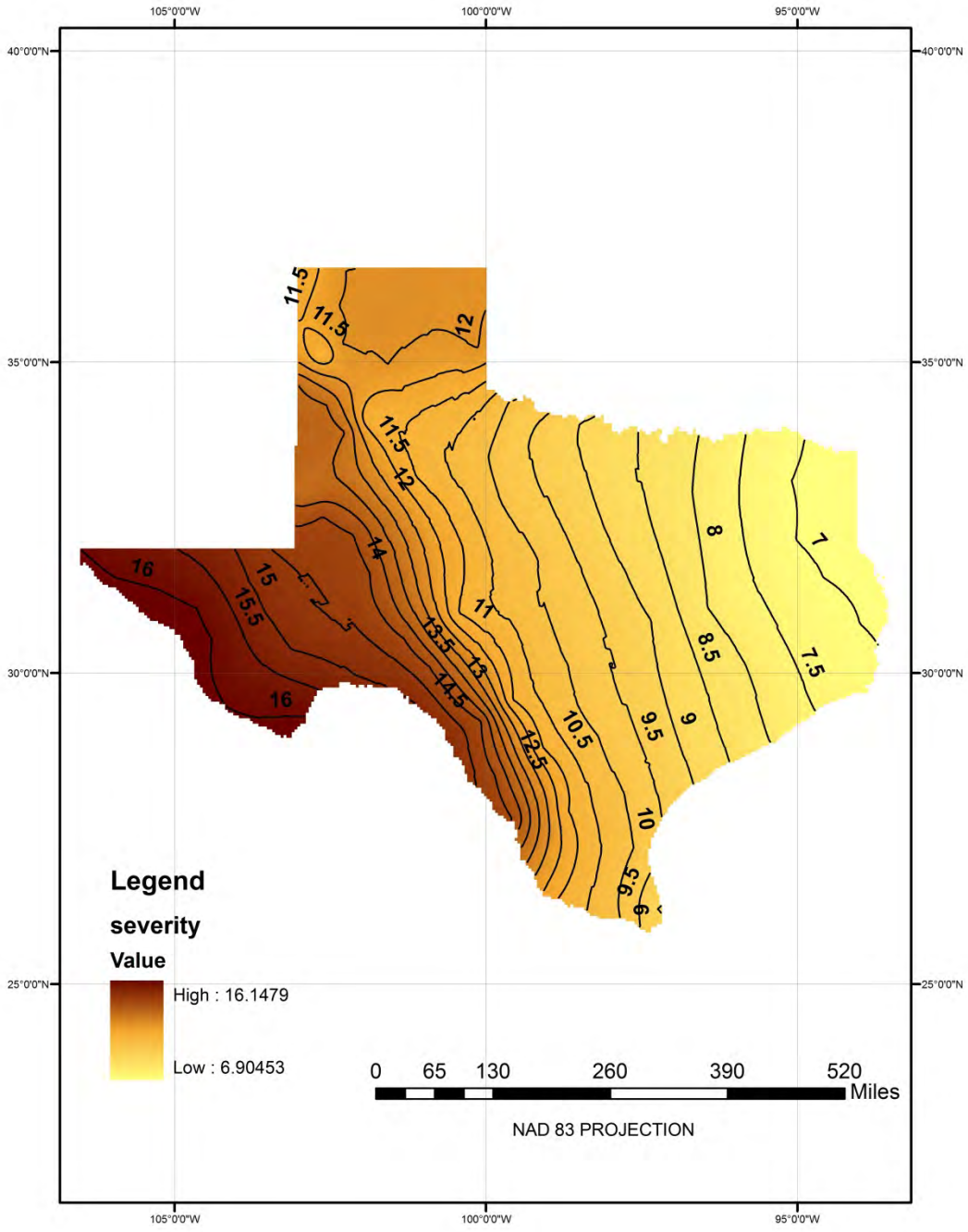

Figure 16ac. Iso severity map for 24 months drought duration with a return period of 50 years

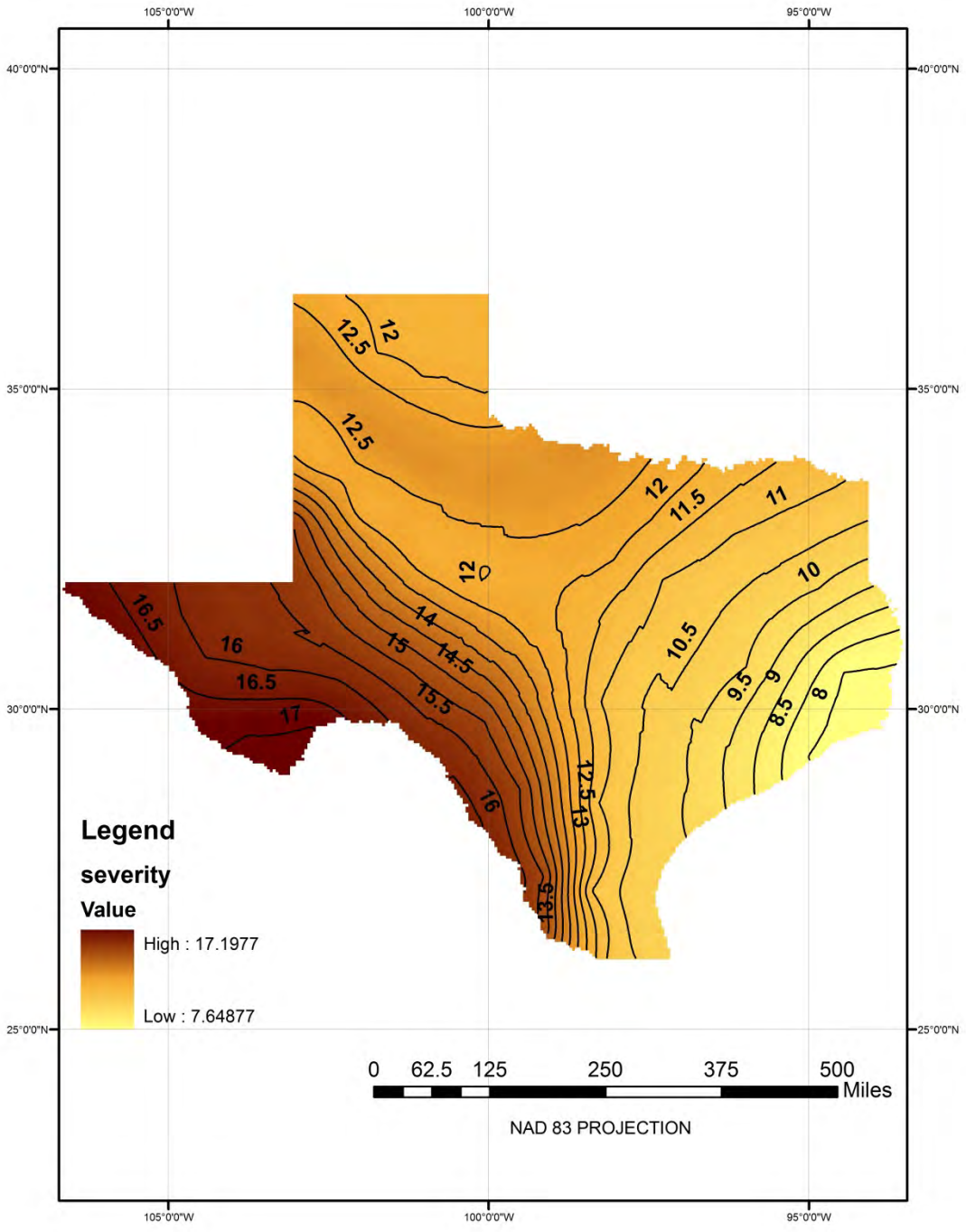

Figure 16ad. Iso severity map for 24 months drought duration with a return period of 100 years

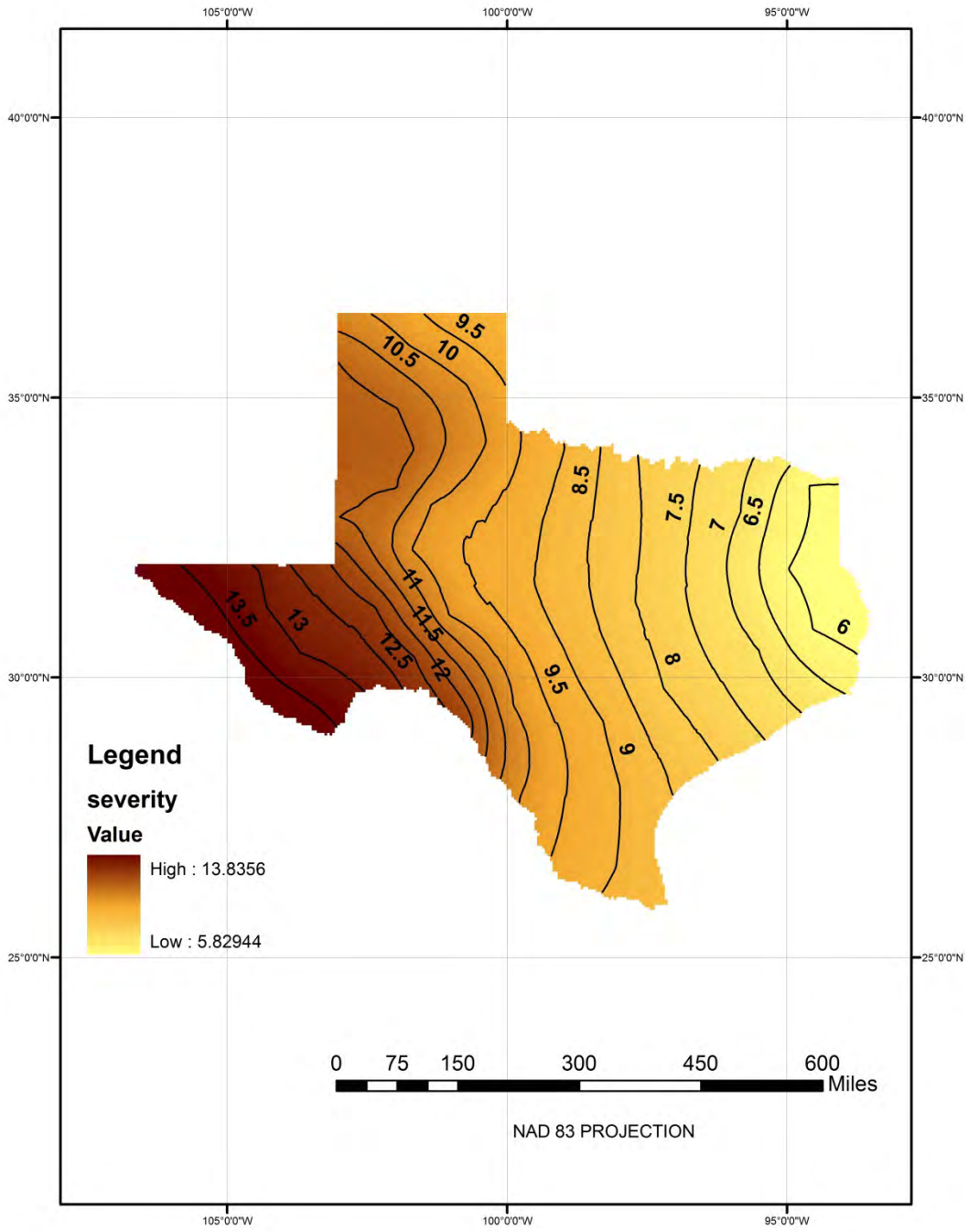

Figure 16ae. Iso severity map for 36 months drought duration with a return period of 5 years

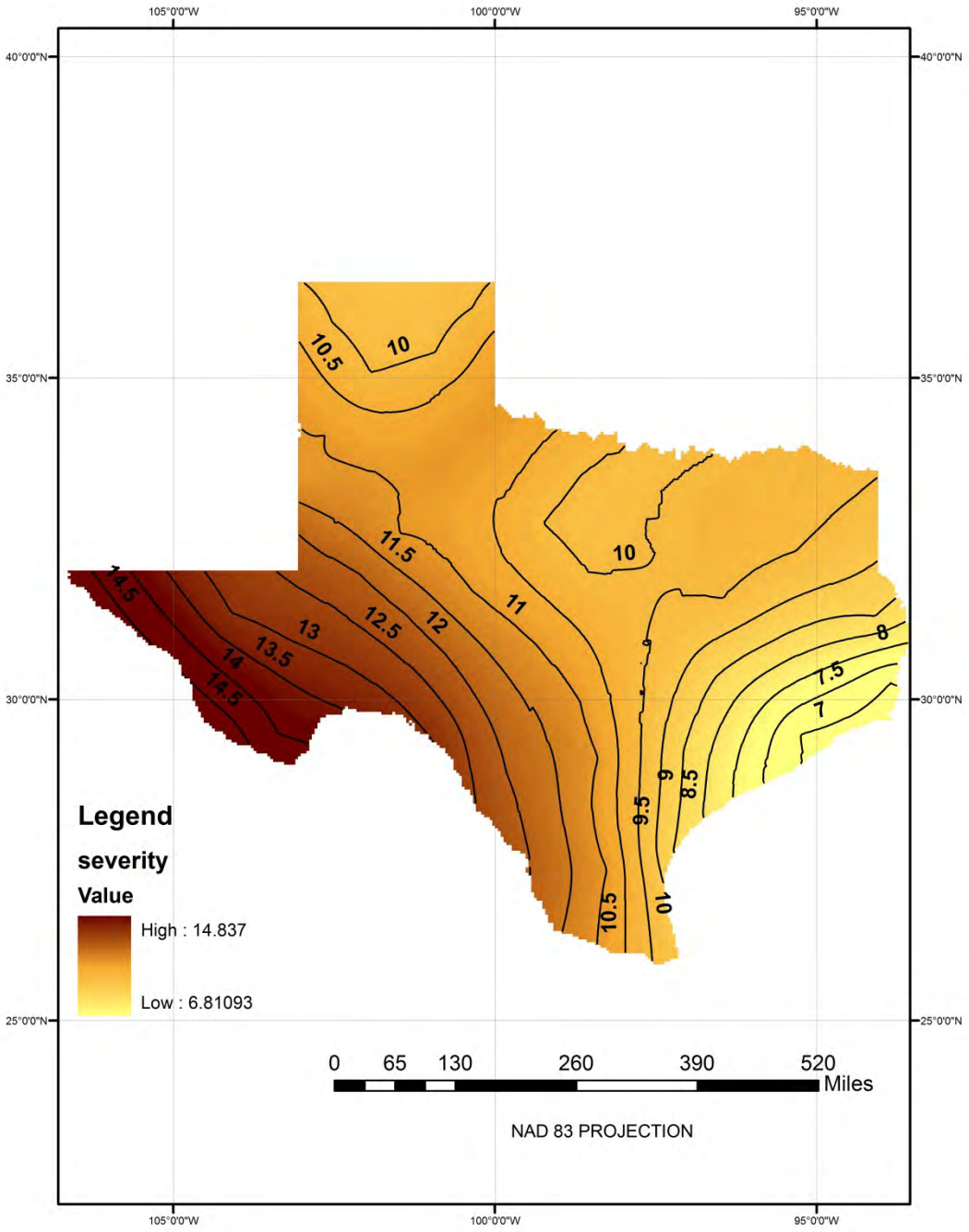

Figure 16af. Iso severity map for 36 months drought duration with a return period of 10 years

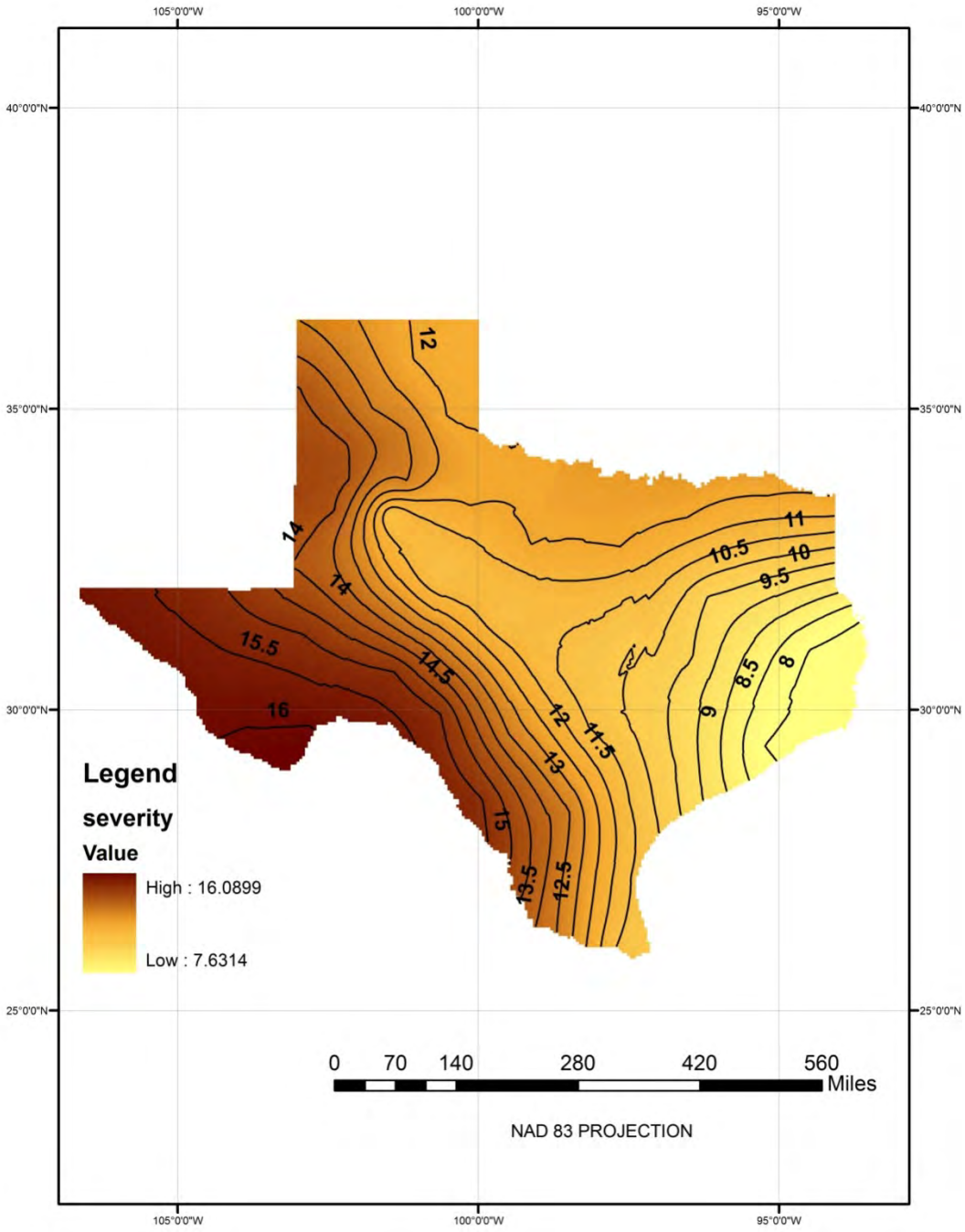

Figure 16ag. Iso severity map for 36 months drought duration with a return period of 25 years

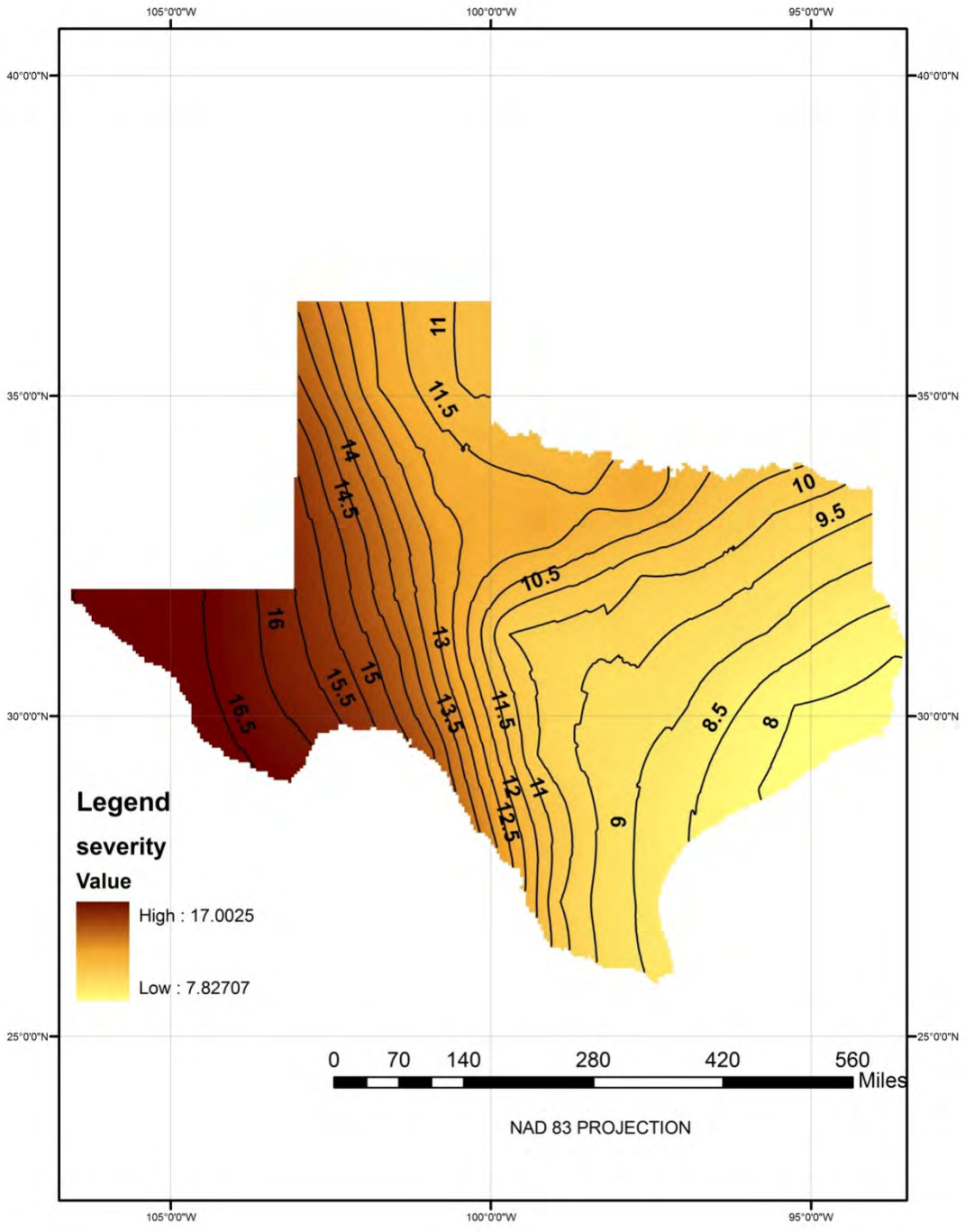

Figure 16ah. Iso severity map for 36 months drought duration with a return period of 50 years

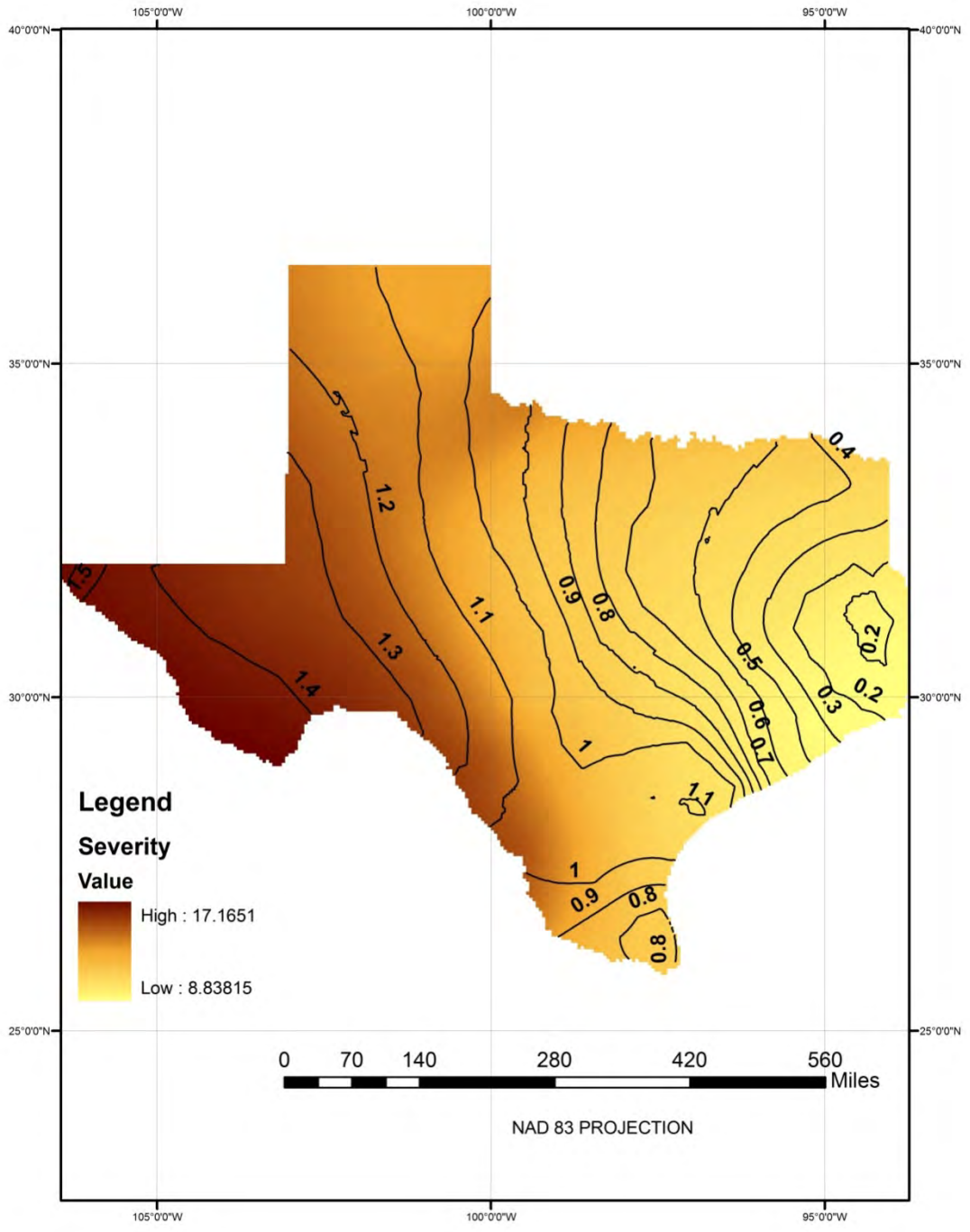

Figure 16ai. Iso severity map for 36 months drought duration with a return period of 100 years

Part 2: Precipitation based Drought maps

The first part of the study derived the drought properties based on simulated stream flow from a large scale hydrological model. It was thus based on a standardized form of stream flow, termed as standardized stream flow index (SSFI). To validate this result, in this section, we develop the drought atlas using drought properties derived based on precipitation. Additionally, it can be used for comparison of the hydrological and meteorological drought conditions over Texas.

The methodology followed will be exactly the same, with the exception that a different drought index, namely standardized precipitation index (SPI) would be used to derive drought properties. SPI is statistically similar to SSFI. There are several pros and cons for the use of SPI. Pros include that, it is a very simple method based only on precipitation; it is usable at any time scale, it can be used universally at any location, and that it can provide early warnings of drought. Cons include the fact that values based on preliminary data may change, and that due to the characteristics associated with the normal distribution, severe and extreme droughts measured by SPI occur with the same frequency at all locations. This means that SPI cannot identify regions that may be more prone to drought than others.

Estimation of SPI

The SPI is calculated through the following steps. Continuous monthly precipitation data for long term will be required for this. This data will be fitted to a suitable distribution. Thom (1966) found that precipitation series are well described by the gamma distribution. The gamma distribution is defined by its probability density function:

$$g(x) = \left(\frac{1}{\beta^{\alpha}\Gamma(\alpha)} \right) x^{\alpha-1} e^{\frac{x}{\beta}} \qquad \text{for } x>0 \tag{25}$$

where $\alpha > 0$ is the shape parameter, $\beta > 0$ is the scale parameter, $x>0$ is the precipitation amount, and Γ is the gamma function.

Calculation of SPI involves fitting a gamma probability density function to the given frequency distribution of the precipitation of a station. Parameters α and β are estimated for each station, for every timescale of interest (1, 3, 6, 12, 24, 48), and for each month of the year. In this case the timescale of interest is 1 month. Using the maximum likelihood estimation method, the parameters are given as:

$$\hat{\alpha} = \frac{1}{4A}\left[1 + \sqrt{1 + \left[\frac{4A}{3} \right]} \right] \tag{25.1}$$

$$\hat{\beta} = \frac{\overline{X}}{\hat{\alpha}} \tag{25.2}$$

where

$$A = \ln(\overline{x}) - \frac{\sum \ln(x)}{n} \tag{25.3}$$

n is number of observations.

After estimating the parameters, the cumulative probability for an observed event for a given precipitation event, in a given month, on a given timescale for the station in question can be calculated. The cumulative probability is given as:

$$G(x) = \frac{1}{\Gamma(\hat{\alpha})} \int_0^x t^{\alpha-1} e^{-t} dt; t = \frac{x}{\hat{\beta}} \tag{25.4}$$

But eq. (25.4) is not defined for x=0, and since precipitation time series will contain zeros, cumulative probability becomes:

$$H(x) = (1-q)\, G(x) + q \tag{25.5}$$

where q is the probability of zero value.

H(x) will then be converted to standard normal variable with mean value of 0, and standard deviation 1, which is the value of SPI. This conversion procedure is same as the methodology for SSFI which is explained in section 1. The classification of SPI is same as that for SSFI, as given in Table 1.

Data Source

Long term monthly precipitation data was necessary for the calculation of SPI and derivation of drought properties for subsequent analysis. The precipitation data required was obtained from the National Climate Data Center (NCDC) website. NCDC gauges have a wide coverage in United States (around 4000 gauges of which over 300 are in Texas).

Kriging for map preparation

Once the S-D-F curves were developed for all the station gauges in Texas, a geostatistical method called kriging was used to produce the drought maps. Kriging techniques can be used to describe and model spatial patterns, predict values at unmeasured locations, and assess the uncertainty associated with a predicted value at the unmeasured locations. Hence, it is an interpolation technique in which the surrounding measured values are weighted to derive a

predicted value for an unmeasured location. Weights are based on the distance between the measured points, the prediction locations, and the overall spatial arrangement among the measured points. Kriging is unique among the interpolation methods in that it provides an easy method for characterizing the variance, or the precision, of predictions. Kriging is based on regionalized variable theory, which assumes that the spatial variation in the data being modeled is homogeneous across the surface. That is, the same pattern of variation can be observed at all locations on the surface.

The ArcGIS geospatial analyst toolbox will be made use of to perform kriging.

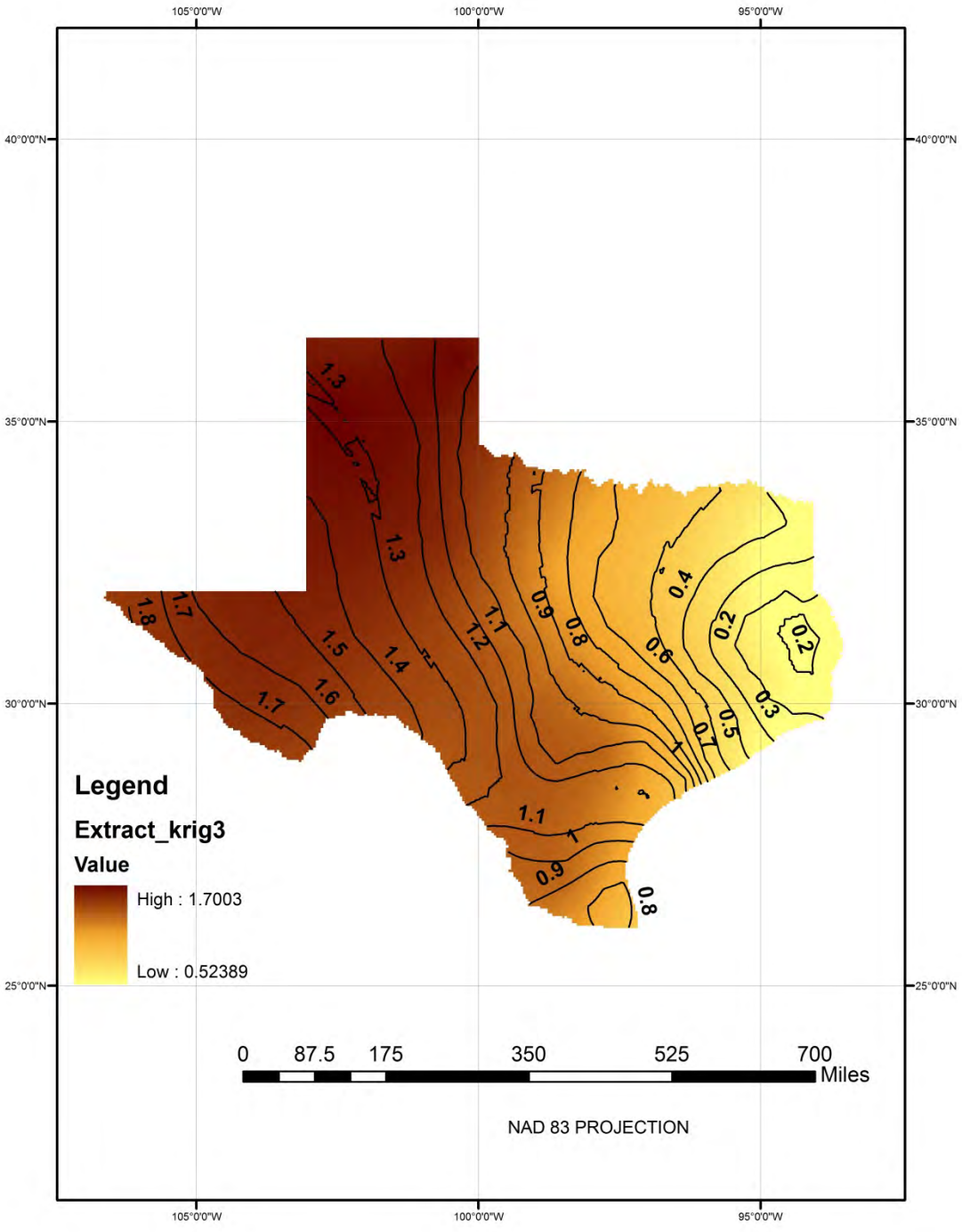

Figure 10a. Precipitation based iso severity map for 3 months drought duration with a return period of 5 years

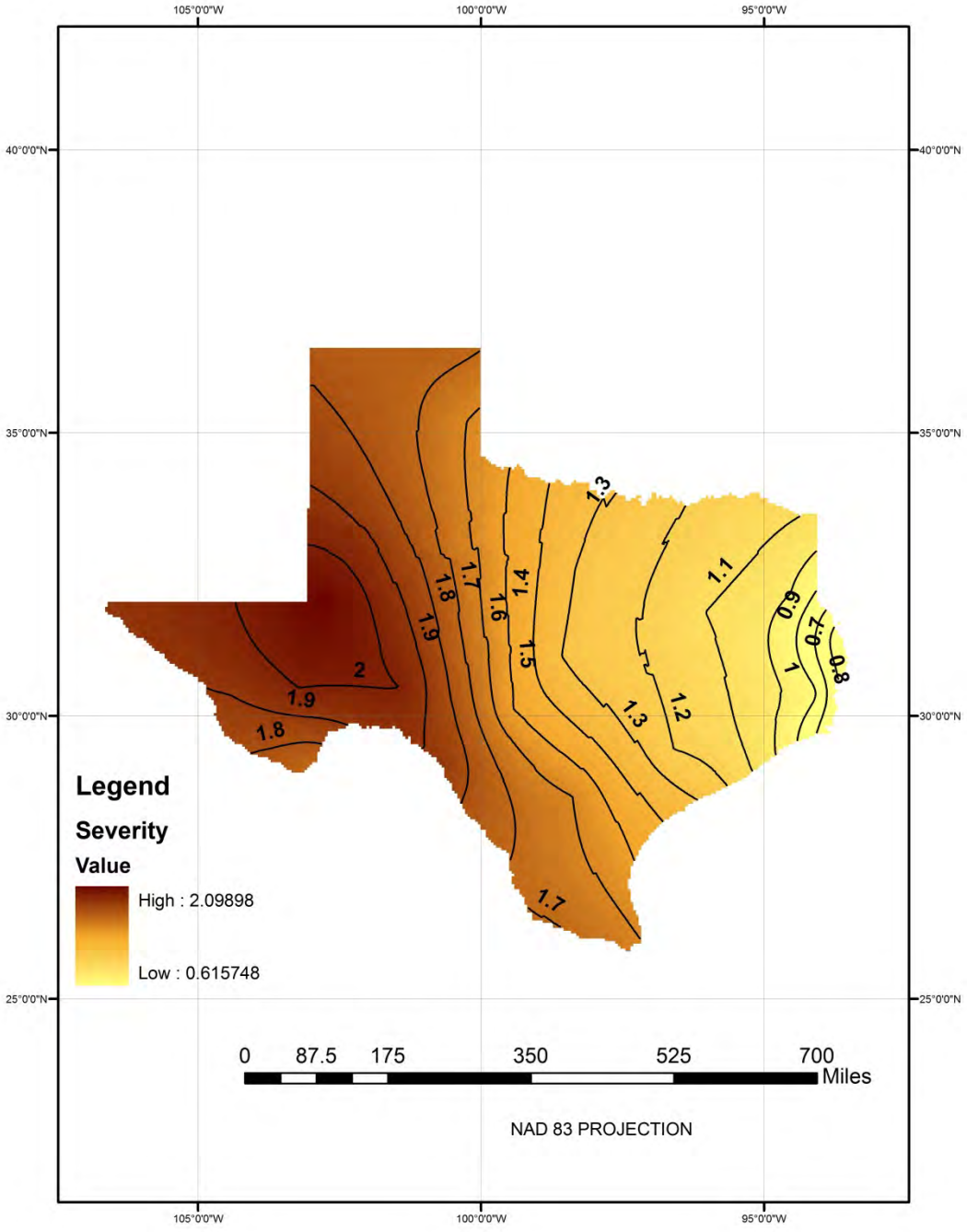

Figure 10b. Precipitation based iso severity map for 3 months drought duration with a return period of 10 years

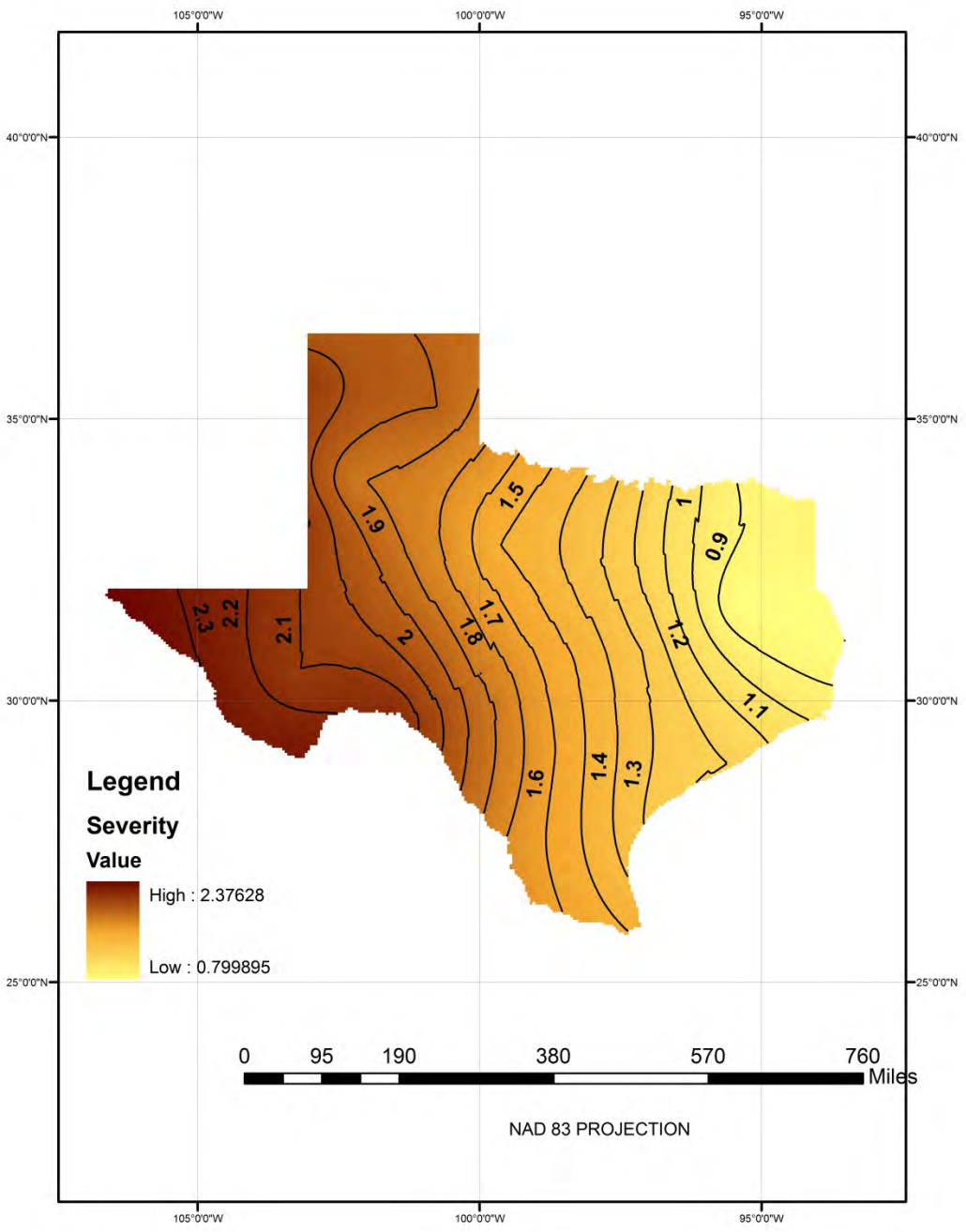

Figure 10c. Precipitation based iso severity map for 3 months drought duration with a return period of 25 years

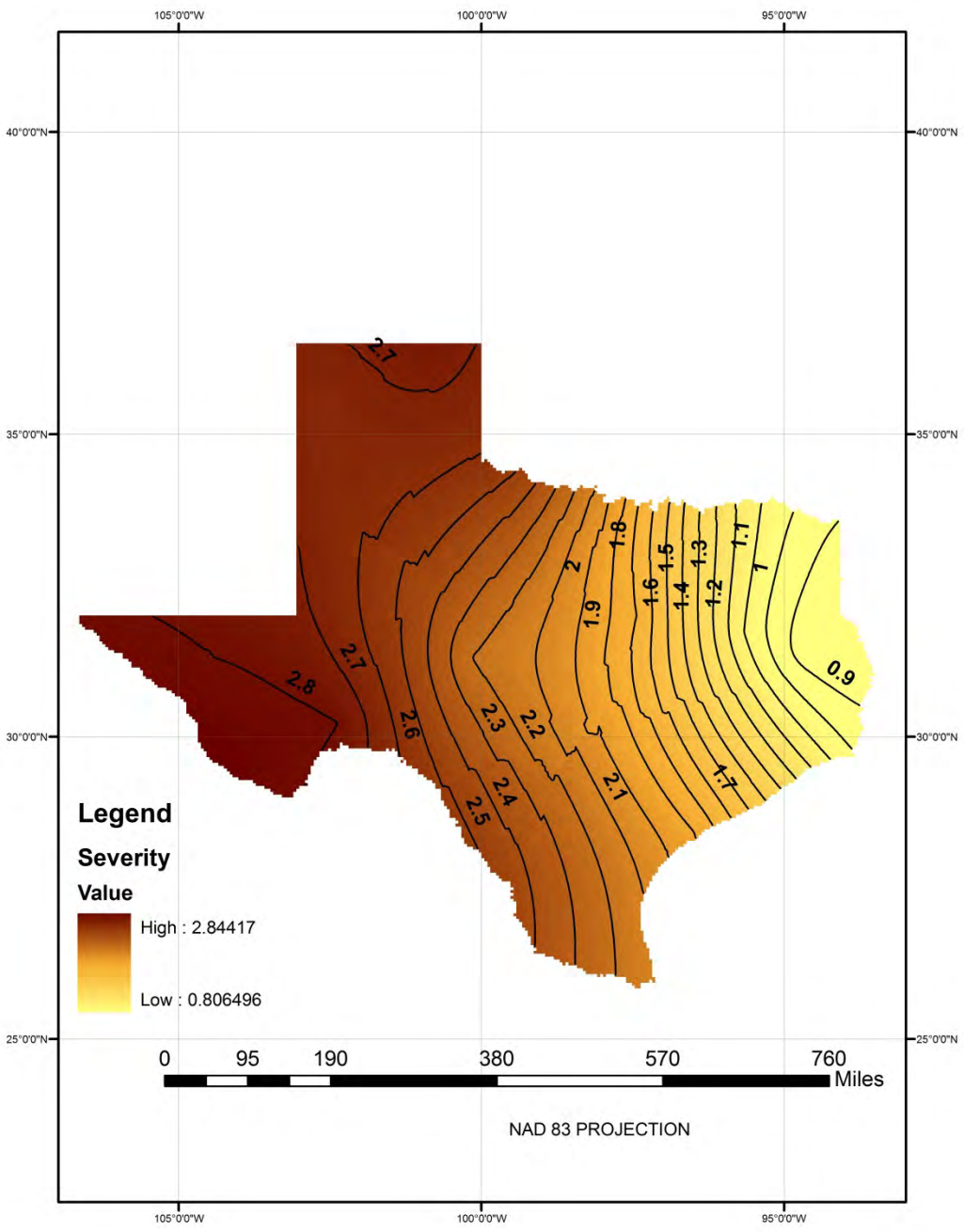

Figure 10d. Precipitation based iso severity map for 3 months drought duration with a return period of 50 years

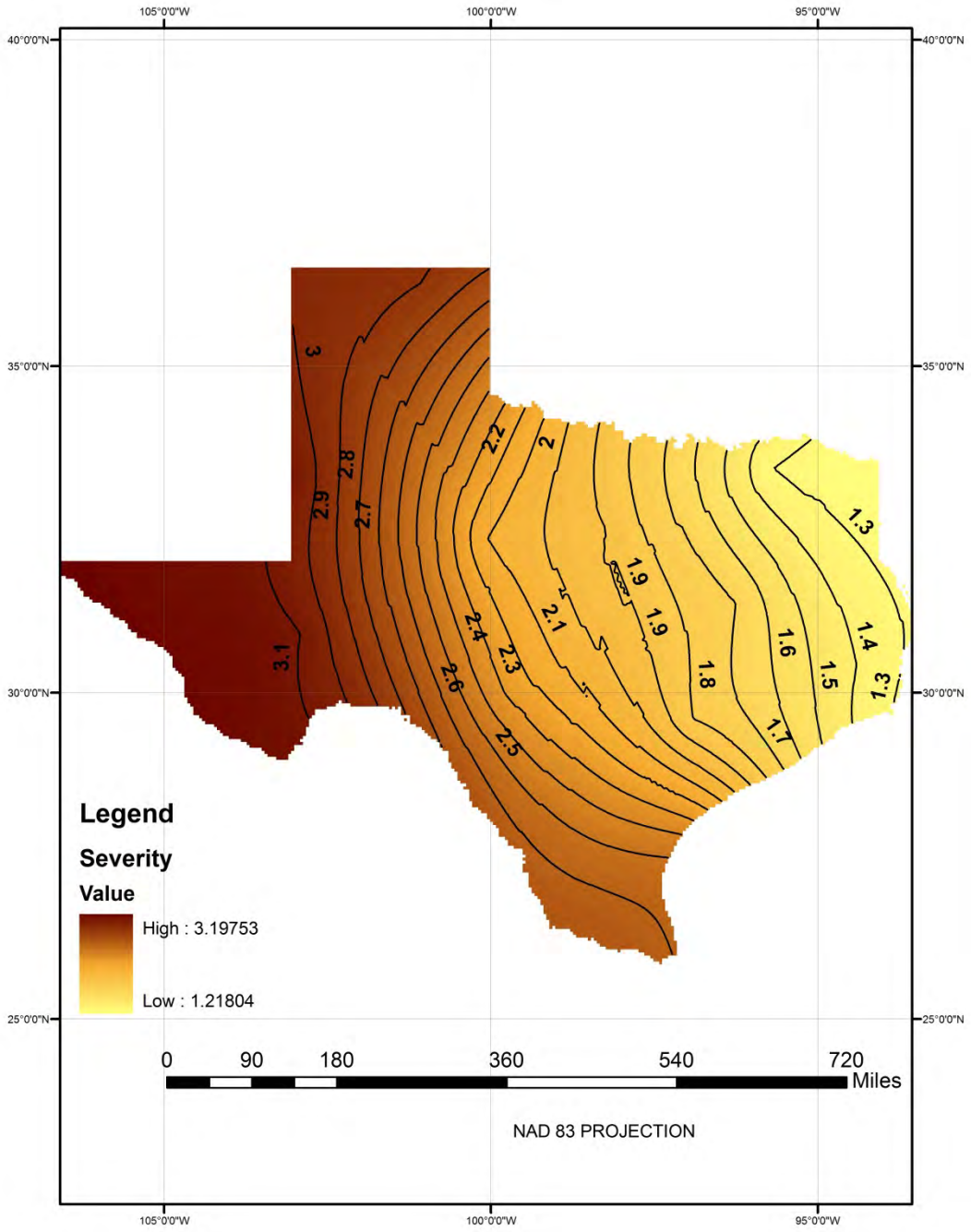

Figure 10e. Precipitation based iso severity map for 3 months drought duration with a return period of 100 years

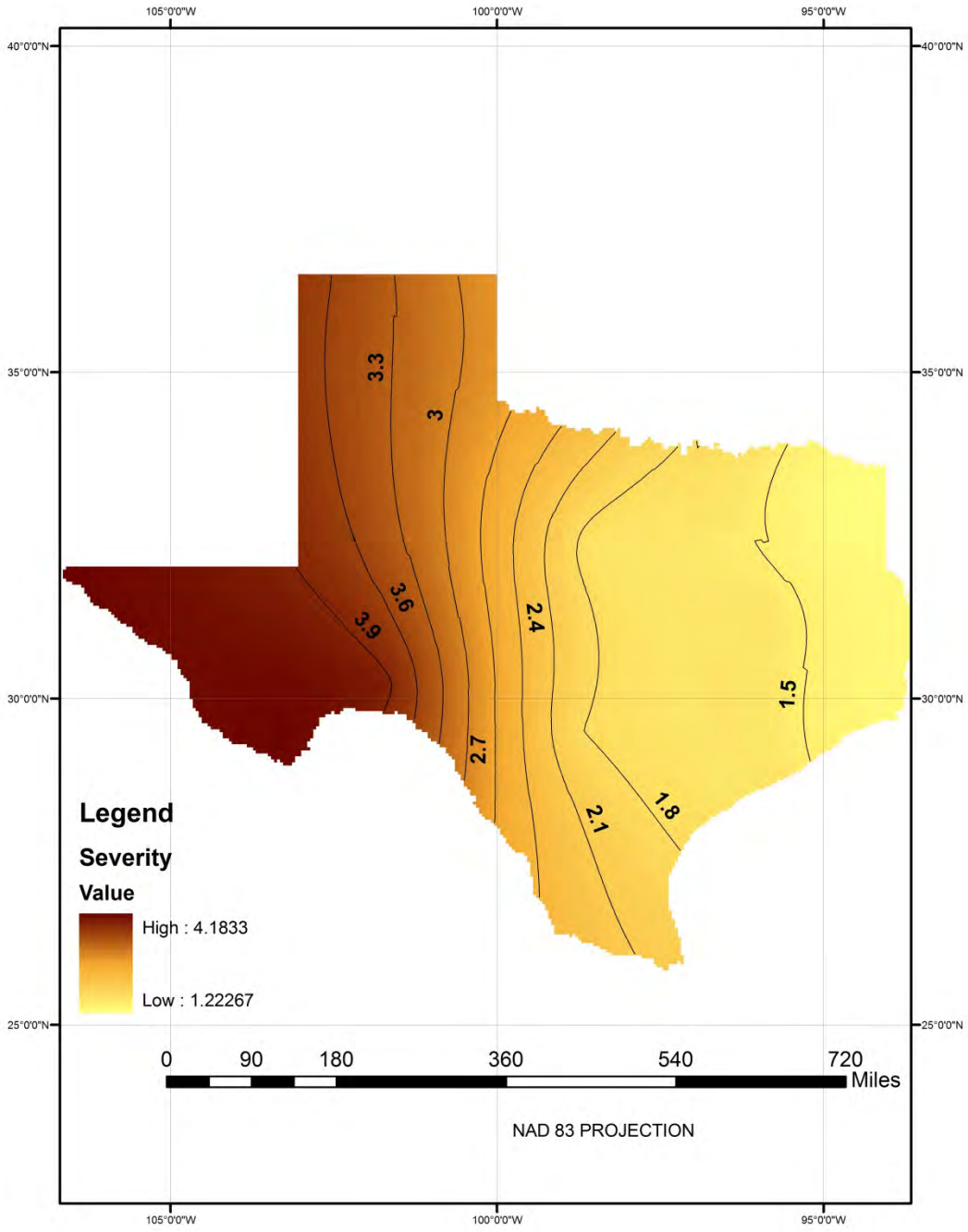

Figure 10f. Precipitation based iso severity map for 6 months drought duration with a return period of 5 years

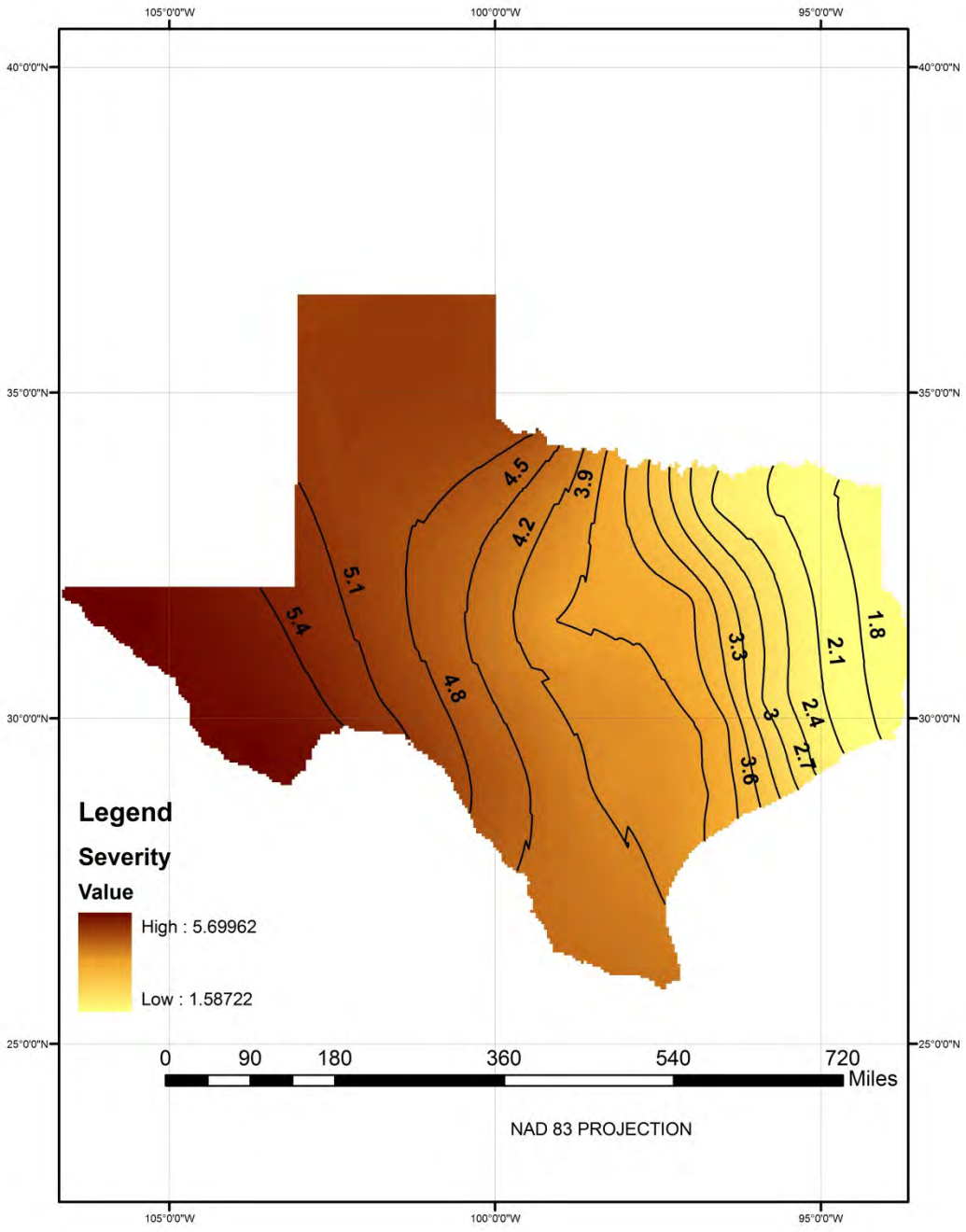

Figure 10g. Precipitation based iso severity map for 6 months drought duration with a return period of 10 years

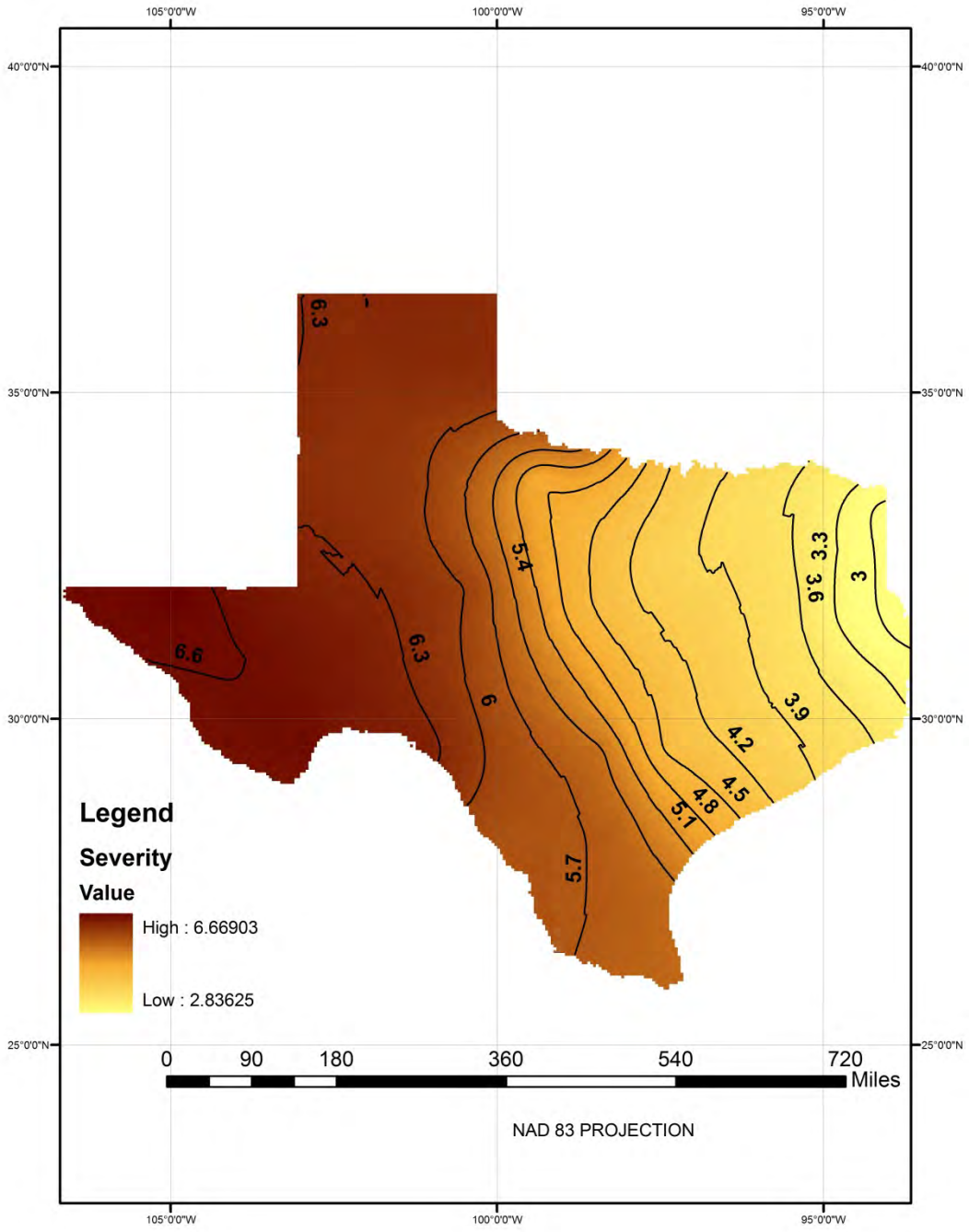

Figure 10h. Precipitation based iso severity map for 6 months drought duration with a return period of 25 years

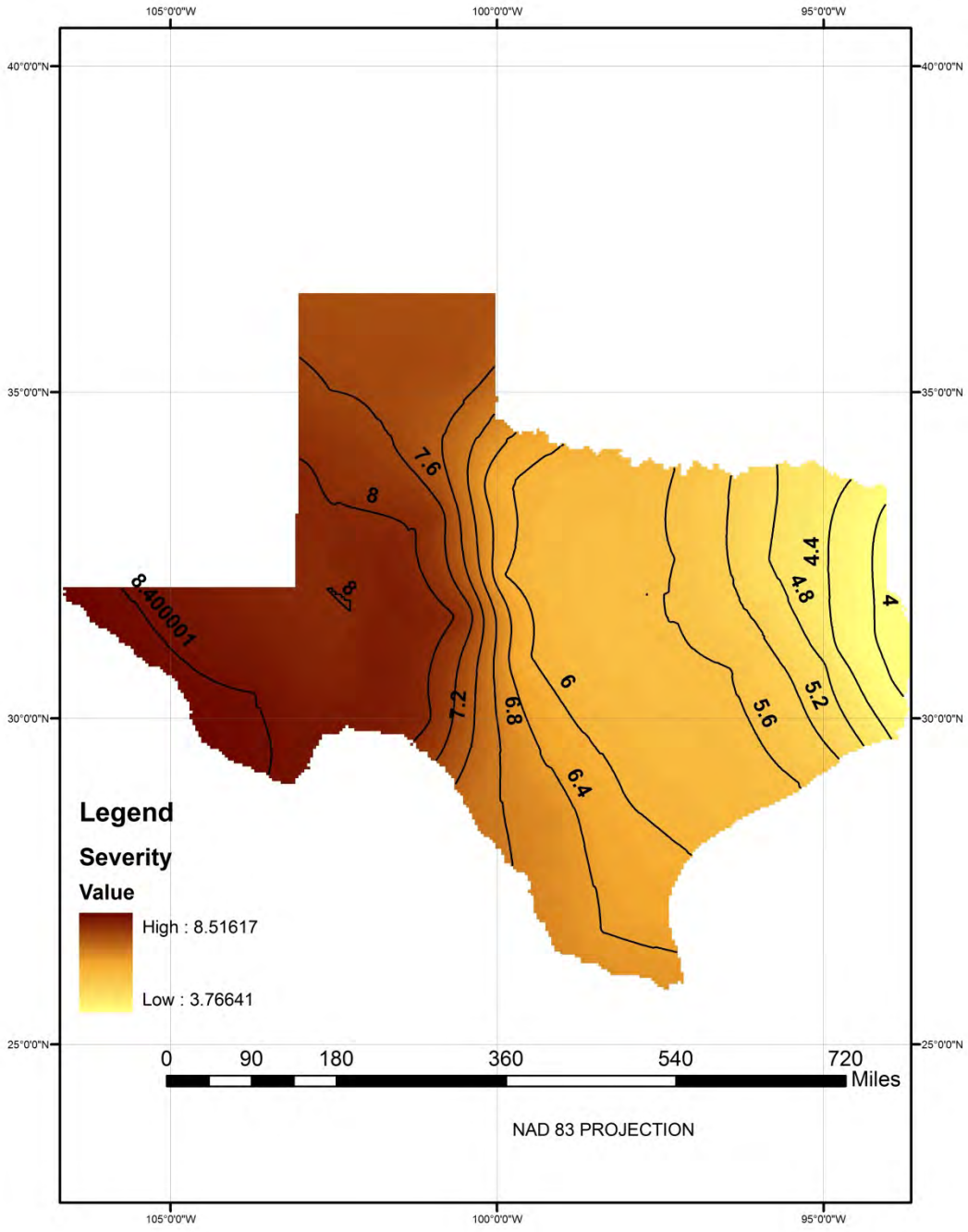

Figure 10i. Precipitation based iso severity map for 6 months drought duration with a return period of 50 years

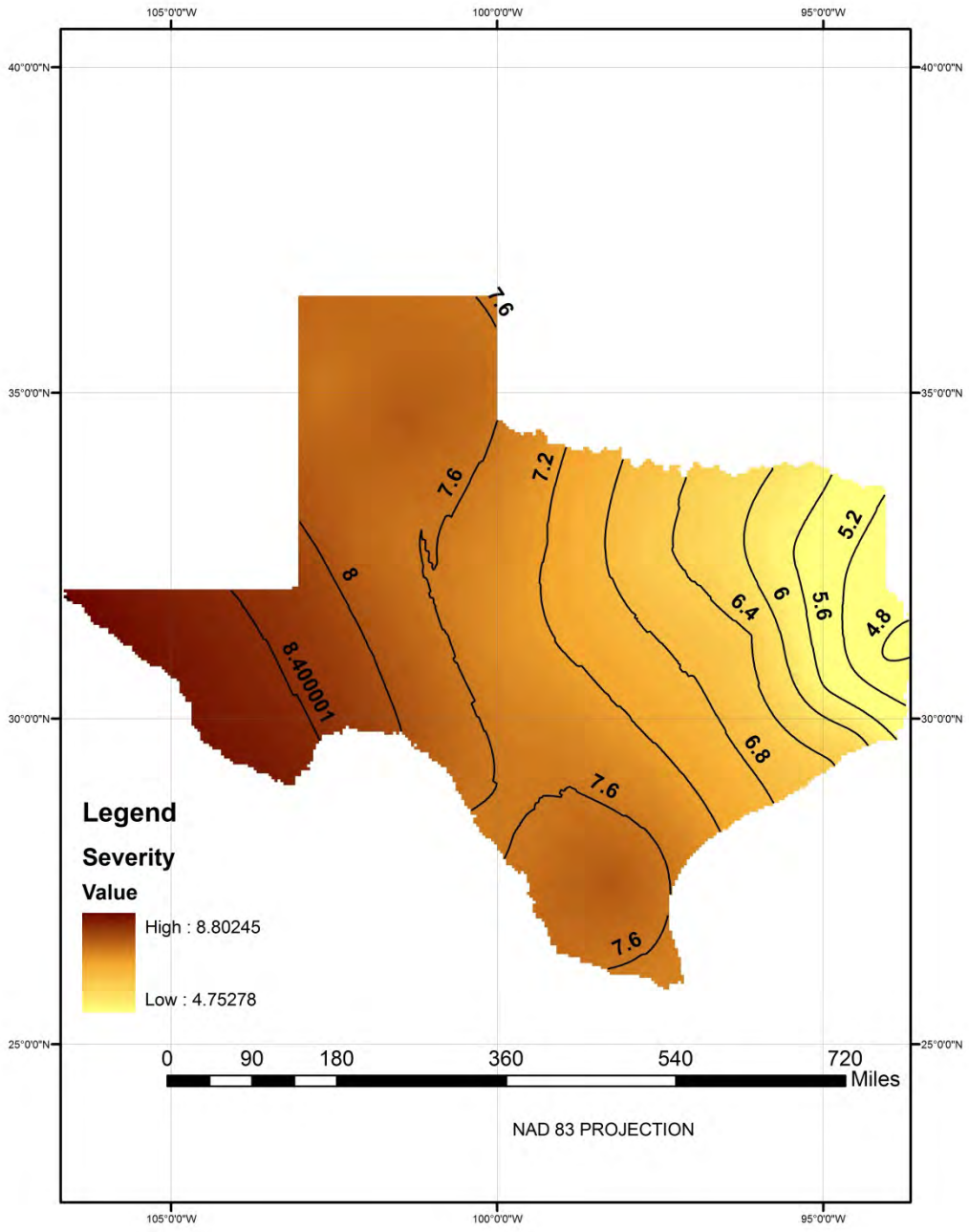

Figure 10j. Precipitation based iso severity map for 6 months drought duration with a return period of 100 years

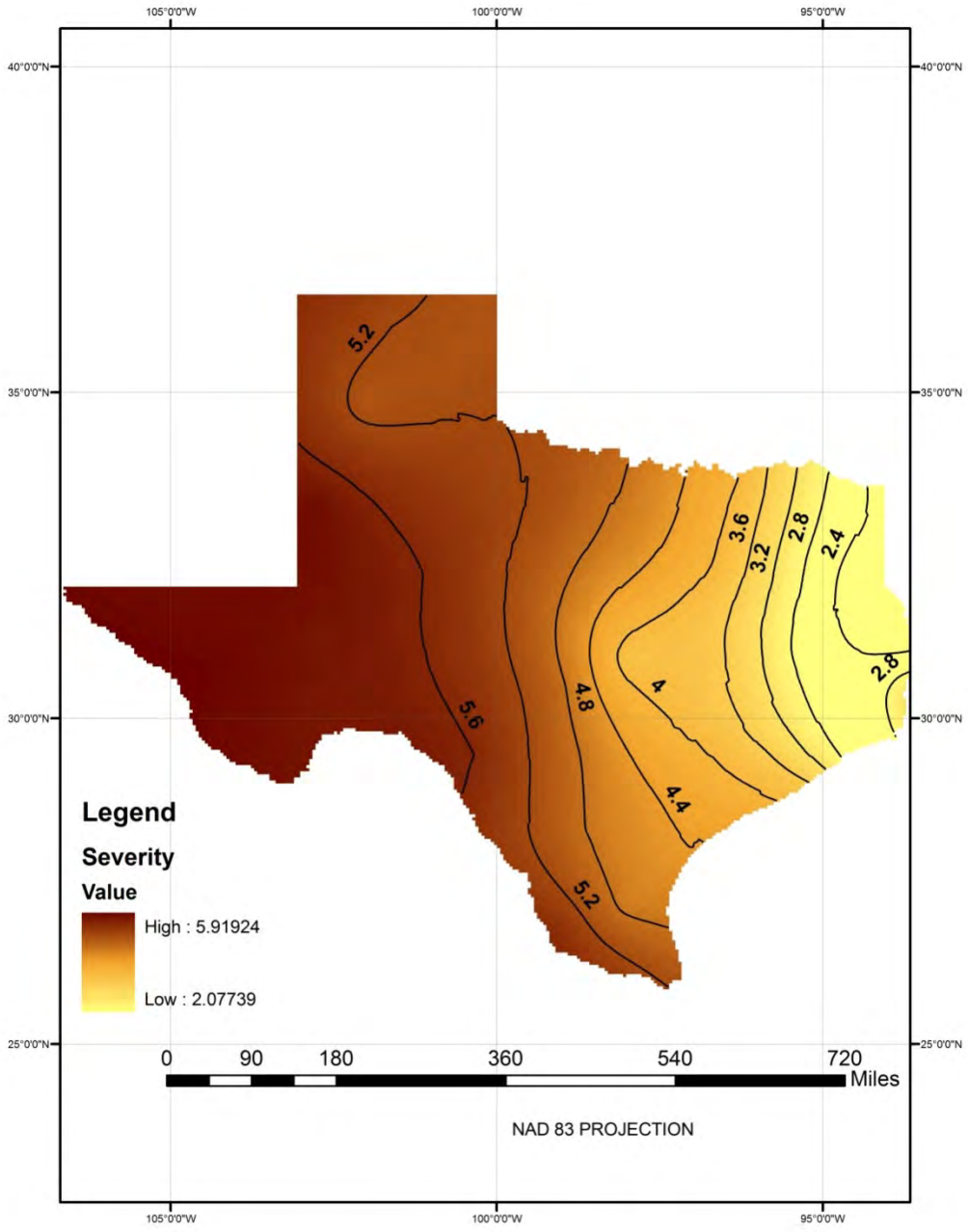

Figure 10k. Precipitation based iso severity map for 9 months drought duration with a return period of 5 years

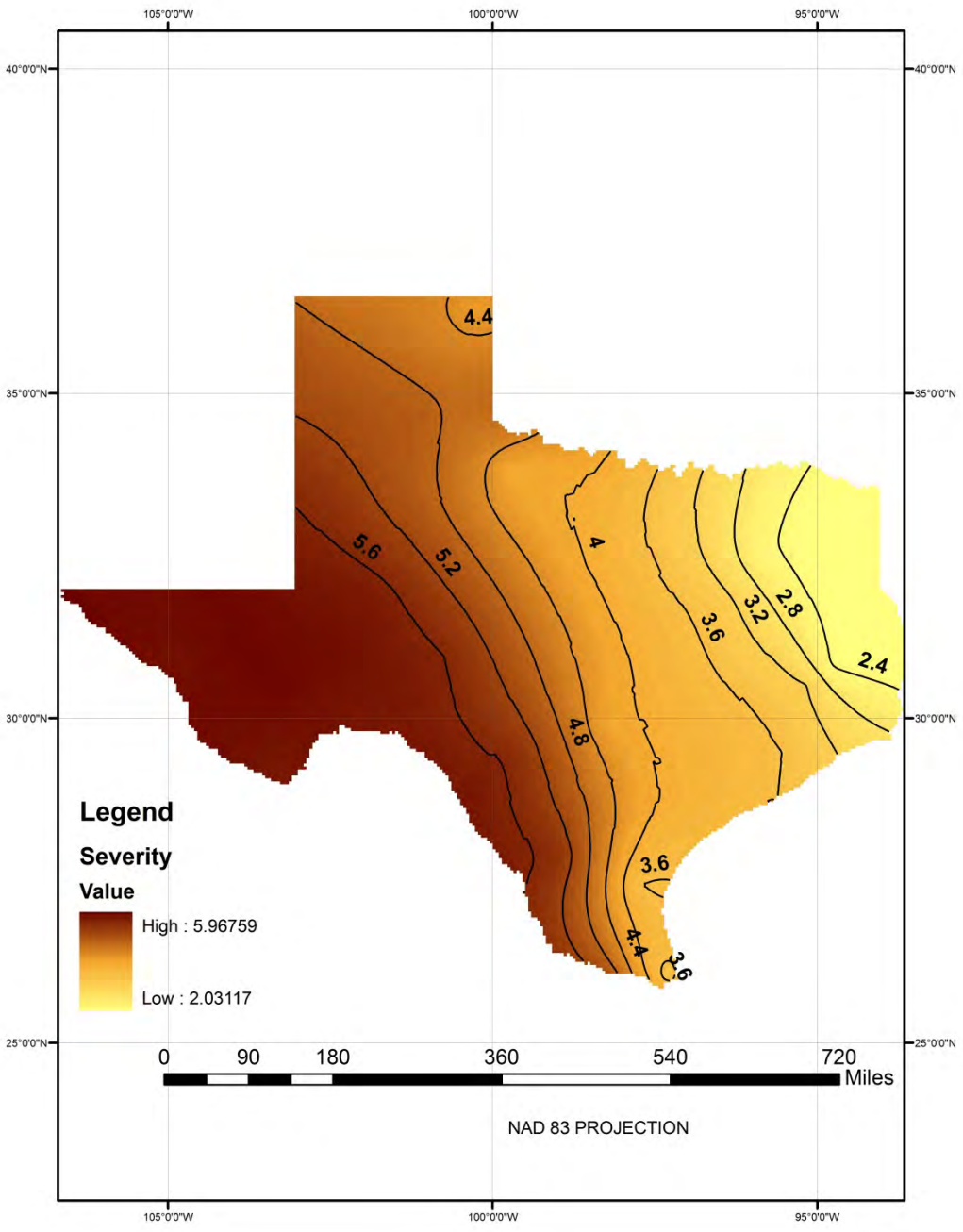

Figure 10l. Precipitation based iso severity map for 9 months drought duration with a return period of 10 years

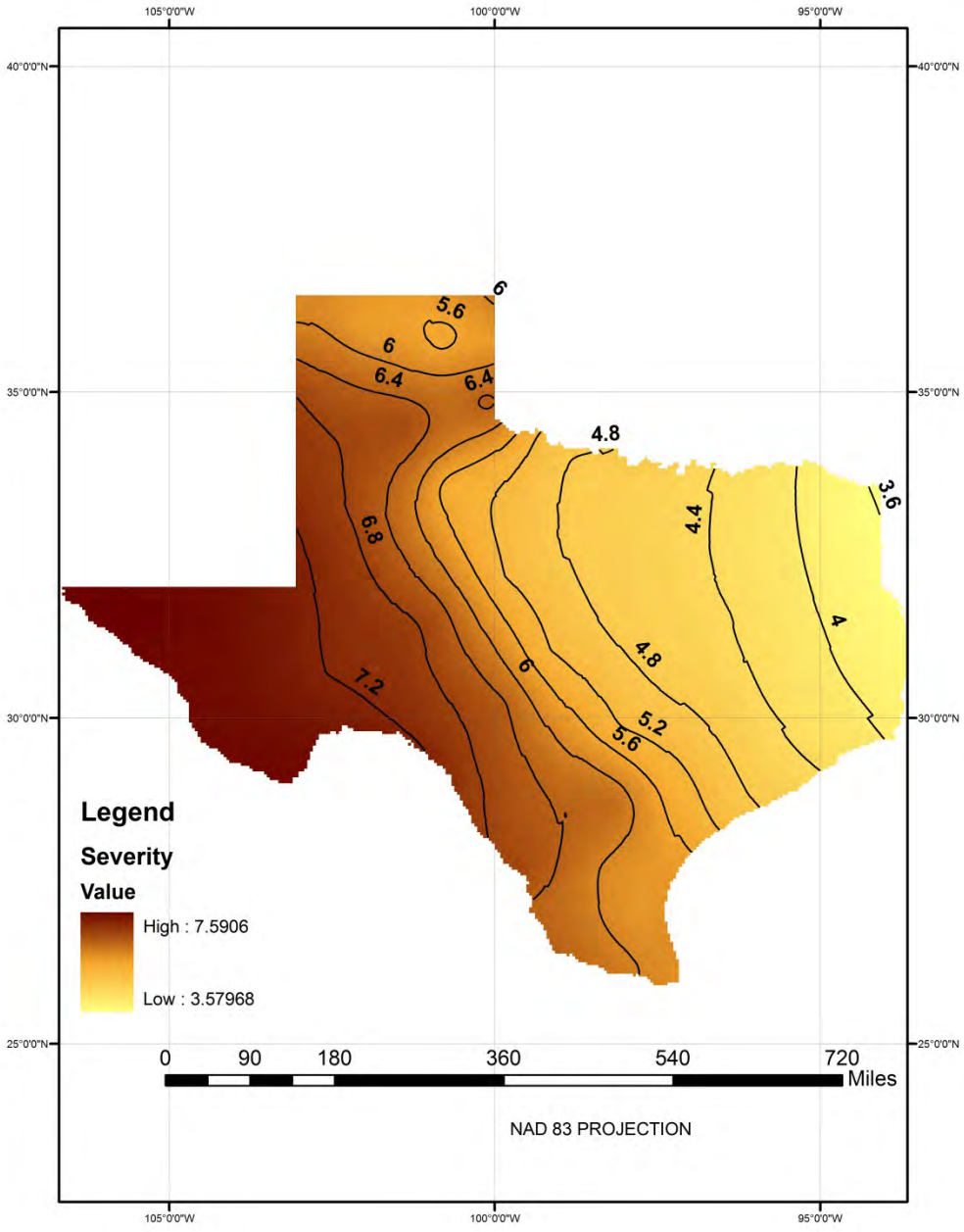

Figure 10m. Precipitation based iso severity map for 9 months drought duration with a return period of 25 years

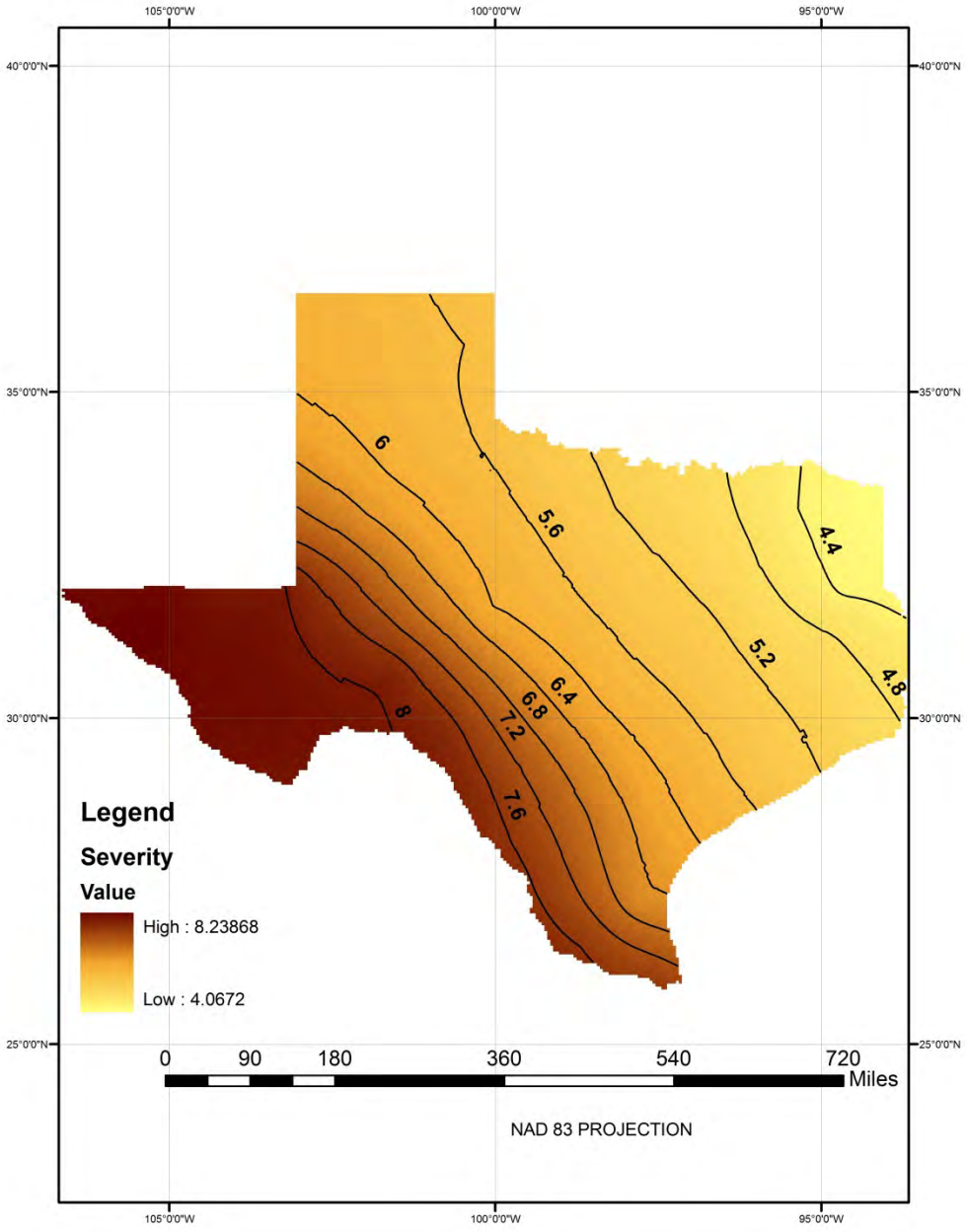

Figure 10n. Precipitation based iso severity map for 9 months drought duration with a return period of 50 years

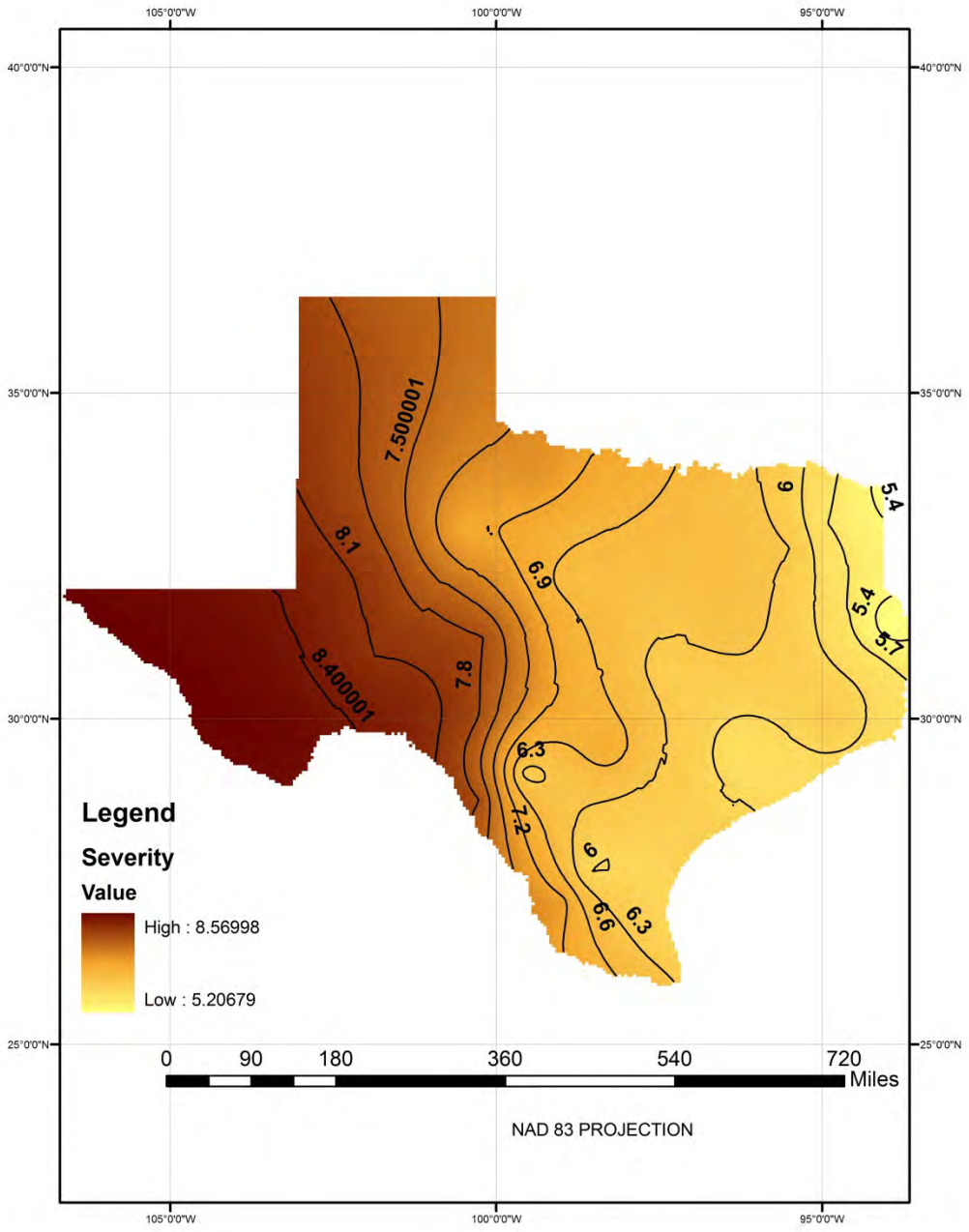

Figure 10o. Precipitation based iso severity map for 9 months drought duration with a return period of 100 years

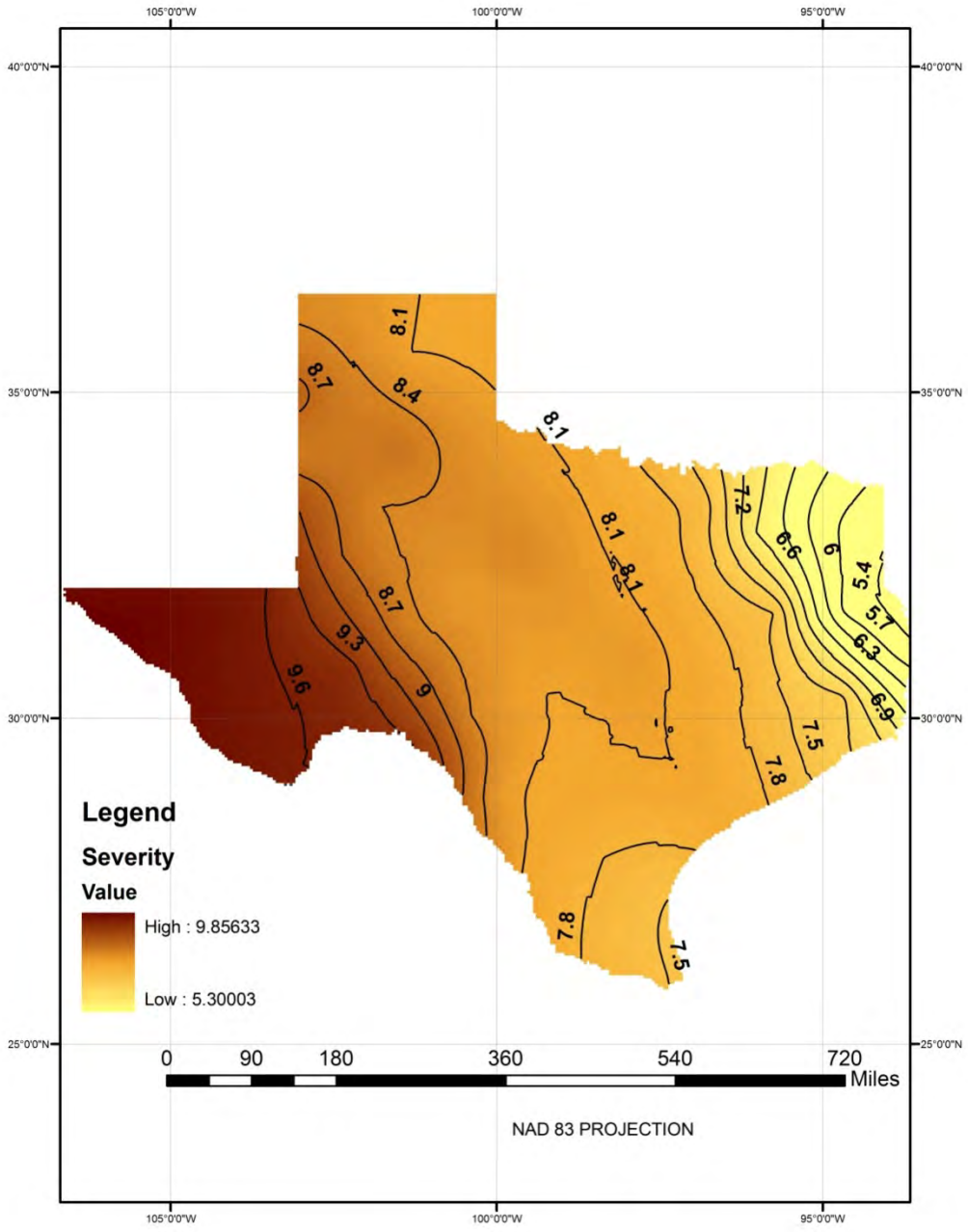

Figure 10p. Precipitation based iso severity map for 12 months drought duration with a return period of 5 years

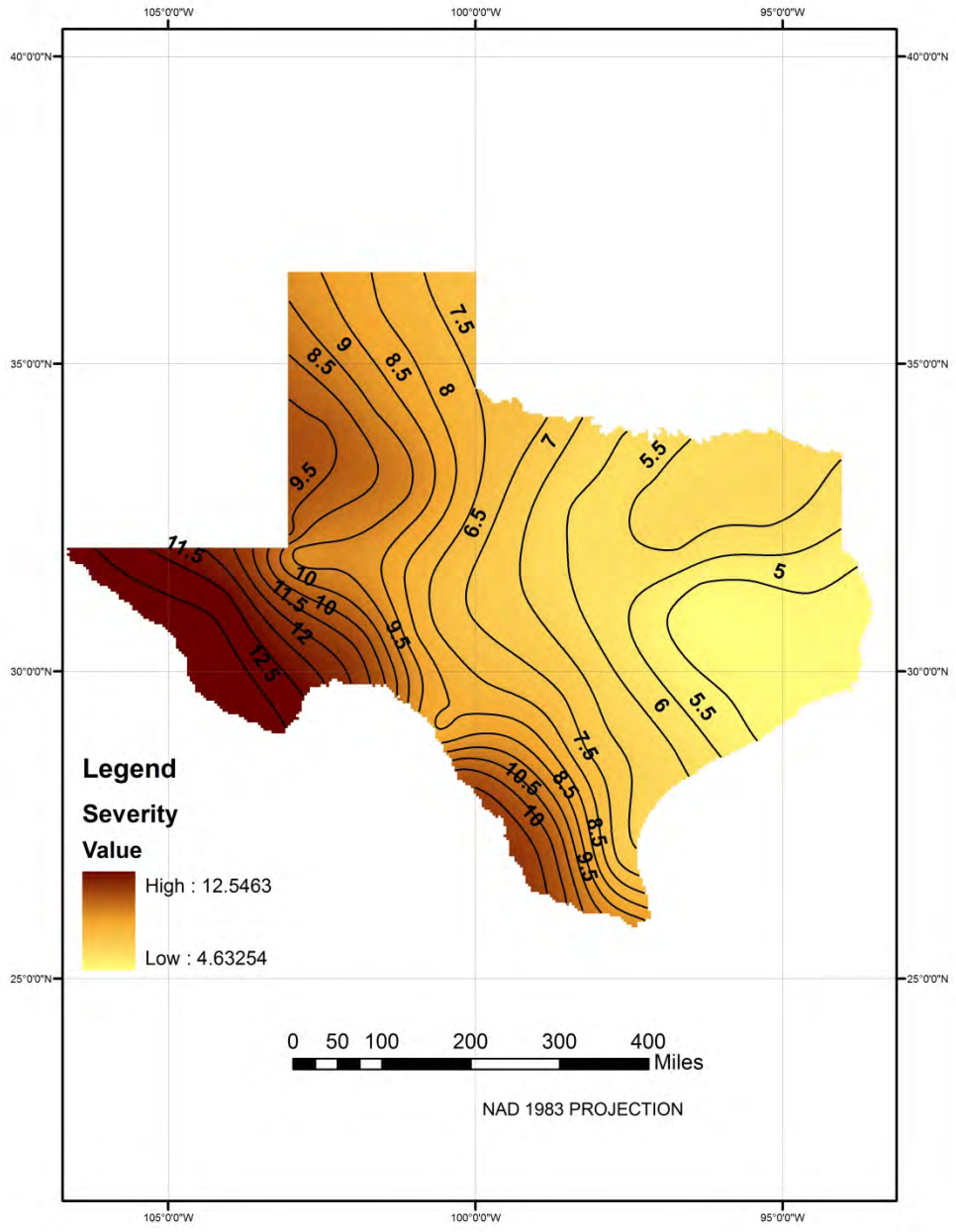

Figure 10q. Precipitation based iso severity map for 12 months drought duration with a return period of 10 years

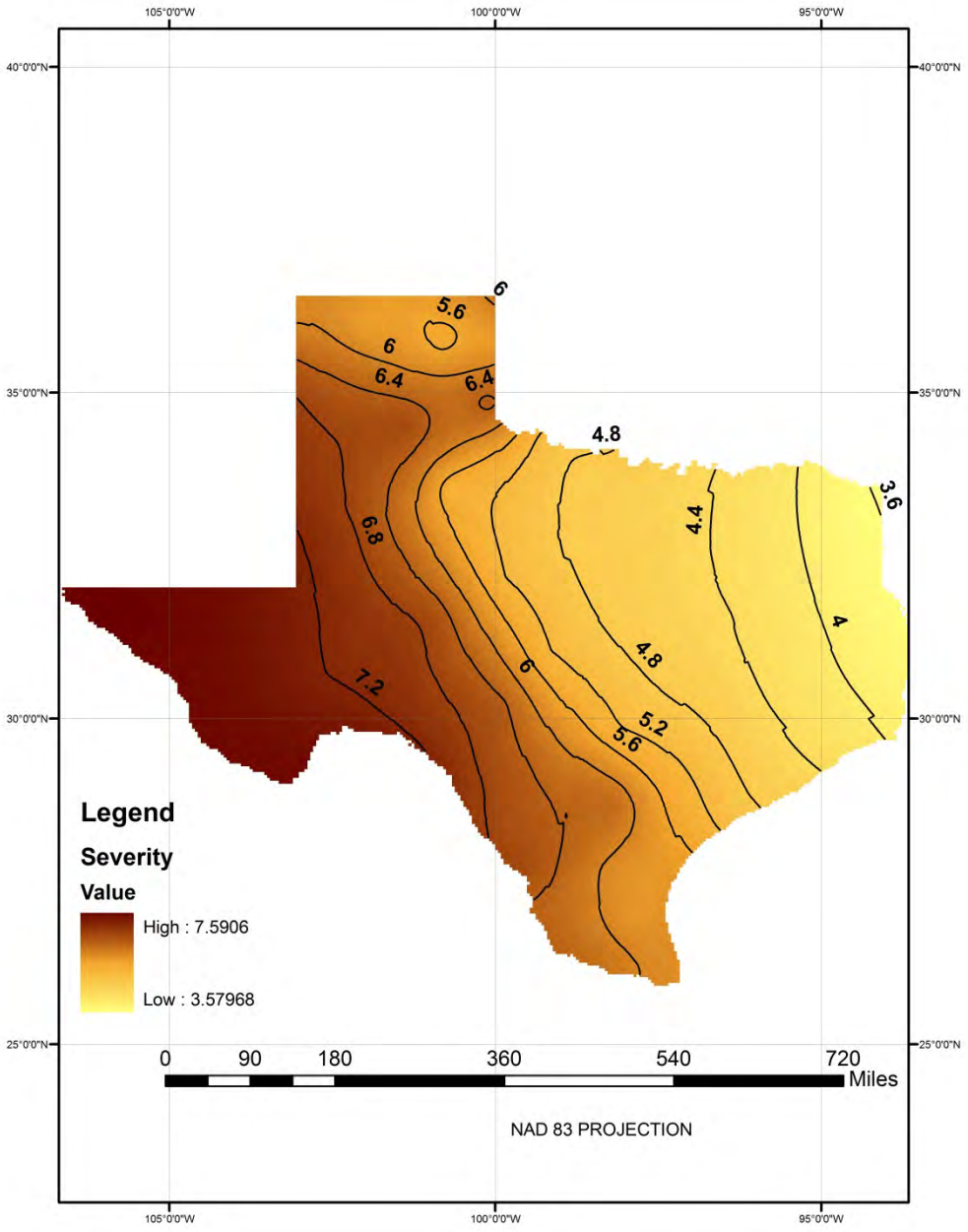

Figure 10r. Precipitation based iso severity map for 12 months drought duration with a return period of 25 years

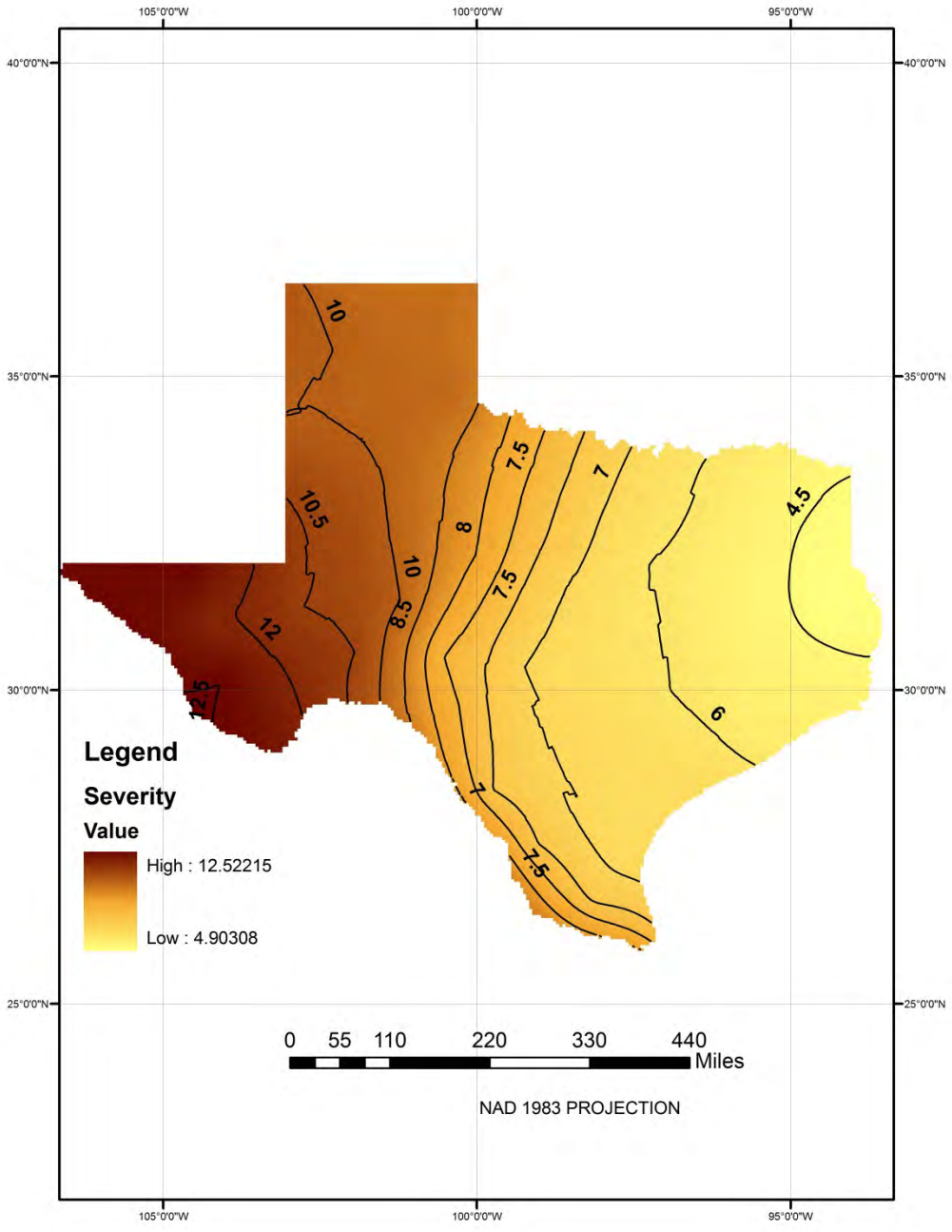

Figure 10s. Precipitation based iso severity map for 12 months drought duration with a return period of 50 years

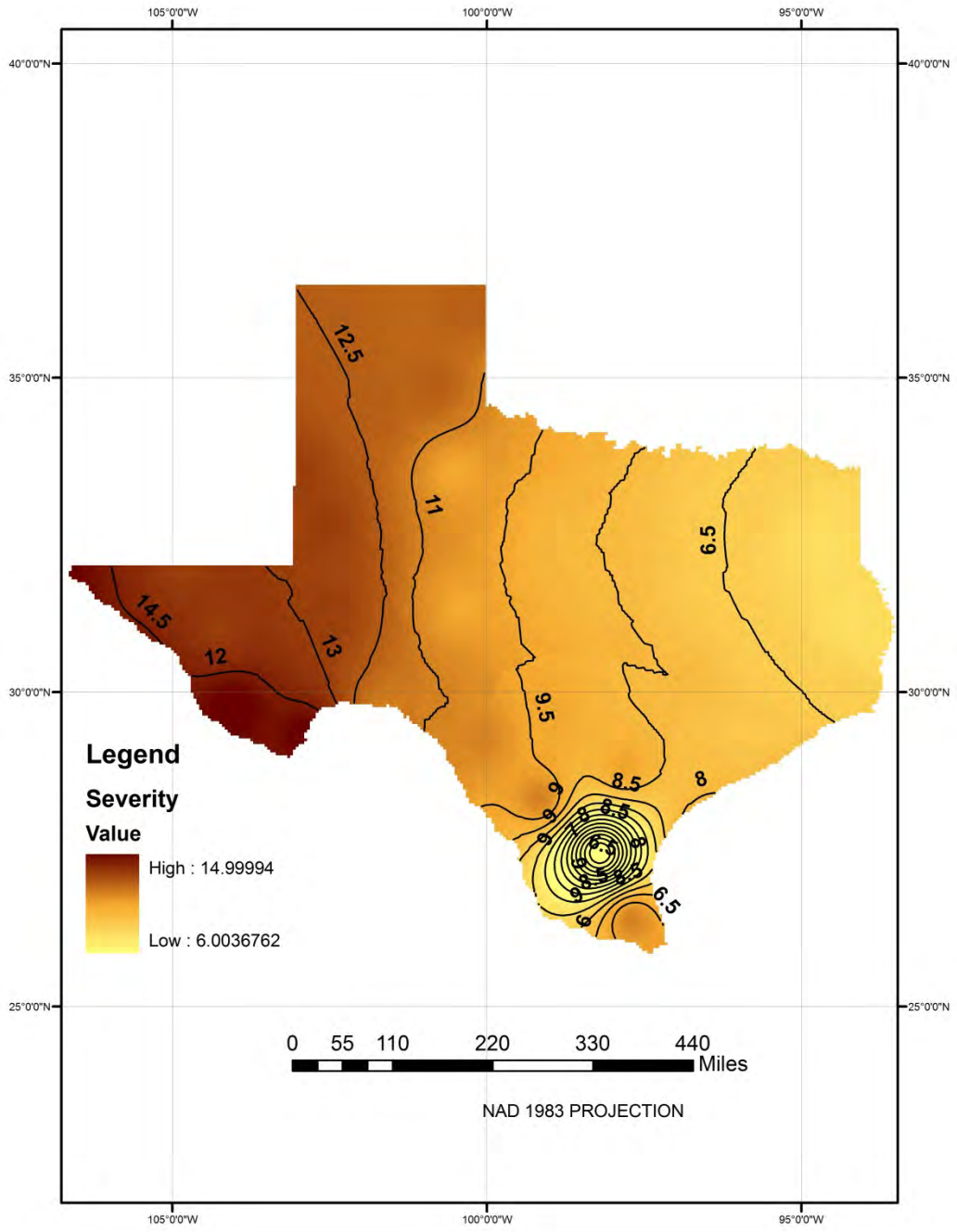

Figure 10t. Precipitation based iso severity map for 12 months drought duration with a return period of 100 years

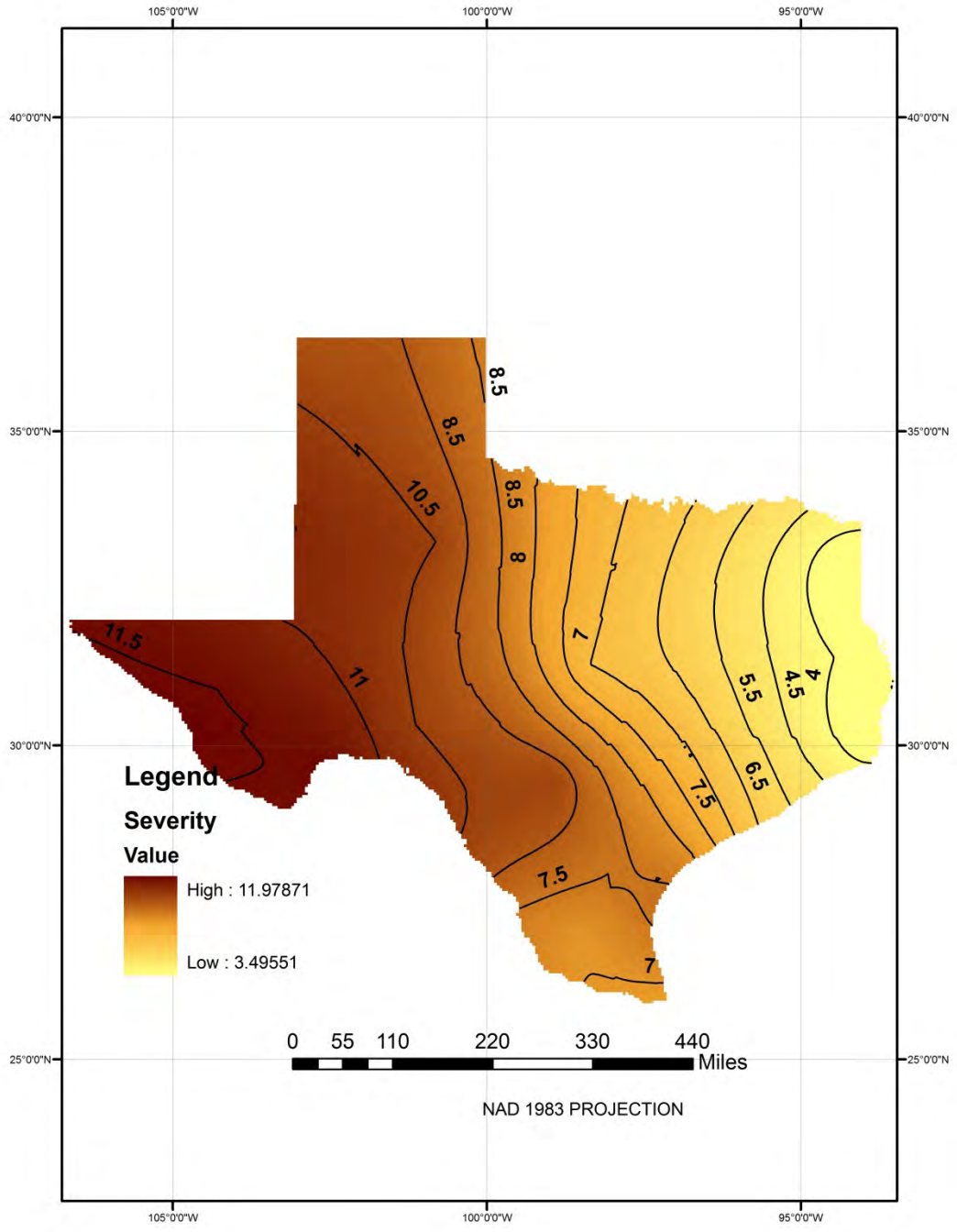

Figure 10u. Precipitation based iso severity map for 18 months drought duration with a return period of 5 years

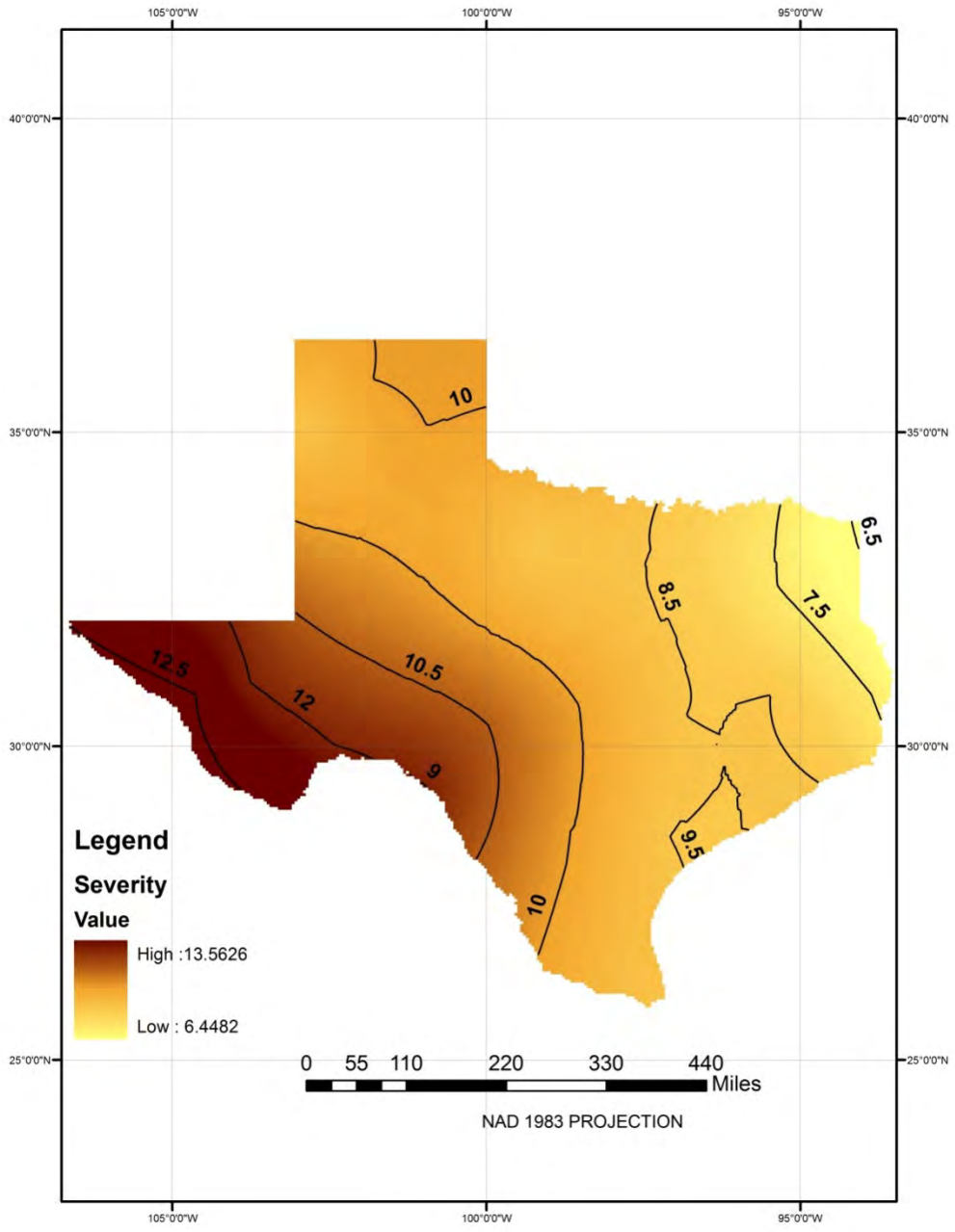

Figure 10v. Iso severity map for 18 months drought duration with a return period of 10 years

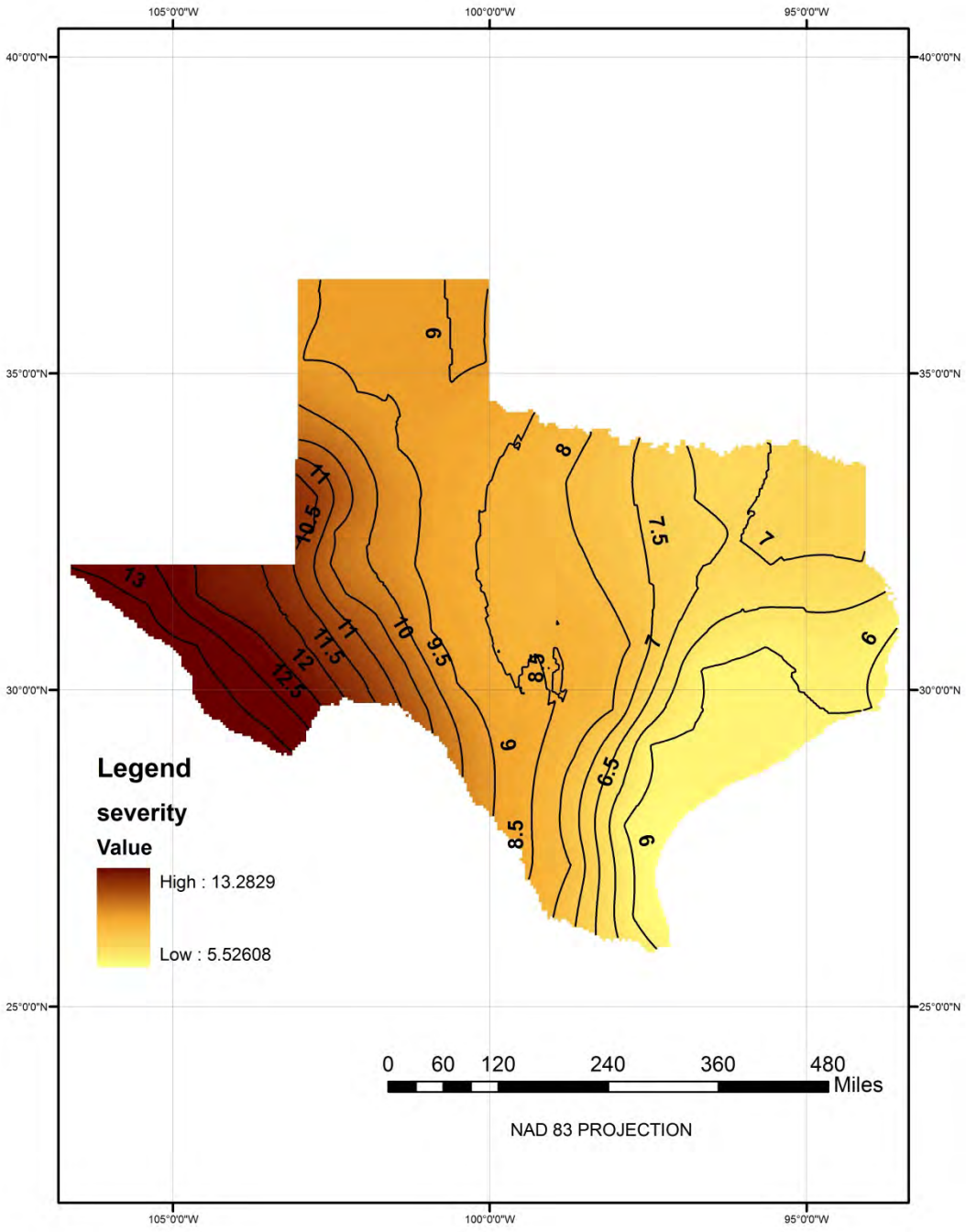

Figure 10w. Precipitation based iso severity map for 18 months drought duration with a return period of 25 years

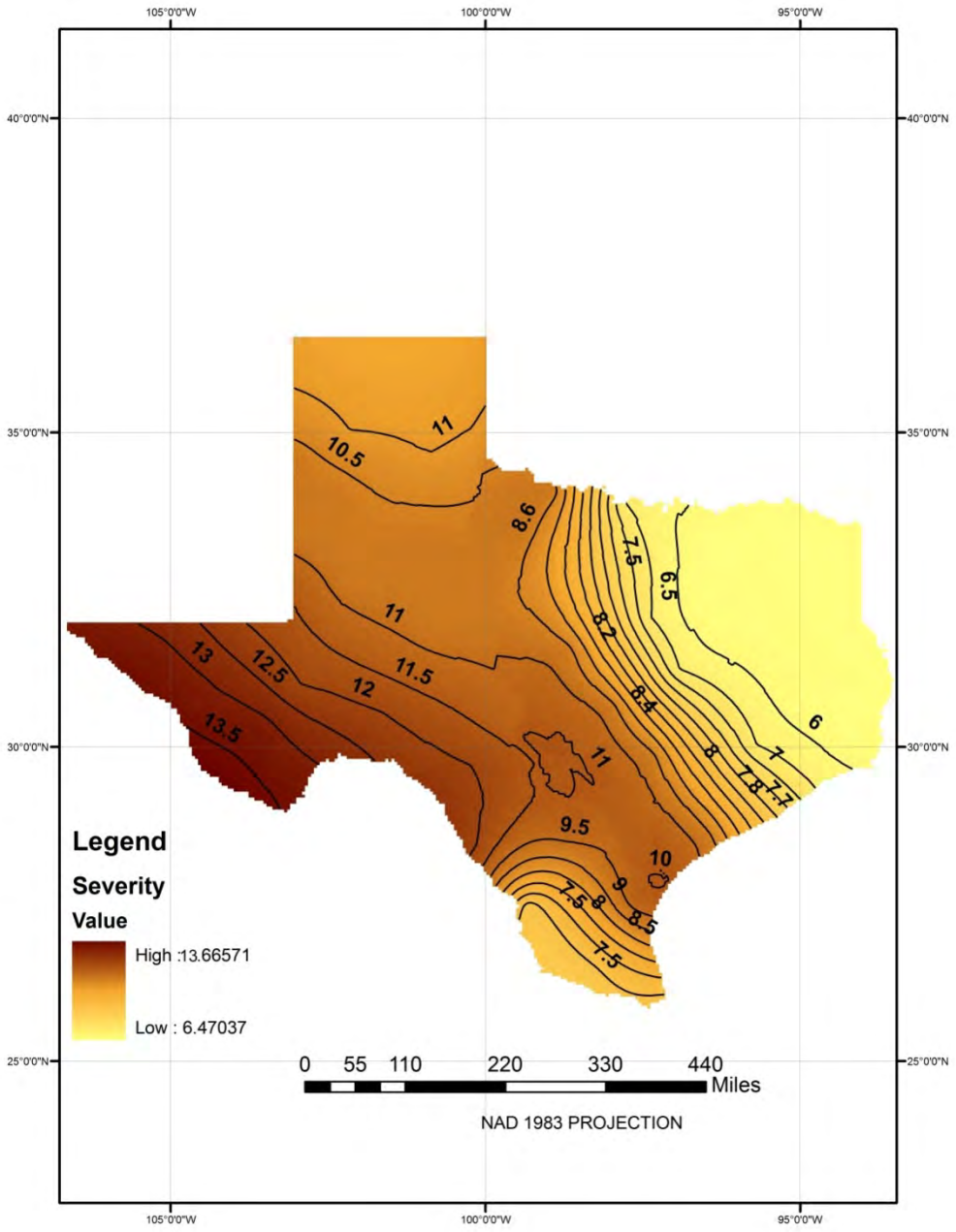

Figure 10x. Precipitation based iso severity map for 18 months drought duration with a return period of 50 years

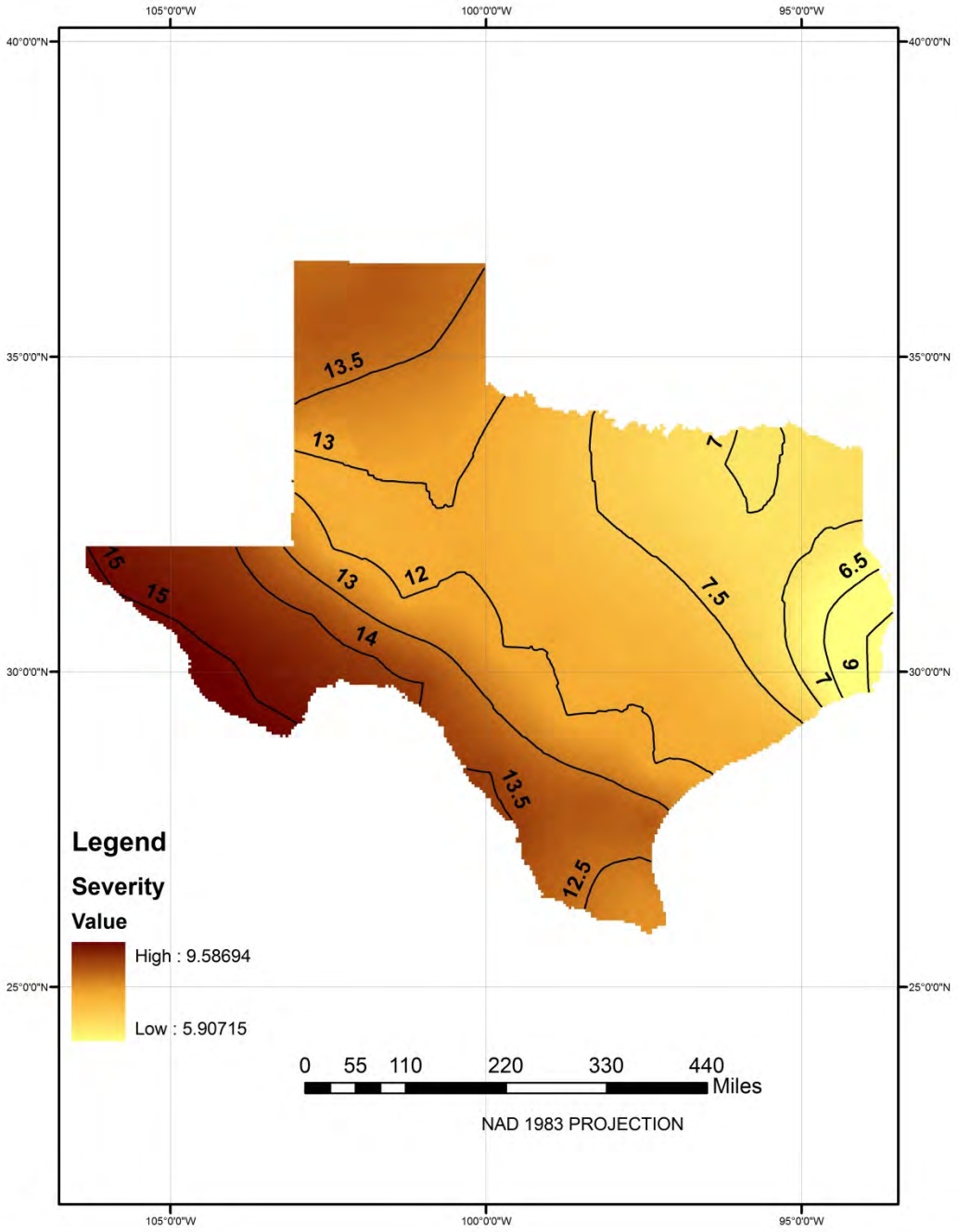

Figure 10y. Precipitation based iso severity map for 18 months drought duration with a return period of 100 years

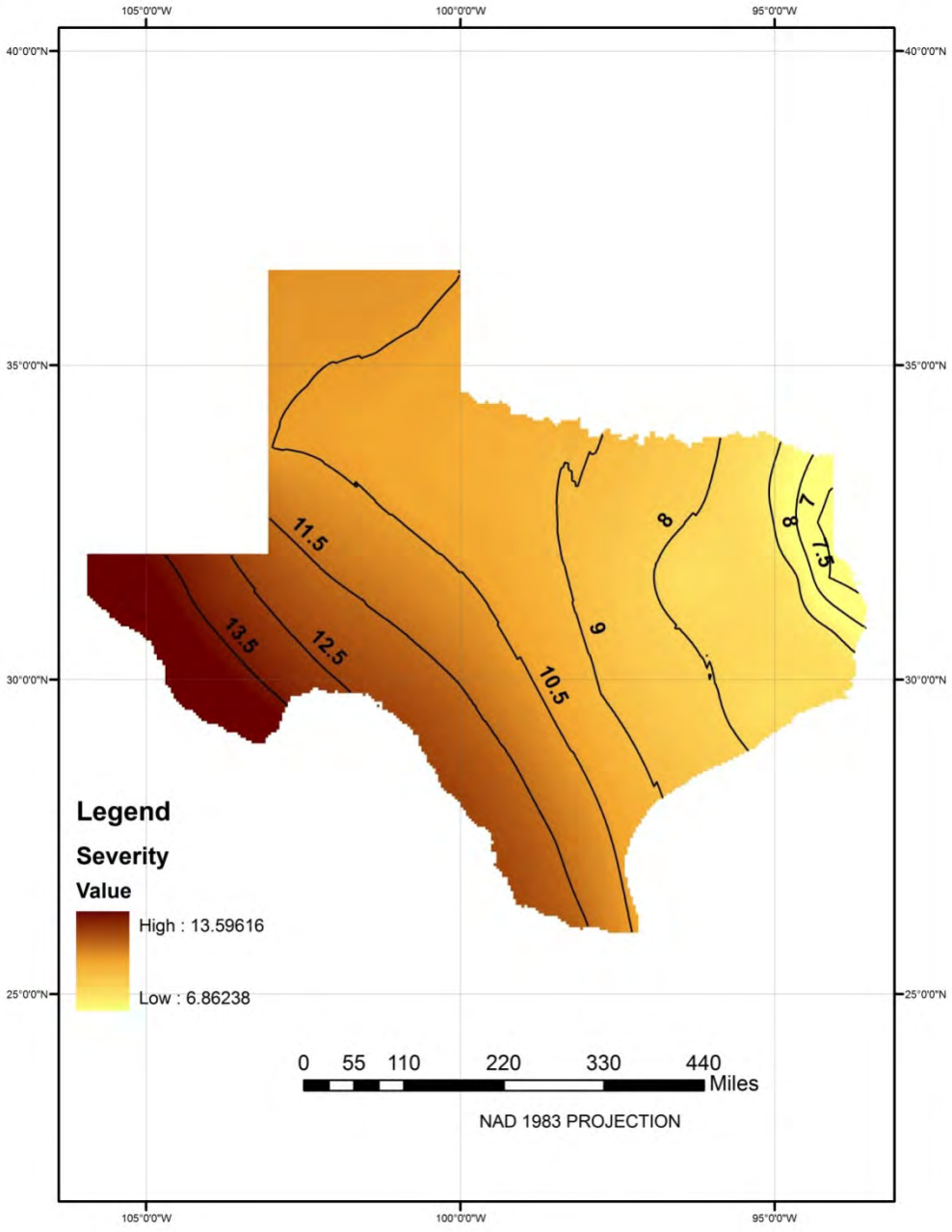

Figure 10z. Precipitation based iso severity map for 24 months drought duration with a return period of 5 years

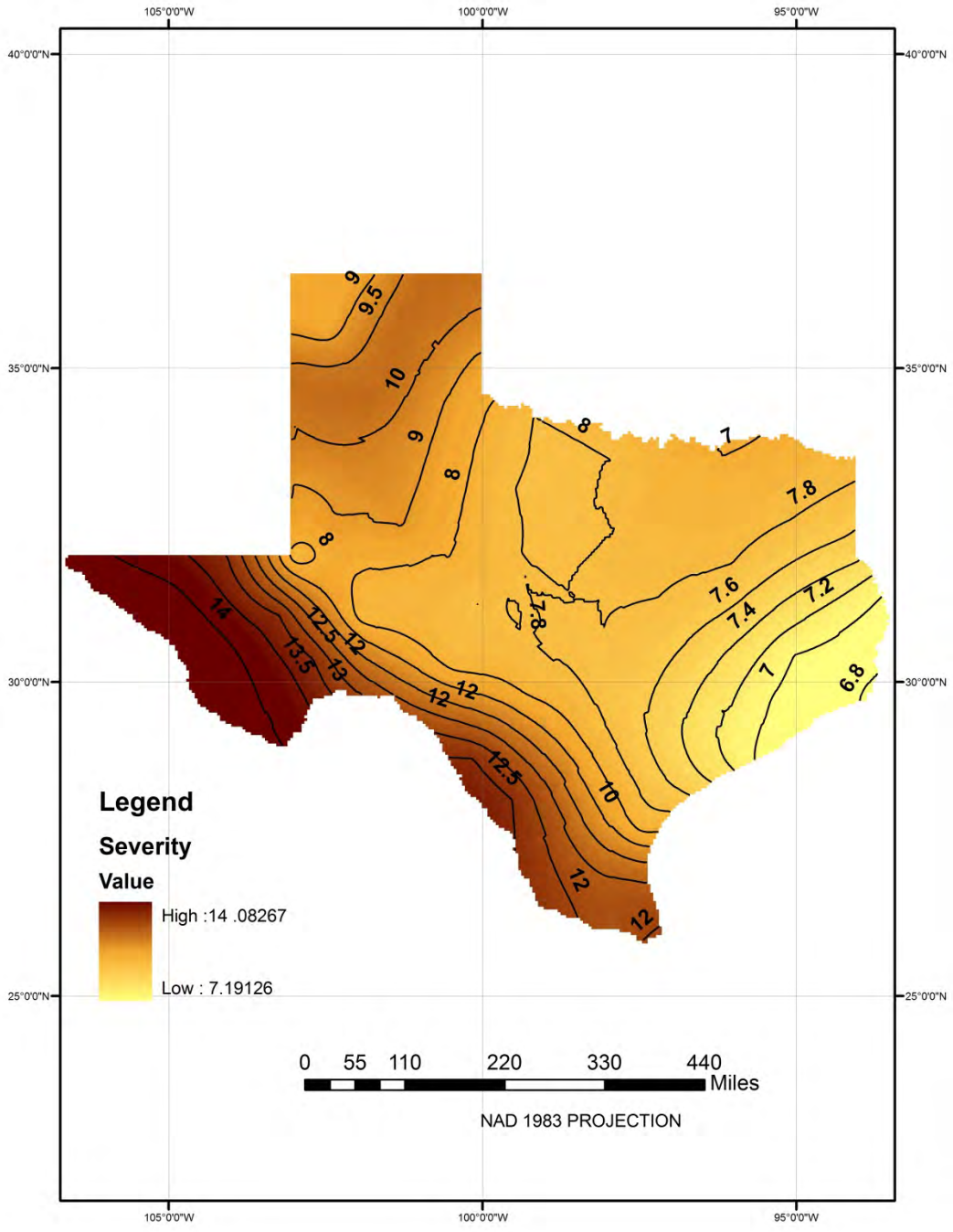

Figure 10aa. Precipitation based iso severity map for 24 months drought duration with a return period of 10 years

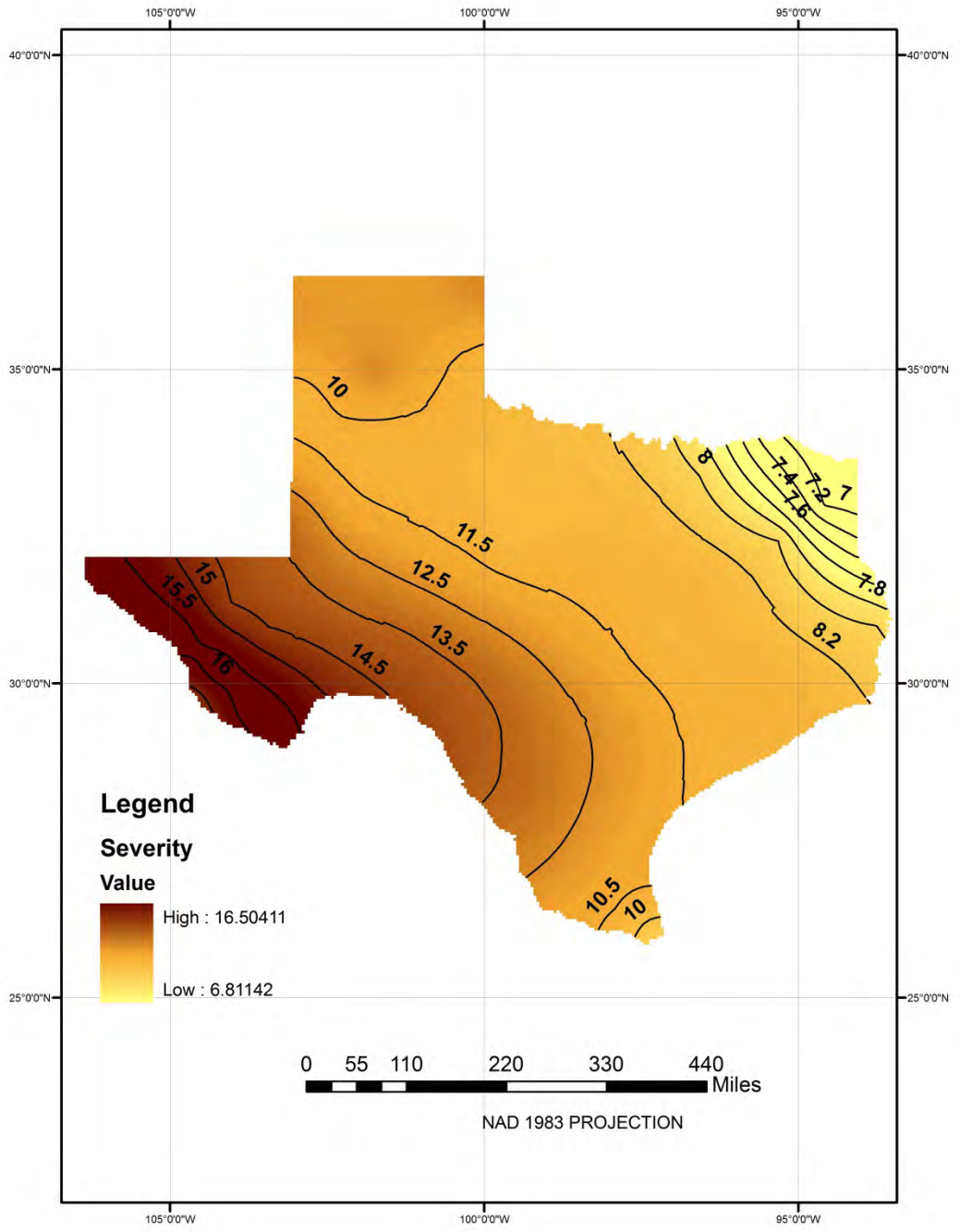

Figure 10ab. Precipitation based iso severity map for 24 months drought duration with a return period of 25 years

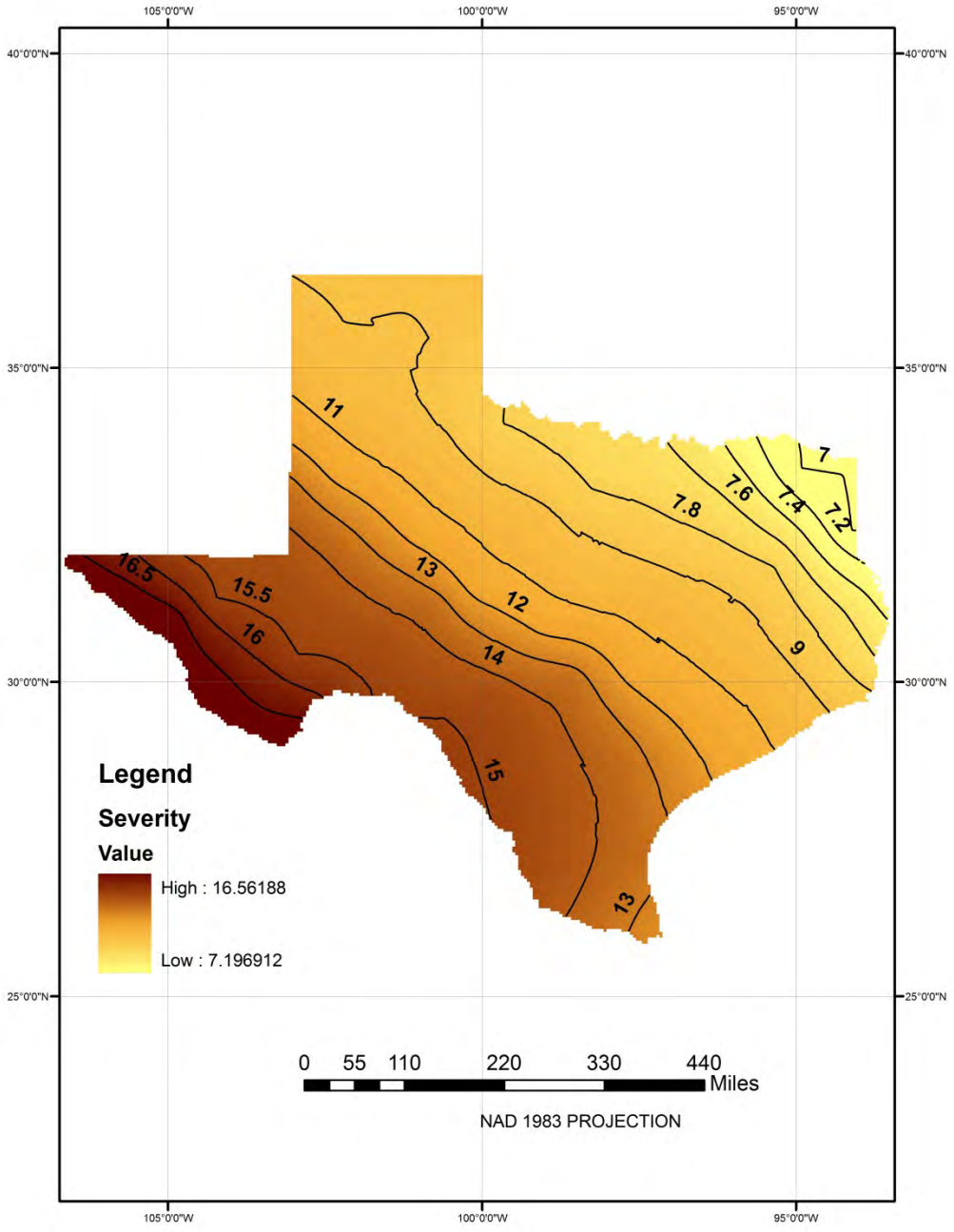

Figure 10ac. Precipitation based iso severity map for 24 months drought duration with a return period of 50 years

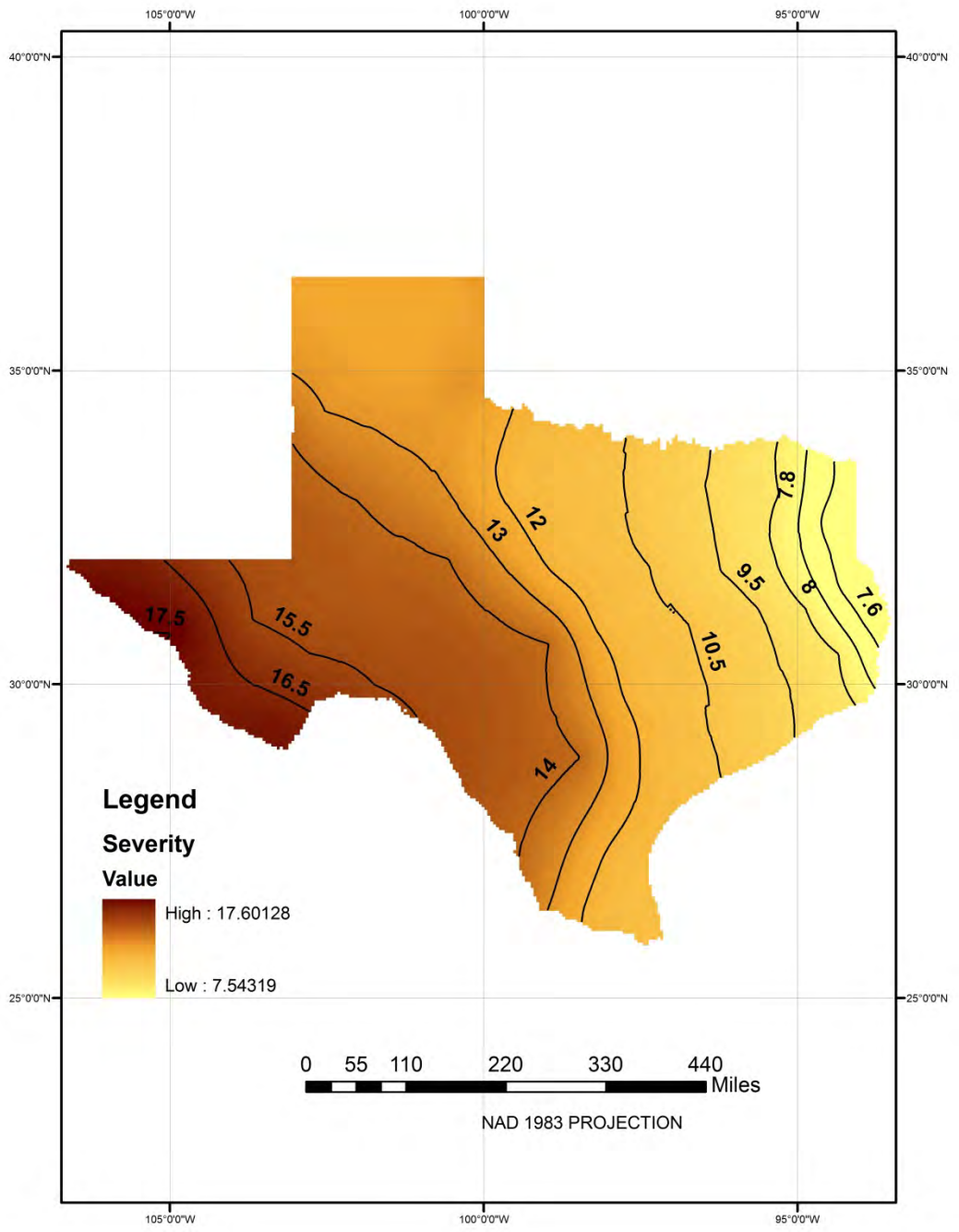

Figure 10ad. Precipitation based iso severity map for 24 months drought duration with a return period of 100 years

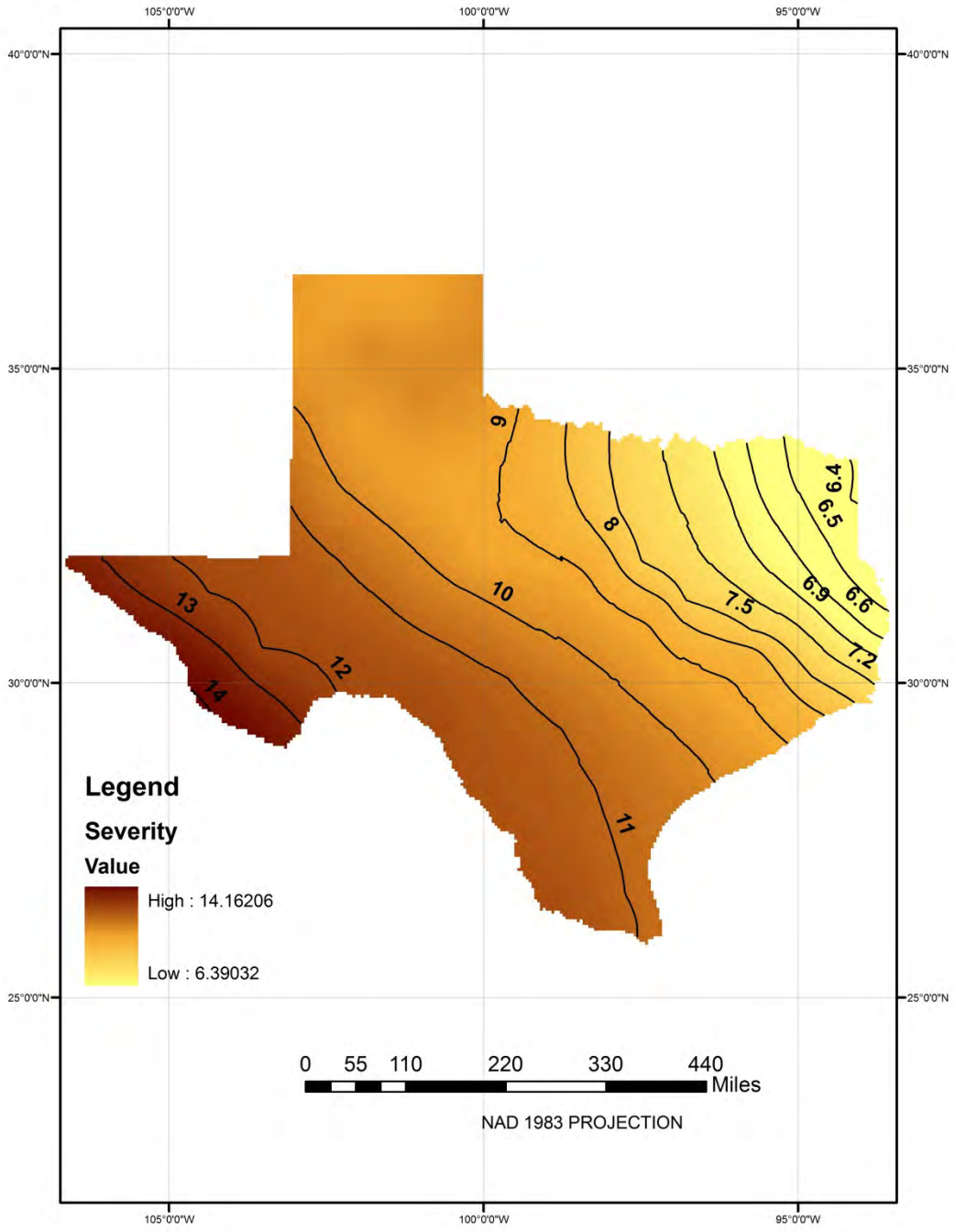

Figure 10ae. Precipitation based iso severity map for 36 months drought duration with a return period of 5 years

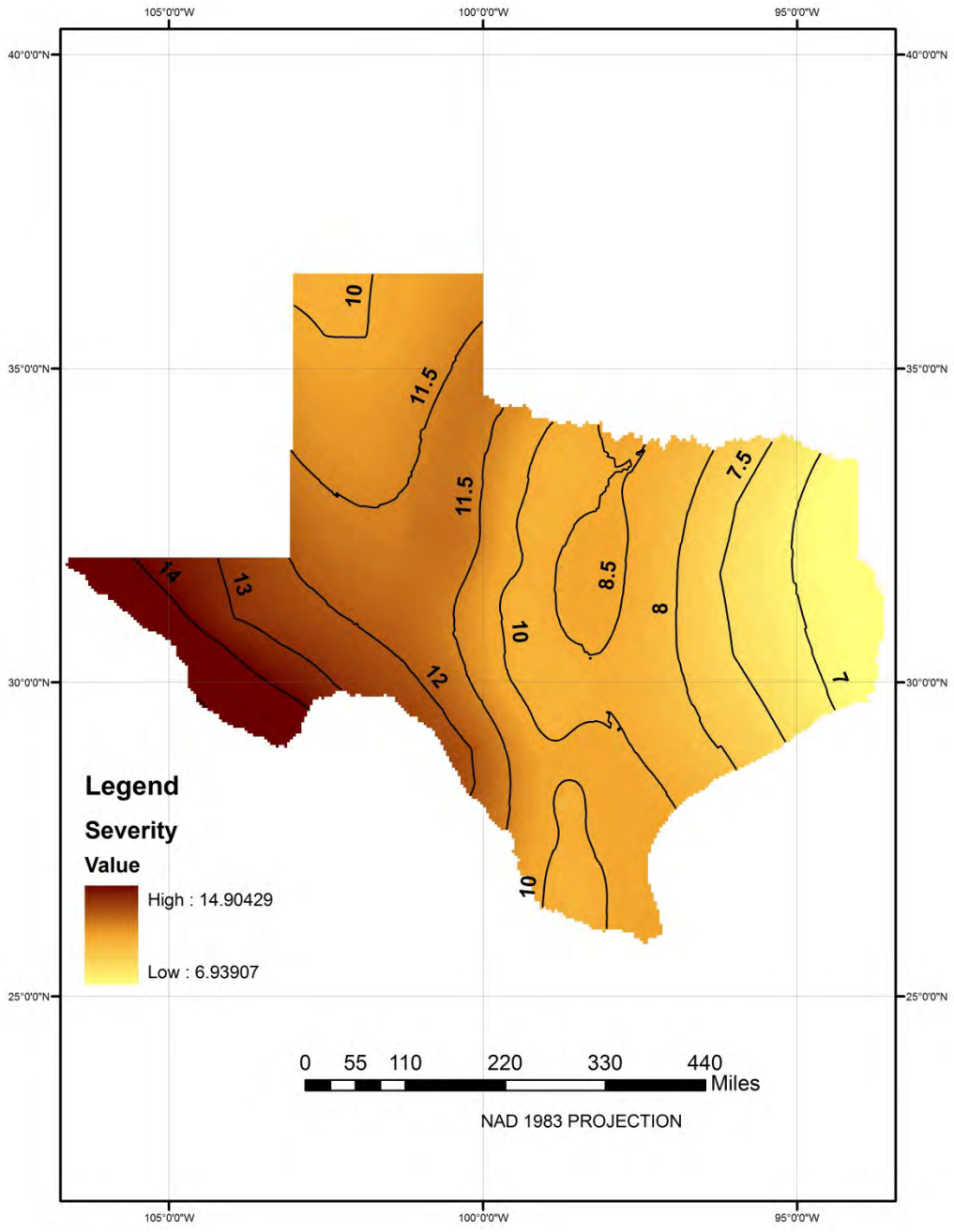

Figure 10af. Precipitation based iso severity map for 36 months drought duration with a return period of 10 years

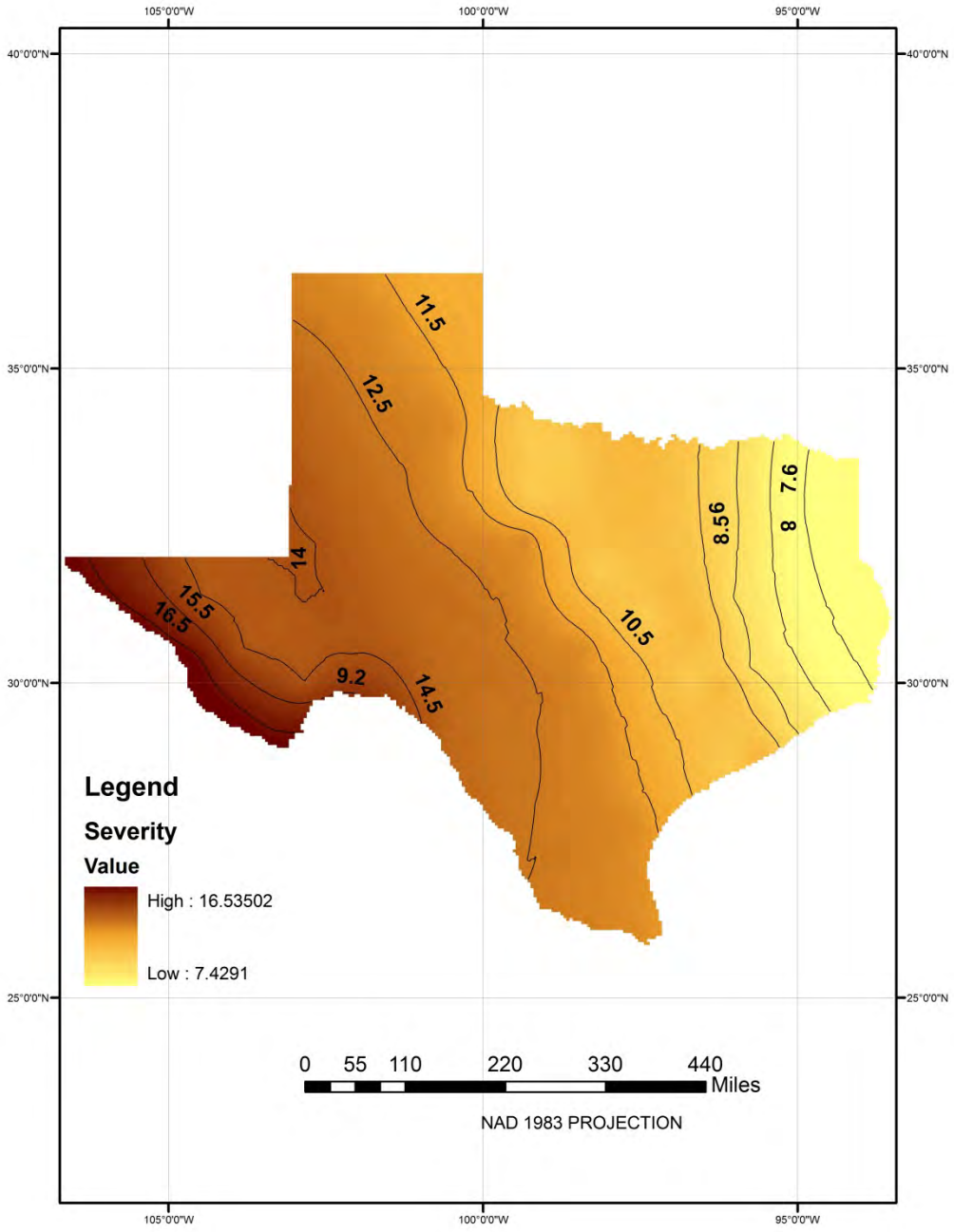

Figure 10ag. Precipitation based iso severity map for 36 months drought duration with a return period of 25 years

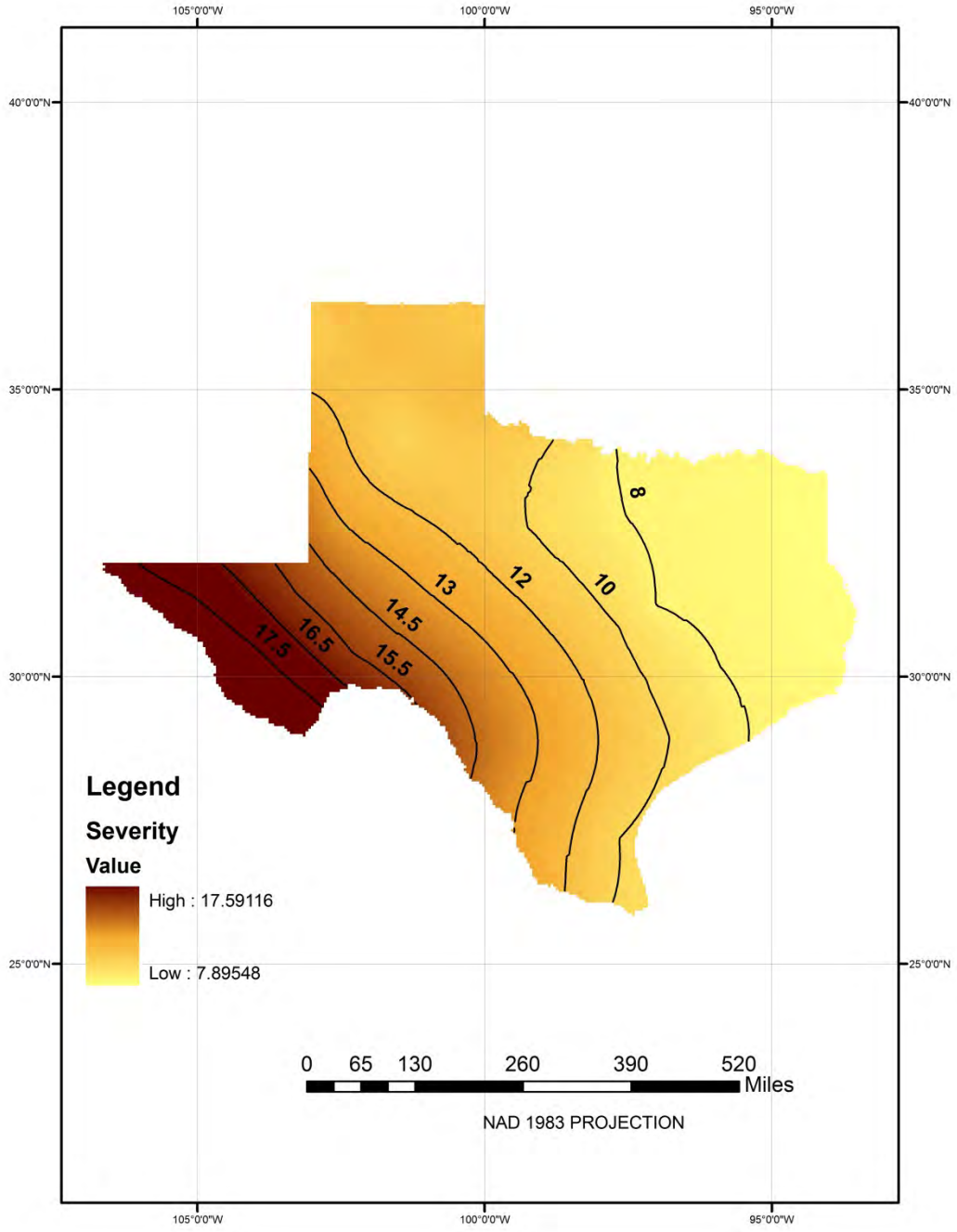

Figure 10ah. Precipitation based iso severity map for 36 months drought duration with a return period of 50 years

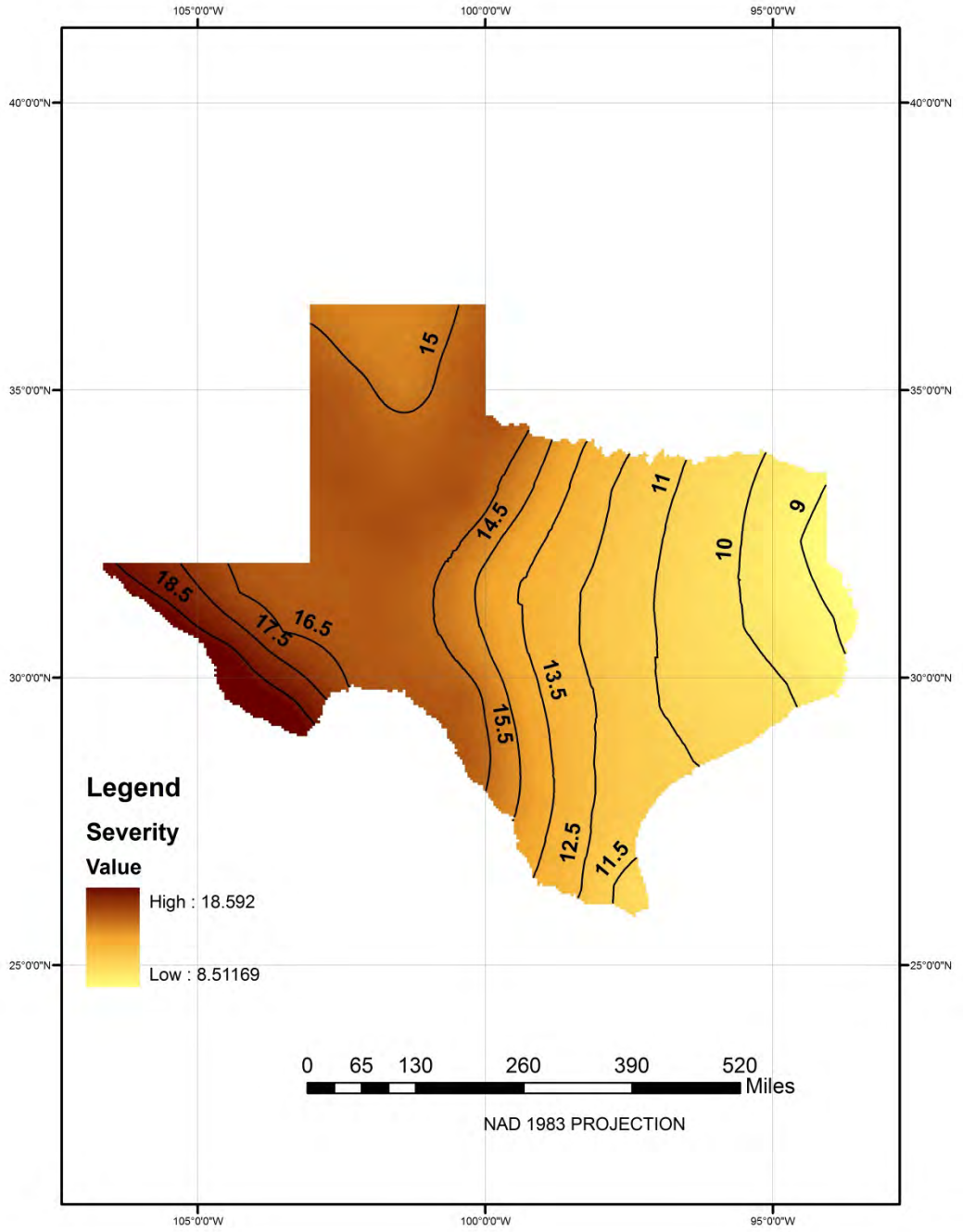

Figure 10ai. Precipitation based iso severity map for 36 months drought duration with a return period of 100 years

Part 3: Naturalized Flow Based Drought Maps

In this part, the naturalized stream flow values from the gauges are used to prepare the drought maps. In this case, the procedure followed is exactly same as in part 1. The only difference is in the data set used. This part would enable us to validate the performance of the land surface model so as to make sure that the model simulations are reliable.

Data Sources

Two data sources were made use of, to obtain the naturalized stream flow data in Texas.

(a) Hydro climatic data network (HCDN)

This is a national data set of stream flow records that are relatively free of confounding anthropogenic influences. The purpose of the dataset is for studying the variation in surface-water conditions throughout the United States. United States Geological Survey (USGS) maintains this record. Naturalized stream flow records for around 89 sites in Texas is available till the water year 1988.

(b) Water Rights analysis package (WRAP)

An alternate source of naturalized flow data is the water rights analysis package (WRAP) developed by Dr. Ralph Wurbs of Texas A&M University. Although it is basically a package for analyzing water rights, naturalized flow is one of the outputs of this package. These flow values have been adjusted to remove anthropogenic effects of both management and use (e.g. reservoirs, diversions). Thus, sequences of monthly flows which represent the historical natural hydrology are typically developed by adjusting recorded flows at gaging stations to remove the past impacts of upstream major reservoirs, water supply diversions, return flows from surface and ground water sources, and other possible factors. The WRAP naturalized flow data is available for 17 river basins in Texas.

Both these data sources have been made use of, depending upon the availability at the location. Kriging is performed after the at-site drought S-D-F curves are derived.

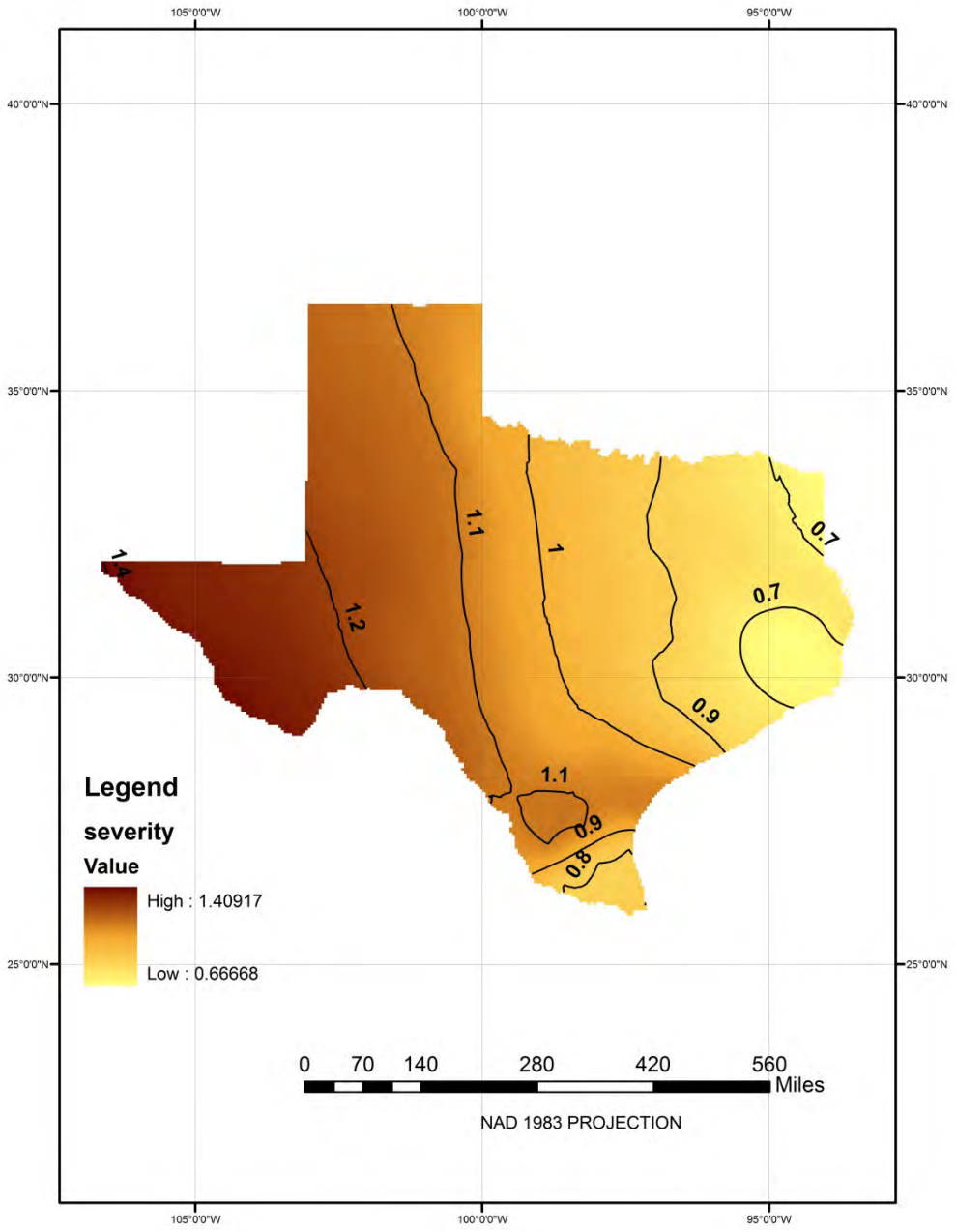

Figure 11a. Naturalized flow based iso severity map for 3 months drought duration with a return period of 5 years

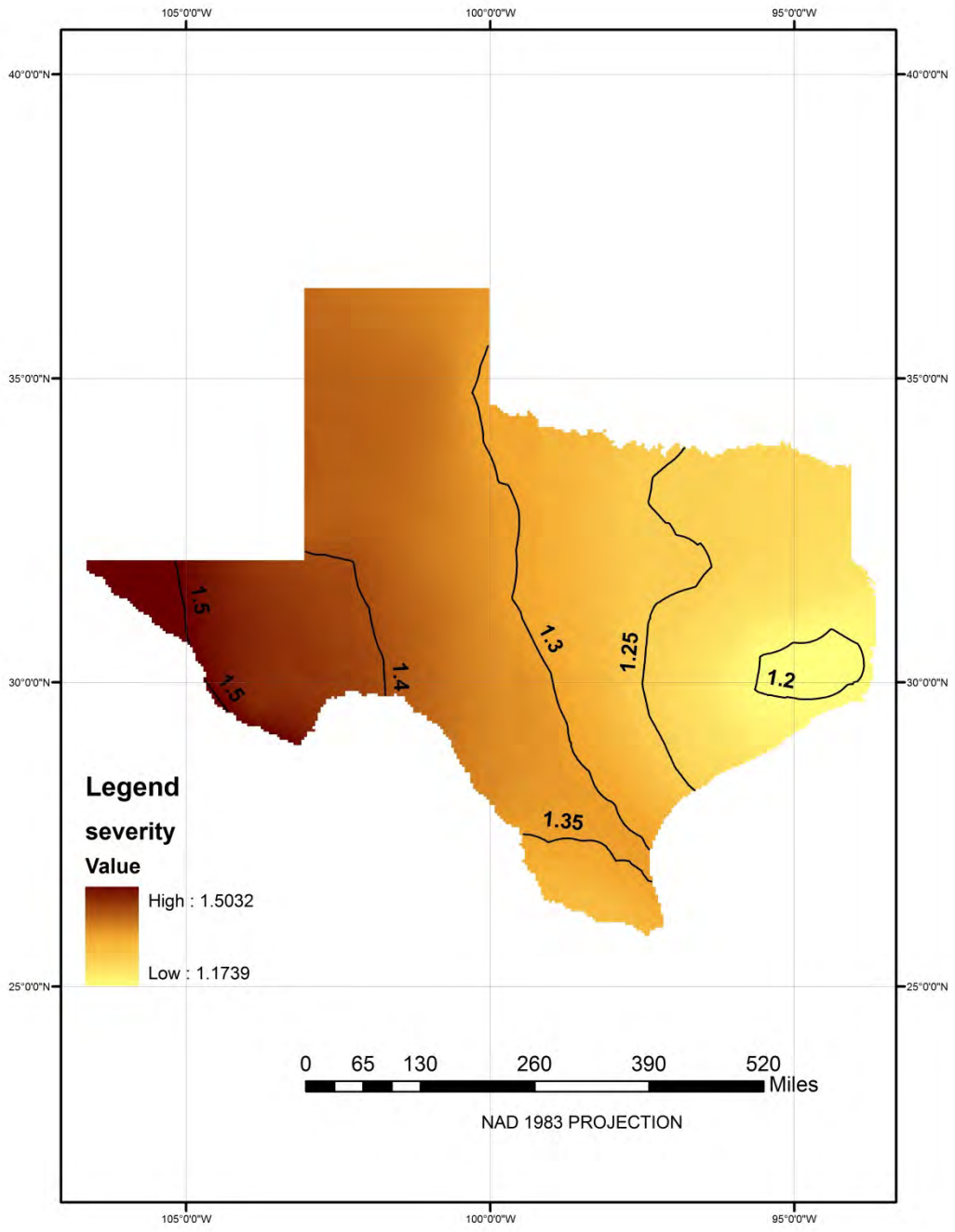

Figure 11b. Naturalized flow based iso severity map for 3 months drought duration with a return period of 10 years

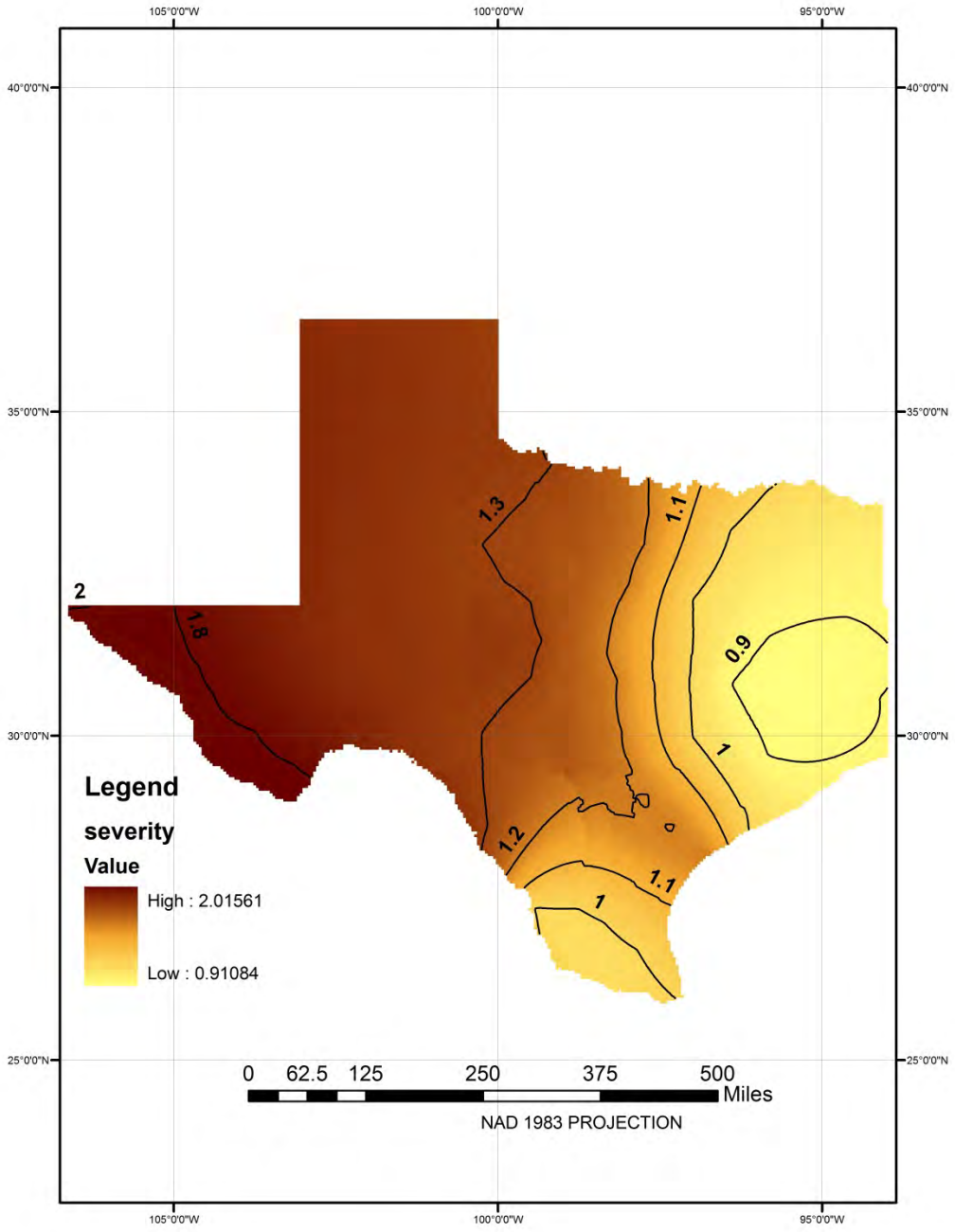

Figure 11c. Naturalized flow based iso severity map for 3 months drought duration with a return period of 25 years

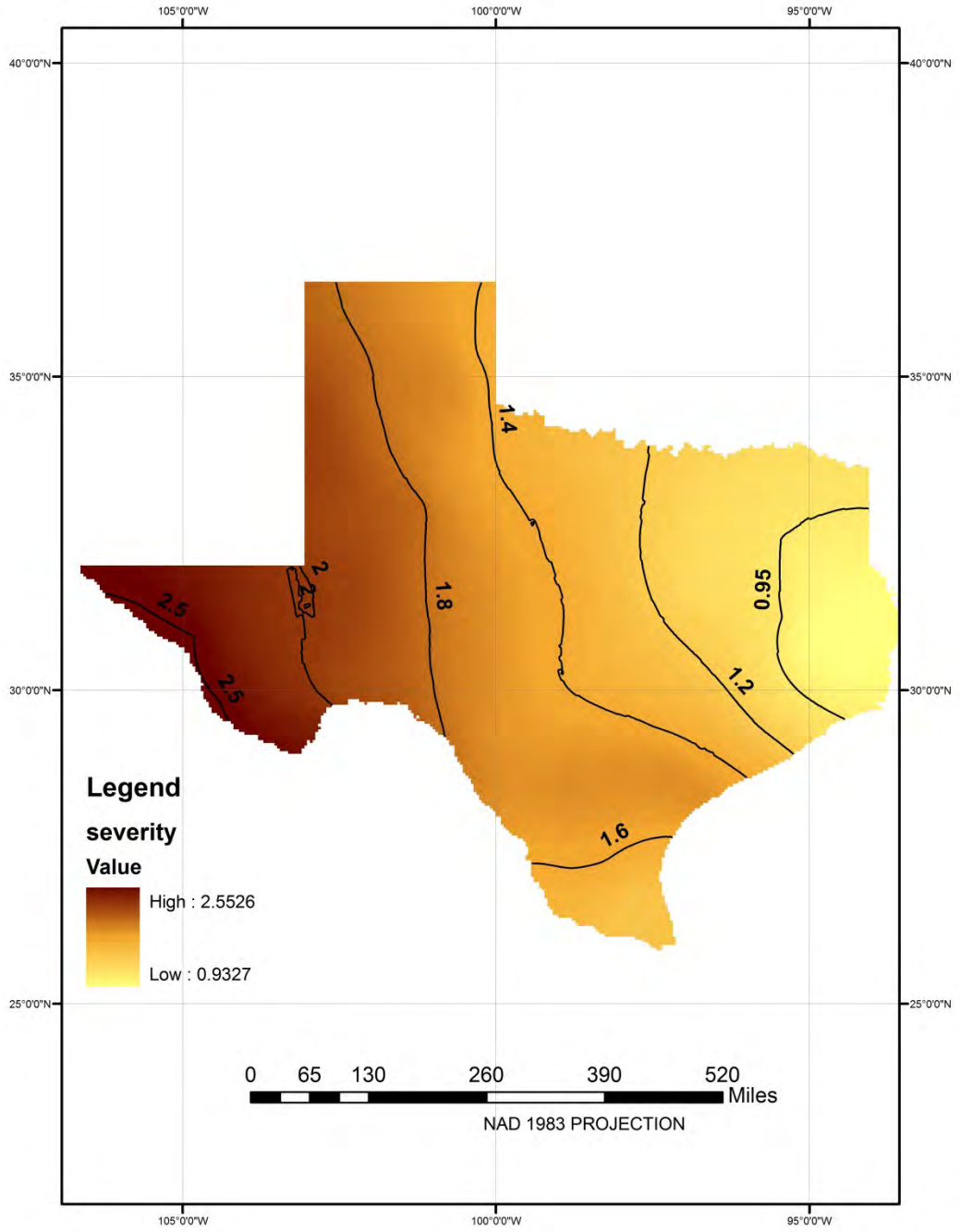

Figure 11d. Naturalized flow based iso severity map for 3 months drought duration with a return period of 50 years

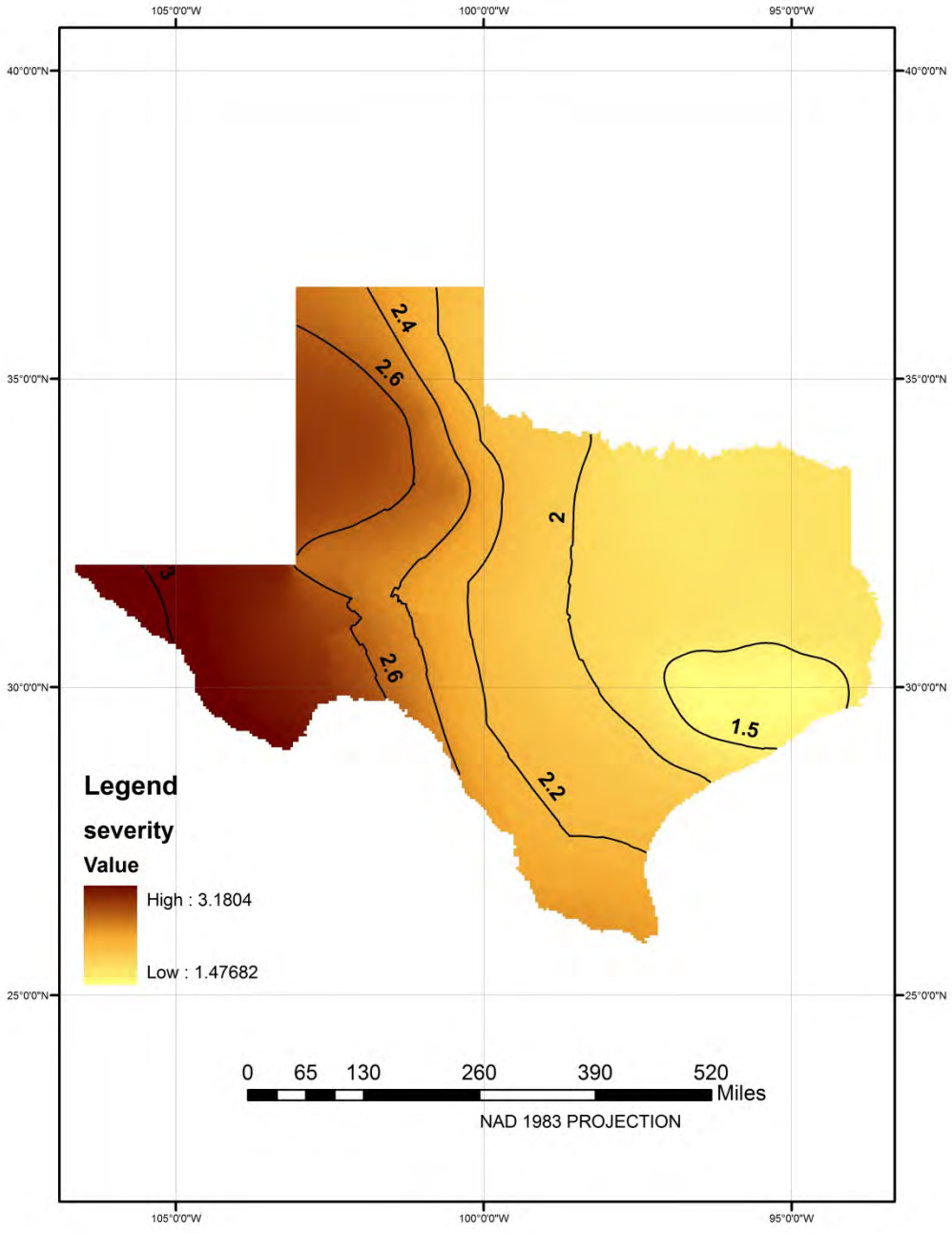

Figure 11e. Naturalized flow based iso severity map for 3 months drought duration with a return period of 100 years

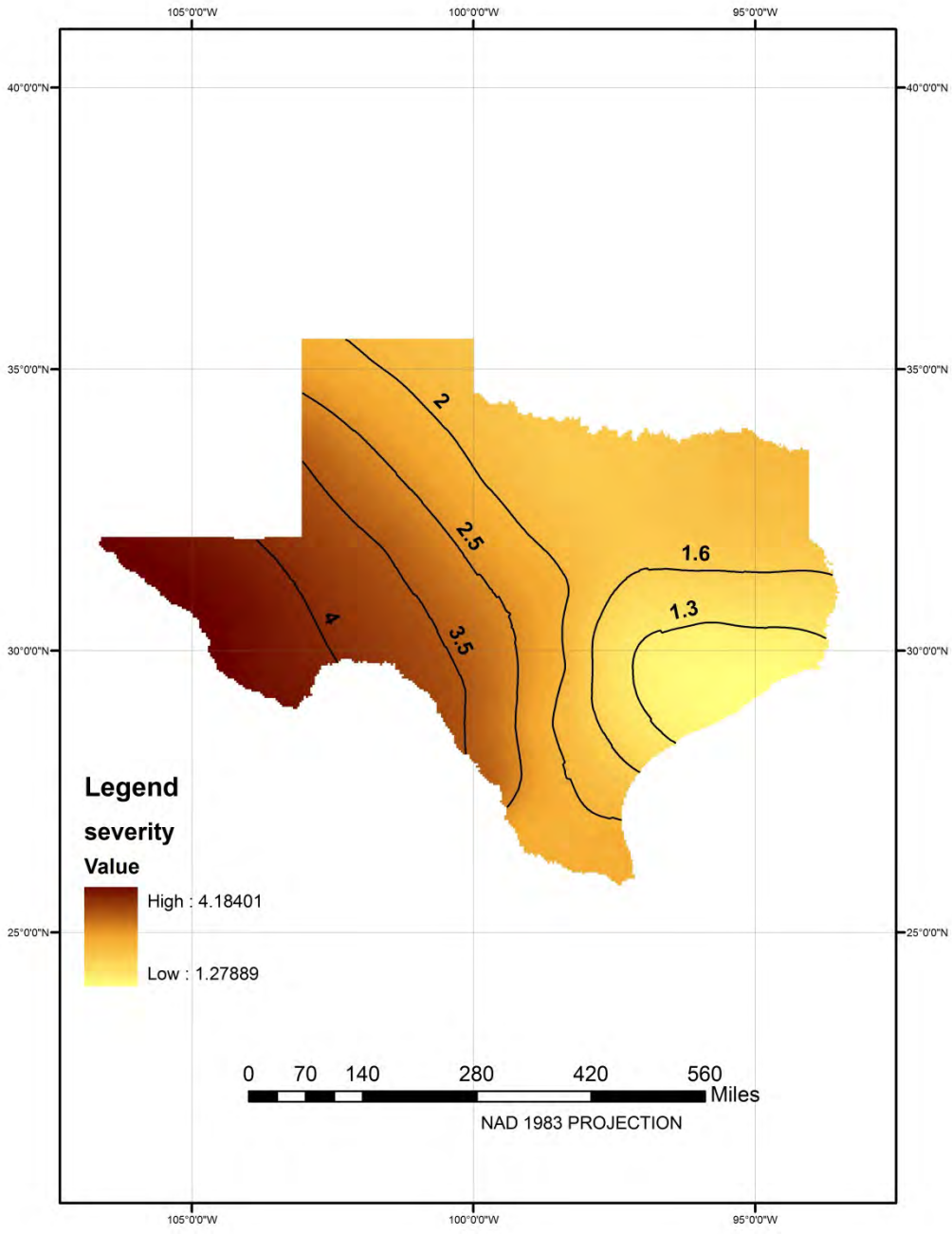

Figure 11f. Naturalized flow based iso severity map for 6 months drought duration with a return period of 5 years

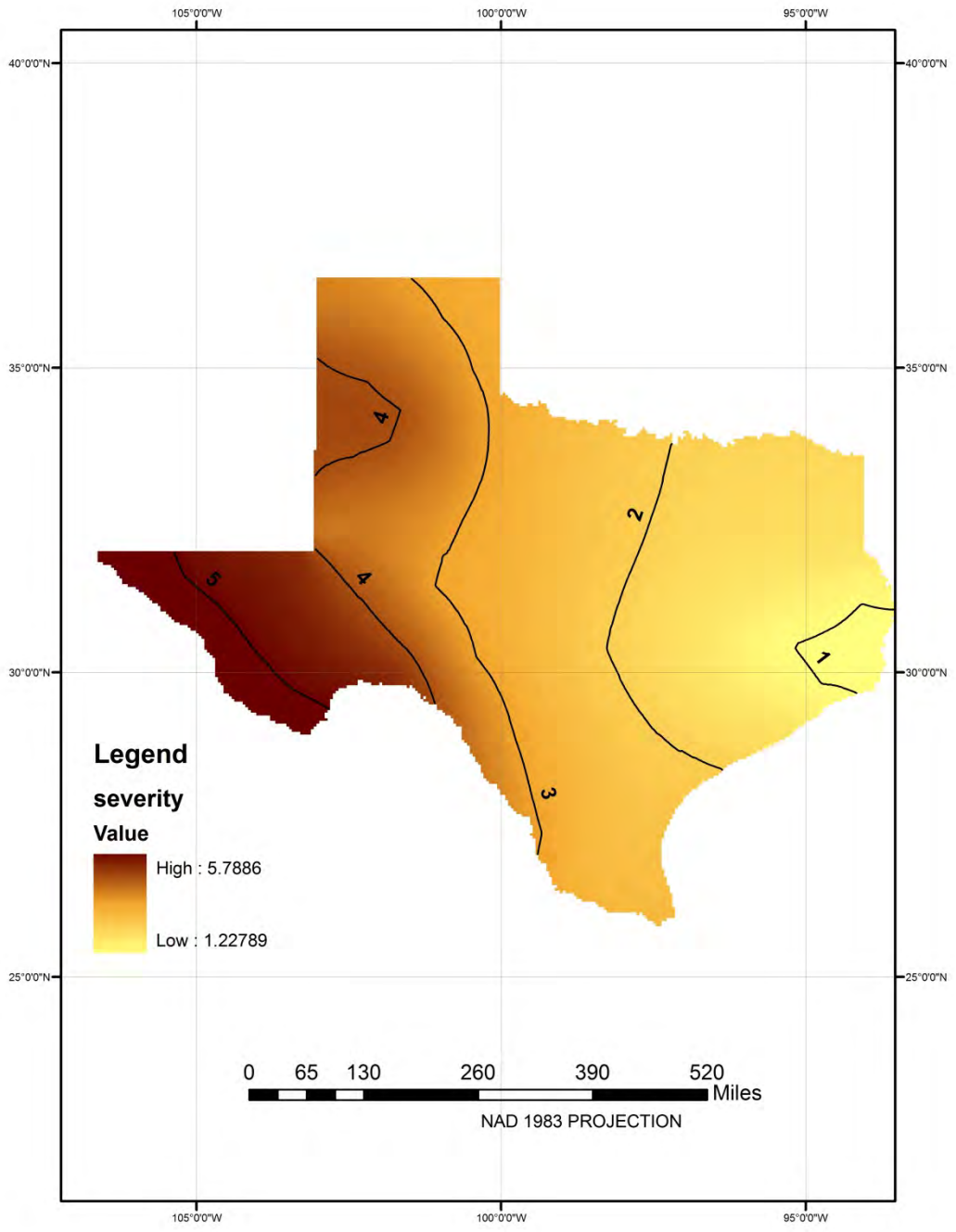

Figure 11g. Naturalized flow based iso severity map for 6 months drought duration with a return period of 10 years

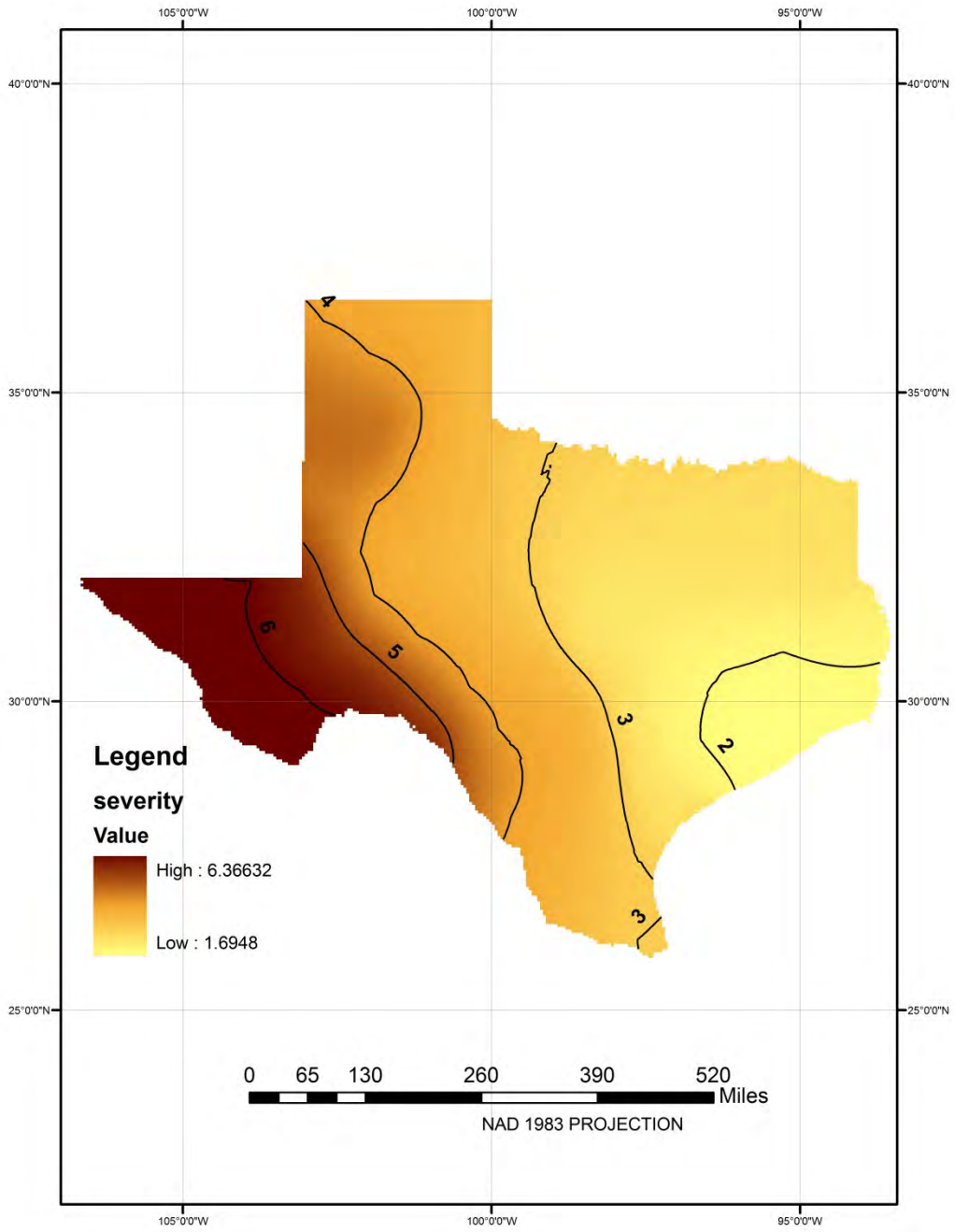

Figure 11h. Naturalized flow based iso severity map for 6 months drought duration with a return period of 25 years

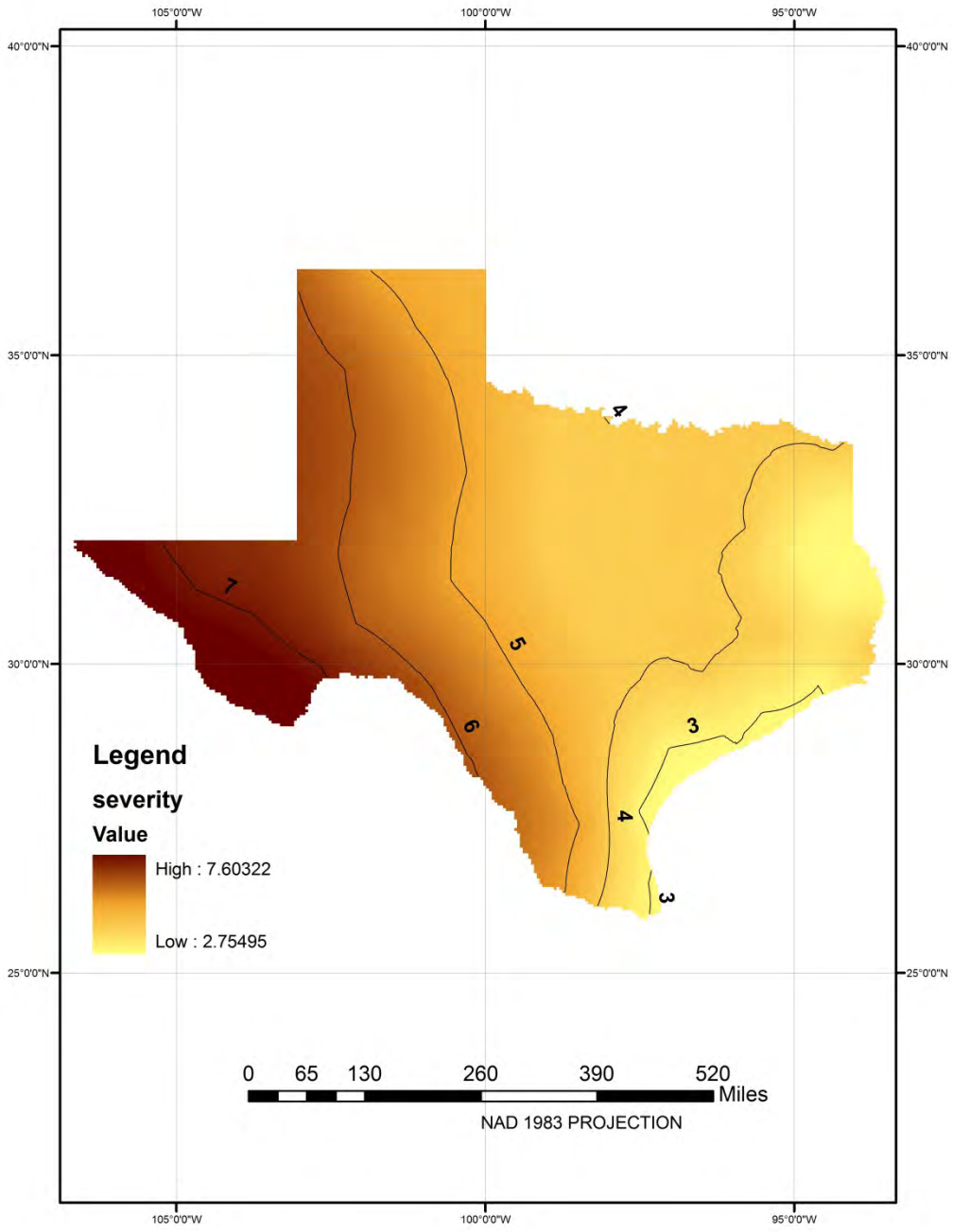

Figure 11i. Naturalized flow based iso severity map for 6 months drought duration with a return period of 50 years

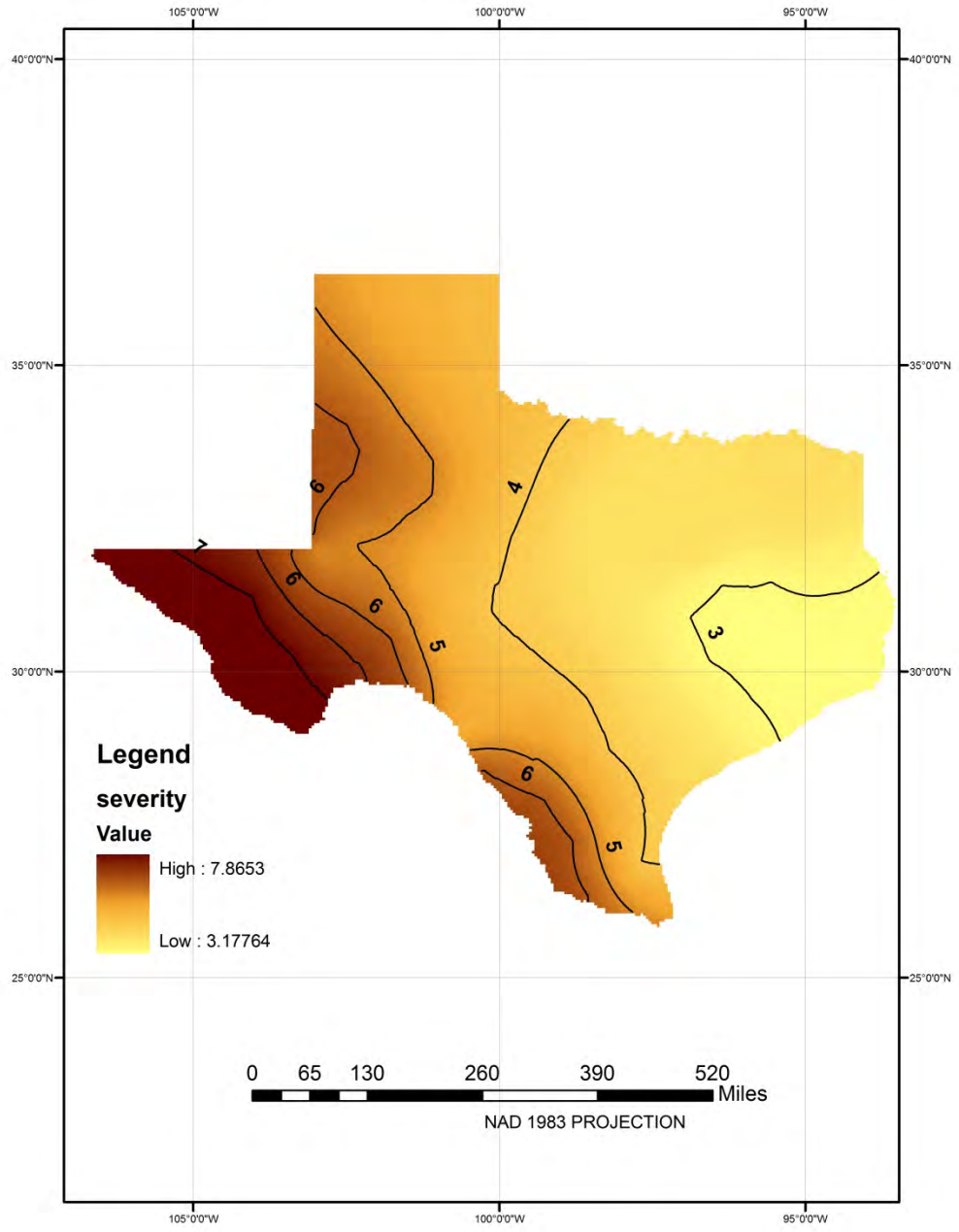

Figure 11j. Naturalized flow based iso severity map for 6 months drought duration with a return period of 100 years

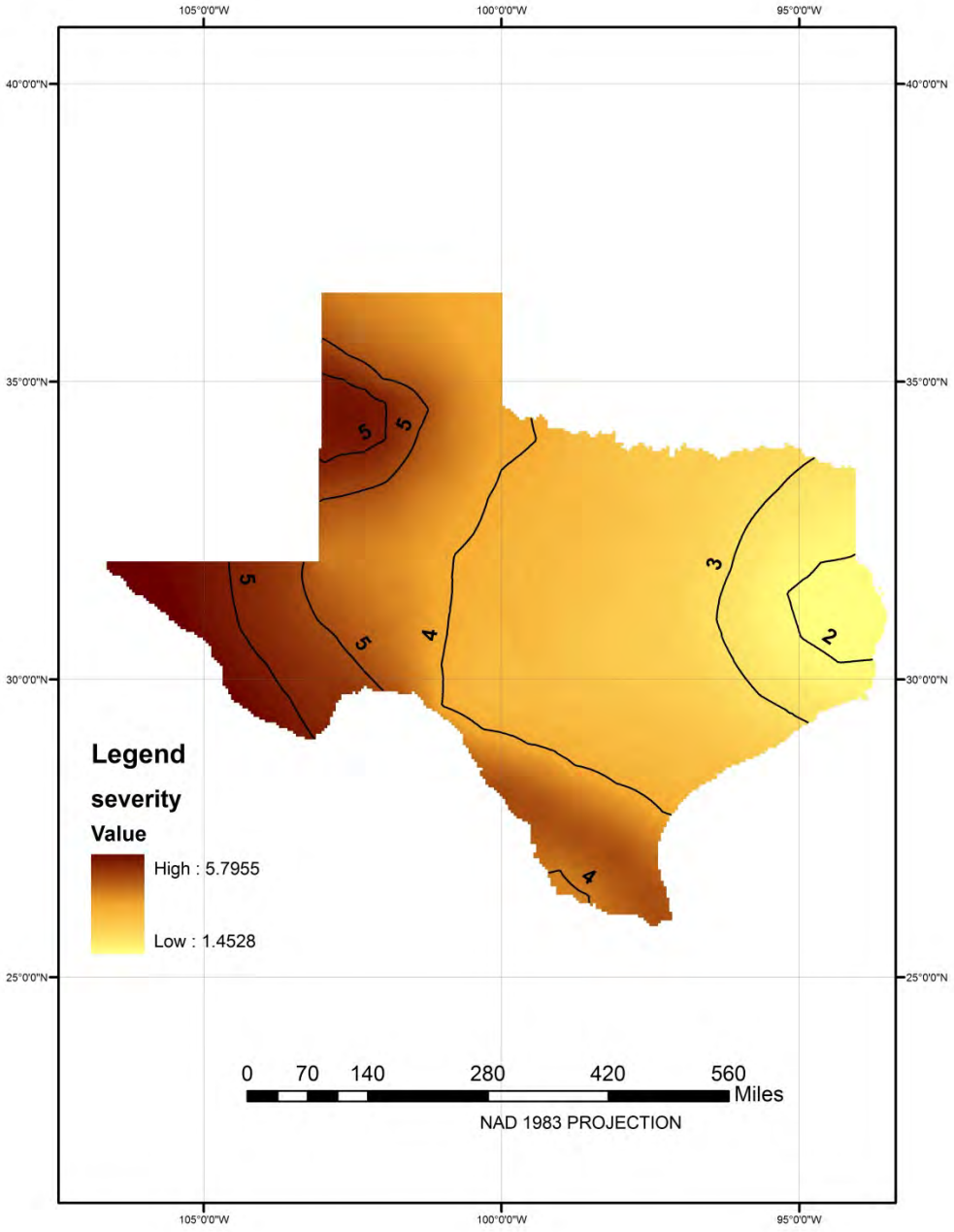

Figure 11k. Naturalized flow based iso severity map for 9 months drought duration with a return period of 5 years

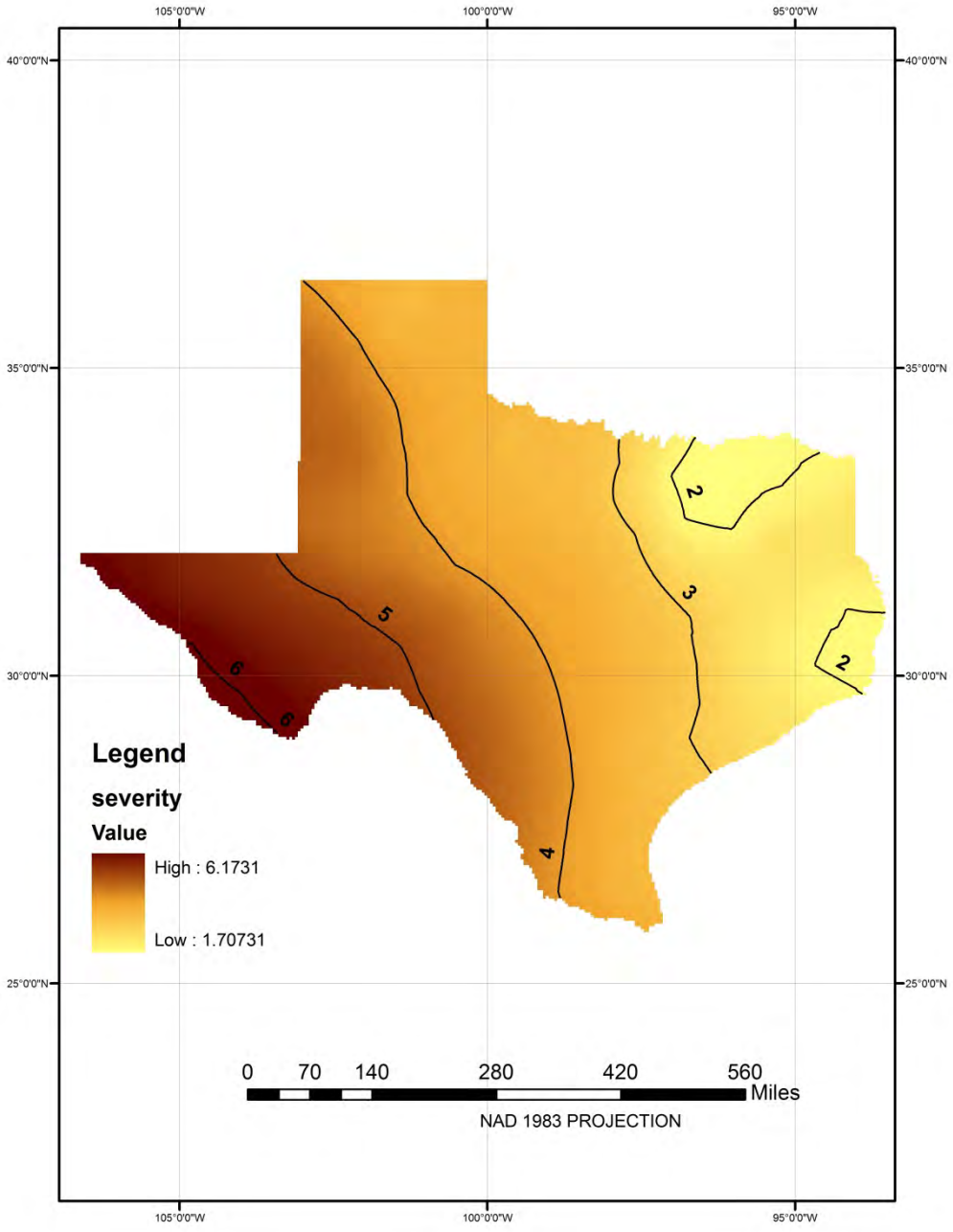

Figure 11l. Naturalized flow based iso severity map for 9 months drought duration with a return period of 10 years

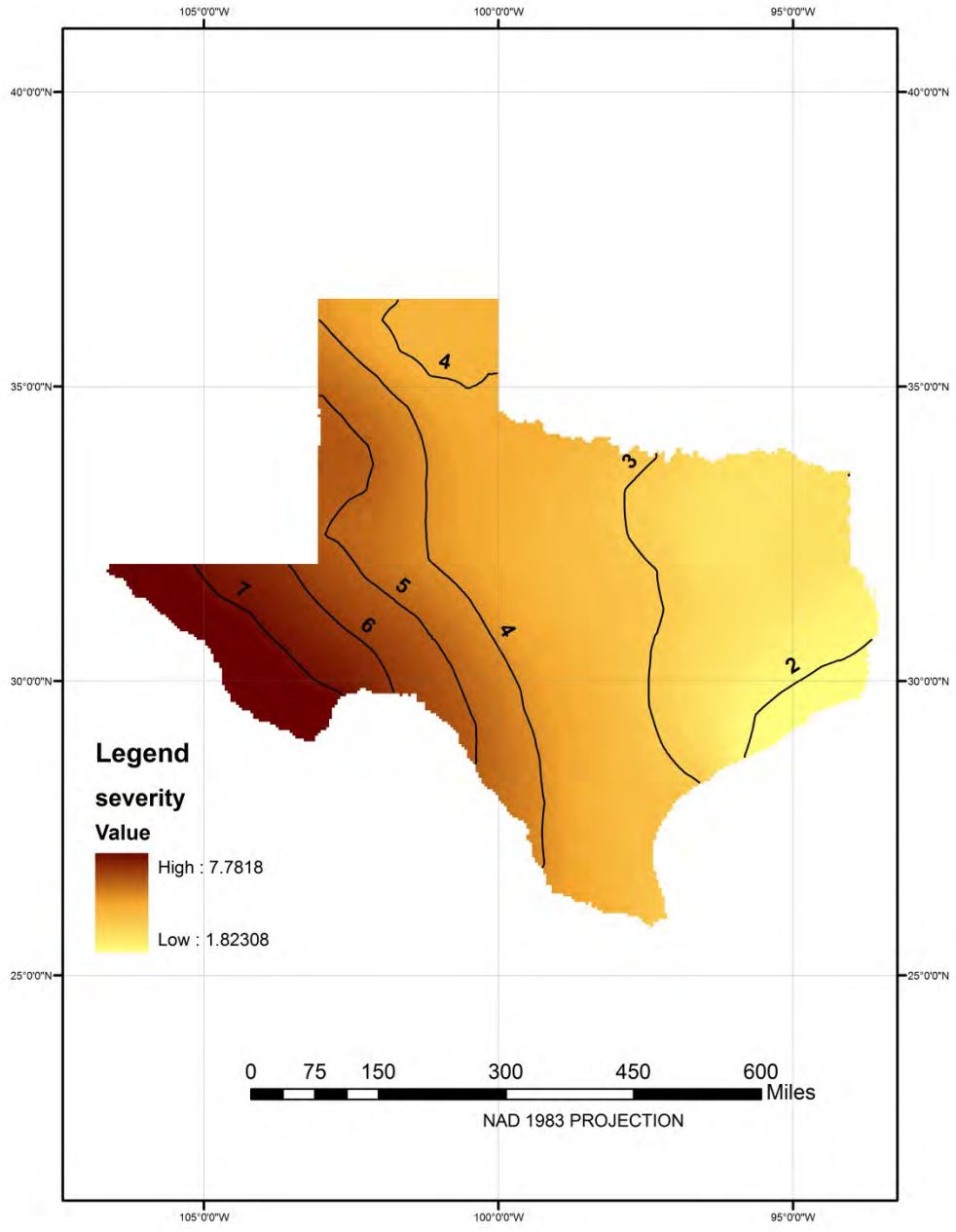

Figure 11m. Naturalized flow based iso severity map for 9 months drought duration with a return period of 25 years

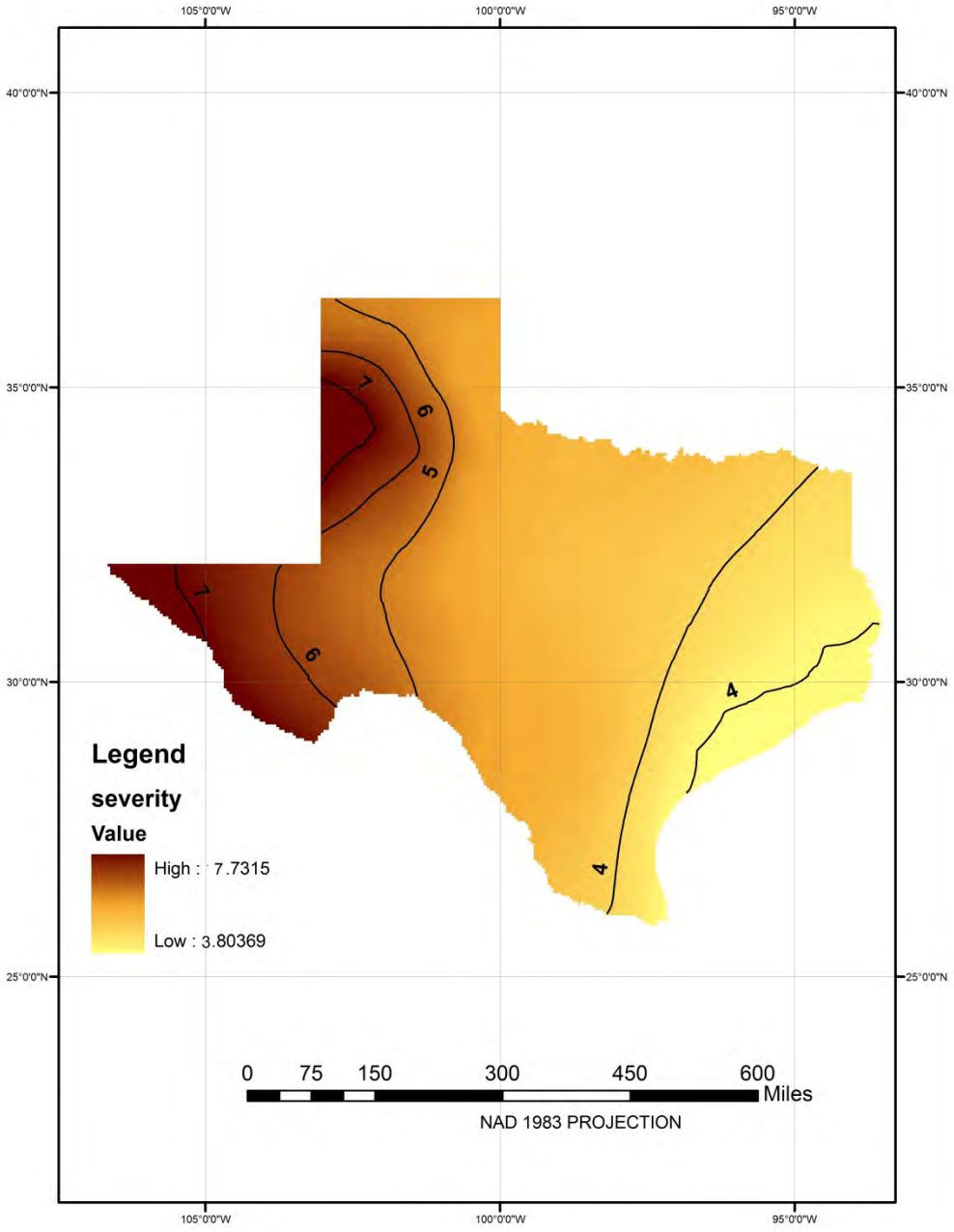

Figure 11n. Naturalized flow based iso severity map for 9 months drought duration with a return period of 50 years

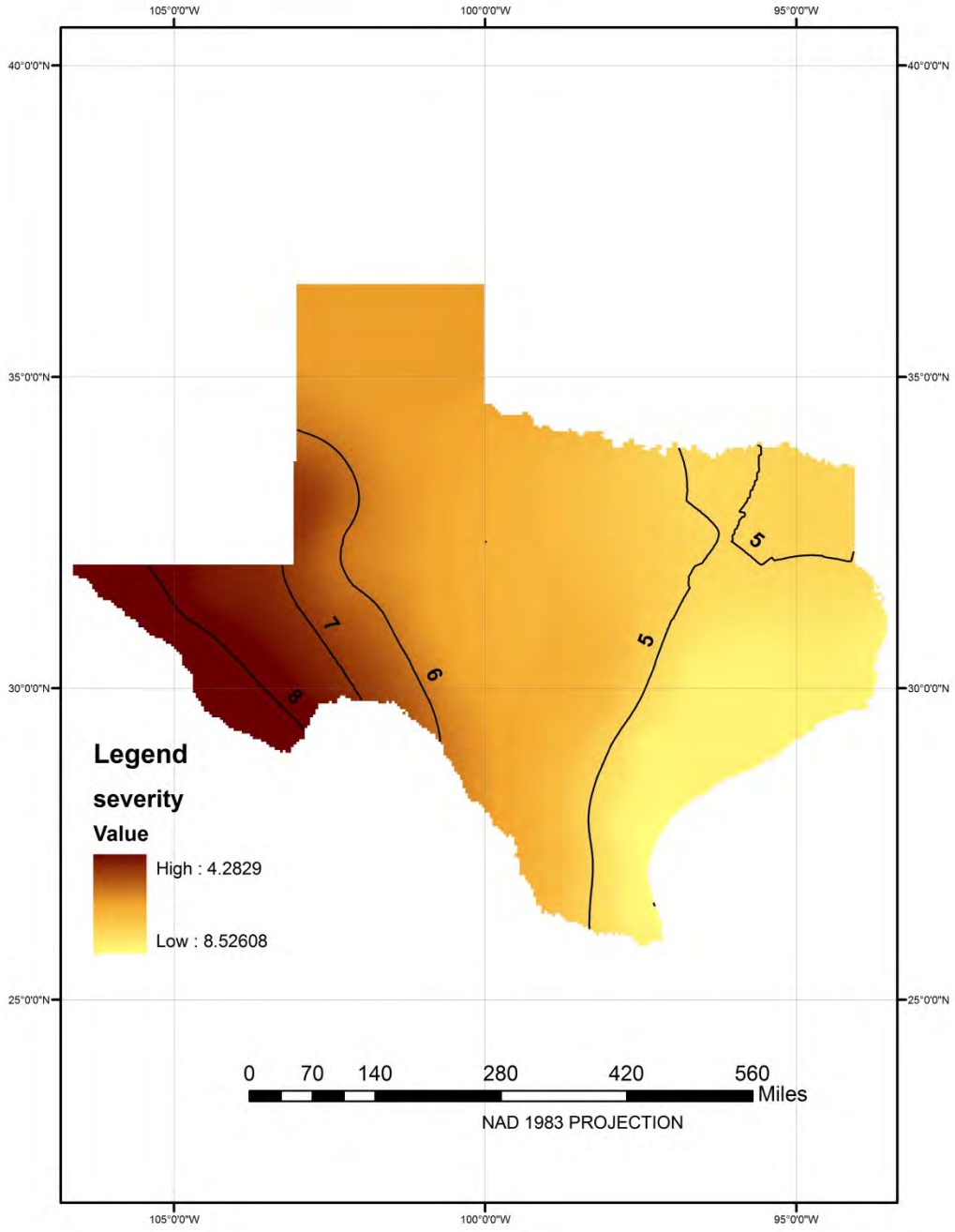

Figure 10o. Precipitation based iso severity map for 9 months drought duration with a return

period of 100 years

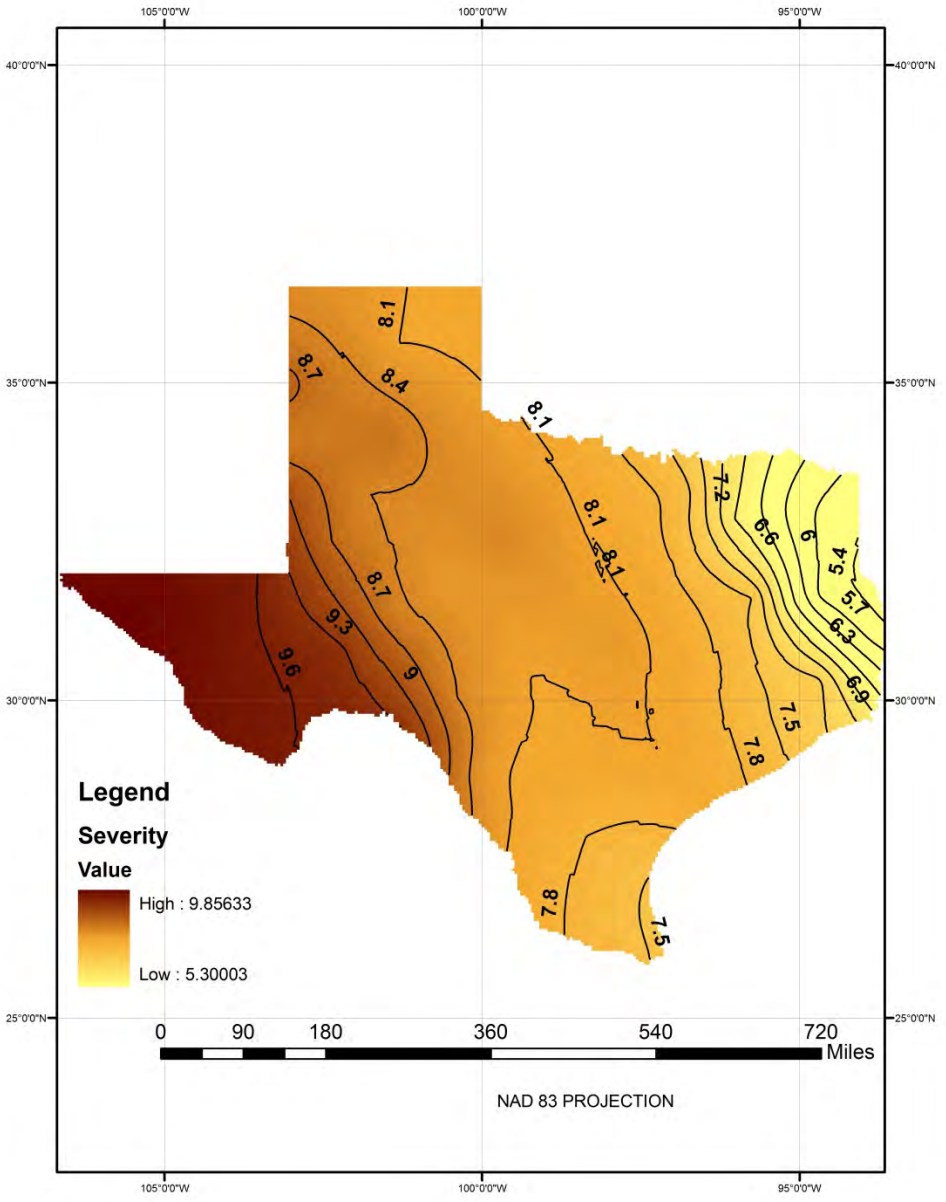

Figure 11p. Naturalized flow based iso severity map for 12 months drought duration with a return period of 5 years

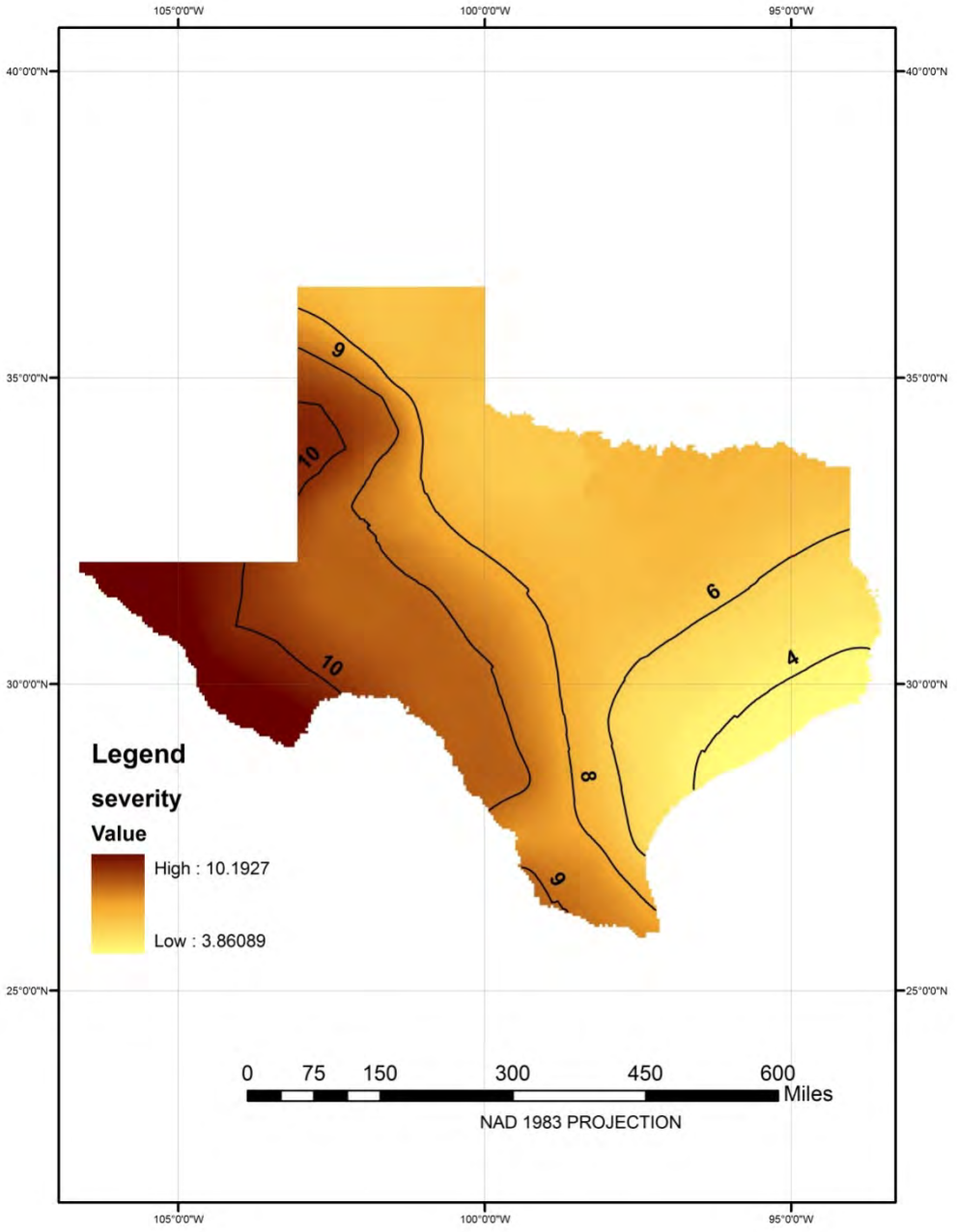

Figure 11q. Naturalized flow based iso severity map for 12 months drought duration with a return period of 10 years

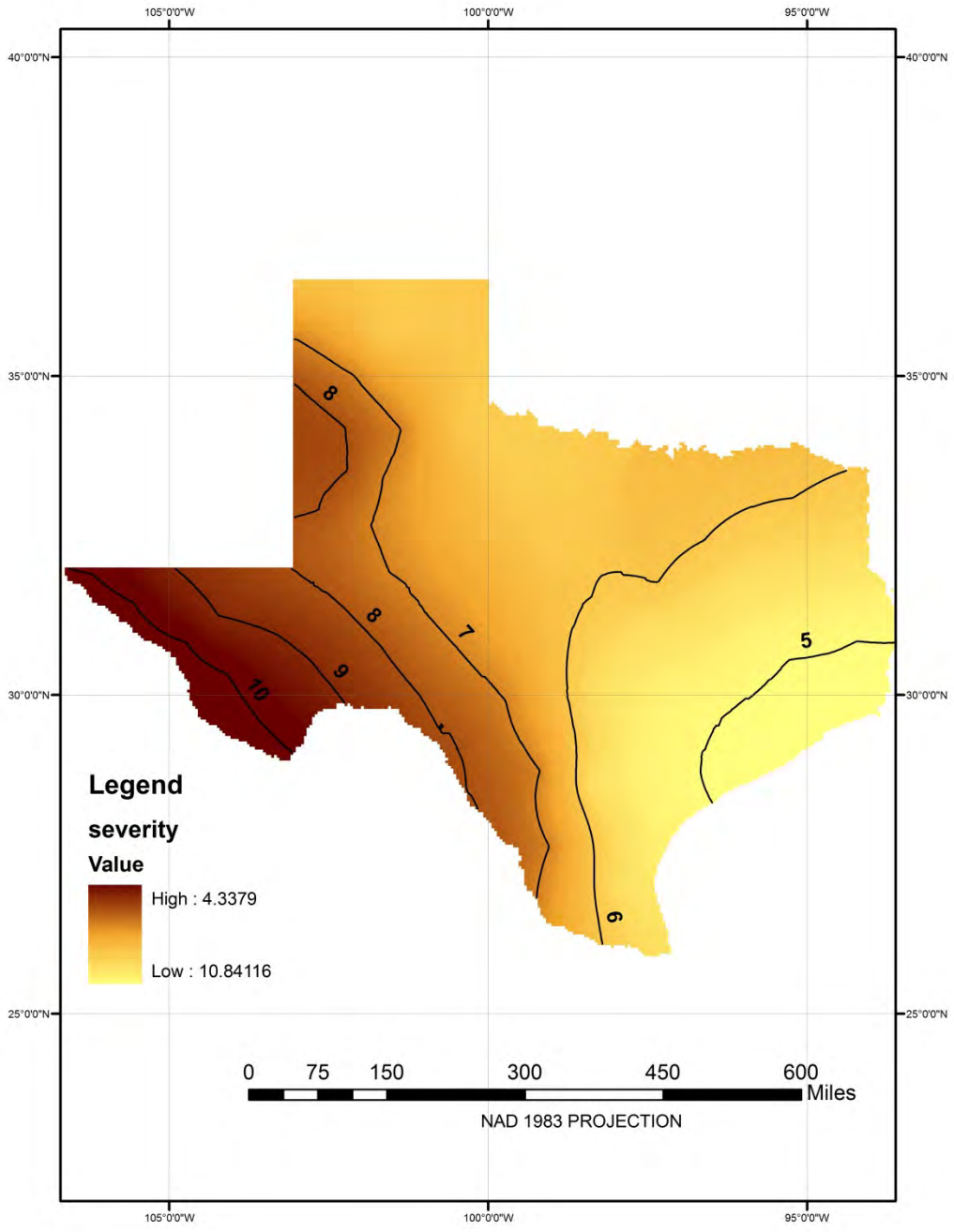

Figure 11r. Naturalized flow based iso severity map for 12 months drought duration with a return period of 25 years

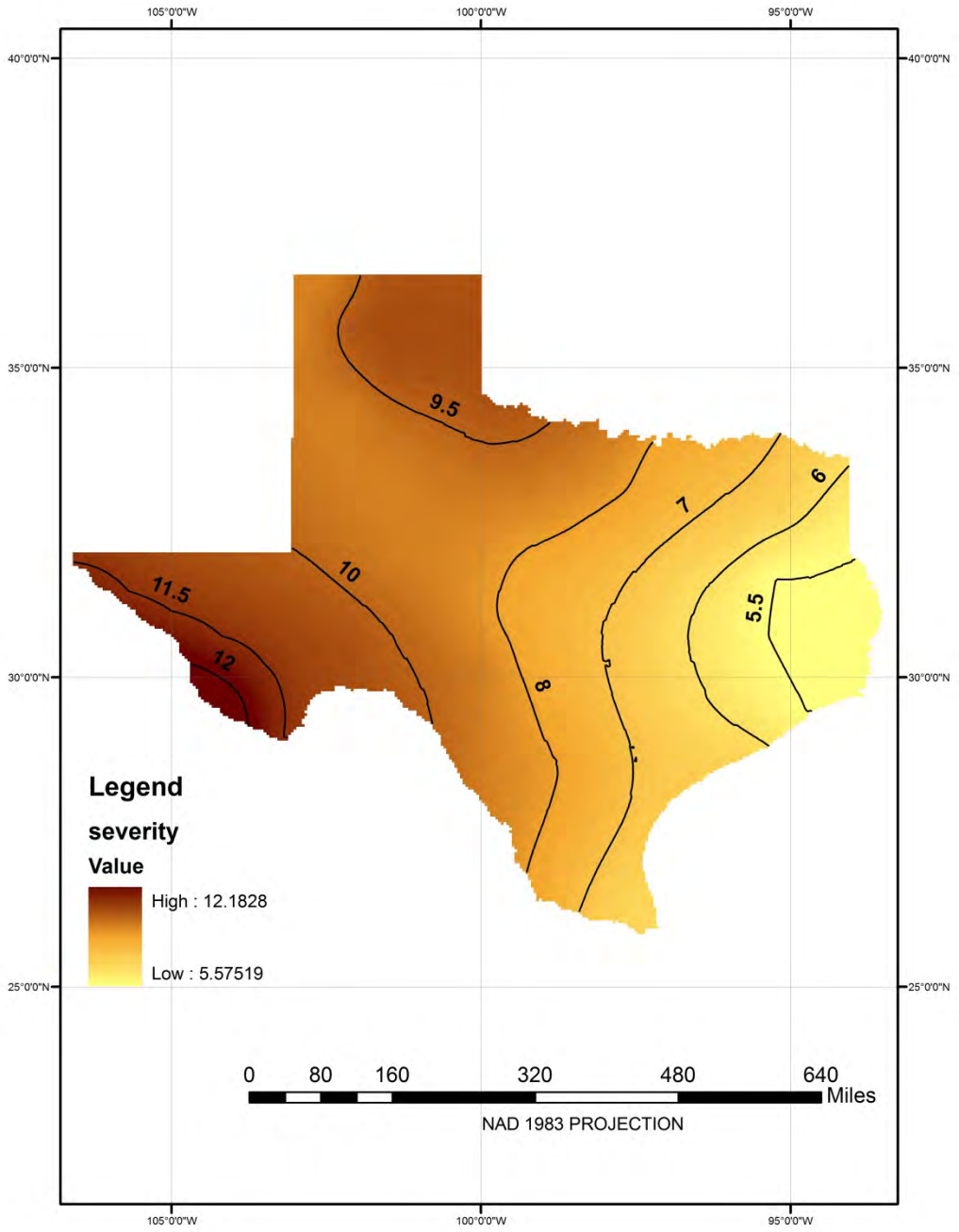

Figure 11s. Naturalized flow based iso severity map for 12 months drought duration with a return period of 50 years

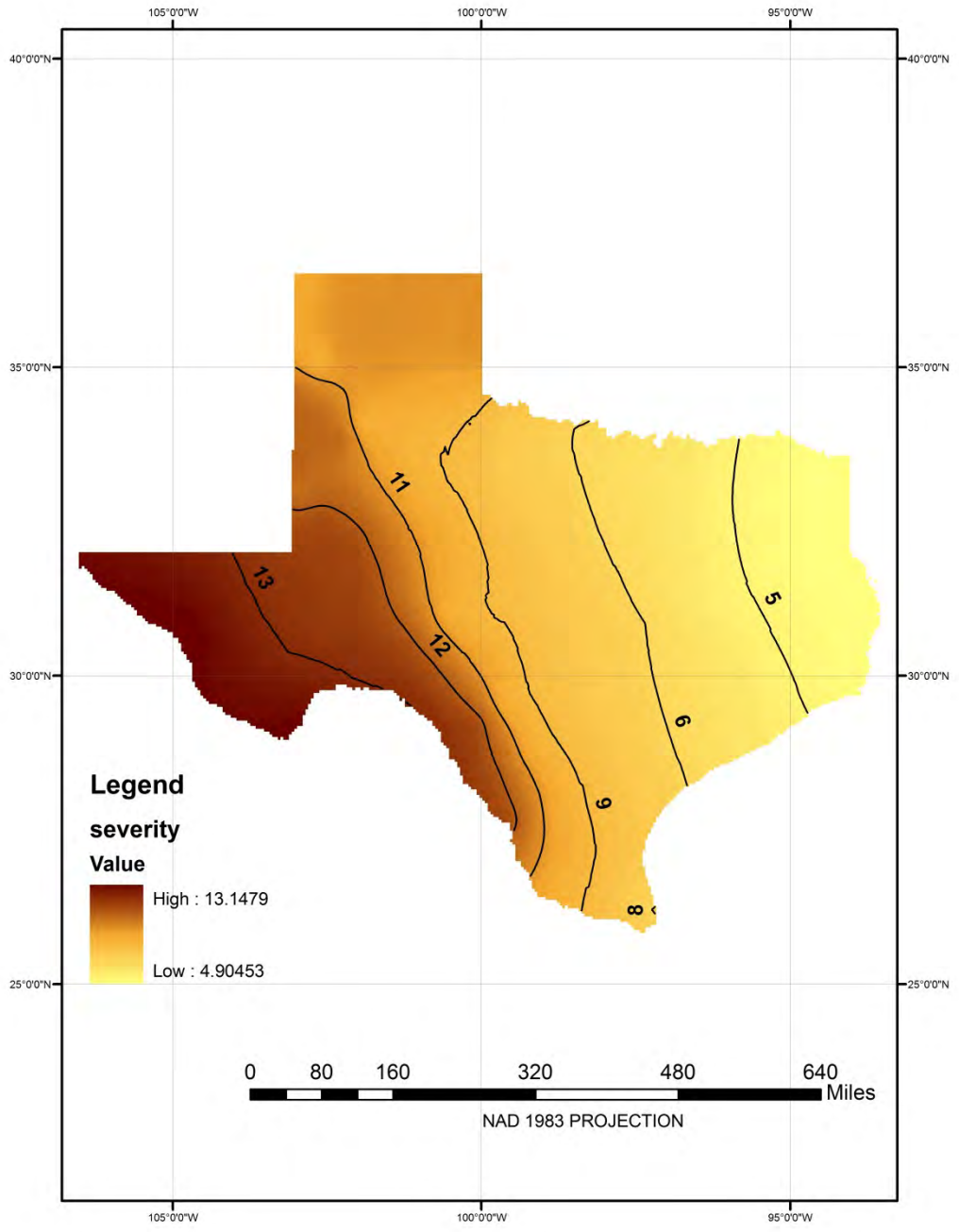

Figure 11t. Naturalized flow based iso severity map for 12 months drought duration with a return period of 100 years

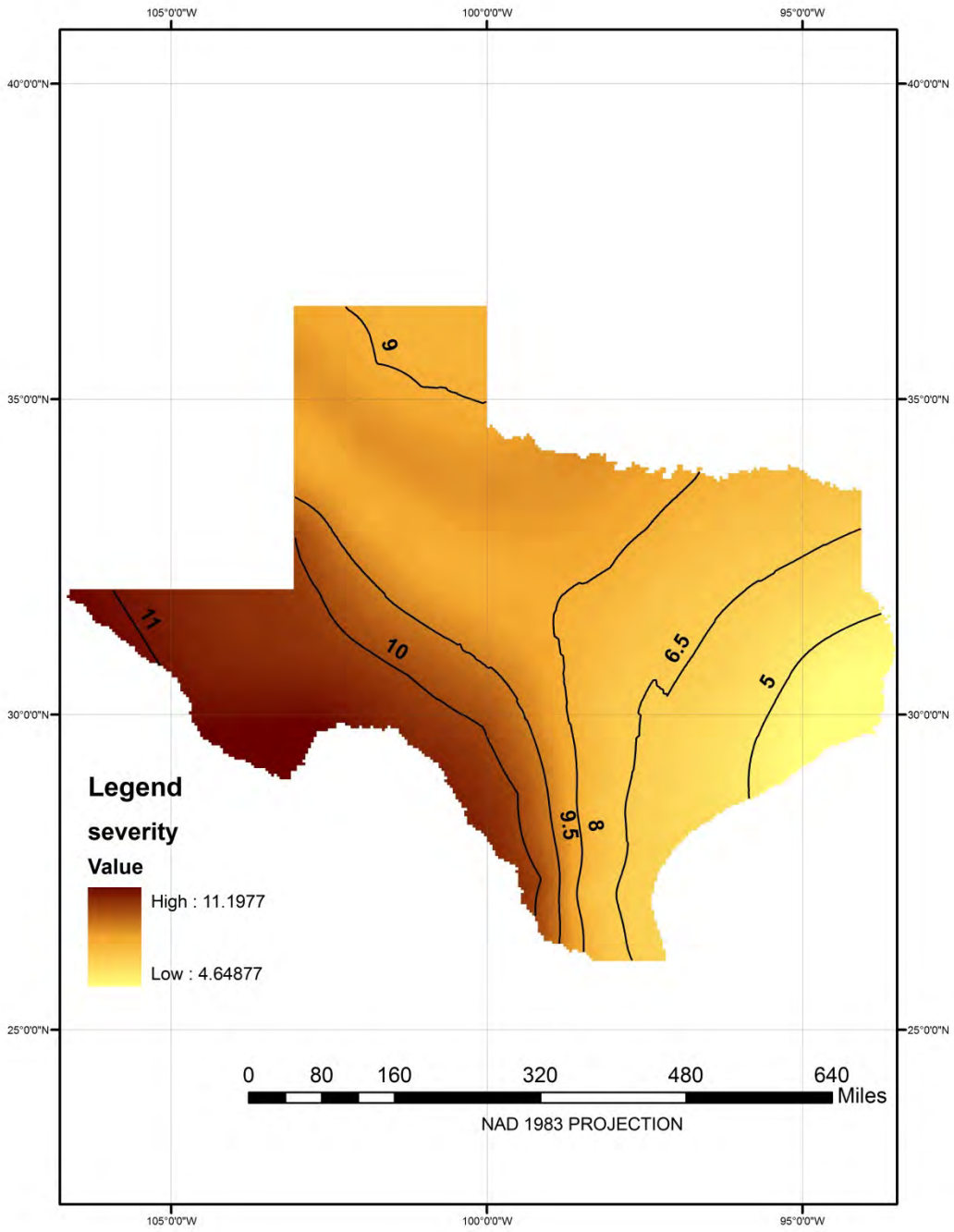

Figure 11u. Naturalized flow based iso severity map for 18 months drought duration with a return period of 5 years

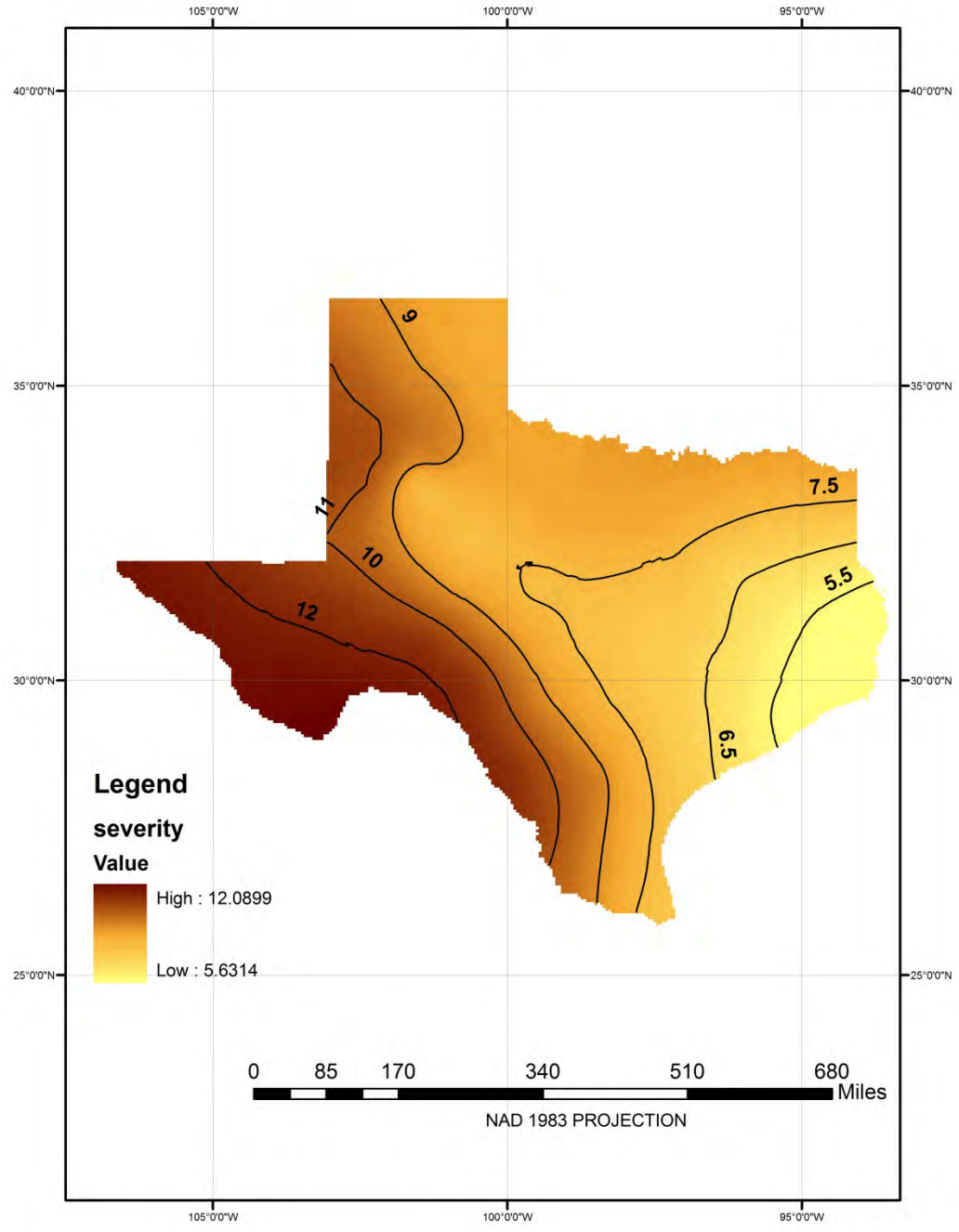

Figure 10v. Iso severity map for 18 months drought duration with a return period of 10 years

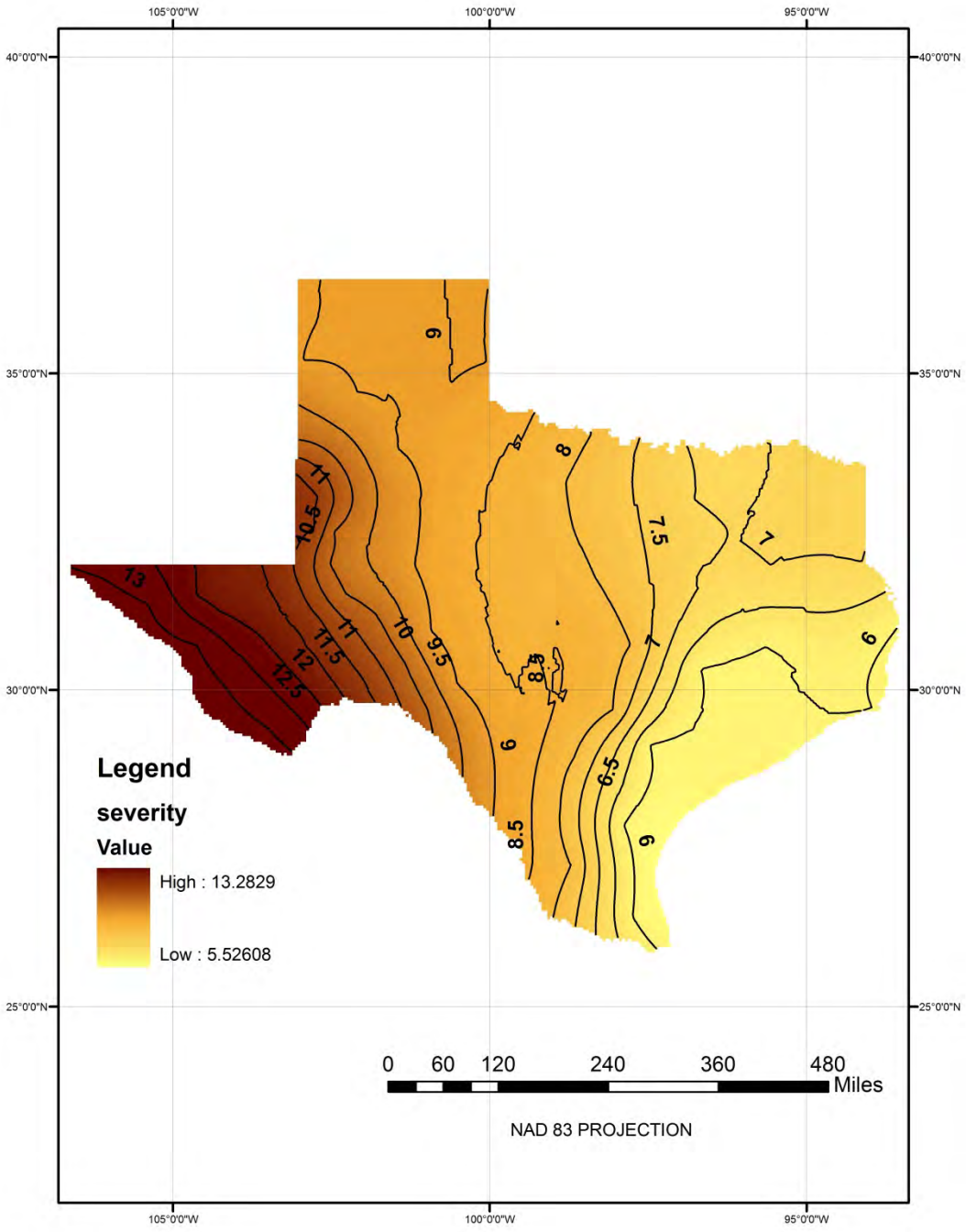

Figure 11w. Naturalized flow based iso severity map for 18 months drought duration with a return period of 25 years

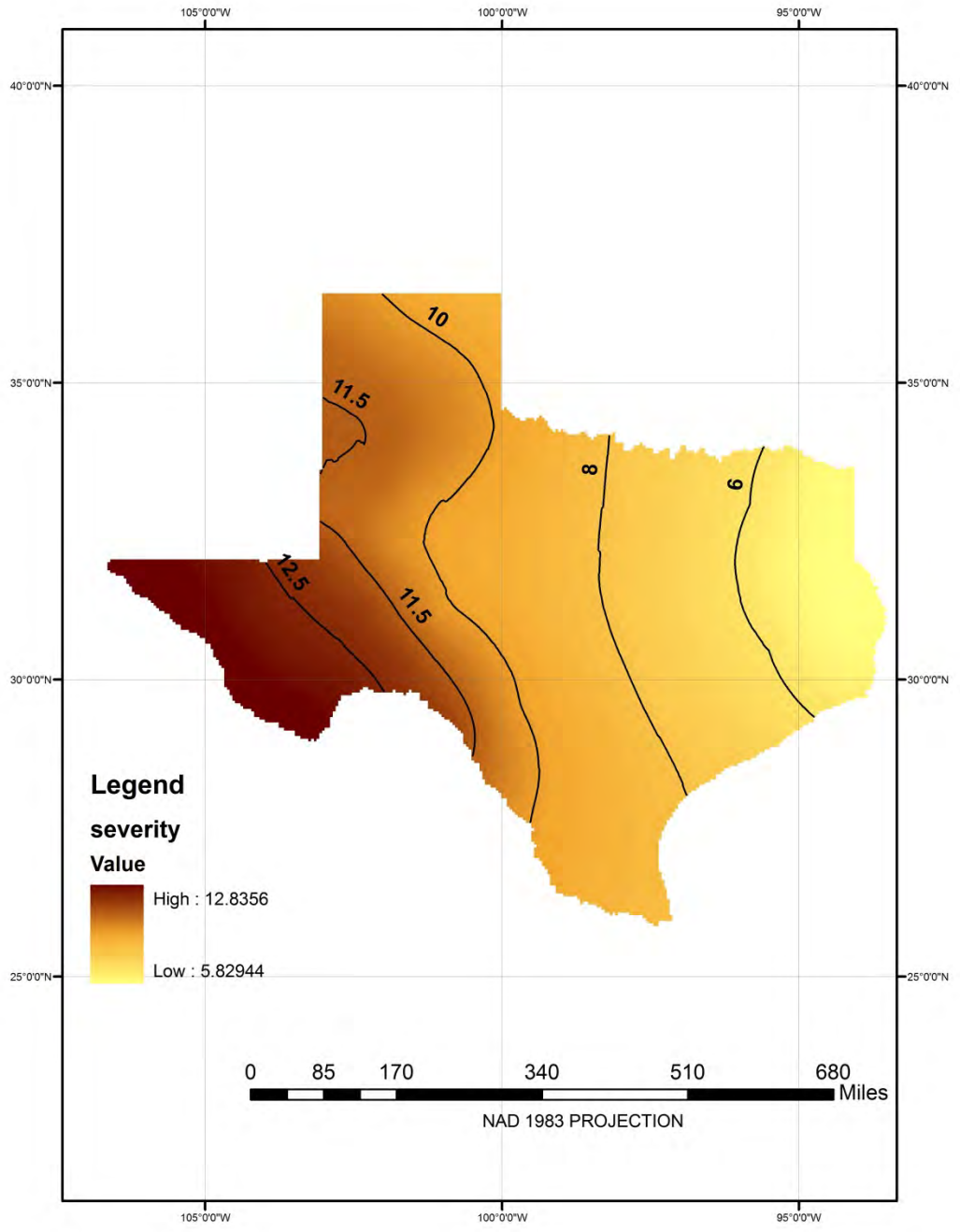

Figure 11x. Naturalized flow based iso severity map for 18 months drought duration with a return period of 50 years

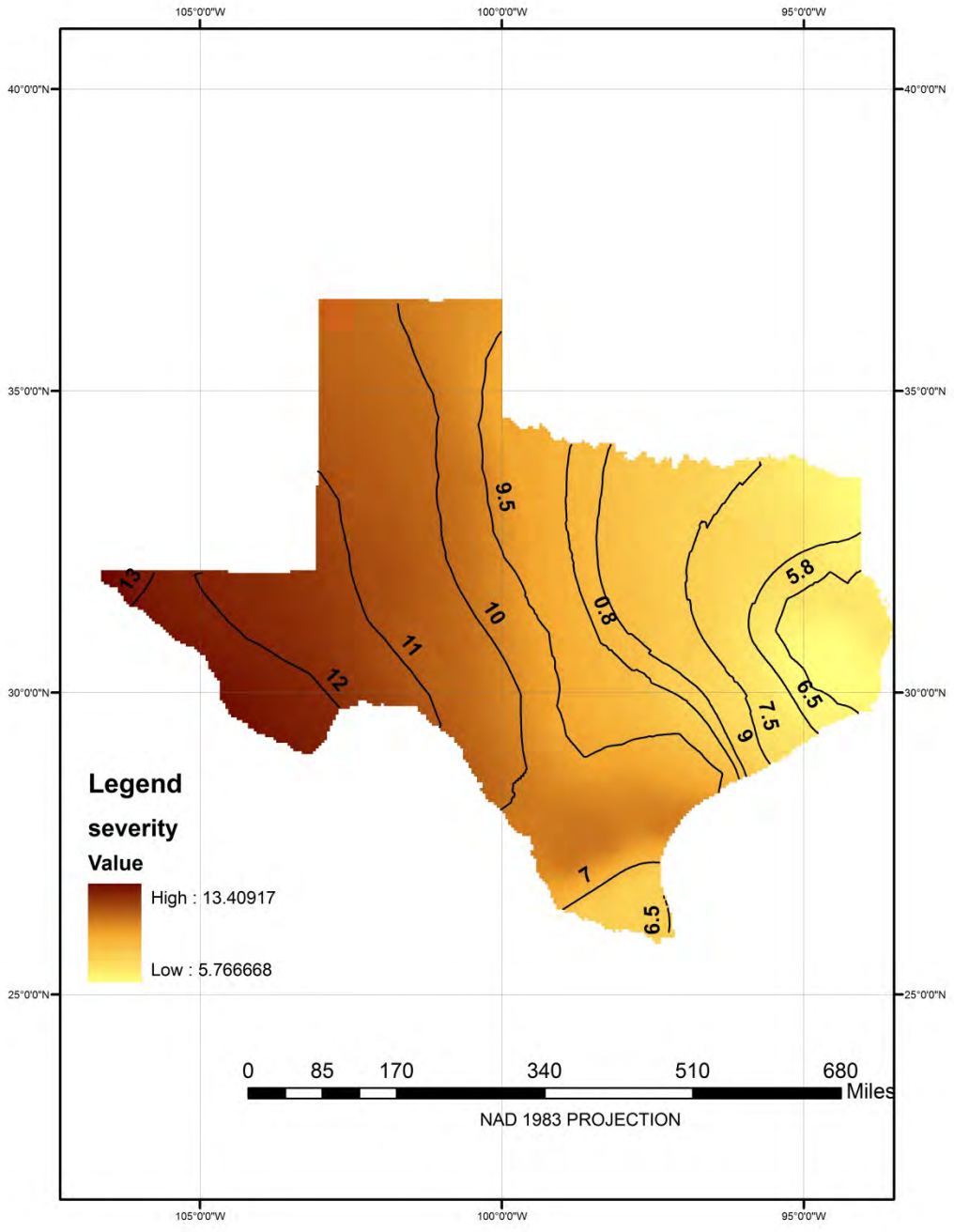

Figure 10y. Precipitation based iso severity map for 18 months drought duration with a return

period of 100 years

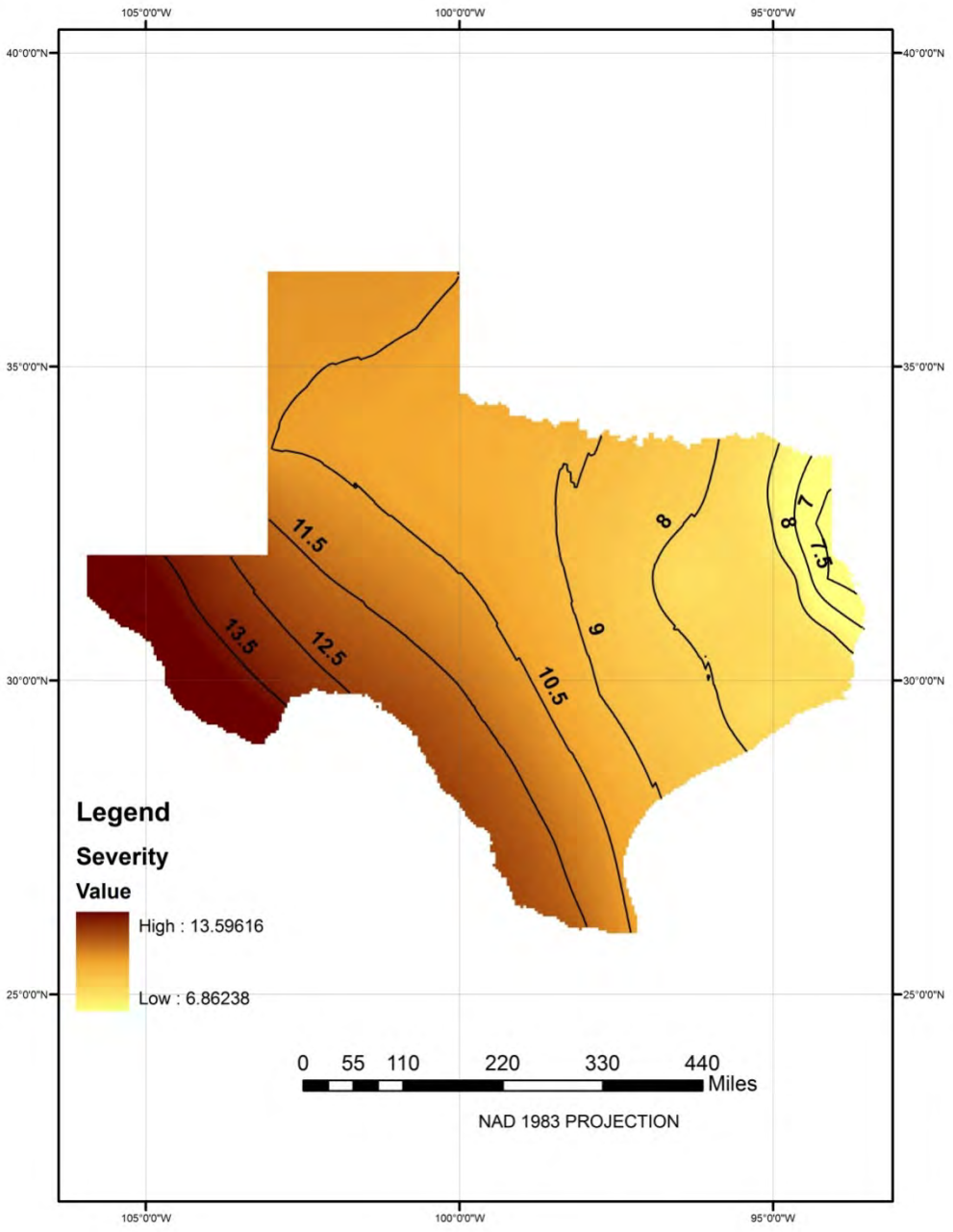

Figure 11z. Naturalized flow based iso severity map for 24 months drought duration with a return period of 5 years

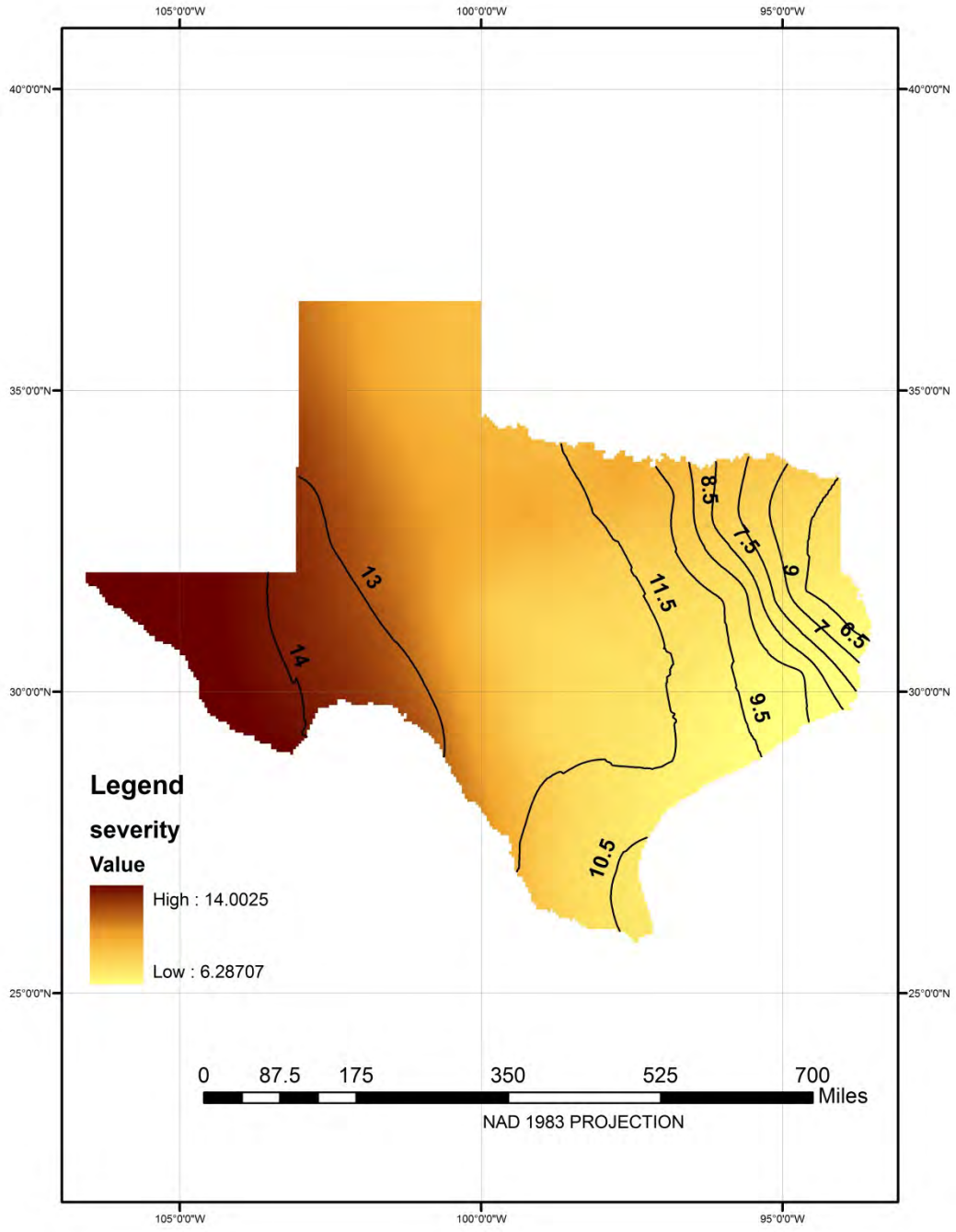

Figure 11aa. Naturalized flow based iso severity map for 24 months drought duration with a return period of 10 years

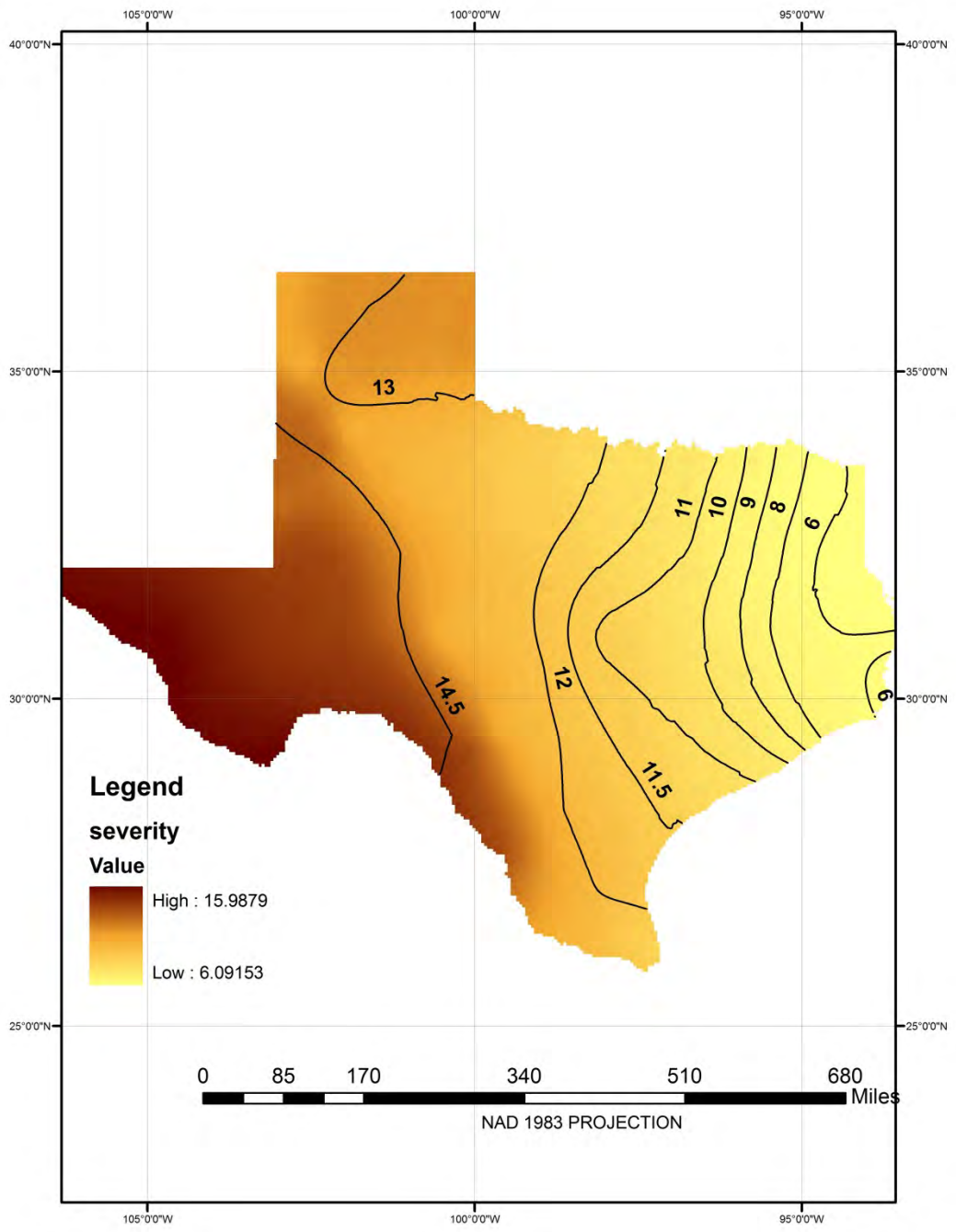

Figure 11ab. Naturalized flow based iso severity map for 24 months drought duration with a return period of 25 years

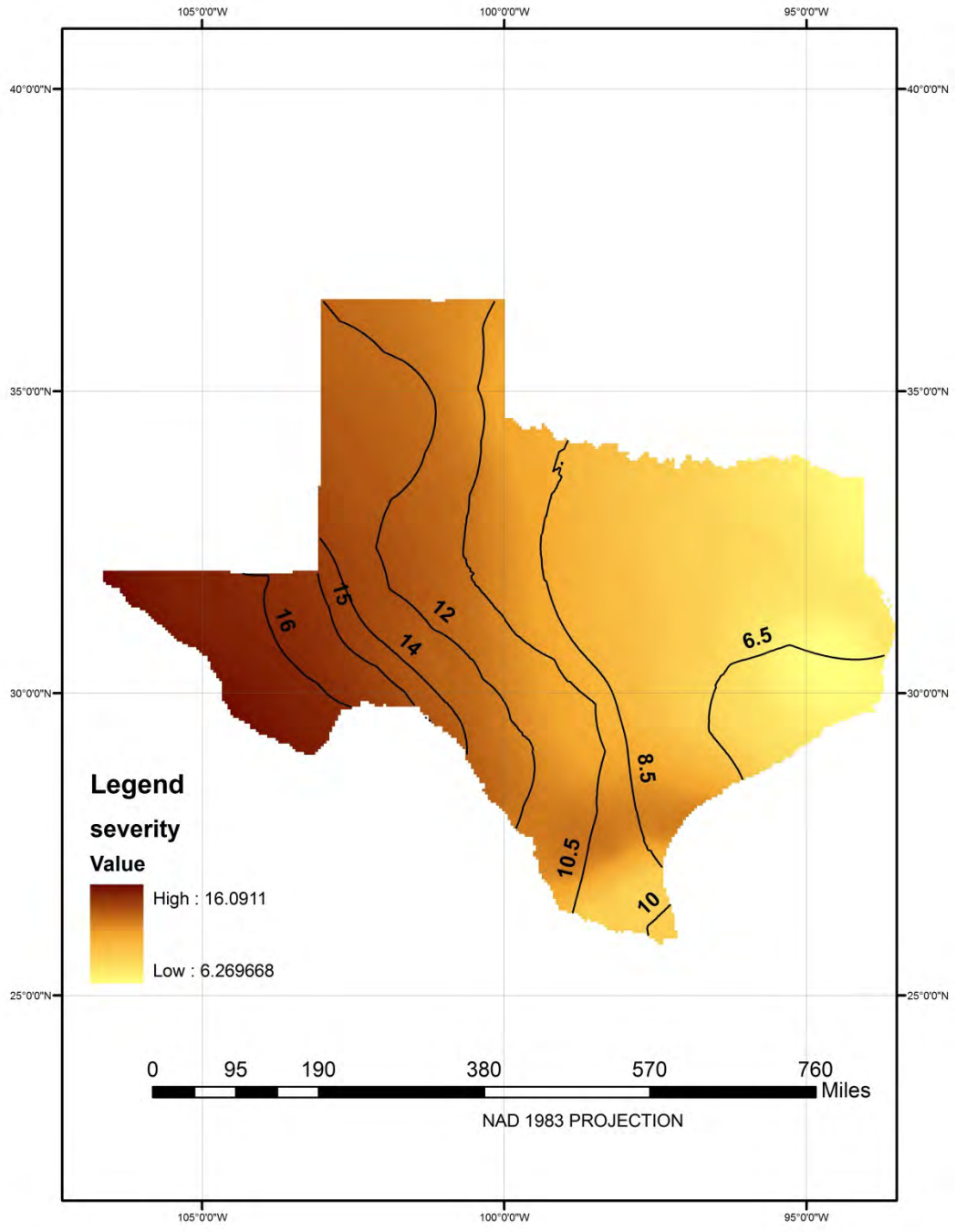

Figure 11ac. Naturalized flow based iso severity map for 24 months drought duration with a return period of 50 years

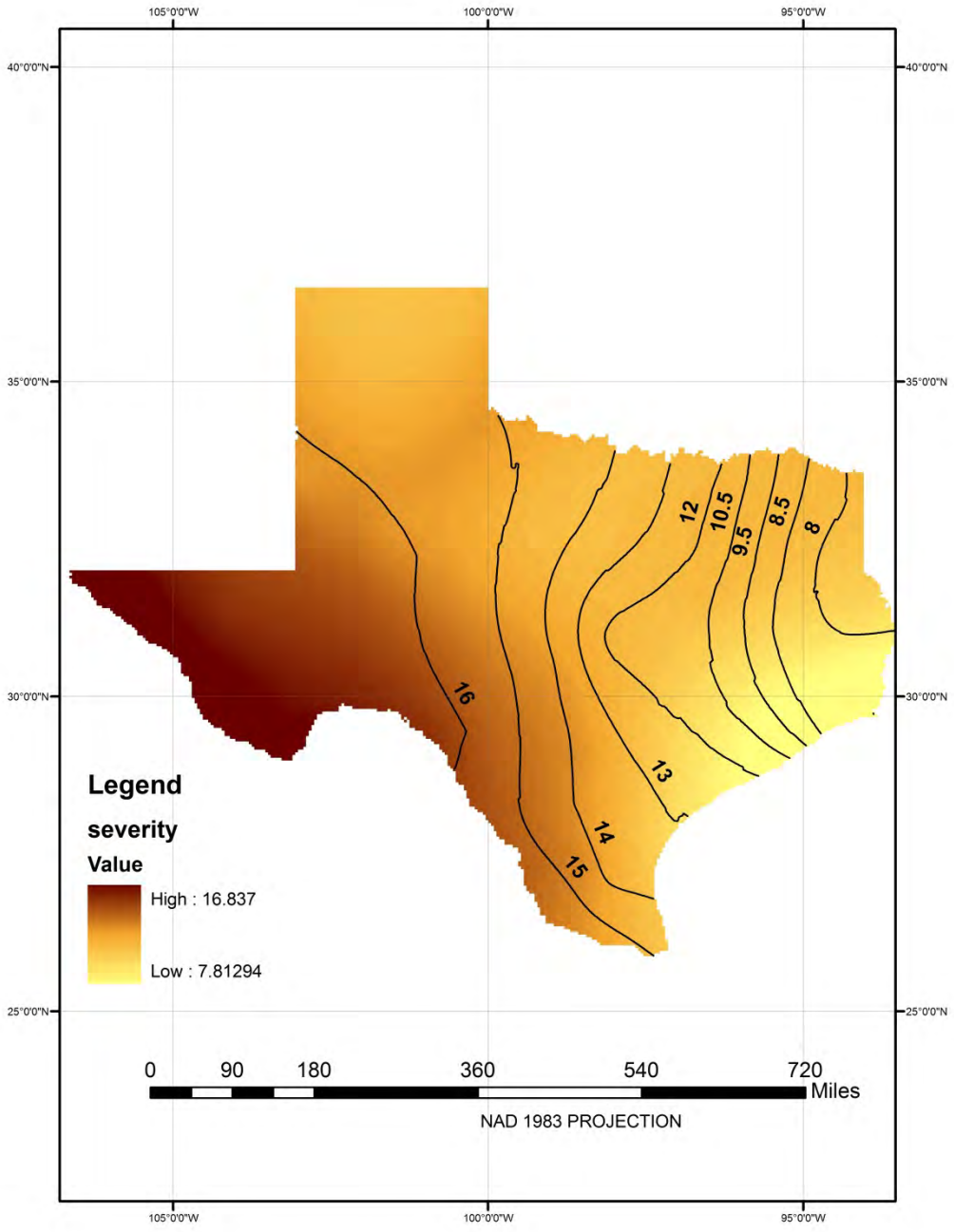

Figure 11ad. Naturalized flow based iso severity map for 24 months drought duration with a return period of 100 years

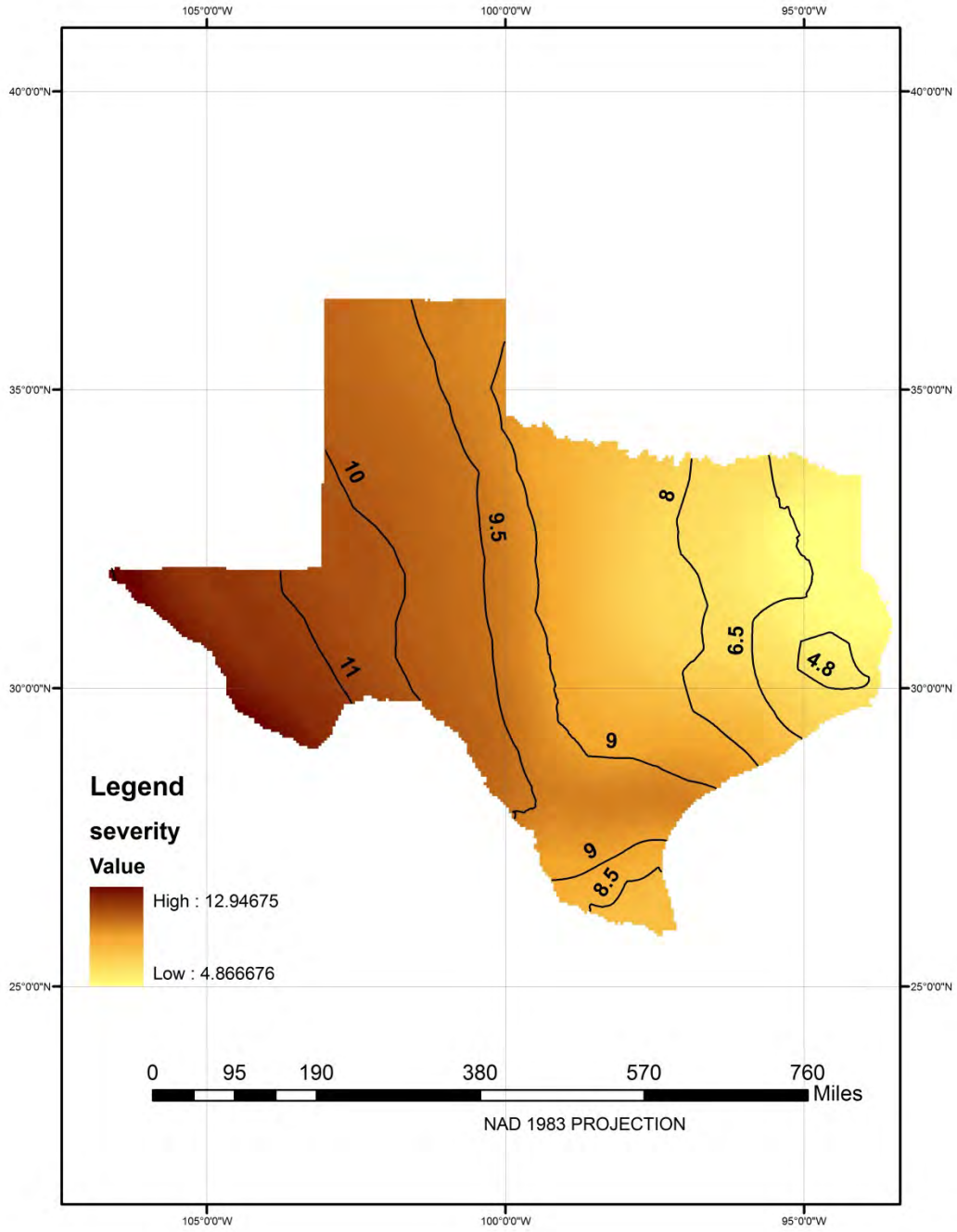

Figure 11ae. Naturalized flow based iso severity map for 36 months drought duration with a return period of 5 years

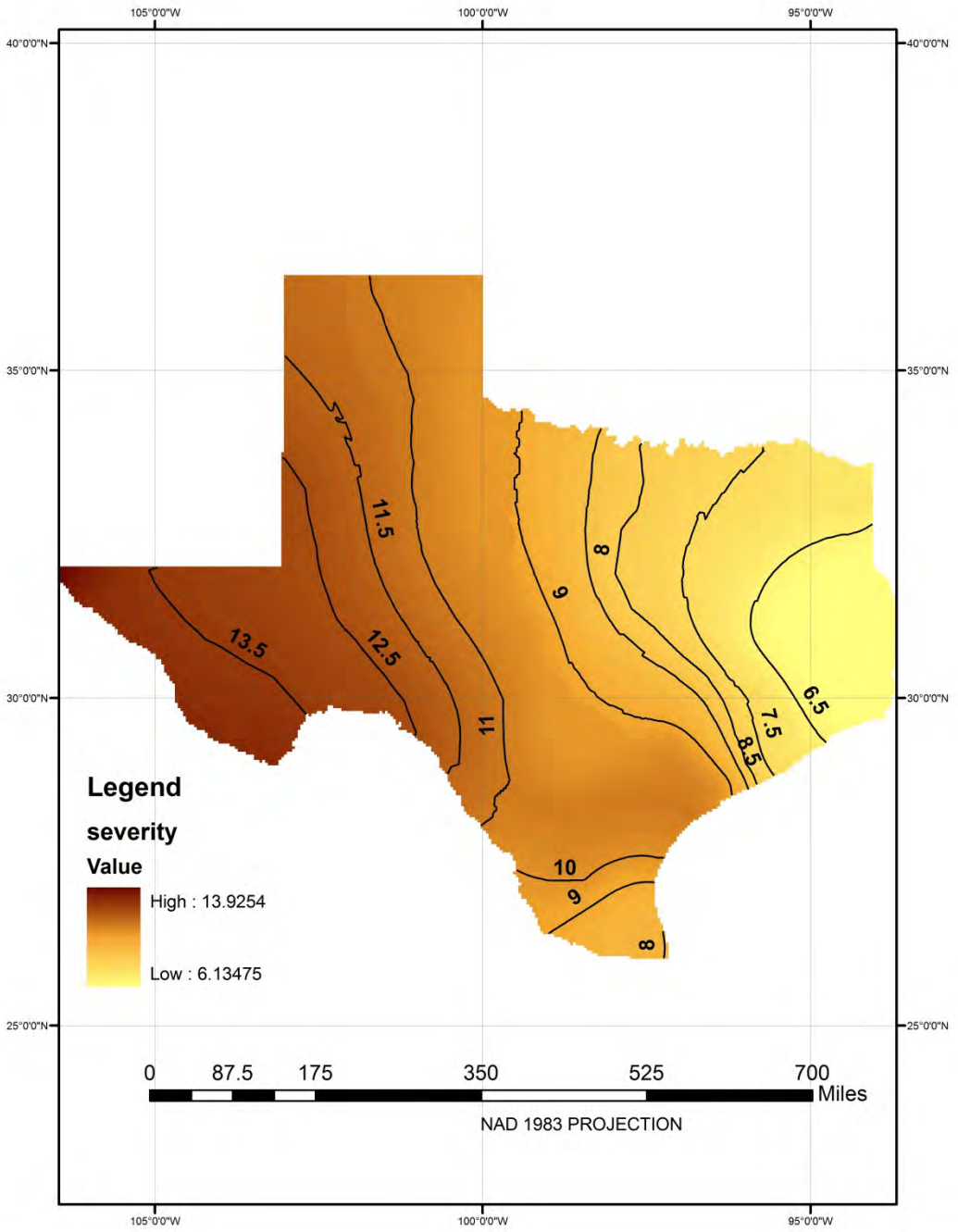

Figure 11af. Naturalized flow based iso severity map for 36 months drought duration with a return period of 10 years

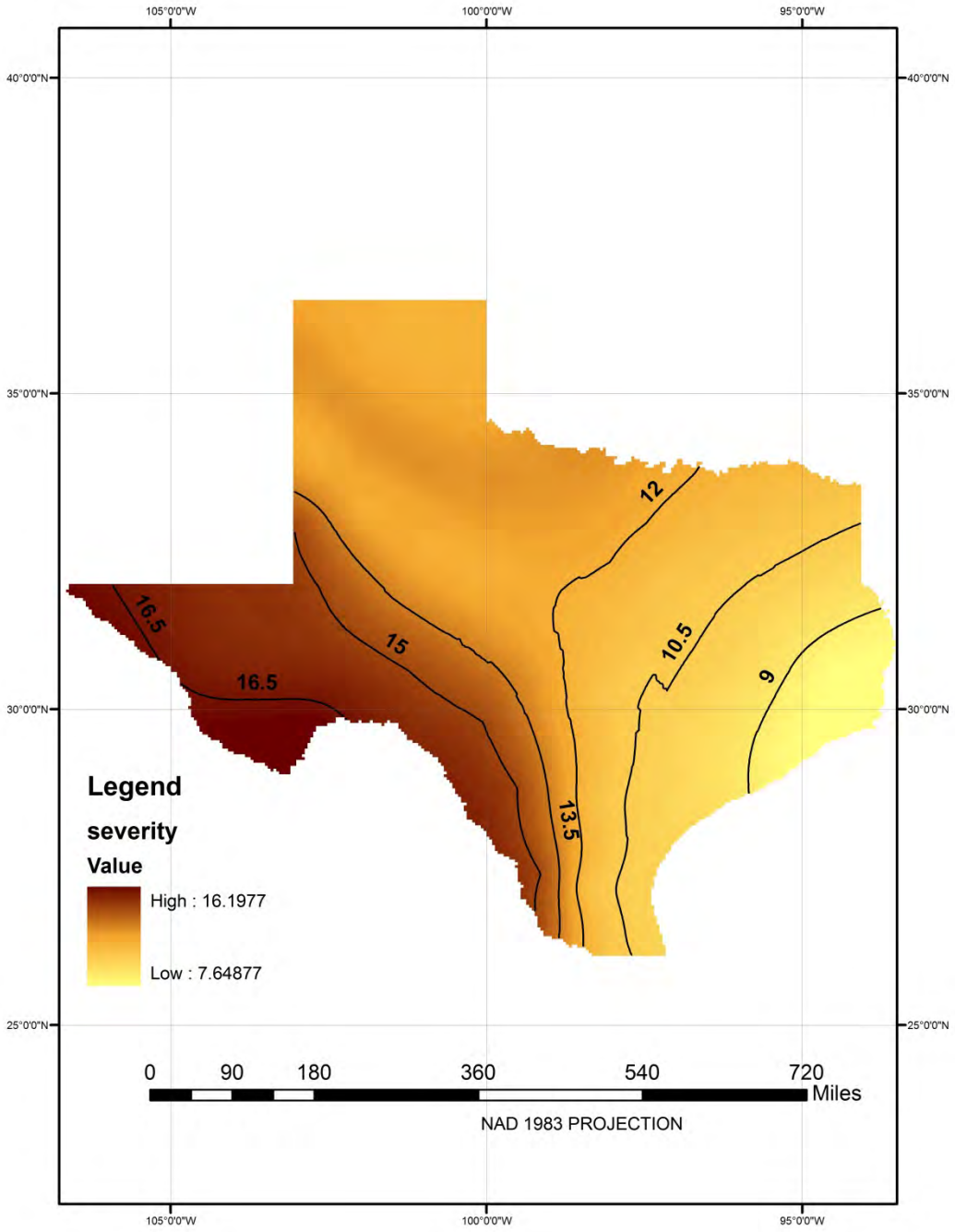

Figure 11ag. Naturalized flow based iso severity map for 36 months drought duration with a return period of 25 years

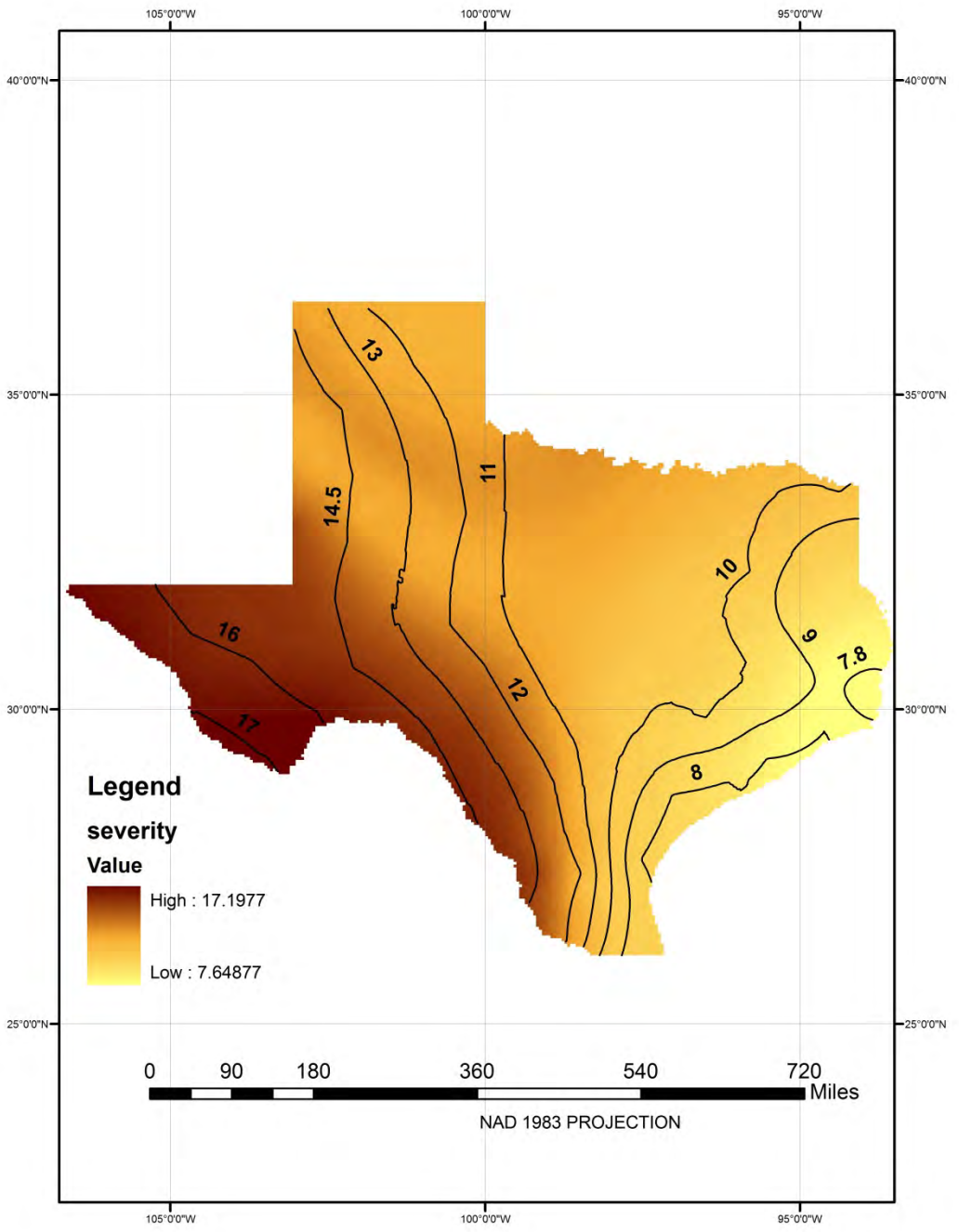

Figure 11ah. Naturalized flow based iso severity map for 36 months drought duration with a return period of 50 years

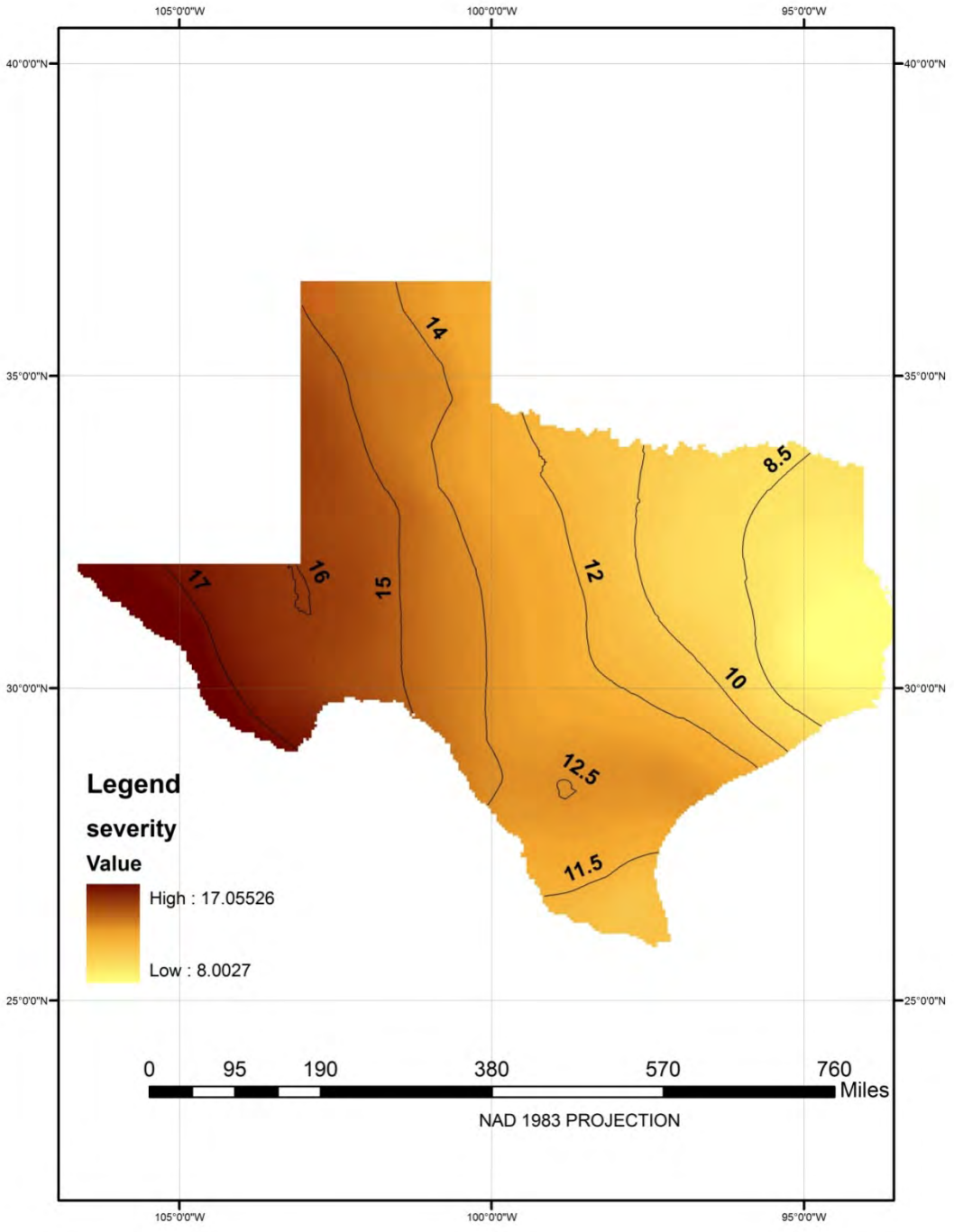

Figure 11ai. Naturalized flow based iso severity map for 36 months drought duration with a return period of 100 years

Appendix 1

Comparison of drought properties at a location when using: (a) Simulated stream flow (b) Precipitation (c) Naturalized stream flow.

Table 9. Summary statistics for drought variables under three conditions

Climatic variable	Statistic	Value
Naturalized streamflow Station : 08029500 Big Cow Creek, TX Lat: 30.49 N, Long: 93.47 W Time: 1953-1988 (monthly)	Mean (cfs) Standard deviation (cfs) Number of droughts Mean severity Minimum severity Maximum severity Mean duration (months) Minimum duration (months) Maximum duration (months)	146.78 216.51 47 3.312 0.064 14.56 4 1 11
VIC model streamflow Lat:30.4375N, Long:93.4125 W Time: 1950-2000 (monthly)	Mean (cfs) Standard deviation (cfs) Number of droughts Mean severity Minimum severity Maximum severity Mean duration (months) Minimum duration (months) Maximum duration (months)	140.75 145.46 57 5.799 0.0084 38.84 8.378 1 12
Precipitation Station: Sabine near Ruliff Lat: 30.18N, Long: 93.44W Time: 1950-2000	Mean (cfs) Standard deviation (cfs) Number of droughts Mean severity Minimum severity Maximum severity Mean duration (months) Minimum duration (months) Maximum duration (months)	53 14.1 54 3.78 0.03 35.9 5.89 1 27

Table 10. Summary of error statistics between (a) simulated and naturalized flow (b) simulated flow and precipitation

Variable	Error%	
	VIC vs. naturalized	VIC vs. precipitation
Number of droughts	17.54	12.96
Mean severity	42.88	12.38
Mean duration	52.25	32.08